Complementary mass spectrometric techniques for the characterization of the organic fraction in atmospheric aerosols

Dissertation

zur Erlangung des Grades eines
`Doktor rerum naturalium (Dr. rer. nat.)´

der Fachbereiche
08 – Physik, Mathematik und Informatik,
09 – Chemie, Pharmazie und Geowissenschaften,
10 – Biologie,
Universitätsmedizin
der Johannes Gutenberg-Universität

vorgelegt von

Alexander L. Vogel

geboren in Bad Schwalbach

Max Planck Graduate Center mit der
Johannes Gutenberg-Universität Mainz

Mainz, Januar 2014

Dekan: XXXXXXXXXXXX

1. Gutachter: XXXXXXXXXXXX

2. Gutachter: XXXXXXXXXXXX

Datum der mündlichen Prüfung: 26.02.2014

I hereby declare that I wrote the dissertation submitted without any unauthorized external assistance and used only sources acknowledged in the work. All textual passages which are appropriated verbatim or paraphrased from published and unpublished texts as well as all information obtained from oral sources are duly indicated and listed in accordance with bibliographical rules. In carrying out this research, I complied with the rules of standard scientific practice as formulated in the statutes of Johannes Gutenberg-University Mainz to insure standard scientific practice.

Mainz, 9. January 2014

„Man merkt nie, was schon getan wurde-
man sieht immer nur das, was noch zu tun bleibt.“

Marie Curie

Zusammenfassung

Atmosphärische Aerosole üben einen starken Einfluss auf das Klima der Erde, auf die Luftqualität und auf die Gesundheit des Menschen aus. Aerosole sind der größte Unsicherheitsfaktor in der Berechnung des Strahlungshaushaltes der Erde. Sie können die Sonnenstrahlung direkt streuen oder absorbieren, oder indirekt als Nukleationskeime für Wolkentröpfchen zu einem erhöhten Reflektionsverhalten von Wolken beitragen. Dabei spielt insbesondere die Anzahlkonzentration, die Größe und die chemische Zusammensetzung der Aerosolpartikel eine wichtige Rolle. Sekundäres organisches Aerosol (SOA), welches durch die atmosphärische Oxidation von flüchtigen organischen Verbindungen entsteht, trägt aufgrund einer Vielzahl verschiedenster organischer Verbindungen maßgeblich zu der Komplexität atmosphärischer Aerosole bei.

Das Ziel dieser Arbeit war es, die Zusammensetzung von atmosphärischem SOA mit Hilfe von massenspektrometrischen Methoden zu untersuchen. Die Echtzeit-Messung von atmosphärischem SOA wurde durch ein Ionenfallen-Massenspektrometer realisiert und ermöglichte somit einen Einblick in dessen Variabilität der chemischen Zusammensetzung. Die Ionisierung der aerosolgetragenen Komponenten erfolgte durch Korona-Entladung bei Atmosphärendruck (*engl.* Atmospheric Pressure Chemical Ionization Ion Trap Mass Spectrometry APCI-IT-MS). Der Vorteil dieser Ionisierungsmethode liegt darin begründet, dass eine Vielzahl organischer Analyten ionisiert werden können, ohne dass diese während des Ionisierungsprozesses fragmentieren. Im Rahmen verschiedener Feldstudien, wurde das APCI-IT-MS in Kombination mit einer Aerosol-Anreicherungseinheit zur Messung von biogenen organischen Säuren eingesetzt. Hierbei konnte dank der begleitenden Messungen eines Aerosol Massenspektrometers (AMS) und der Filterprobenahme für die Analyse mittels Flüssigchromatographie / hochauflösende Massenspektrometrie (LC/UHRMS) die Aerosolzusammensetzung umfassend charakterisiert werden.

Insbesondere konnte im Rahmen einer Feldmesskampagne im borealen Nadelwald in Hyytiälä, Finnland, die Partitionierung einzelner organischer Säuren zwischen der Gas- und der Partikelphase gemessen werden. Es konnte gezeigt werden, dass schwerflüchtige organische Verbindungen zu einem Großteil in die Gasphase partitionieren. Diese Beobachtung wurde als ein Hinweis auf eine nicht unmittelbare Gleichgewichtseinstellung zwischen Gas- und Partikelphase interpretiert, welche entweder durch die kontinuierliche Produktionsrate von schwerflüchtigen Verbindungen in der Gasphase oder durch einen viskosen Phasenzustand der Aerosolpartikel bedingt sind. Des Weiteren ermöglichte der MS/MS-Modus des Ionenfallenmassenspektrometers Messungen, die *in-situ* Rückschlüsse auf die strukturelle Beschaffenheit einzelner Moleküle erlaubten. Der Vergleich zu der experimentellen Ozonolyse bestimmter Monoterpene im Labor zeigte, dass das atmosphärische Aerosol in Finnland zu Teilen aus noch unbekannten Oxidationsprodukten besteht. Des Weiteren zeigten die aufgenommen Massenspektren der atmosphärischen Gasphase eine große Übereinstimmung zu der im Experiment erzeugten Partikelphase. Die atmosphärische Partikelphase hingegen erschien höher oxidiert als die experimentell erzeugte Partikelphase. Diese Beobachtungen verdeutlichen, dass ein besseres Verständnis des Ausmaßes der atmosphärischen Oxidation sowie der Partitionierung der Oxidationsprodukte zwischen Gas- und Partikelphase für eine präzisere Vorhersage der atmosphärischen SOA Konzentrationen erforderlich ist.

Aufgrund einer Modifikation des experimentellen Aufbaus konnte, während einer Feldstudie auf dem Kleinen Feldberg/Taunus in Deutschland, die Empfindlichkeit für organische Verbindungen in der Partikelphase verbessert werden. Dies ermöglichte unter Anderem die

Messung der chemischen Zusammensetzung während eines Partikelneubildungsprozesses. Dabei wurden organische Verbindungen mit einem Molekulargewicht von ~ 300 Da gemessen, deren Summenformel durch die Analyse einer gleichzeitigen Filterprobe mittels LC/UHRMS bestimmt werden konnte. Hierbei konnte gezeigt werden, dass Oxidationsprodukte von Sesquiterpenen eine wichtige Rolle in der Neubildung von Partikeln und deren Wachstum zu klimatisch relevanten Größen spielen können.

Die eingehende Analyse der Filterproben mittels LC/UHRMS zeigte des Weiteren, dass eine Vielzahl verschiedener Organosulfate und Nitrooxy-Organosulfate im atmosphärischen Aerosol am Kleinen Feldberg nachgewiesen werden konnten. Diese Beobachtung konnte durch die Echtzeit-Messung einzelner Massenspuren des APCI-IT-MS bestätigt werden. Der simultane quantitative Vergleich von Sulfat-Messungen durch Ionenchromatographie und die Aerosol Massenspektrometrie verdeutlichte, dass ein erheblicher Anteil des Gesamt-Sulfats an organischen Molekülen gebunden war.

Schließlich wurde die umfangreiche chemische Charakterisierung des atmosphärischen Aerosols mit der durch einen Wolkenkondensationskeimzähler ermittelten Hygroskopizität der Aerosolpartikel verglichen. Gleichzeitig wurde die oxidative Alterung des Aerosols durch das Verhältnis zweier biogener Oxidationsprodukte zueinander bestimmt. Hierbei zeigte sich, dass die Hygroskopizität des Aerosols mit oxidativer Alterung zunimmt. Des Weiteren wurde beobachtet, dass mit der chemischen Bindung von Sulfat an organischen Molekülen die Hygroskopizität der Aerosolpartikel, im Vergleich zu einer internen Mischung aus anorganischem Sulfat und rein organischen Verbindungen, deutlich verringert ist. Abschließend lässt sich zusammenfassen, dass die Applikation moderner massenspektrometrischer Methoden detaillierte Einblicke in chemische und physikochemische Prozesse atmosphärischer Aerosole ermöglicht.

Abstract

Aerosol particles are strongly related to climate, air quality, visibility and human health issues. They contribute the largest uncertainty in the assessment of the Earth´s radiative budget, directly by scattering or absorbing solar radiation or indirectly by nucleating cloud droplets. The influence of aerosol particles on cloud related climatic effects essentially depends upon their number concentration, size and chemical composition. A major part of submicron aerosol consists of secondary organic aerosol (SOA) that is formed in the atmosphere by the oxidation of volatile organic compounds. SOA can comprise a highly diverse spectrum of compounds that undergo continuous chemical transformations in the atmosphere.

The aim of this work was to obtain insights into the complexity of ambient SOA by the application of advanced mass spectrometric techniques. Therefore, an atmospheric pressure chemical ionization ion trap mass spectrometer (APCI-IT-MS) was applied in the field, facilitating the measurement of ions of the intact molecular organic species. Furthermore, the high measurement frequency provided insights into SOA composition and chemical transformation processes on a high temporal resolution. Within different comprehensive field campaigns, online measurements of particular biogenic organic acids were achieved by combining an online aerosol concentrator with the APCI-IT-MS. A holistic picture of the ambient organic aerosol was obtained through the co-located application of other complementary MS techniques, such as aerosol mass spectrometry (AMS) or filter sampling for the analysis by liquid chromatography / ultrahigh resolution mass spectrometry (LC/UHRMS).

In particular, during a summertime field study at the pristine boreal forest station in Hyytiälä, Finland, the partitioning of organic acids between gas and particle phase was quantified, based on the online APCI-IT-MS and AMS measurements. It was found that low volatile compounds reside to a large extent in the gas phase. This observation can be interpreted as a consequence of large aerosol equilibration timescales, which build up due to the continuous production of low volatile compounds in the gas phase and/or a semi-solid phase state of the ambient aerosol. Furthermore, *in-situ* structural informations of particular compounds were achieved by using the MS/MS mode of the ion trap. The comparison to MS/MS spectra from laboratory generated SOA of specific monoterpene precursors indicated that laboratory SOA barely depicts the complexity of ambient SOA. Moreover, it was shown that the mass spectra of the laboratory SOA more closely resemble the ambient gas phase composition, indicating that the oxidation state of the ambient organic compounds in the particle phase is underestimated by the comparison to laboratory ozonolysis. These observations suggest that the micro-scale processes, such as the chemistry of aerosol aging or the gas-to-particle partitioning, need to be better understood in order to predict SOA concentrations more reliably.

During a field study at the Mt. Kleiner Feldberg, Germany, a slightly different aerosol concentrator / APCI-IT-MS setup made the online analysis of new particle formation possible. During a particular nucleation event, the online mass spectra indicated that organic compounds of approximately 300 Da are main constituents of the bulk aerosol during ambient new particle formation. Co-located filter analysis by LC/UHRMS analysis supported these findings and furthermore allowed to determine the molecular formulas of the involved organic compounds. The unambiguous identification of several oxidized C-15 compounds indicated that oxidation products of sesquiterpenes can be important compounds for the initial formation and subsequent growth of atmospheric nanoparticles.

The LC/UHRMS analysis furthermore revealed that considerable amounts of organosulfates and nitrooxy organosulfates were detected on the filter samples. Indeed, it was found that several nitrooxy organosulfate related APCI-IT-MS mass traces were simultaneously enhanced. Concurrent particle phase ion chromatography and AMS measurements indicated a strong bias between inorganic sulfate and total sulfate concentrations, supporting the assumption that substantial amounts of sulfate was bonded to organic molecules.

Finally, the comprehensive chemical analysis of the aerosol composition was compared to the hygroscopicity parameter kappa, which was derived from cloud condensation nuclei (CCN) measurements. Simultaneously, organic aerosol aging was observed by the evolution of a ratio between a second and a first generation biogenic oxidation product. It was found that this aging proxy positively correlates with increasing hygroscopicity. Moreover, it was observed that the bonding of sulfate to organic molecules leads to a significant reduction of kappa, compared to an internal mixture of the same mass fractions of purely inorganic sulfate and organic molecules. Concluding, it has been shown within this thesis that the application of modern mass spectrometric techniques allows for detailed insights into chemical and physico-chemical processes of atmospheric aerosols.

Table of contents

1 Introduction

1.1 Atmospheric aerosols and their impact on Earth´s climate

Atmospheric aerosols are liquid or solid particles suspended in air. They are ubiquitous throughout the atmosphere and originate from natural and anthropogenic sources. According to their formation processes, it is distinguished between primary and secondary aerosols. Primary aerosols consist of particles which are directly emitted into the air (e.g. in form of wind-blown dust, sea-salt, pollen, fungal spores or plant debris) whereas secondary aerosols contain particles that are formed in the atmosphere through the oxidation of gaseous precursors and subsequent gas-to-particle conversion (e.g. the oxidation of SO_2 to H_2SO_4) (Pöschl, 2005; Hallquist et al., 2009). The size of the particles depends on their formation mechanisms. Particles larger than 1 µm in diameter (*coarse mode*) are usually primary in nature and contribute largely to the mass of aerosol populations. They have short atmospheric lifetimes due to fast gravitational settling (Seinfeld and Pandis, 2006). Particles smaller than 1 µm (*fine mode*) are usually secondary in nature and contribute largely to the number and surface area of particle populations. The *fine mode* can furthermore be classified into three different submicron size modes: The smallest particles, which can be less than 10 nm in diameter (*nucleation mode*), are secondary in nature, formed by the condensation of low volatile compounds onto thermodynamically stable clusters (e.g. Kulmala et al., 2013). They usually grow rapidly to larger sizes by condensation of vapors or coagulation with other particles. Diameters between 10 to 100 nm refer to the *Aitken mode.* The *accumulation mode* spans from 100 nm to 1 µm and comprises the aerosol particles with the longest atmospheric lifetime. Particles of this size mode are mainly removed from the atmosphere by wet deposition. It is mentioned that, despite of their large size and low number concentration, primary super-micron particles are essentially important for the formation of precipitation due to the ability to act as ice nuclei (IN) (Cantrell and Heymsfield, 2005).

Aerosols influence the Earth´s radiative balance directly by scattering or absorbing solar radiation (Satheesh and Moorthy, 2005) or indirectly by acting as cloud condensation nuclei (CCN) (Lohmann and Feichter, 2005). The properties of aerosol particles determine whether the net effect on the radiative balance of the Earth´s energy budget is positive or negative. Emissions of black carbon (BC) and the formation of atmospheric brown clouds (ABCs), for example, heat the Earth´s atmosphere due to the absorption of solar radiation and are, after carbon dioxide emissions, the second strongest contribution to global warming (Figure 1.1) (IPCC, 2013; Ramanathan and Carmichael, 2008).

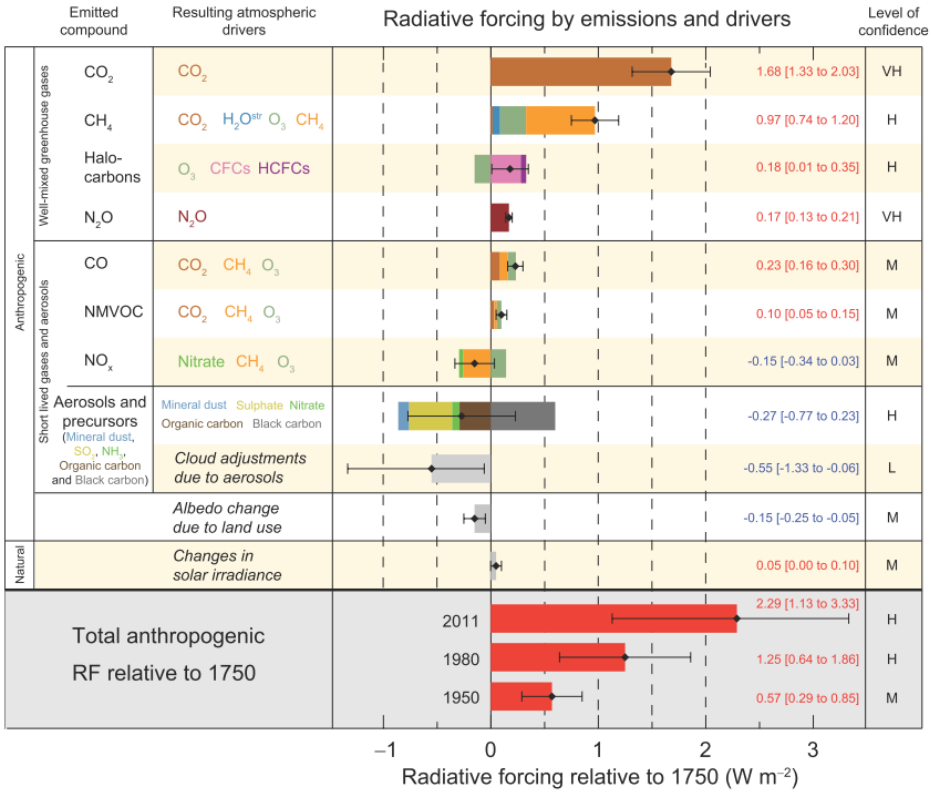

Figure 1.1 Radiative forcing estimates in 2011 compared to 1750 induced by anthropogenic gaseous and particulate emissions. The best estimates of the sum contribution of each category are depicted as black diamonds and the uncertainties as black errorbars. The level of confidence of the net forcing is abbreviated as follows: VH-*very high*, H-*high*, M-*medium*, L-*low*, VL-*very low*. Reprinted from IPCC (2013).

In contrast to BC, sulfate particles cause brighter clouds due to a larger number of smaller droplets, resulting in a net cooling effect (*cloud albedo effect*) (Twomey, 1977; Boucher and Lohmann, 1995). Additionally, these brighter clouds mostly have prolonged average lifetimes (*cloud lifetime effect*) (Albrecht, 1989). This effect is often observed over polluted regions, where the available amount of water vapor condenses onto a larger number of CCN, producing many small cloud droplets. As a consequence, precipitation is suppressed due to a slower coalescence of a higher number concentration of small cloud droplets into rain droplets (Rosenfeld et al., 2008). Thus, in addition to the effects on the radiative balance, atmospheric aerosols also have a significant influence the Earth´s hydrological cycle (e.g. Ramanathan et al., 2001).

Aerosol particles continue to contribute the largest uncertainty in the estimation of the global radiative forcing (IPCC, 2013). This is due to the fact that the average aerosol lifetime is relatively short and hence the temporal and spatial distribution highly variable, whereas long-lived greenhouse gases (GHG) are homogeneously distributed throughout the atmosphere. Furthermore, aerosol particles have no uniform properties since they can undergo continuous

chemical and physical alteration throughout their life cycle and interact with atmospheric trace gases in heterogeneous or multiphase chemical reactions (Ravishankara, 1997).

However, it is still uncertain to which extent the net negative radiative effect of aerosols involves the danger of masking the global greenhouse effect by compensating the positive radiative forcing of GHG emissions. Moreover, as anthropogenic aerosol precursor gases, such as SO_2, are reduced in a future scenario, global warming might accelerate, because of a much shorter lifetime of cooling aerosols compared to the warming GHG (Charlson et al., 1992; Andreae et al., 2005).

Furthermore, epidemiological studies have shown that particulate matter (PM) can also be associated to adverse human health effects, especially affecting the respiratory and cardiovascular system (Schwartz et al., 1996; Pope and Dockery, 2006). However, due to the complexity or the organic aerosol fraction, it is argued that the "organic aerosol" cannot be regarded as an aggregate category when examining its potential health effects. Therefore, multidisciplinary approaches are necessary for a thorough risk assessment of organic aerosol constituents (Mauderly and Chow, 2008).

1.2 Secondary organic aerosol (SOA)

Depending on the location, the continental submicron organic aerosol (OA) fraction ranges between 20 and 90% (Lim and Turpin, 2002; Murphy et al., 2006; Zhang et al., 2007) and there is increasing evidence that a large stake of the OA can be attributed to secondary organic aerosol (SOA) (Heald et al., 2005; Jimenez et al., 2009). Current atmospheric models underestimate the measured SOA mass (Figure 1.2), which indicates that fundamental knowledge gaps are contributing to aerosol related uncertainties in global climate and air quality models (Volkamer et al., 2006; Goldstein and Galbally, 2007; Jimenez et al., 2009). These knowledge gaps are closely related to the chemical complexity, to the continuous transformation and degradation, and to the composition dependent physical and physico-chemical properties of organic gaseous and particulate emissions, as discussed in the following sections.

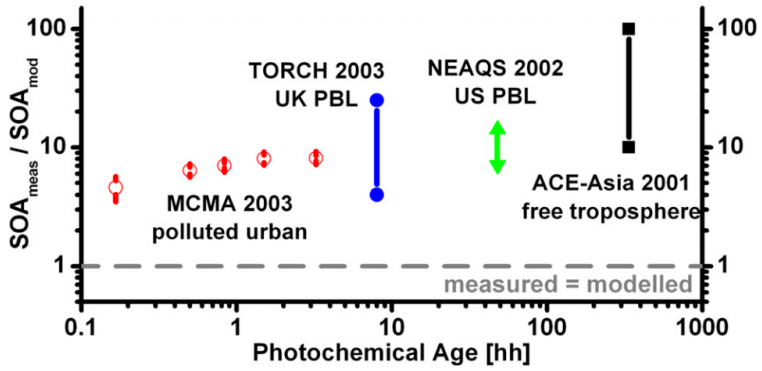

Figure 1.2 Comparison of the ratio between measured and modelled secondary organic aerosol (SOA) as a function of the photochemical age (calculated with the assumption of [OH] = $3*10^6$ molecules cm^{-3}) (Volkamer et al., 2006).

1.2.1 Formation of SOA

A prerequisite for the formation of SOA is the emission of volatile organic compounds (VOCs) into the atmosphere– either biogenic or anthropogenic in origin. On a global scale, biogenic emissions of VOCs are almost one order of magnitude higher than anthropogenic emissions (Guenther et al., 1995). The emitted VOCs are mainly secondary metabolites, such as the terpenoid isoprene (C_5H_8), the monoterpenes ($C_{10}H_{16}$) and sesquiterpenes ($C_{15}H_{24}$), which can be experienced as the refreshing odour of forests. Other VOCs (e.g. alkanes and non-terpenoid alkenes) as well as oxygenated VOCs (e.g. carbonyls, alcohols, organic acids) are also emitted by plants, but not in the same amount as isoprene and monoterpenes (Kesselmeier and Staudt, 1999). Once released into the air, the reaction of VOCs with the atmospheric oxidants hydroxyl radical (OH), ozone (O_3) and nitrate radical (NO_3) proceeds, resulting in products with very different properties. If the oxidation results in functionalization or oligomerization of the initial VOCs, the oxidation products´ vapor pressure is reduced by several orders of magnitude. This facilitates the gas-to-particle conversion of VOCs to SOA in form of condensation onto pre-existing particles or the formation of new particles (Figure 1.3). If the oxidation is accompanied by fragmentation, however, the vapor pressure of the products is usually increased, implying that the oxidation products remain in the gas phase and do not contribute to the SOA fraction (Kroll et al., 2011).

Large emission fluxes of VOCs over forested areas thus contribute to an increasing SOA fraction of local aerosol populations. SOA can be observed in form of a “blue haze” over large forested areas during summertime, due to wavelength dependent Rayleigh scattering of light. The

connection between gaseous emissions of forests and the formation of particles that cause the blue haze was described by Went et al. back in 1960.

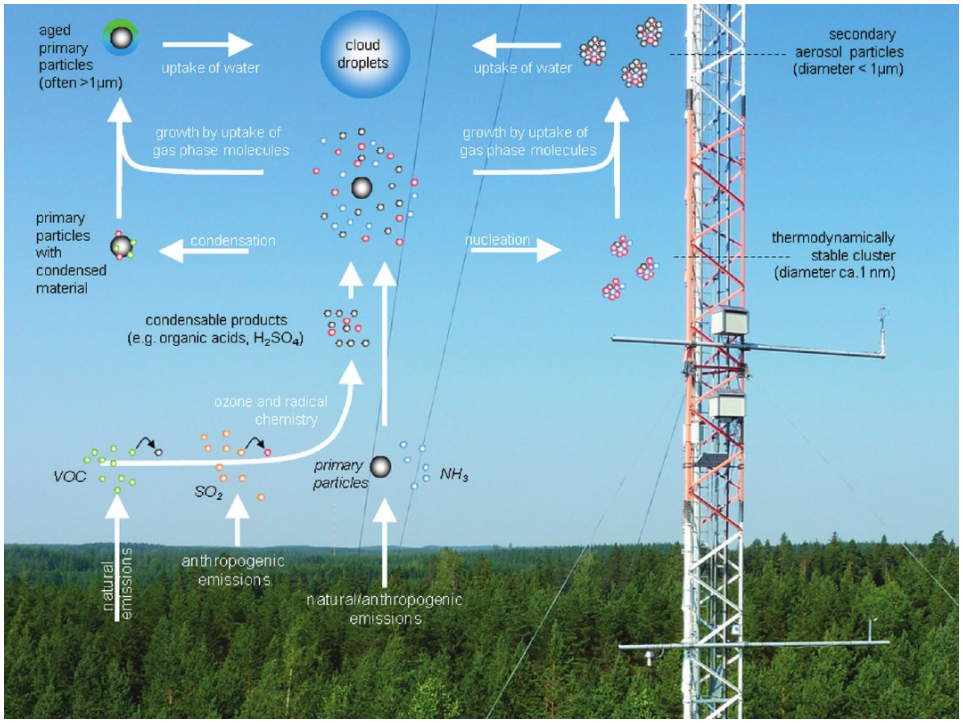

Figure 1.3 Formation mechanisms of atmospheric aerosols (Hoffmann et al., 2011).

Since atmospheric oxidation involves several radical reactions, radical intermediates and continuous multigeneration oxidative steps, the oxidation of the (already large) variety of different VOC precursors results in a manifold variety of different compounds present in SOA (Goldstein and Galbally (2007) estimate that 10^4 to 10^5 different organic compounds are present in atmospheric aerosols). An overview of the initial gas phase chemistry of VOC oxidation is given in Figure 1.4.

The initial reaction of a VOC with OH, NO_3 and ozone forms an alkyl radical (in the case of ozone through the hydroperoxide channel, Kroll and Seinfeld, 2008) which further reacts with oxygen producing an alkylperoxy radical RO_2. Depending on the concentration of NO_x, HO_2 and RO_2 radicals, the alkylperoxy radical either recombines to products such as alcohols, hydroperoxides, peroxynitrates or organic nitrates or it reacts with NO forming alkoxy radicals (RO). Alkoxy radicals can isomerize or dissociate resulting again in an alkyl radical or reacting with oxygen to produce a carbonyl and HO_2 (Kroll and Seinfeld, 2008). As these reactions proceed, the functionalization and fragmentation reactions of the initial VOCs finally result in the oxidation to CO_2 and water, as long as the compounds are not removed from atmosphere by dry or wet deposition.

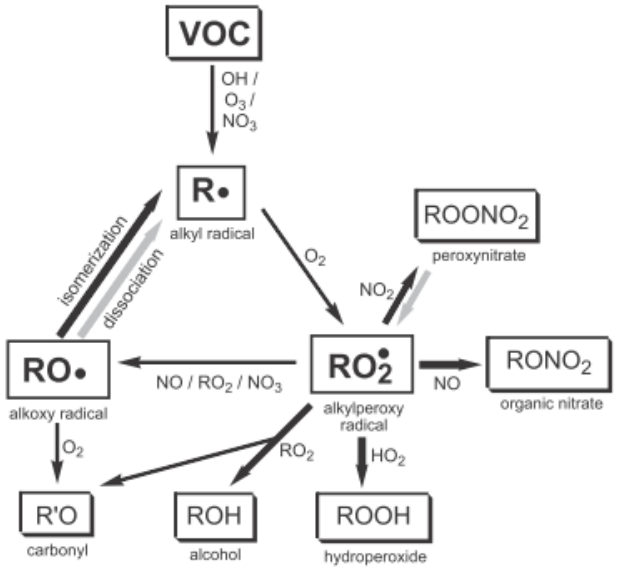

Figure 1.4 Initial gas phase oxidation mechanism of volatile organic compounds (VOCs) by atmospheric oxidants. Bold black arrows indicate reactions that are associated with a significant reduction of the vapor pressure (Kroll and Seinfeld, 2008).

1.2.2 Gas-to-particle partitioning

The molecular structure of many biogenic VOCs, in form of cyclic molecules incorporating an endocyclic double bond, prevents the fragmentation of the molecule upon the initial radical or ozone attack at the C-C double bond. Although the double bond is cleaved during the oxidation, the molecule only undergoes a ring-opening reaction instead of fragmentation into two products. Thus, the incorporation of two polar functional groups without fragmentation decreases the vapor pressure of a compound to an extent of several orders of magnitude (Pankow and Asher, 2008). However, the large amounts of first generation oxidation products of VOCs do not necessarily condense onto particles. They are rather considered as semi-volatile organic compounds (SVOCs), implying that SVOCs partition between the gas and particle phase depending on the available particle mass (*PM* (µg/m^3)) (see Eq. 1.1, where $f_{p,i}$ is the fraction of the compound *i* in the particle phase) (Pankow, 1994a).

$$f_{p,i} = \frac{K_{p,i} PM}{1 + K_{p,i} PM} \tag{1.1}$$

The partitioning constant $K_{p,i}$ (m^3/µg) of the compound *i* (Eq. 1.2) is determined by the complex thermodynamics of the aerosol system where f_{om} is the fraction of *PM* that is organic

matter, $\overline{MW_{om}}$ (g/mol) is the average molecular weight of the organic matter, γ_i is the activity coefficient and $p_{L,i}^o$ (Torr) the liquid vapor pressure of the compound *i* (Pankow, 1994b).

$$K_{p,i} = \frac{f_{om} 760 RT}{\overline{MW_{om}} \gamma_i p_{L,i}^o 10^6} \quad (1.2)$$

The semi-volatile character of a large fraction of organic aerosol (OA) implies the exposition of SVOCs to OH-radicals in the gas phase. Further oxidation of the SVOCs by OH might substantially affect the oxidation capacity of the atmosphere and produce higher oxidized organic compounds which have a larger SOA formation potential than the initial VOC precursor gases (Donahue et al., 2012b). Moreover, particulate emissions (e.g. from vehicle emissions) which contain a large fraction of SVOCs in the condensed phase, as soon as diluted into the atmosphere, the SVOCs will partially evaporate into the gas phase where they are oxidized. Subsequently, the formed less volatile oxidation products will partition back into the particle phase, and therefore contribe to an increase in particle mass (Robinson et al., 2007). As this SOA formation potential of particulate emissions was included in a regional air quality model, a much more precise prediction of ambient aerosol concentrations was achieved (Robinson et al., 2007).

1.2.3 Condensed phase chemistry

Another important aspect of secondary organic aerosols in the atmosphere are heterogeneous (on the surface of a particle) or multiphase (in the liquid condensed phase) chemical reactions (Ravishankara, 1997), which can substantially increase SOA mass. Through oligomerization reactions, even volatile reactive compounds, such as isoprene and glyoxal, were observed to participate in the formation of SOA (Claeys et al., 2004; Carlton et al., 2009; Lim et al., 2010), possibly catalyzed by both inorganic and organic acids (Jang et al., 2002; Kalberer et al., 2004). Condensed phase reactions between inorganic (ammonium, nitrate and sulfate) and organic aerosol constituents, lead to the formation of low volatile irreversible products like imines and imidazoles (Shapiro et al., 2009; Kampf et al., 2012), organosulfates from the isoprene derived epoxydiol IEPOX (Surratt et al., 2010), as well as monoterpene derived organosulfates and nitrooxy organosulfates (Surratt et al., 2008). These observations indicate the necessity to account for the chemical diversity of aerosols in order to predict SOA mass and properties more reliably.

1.3 Cloud condensation nuclei

Whether a particle is able to nucleate a cloud droplet depends primarily on the size of the particle (Dusek et al., 2006). According to the Köhler theory, larger particles are activated into cloud droplets at lower water vapor supersaturations (see Figure 1.5, Andreae and Rosenfeld, 2008). A key variable of the impact of aerosols on cloud radiative properties is the particle number concentration. Therefore, it is crucial to understand which source processes lead to an enhancement or decrease in the number of cloud active particles in the atmosphere (Andreae and Rosenfeld, 2008).

The upper limit of atmospherically relevant supersaturation is ~1%, as this is the maximum value at the cloud base. Particles that are smaller than ~50 nm are generally not activated under these conditions (Dusek et al., 2006). However, CCN measurements only represent the number of potential CCN particles. Under realistic conditions, where physicochemical kinetics come into play, the actual number of activated particles might be different from the measurements. The competition for a limited amount of water vapor might become affected by the chemical composition, thus enhancing or decreasing the activation of particles due to different solubility/hygroscopicity of the involved compounds, surface tension alteration by organic compounds or by the uptake of soluble gases (Laaksonen et al., 1998; Kreidenweis et al., 2006; Nenes et al., 2002; McFiggans et al., 2006).

In order to describe the dependency between CCN activity and the dry diameter of a particle, Petters and Kreidenweis (2007) have introduced the hygroscopicity parameter κ. Considering atmospheric relevant aerosols, κ values range between 0 for nonhygroscopic compounds (e.g. soot) and 1.4 for highly hygroscopic salts such as sodium chloride (Petters and Kreidenweis, 2007).

The hygroscopicity of laboratory generated secondary organic aerosol from the monoterpenes α- and ß-pinene appears to be slightly soluble with κ values around 0.1 (Prenni et al., 2007), whereas the secondary inorganic species $(NH_4)_2SO_4$ and NH_4NO_3 are very hygroscopic with κ ~0.61 and ~0.67, respectively (Clegg et al., 1998; Svenningsson et al., 2006). The biogenic organic acids pinonic acid, norpinic acid and pinic acid are ubiquitous in SOA over forested areas. Due to their polar functional groups, they are more soluble than the average laboratory generated SOA with κ values of 0.11, 0.18 and 0.25 (Raymond and Pandis, 2003).

As ambient aerosol particles throughout the northern hemisphere are usually an internal mixture of inorganic and organic compounds (Zhang et al., 2007), the average κ for continental and marine aerosol can be estimated to 0.3±0.1 and 0.6±0.1, respectively (Andreae and Rosenfeld, 2008). This implies that the low κ variability due to the chemical composition of

particles is a smaller uncertainty factor than the numerous chemical mechanisms that contribute to the growth of particles to atmospherically relevant sizes.

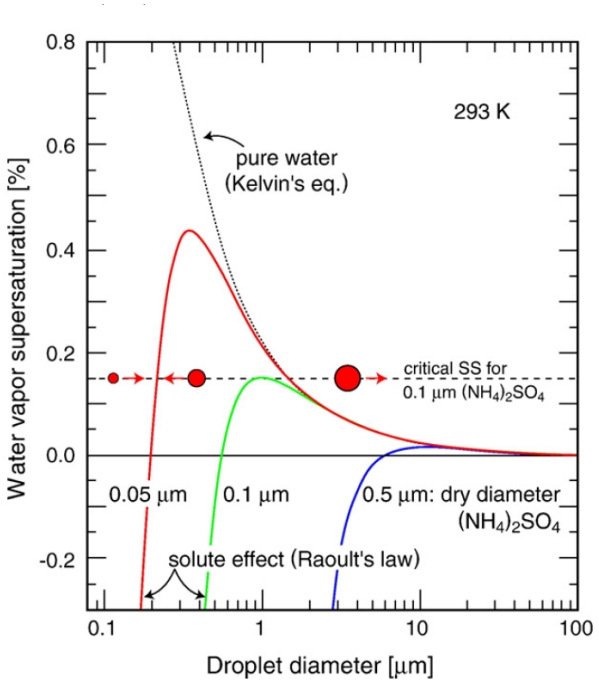

Figure 1.5 The droplet diameter as a function of the water vapor supersaturation (Köhler curves) for different dry diameters of ammonium sulfate particles at 293 K. The maximum of each Köhler curve refers to the critical supersaturation, above which particles can grow into cloud droplets. (Andreae and Rosenfeld, 2008)

The growth rates of particles need to be quantified, since the loss of particles due to coagulation decreases with increasing size of the particles. Therfeore, the chemical processes of particle growth need to be understood in order to predict the number concentration of CCN more reliably (Riipinen et al., 2012). Furthermore it has recently been calculated by using a cloud parcel model, that the co-condensation of semi-volatile compounds during the updraught of air masses facilitates the additional uptake of water and thereby enhances the cloud droplet number (as a function of updraught velocity) up to 30 % (Topping et al., 2013). This finding demonstrates that the whole picture of both gas and particle phase composition is indispensable for a reliable prediction of the number concentration of cloud droplets. Furthermore, the investigation to which extent anthropogenic gas and particle phase emissions alter the number of cloud active particles by the amount of condensable inorganic and organic species is cutting edge research in atmospheric science.

1.4 Mass spectrometry for the analysis of atmospheric aerosol

Mass spectrometry (MS) is the most commonly applied technique for the chemical analysis of atmospheric aerosol particles (Farmer and Jimenez, 2010). It provides high sensitivity and selectivity towards single chemical compounds. Some techniques allow to probe ambient aerosol in real-time (online), thus revealing the dynamics of diurnal cycles or transient events and avoiding artefacts which can be associated with aerosol sampling (Pratt and Prather, 2012).

Generally, online MS can be distinguished into bulk aerosol mass spectrometry and single particle mass spectrometry. Bulk aerosol MS means that the average chemical composition of thousands of particles in the submicron size range is analyzed. Single particle MS uses pulsed laser ionization techniques for the evaporation and ionization of particles in the size range between ~100 nm and ~3 µm (Pratt and Prather, 2012). As the focus of this study lies on the chemical analysis of the bulk aerosol composition, a brief introduction of the applied methods is provided in the following section:

1.4.1 Aerosol Mass Spectrometry

The Aerosol Mass Spectrometer (AMS) is the most established mass spectrometer for the chemical analysis of submicron aerosol particles in real time (Canagaratna et al., 2007). The inlet of the instrument consists of an aerodynamic lens, which is the interface between the ambient air and the instruments vacuum (Figure 1.6). The lens focuses submicron aerosol particles into a narrow beam of which the non-refractory compounds become evaporated in the ionization chamber by a heated tungsten vaporizer. The particle beam can be divided by a rotating chopper in order to obtain size resolved chemical composition. Refractory compounds that cannot be evaporated under high vacuum (~10^{-5} Pa) at ~600 °C (e.g. black carbon) are not accessible by the AMS. Ionization of the vaporized compounds is achieved by electron impact (EI) ionization and the formed positive ions are mass analyzed by a time of flight (ToF) mass spectrometer. In this study, the compact time of flight version of the AMS was utilized (Drewnick et al., 2005) that provides unit mass resolution spectra which translate into quantitative mass concentrations of sulfate, nitrate, ammonium, chloride and organics. The detection limit of the AMS for the individual chemical species depends on the average time over which one spectrum is acquired. Drewnick et al. (2009) report detection limits between 3 ng m^{-3} for nitrate and sulfate and 30 ng m^{-3} for ammonium and organics based on a 30 seconds average time interval.

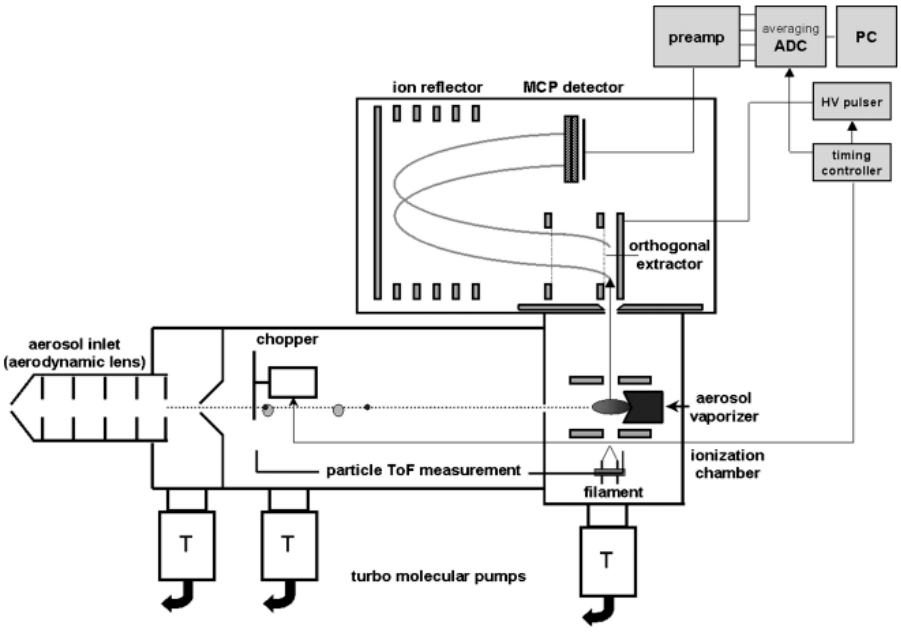

Figure 1.6 Scheme of the Compact Time of Flight Aerosol Mass Spectrometer (Drewnick et al., 2005)

Due to the EI process, organic compounds usually undergo severe fragmentation, resulting in mass spectra with the majority of ion signals below mass/charge (*m/z*) 120. Therefore, the quantitative and size resolved chemical analysis in real time can be seen as the strength of the AMS. The detailed analysis of certain organic compounds requires the application of soft ionization techniques that preserve the molecular structure upon ionization, as discussed in the following chapter.

1.4.2 Atmospheric pressure chemical ionization mass spectrometry

An ionization technique that preserves the molecular structure of organic compounds to a great extent is the atmospheric pressure chemical ionization (APCI). This technique goes back to the work of Carroll and co-workers (1975) who coupled liquid chromatography to an APCI source, hence enabling the analysis of chromatographically separated molecules by mass spectrometry. Whether the ionization of sprayed liquid droplets after LC separation or the ionization of ambient aerosol particles is desired, the fundamental principles of both applications of the APCI are identical.

The aerosol particles are heated in a ceramic tube in order to evaporate the analytes into the gas phase, which is a prerequisite for the ionization process. The primary reagent ions are formed by corona discharge between the tip of a needle and the inlet capillary of the MS. The potential difference usually ranges between 1.5 and 5 kV and a discharge current between 2 and 10 µA.

The primary reagent ions that react with the analytes are H_3O^+ ions and O_2^--radicals. Analyte molecules (M) that have higher gas phase basicity than H_3O^+ are ionized in the proton transfer reaction

$$M + H_3O^+ \rightarrow [M+H]^+ + H_2O$$

and those molecules having a higher gas phase acidity are ionized in the proton abstraction reaction with O_2^--radicals

$$M + O_2^{-\cdot} \cdot (H_2O)_n \rightarrow [M-H]^- + HO_2\cdot + n\ H_2O.$$

Due to the high molecular density at atmospheric pressure, two favorable features of the APCI are achieved: (1) a large fraction of the gaseous molecules that are introduced into the ionization region are ionized due to sufficient collisions with the reagent ions and (2) the formed ions (possibly in an excited and unstable state due to the exothermal proton abstraction reaction) rapidly attain thermal equilibrium, typically after a few collisions with the neutral carrier gas, also referred to as “collisional stabilization” (Mitchum and Korfmacher, 1983).

Depending on the chosen polarity of the ion source, the positive or negative ions are transferred into the vacuum system of the mass spectrometer. In this work, the APCI source was applied in conjunction with a quadrupole ion trap (QIT) mass analyzer. The QIT consists of two hyperbolic electrodes (end-cap electrodes) which are arranged opposite of each other and a ring electrode in between (Figure 1.7 A).

The ions which are entering the ion trap through an aperture in the apex of one end-cap electrode are exposed to an electric field inside the ion trap. The end-cap electrodes are grounded and the applied electrical potential at the ring electrode ϕ_0 consists of the direct current (DC) voltage U and the radio frequency (RF) voltage $Vcos\Omega t$, where V is the amplitude and Ω equals $2\pi f$ with f being the fixed frequency of RF (~1.1 MHz) (Eq. 1.3).

$$\phi_0 = U + Vcos\Omega t \qquad (1.3)$$

The RF field of the ring electrode induces oscillation of ions (Figure 1.7 B). Whether the trajectory of an ion along the radial (r) and axial (z) dimension is stable or not, is described by the variables a and q which depend on the applied RF (V) and DC (U) components (where z^* is the number of the charge e).

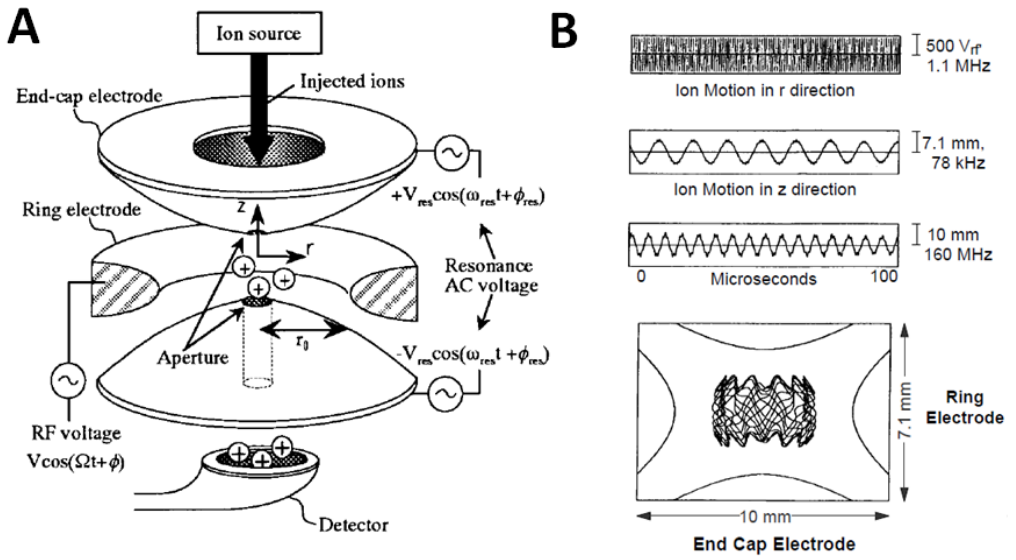

Figure 1.7 (A) Scheme of the quadrupole ion trap (Yoshinari, 2000) (B) Ion trajectory simulation in a quadrupole ion trap (Cooks et al., 1991)

$$a_z = -2a_r = \frac{-16z^*eU}{m(r_0^2 + 2z_0^2)\Omega^2} \tag{1.4}$$

$$q_z = -2q_r = \frac{8z^*eV}{m(r_0^2 + 2z_0^2)\Omega^2} \tag{1.5}$$

The solution of Eq. 1.4 and 1.5 can be illustrated by the Mathieu stability diagram, where the shaded area represents stable ion trajectories along both (*r* and *z*) dimensions. For the most commercially available ion traps no DC component is applied (*U*=0), hence a_z equals zero and the stability is determined by q_z only. As it can be seen in Figure 1.8, the operating line for the mass selective instability is confined by the *z* stability at q_z=0.908. Above this value, ions are becoming unstable in the *z* direction and are therefore ejected from the ion trap to the detector, which is usually a conversion dynode and an electron multiplier. As it can be seen from Eq. 1.5, q_z increases with larger *V* and smaller *m*. Therefore, in the operation mode of the *mass selective instability*, one mass scan proceeds via the destabilization from small to large *m/z* ions through the continuous increase of the RF amplitude *V*.

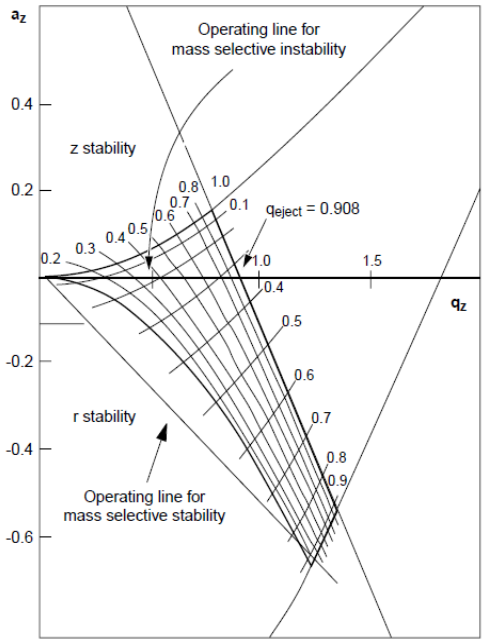

Figure 1.8 Mathieu stability diagram of the quadrupole ion trap. The shaded area illustrates where the Mathieu parameters a_z and q_z describe stabilized ions in the *r*- and *z*-direction simultaneously (Wong and Cooks, 1997).

In order to improve the mass resolution, the ion trap is filled with inert gas (usually ~1 mTorr helium) that dampens the kinetic energy of the ions. Furthermore, the helium is also needed for MS/MS studies (also referred to as "tandem-in-time" or MS^n) that enable the observation of fragments of single precursor ions. For this kind of analysis, all ions of a smaller *m/z* than the target *m/z* are removed from the ion trap by the *mass selective instability* mode. Ions with *m/z* larger than the target *m/z* are ejected by applying additional RF voltage on the end caps. The frequency is adjusted to come into resonance with the *m/z* ratios that need to be ejected (*resonant ion ejection*). As one *m/z* ratio is now isolated, it is stored at q_z=0.25 and additional energy is transferred to the target *m/z* (*resonance excitation*). The kinetically accelerated ions collide with the helium atoms inside the ion trap and form fragments that can be used for the structural elucidation of the isolated *m/z* ion. This process is called *collisional induced dissociation* (CID) and was applied within this work for the *in-situ* structural elucidation of compounds in ambient aerosol.

1.4.3 Orbitrap mass spectrometry

In chapter 4 of this work, additionally to the online analysis by AMS and APCI-MS, the ambient aerosol was sampled on filters and subsequently analyzed in the laboratory by liquid chromatography (LC) coupled to electrospray ionization (ESI)-Orbitrap mass spectrometry. As this mass spectrometric technique offers the possibility to measure ions with a mass resolution up to *R*=150,000, it is also referred to as high resolution mass spectrometry (HRMS) (Nizkorodov et al., 2011) or ultrahigh resolution mass spectrometry (UHRMS) (Lin et al., 2012; Kourtchev et al., 2013). Combined with the separation of complex molecular mixtures by liquid chromatography, this technique provides unambiguous evidence for the presence of certain compounds. Furthermore, the high mass resolution and accuracy (<2 ppm) of the Orbitrap enables the determination of the elemental composition by exact mass measurements (Figure 1.9 (b)).

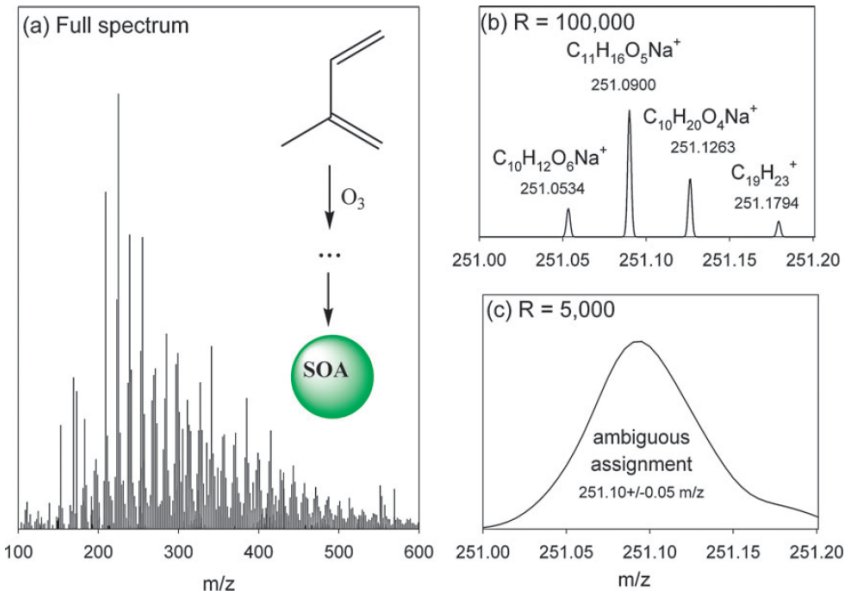

Figure 1.9 (a) positive ion mode ESI-MS stick spectrum of isoprene/ozone SOA, (b) HR-MS of an Orbitrap instrument (*R*=100,000) allows for elemental composition assignment whereas (c) isobar interfering molecules cannot be resolved at *R*=5000 (Nizkorodov et al., 2011).

The Orbitrap technique is a new type of mass analyzer that was commercialized within the last decade (Makarov, 2000; Hu et al., 2005). The working principle is the trapping of ions around an axial central electrode in an electrostatic field. The ions are injected into the Orbitrap perpendicular to the *z*-axis by the C-Trap (Figure 1.10). The trapped ions undergo rotation around the axial central electrode which is shaped in form of a spindle. Due to this shape, the ions start to harmonically oscillate around the spindle electrode along its length (*z*-axis) (Perry et al., 2008). The axial harmonic oscillation ω depends on the *m/z* of the ions according to Eq. 1.6, where *k* is the force constant of the electrical potential (axial restoring force). Since the harmonic

oscillation along the *z*-axis is independent from the initial kinetic energy of the ions, spectra of high mass resolution and accuracy can be recorded (Makarov, 2000).

$$\omega = \sqrt{\frac{z}{mk}} \tag{1.6}$$

A coaxial outer electrode, that consists of two axial halves, measures the ion image current of the frequency of the harmonic oscillation of ions orbiting in the space between the inner and outer electrodes (Figure 1.10). Hence, all ions are measured simultaneously and the amplified ion current signal is deconvolved by fast Fourier-transformation (FT) into high resolution mass spectra (Perry et al., 2008).

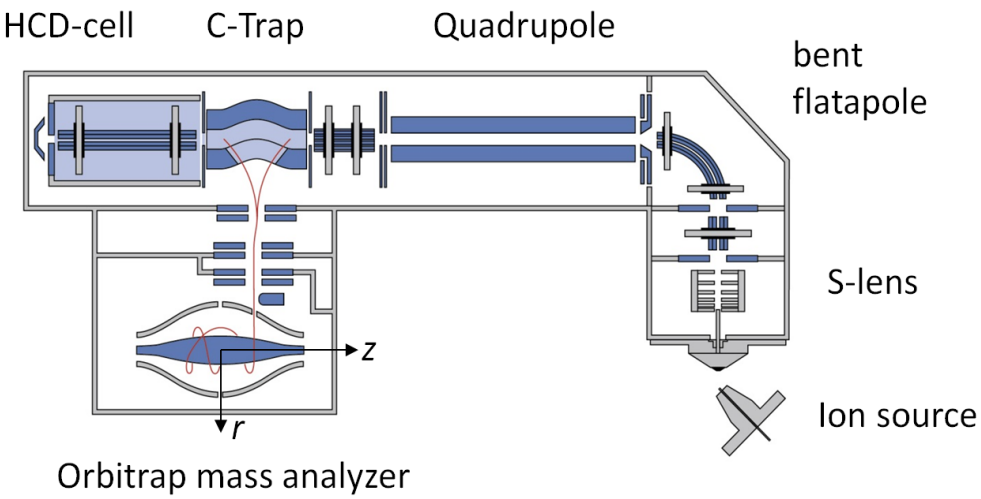

Figure 1.10 Schematic of the Q-Exactive Orbitrap-MS, Figure adapted from ThermoFisher Scientific (2013)

1.5 Thesis objectives and outline

Ambient aerosols are a highly complex chemical mixture of thousands of different compounds with different chemical composition and physical properties. Especially the atmospheric oxidation of biogenic emissions greatly contributes to the mass and to the chemical diversity of aerosols, hence making the secondary organic fraction an important contributor to the aerosol related uncertainties in global climate models.

The aim of this work was to establish a soft ionization mass spectrometer for field measurements of SOA at biogenically dominated locations. The application of the instrument of choice (an atmospheric pressure chemical ionization mass spectrometer (APCI-MS)) in field studies, where low SOA concentration levels can be encountered, required the combination of the APCI-MS with an online aerosol concentration unit, that needed to be built based on the work of Geller et al. (2005).

The main idea of the online field application was to achieve highly time resolved chemical analysis of the organic aerosol fraction, which possibly allows for the observation of organic aerosol formation, gas-to-particle partitioning of specific compounds, bulk aerosol aging and condensed phase chemistry in ambient air. Preferentially, the APCI-MS was applied within field studies, as simultaneous measurements of other aerosol instrumentation allowed to obtain a comprehensive characterization of the aerosol and therefore achieving new insights. Furthermore, laboratory terpene ozonolysis studies should be carried out in order to study how different biogenic emissions and different oxidative environments in the field affect the chemical composition of SOA.

The specific field studies, where the APCI-MS in conjunction with the aerosol concentration unit was applied, are the

1. HUMPPA-COPEC campaign at Hyytiälä, Finland in summer 2010, the
2. BEACHON-RoMBAS campaign in Colorado, USA, in summer 2011 and the
3. INUIT-TO campaign at the Taunus Observatory, Germany in August 2012.

During the HUMPPA-COPEC 2010 campaign, the initial aim was the field application of the APCI-MS, operating in real-time at ambient concentration levels. New insights on the ambient aerosols chemical diversity were obtained through the comparison between the field observations and chamber ozonolysis experiments of the most abundant biogenic precursors. Furthermore, the measurements of the ambient gas-to-particle partitioning of specific known organic acids was compared to the calculated equilibrium partitioning behavior of these

compounds. The results of the associated field and laboratory measurements are discussed in detail in chapter 2 and 3 of this work, which are the reprints of two first author publications.

An additional aim of this work was to compare the APCI-MS with a similar soft ionization MS technique, namely the MOVI-HRToF-CIMS (Yatavelli et al., 2012), within the BEACHON-RoMBAS campaign. Due to experimental difficulties of both instruments during the campaign, simultaneous measurements were not achieved. However, the application of a semi-continuous pre-concentration unit (MOVI) in conjunction with the APCI-MS operated successfully during the campaign and resulted in a co-author publication (Brüggemann et al., 2014).

Finally, the INUIT-TO 2012 campaign was conducted at a rural mountaintop field site which is surrounded by a mixed forest environment. A different setup of the aerosol concentrator was applied, in order to improve the detection limit of the system. Co-located filter sampling was carried out for the subsequent analysis by LC-UHRMS analysis in the laboratory, providing information of the elemental composition of single organic species. Together with the online APCI-MS, AMS, ion-chromatography of particulate sulfate, and CCN counter measurements, a unique dataset was recorded, that allowed to resolve the chemical complexity of the ambient aerosol in detail. The discussion of the outcome of this field campaign is presented in chapter 4 of this work, which is a manuscript in prepartation.

2 Application of online APCI-MS in a boreal forest field study

This chapter is a reprint of the article:

A. L. Vogel, M. Äijälä, M. Brüggemann, M. Ehn, H. Junninen, T. Petäjä, D. R. Worsnop, M. Kulmala, J. Williams, and T. Hoffmann

Online atmospheric pressure chemical ionization ion trap mass spectrometry (APCI-IT-MS^n) for measuring organic acids in concentrated bulk aerosol – a laboratory and field study

Atmospheric Measurement Techniques, *6*, 431-443, doi:10.5194/amt-6-431-2013, **2013**.

Abstract. The field application of an aerosol concentrator in conjunction with an atmospheric pressure chemical ionization ion trap mass spectrometer (APCI-IT-MS) at the boreal forest station SMEAR II at Hyytiälä, Finland, is demonstrated in this study. APCI is a soft ionization technique allowing online measurements of organic acids in the gas and particle phase. The detection limit for the acid species in the particle phase was improved by a factor of 7.5 to 11 (e.g. ~40 ng/m³ for pinonic acid) by using the miniature Versatile Aerosol Concentration Enrichment System (mVACES) upstream of the mass spectrometer. The APCI-IT-MS was calibrated in the negative ion mode with two biogenic organic acid standards - pinic acid and pinonic acid. Pinic acid was used as a surrogate for the quantification of the total amount of organic acids in the ambient aerosol based on the total signal intensities in the negative ion mode. The results were compared with the total organic signal of a C-ToF-AMS during the HUMPPA-COPEC 2010 field campaign. The campaign average contribution of organic acids measured by APCI-IT-MS to the total sub-micron organic aerosol mass was estimated to be about 60%, based on the response of pinic acid. Very good correlation between APCI-IT-MS and C-ToF-AMS (Pearson´s R = 0.94) demonstrates soft ionization mass spectrometry as a complimentary technique to AMS with electron impact ionization. MS^2 studies of specific *m/z* ratios recorded during the HUMPPA-COPEC 2010 field campaign were compared to MS^2 studies of selected monoterpene oxidation products formed in simulation chamber experiments. The comparison of the resulting fragments shows that oxidation products of the main VOCs emitted at Hyytiälä (α-pinene and Δ^3-carene) cannot account for all of the measured fragments. Possible explanations for those unaccounted fragments are the presence of unidentified or underestimated biogenic SOA precursors, or that different products are formed by a different oxidant mixture of the ambient air compared to the chamber ozonolysis.

2.1 Introduction

It is well known that atmospheric aerosols play an important role in global climate and human health (IPCC, 2007; Pope, III et al., 2009). Hence, a large scientific community is focussing their research on the physical properties and chemical composition of submicron aerosol particles to understand radiative forcing and air quality (Kulmala et al., 2011). Organic Aerosol (OA) represents the major fraction of non-refractory submicron particle mass (between 18 and 70%) and in tropical forest regions OA can even account for 90% of total fine aerosol mass (Zhang et al., 2007; Kanakidou et al., 2005). OA makes up the most abundant but least characterized fraction of atmospheric aerosol particles. This is because OA is a highly complex mixture consisting of thousands of different chemical species at very low concentrations. Goldstein and Galbally (2007) estimate a number of 10^4-10^5 measured organic atmospheric

species which still might be only a fraction of the number actually present. However, a major fraction of OA is believed to consist of organic acids (or multifunctional compounds including organic acid groups) since atmospheric oxidation not only favours the incorporation of oxygen over the atmospheric lifetimes of atmospheric organics, but the low vapour pressure of organic acids also drives these compounds into the particle phase (Kroll et al., 2011).

Common offline techniques for measuring single organic compounds from filter samples are liquid- or gas-chromatography coupled to mass spectrometry (LC/MS, GC/MS); off-line techniques for measuring bulk properties such as functional group contributions are nuclear magnetic resonance spectroscopy (NMR) or direct filter analysis using Fourier transformation infrared spectroscopy (FTIR) (Hallquist et al., 2009; Hoffmann et al., 2011). Unfortunately, offline techniques offer only relatively poor time resolution (several hours to weeks) and can be seriously biased by positive (gas phase condensation, reactions on the filter surface) and/or negative (evaporation during sampling, degradation on the filter surface, losses or degradation during sample preparation and analysis) sampling artefacts. Turpin et al. (1994) showed that gas phase adsorption is the dominant artefact in sampling of organic aerosol. The question therefore arises whether filter samples faithfully display the real atmospheric organic aerosol composition (Prather et al., 2008). Warnke et al. (2006) mentioned that more volatile organic compounds (pinonic acid) produce higher artefacts (up to 50%) than the less volatile organics. As a consequence, further development and field application of online techniques for directly measuring the chemical composition of the gas and particle phase is required in order to improve our understanding of formation, composition and fate of atmospheric aerosols.

The Aerodyne aerosol mass spectrometer (AMS) enables online chemical composition measurements of aerosol particles by flash vaporization of non-refractory components and subsequent ionization using electron impact ionization (EI) (Jayne et al., 2000). Due to the relatively high energy of the ionizing electrons (70 eV) most organic molecules are fragmented. Selected fragments can then be used for the determination of the oxygen-to-carbon ratio, and indirectly, certain individual sources or the volatility of the organic aerosol components. Using positive matrix factorization (PMF) analysis, the AMS can be used to classify organic aerosol into hydrocarbon-like OA (HOA), biomass burning OA (BBOA), semi-volatile oxygenated OA (SV-OOA) and low volatility oxygenated OA (LV-OOA) (Zhang et al., 2011; Jimenez et al., 2003; Jimenez et al., 2009). Based on such an approach also complex processes, such as photochemical ageing of organic aerosols, can be investigated (Ng et al., 2010; Ng et al., 2011). However, identification and quantification of specific molecular tracer compounds is not easily accomplished with EI-AMS (Canagaratna et al., 2007). This goal can only be achieved through low energy ionization processes, resulting in no or minor fragmentation of the molecular tracers (soft-ionization techniques). In the extreme case, each ionized organic molecule results in a

single signal representative for the molecular ion of the compound of interest. One possibility is the use of corona discharge (CD) at atmospheric pressure; a technique that is well established when liquid chromatography is hyphenated with mass spectrometry (atmospheric pressure chemical ionization (APCI)). The technique represents a soft ionization method, where fragmentation of the analyte molecules plays a minor role and mostly molecular ions are observed. The application of this technique measuring organic compounds in the particle phase was reported as early as 1998 by Hoffmann et al. using CD for the generation of O_2^--ions at atmospheric pressure (Hoffmann et al., 1998). Prior to the ionization process, the organic compounds are thermally evaporated from the particle phase by a vaporizer within the ion source. Gas phase compounds are removed upstream of the ion source by an activated charcoal denuder. For higher organic mass loadings, e.g. for measurements in simulation chamber experiments, the atmospheric pressure chemical ionization ion trap mass spectrometer (APCI-IT-MS) is well suited for online measurements of organic acids in the negative ionization mode, providing new insights into product structures (Warscheid and Hoffmann, 2001, 2002) and multiphase chemical mechanism of secondary organic aerosol ageing (Mueller et al., 2012). Measuring in the positive ion mode, hydroperoxides and hydroperoxy acids, formed during ozonolysis of biogenic volatile organic compounds (BVOCs), can be identified by a characteristic loss of 34 Da during MS^2 experiments (Reinnig et al., 2009). However, for measuring secondary biogenic organic acids at ambient concentrations below 100 ng/m³, this technique is not sensitive enough.

Other approaches towards soft-ionization AMS are described by Dreyfus and Johnston (2008), Dreyfus et al. (2009) and Geddes et al. (2010). An overview article on soft ionization mass spectrometry of atmospheric organic aerosols was recently published by Zahardis et al. (2011). Hearn and Smith (2006) describe an aerosol CIMS as an online measurement technique, using a radioactive polonium source (^{210}Po) to generate SF_6^- as primary ions. The reported detection limit of 100-200 ng/m³ is sufficiently low for sulfate measurements in ambient aerosols; however, it is not sensitive enough for most organic species in the particle phase. By using a cold trap U-tube they were able to measure ambient aerosol organic compounds after sampling for 6 h. Another promising semi-online method for measuring organic acids in the gas and particle phase has recently been reported by Yatavelli and Thornton (2010) using a Micro Orifice Volatilization Impactor (MOVI) in front of a CI-MS. This technique has the advantage of sampling particles by inertial impaction at a relativly high flow rate (10 SLPM) within 15% of the ambient pressure. During sampling periods gas phase concentration can be measured online. An instrumental approach towards measuring nanoparticle composition is the TDCIMS (Thermal Desorption Chemical Ionization Mass Spectrometer, Smith and Rathbone, 2008). The authors use a unipolar charger and a nano-DMA to collect 8 – 40 nm particles on an

electrostatic precipitator. Subsequent thermal desorption and chemical ionization allows measurements of mono- and dicarboxylic acids in nucleation mode particles. Further instrumentation which is based on collection, thermal desorption and ionization of the analytes are the aerosol collection module coupled to GC-MS (Hohaus et al., 2010), the thermal desorption particle beam MS (TD-PBMS, Tobias and Ziemann, 1999) and the thermal desorption PTR-MS (TD-PTR-ITMS, Thornberry et al., 2009). However, these semi-online techniques are all based on thermal desorption of surface-deposited analytes, which increases the hazard of decomposition during desorption. Furthermore, a constant collection efficiency is not guaranteed since particle bounce effects of glassy SOA particles might change with chemical composition, relative humidity and liquid water content of the aerosol particles (Virtanen et al., 2010; Saukko et al., 2012).

In this paper we describe for the first time the coupling of the miniature versatile aerosol concentration enrichment system (mVACES, Geller et al., 2005) with the soft ionization APCI-IT-MS, allowing online measurements of the composition of laboratory generated OA and ambient OA during the HUMPPA-COPEC2010 field campaign at Hyytiälä, Finland (Williams et al., 2011). The mVACES works by first supersaturating the incoming particles with respect to water vapor and then rapidly cooling the aerosols to force water condensation, followed by enrichment with a virtual impactor. Consequently, the aerosol particles are not enriched by sampling onto a surface but rather the enriched minor flow is measured directly by APCI-IT-MS. Geller et al. (2005) showed that the particle size distribution before and after enrichment and drying is not altered. Khlystov et al. (2005) investigated the VACES technology with focus on artefacts due to repartitioning from gaseous compounds into the particle-phase. They observed significant positive artefacts for semi-volatile nitrate, based on the enrichment factor of sulfate. Artefacts for organic material were less pronounced; however, the artefacts of semi-volatile organics were not investigated by Khlystov et al. (2005) and further fundamental studies are needed in order to clarify those issues. Field applications of the mVACES have been done in combination with online and offline techniques, resulting in a better signal-to-noise ratio of low flow rate instruments or shorter filter sampling time, respectively (Ning et al., 2006). Previously, the mVACES has been demonstrated to measure bulk aerosol composition in a remote region in conjunction with HR-ToF-AMS (Sun et al., 2009) or in an urban environment in conjunction with the soft ionization PIAMS (photoionization AMS, Dreyfus and Johnston, 2008).

2.2 Experimental

Online analysis of organic acids in the bulk aerosol was realized by using a Finnigan LCQ ion trap mass spectrometer (IT-MS) (Finnigan MAT, San Jose, USA). The instrument was equipped with a modified atmospheric pressure chemical ionization (APCI) ion source (Kuckelmann et al., 2000). It was operated in the negative mode to form $[M-H]^-$ ions. The APCI-IT-MS used has been described in detail by Hoffmann et al. (2002) for online measurements of gaseous and particulate organic compounds in chamber experiments. Briefly, O_2^- ions are formed at atmospheric pressure by a 3 kV corona discharge between a needle and the transfer capillary (Figure 2.1). Gaseous analytes, which have a higher gas-phase acidity than O_2^-, become ionized by proton transfer reactions. Remaining excess energy of the proton transfer reaction is transferred by collision to a third neutral molecule. The O_2^- reagent ion is selective towards organic acids, inorganic acids, nitrophenols and combination between those compound classes (e.g. organosulfates). Veres et al. (2008) described a similar CI-MS method using acetic acid as reagent ion. Due to a lower gas-phase acidity of O_2^- compared to acetic acid (Bartmess, 2011), most atmospherically relevant organic acids are detected by the O_2^--ionization method. Both techniques show limited response on organic acids which rapidly undergo thermal decomposition, e.g. oxalic acid or malonic acid.

To enhance signal intensities of the particle phase compounds, the APCI-IT-MS was equipped with a miniature versatile aerosol concentration enrichment system (mVACES) in front of the MS (Geller et al., 2005). A scheme of the instrumental setup is shown in Figure 2.1.

2.2.1 mVACES/APCI-IT-MS setup during the HUMPPA-COPEC 2010 field campaign

During July and August 2010 the HUMPPA-COPEC 2010 field campaign was carried out at the SMEAR II station at Hyytiälä, Finland (Hari and Kulmala, 2005). The aim of this campaign was to investigate summertime boreal forest chemistry, mainly focusing on the photochemistry of biogenic emissions. Periods influenced by biomass burning, anthropogenic emissions and sawmill emissions were contrasted to clean natural conditions (Williams et al., 2011).

The measurements described here took place at the main SMEAR II cottage. Ambient air was sampled from canopy level height through a stainless steel tube as the main inlet. The OD of the tube was app. 5 cm and the flow speed was set to 0.5 m/s using a fan at the end of the tube. The mVACES/APCI-IT-MS and the Aerodyne C-ToF-AMS were sampling from this tube using Pitot-tube-like sampling ports (Figure 2.1). The sampling port and the mVACES/APCI-IT-MS were connected by a 12.0 mm ID and 2.00 m long conductive PTFE tube (Type PTFE EX,

Bohlender GmbH, Grünsfeld, Germany). A 2.5 cm ID circular channel was shaped into a cellulose sponge inside the saturator. The sponge was kept moist using a peristaltic pump which continuously purged water onto the top of the sponge.

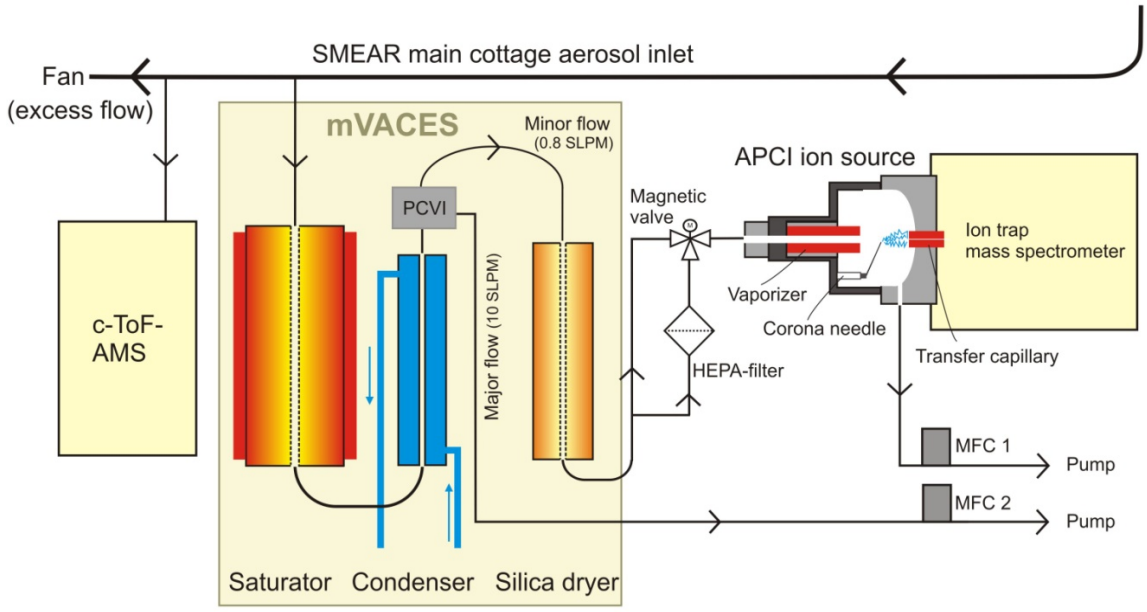

Figure 2.1 Scheme of the instrumental setup of mVACES/APCI-IT-MS and C-ToF-AMS during the HUMPPA-COPEC 2010 field campaign (dimensions are not true to scale).

The water reservoir was exchanged twice a day with ultrapure water to avoid memory effects by absorbed gas phase species. A heating tape (HBSI, Horst GmbH, Lorsch, Germany) with a temperature regulator (HT30, Horst GmbH, Lorsch, Germany) was adjusted to keep the temperature at the center of the saturator at 35 °C. The air at the end of the saturator had a relative humidity (RH) above 90 % and a temperature of approximately 30 °C (depending on the conditions of the sampled air). The temperature of the cooling liquid in the condenser (2.0 cm ID, 40 cm length) was kept at − 1°C using a cooling thermostat (Lauda ECO RE 415 S, Lauda Dr. R. Wobser GmbH & Co. KG, Lauda-Königshofen, Germany). A mixture of ethylene glycol and water (1:1, v/v) was used as the cooling liquid. Downstream of the condenser a virtual impactor was used to let the grown aerosol particles transit into the minor flow. The virtual impactor used was originally designed as a pumped counterflow virtual impactor (PCVI, Boulter et al., 2006) which separates gas phase and low inertia particles from high inertia particles. In this study the PCVI was operated without counterflow to maximize the transition of low inertia particles into the minor flow. The absolute pressure inside the virtual impactor depends on the input and output flow rates and ranged between 880 and 910 mbar. The major flow was set to 10 standard liters per minute (SLPM) and the minor flow to 0.8 SLPM using two distinct mass flow

controllers (MKS Instruments, Andover, USA) resulting in a theoretical enrichment factor of 12.5. A 1/4" stainless steel tube was used to connect the PCVI with a silica gel diffusion dryer (1 cm ID x 40 cm). Each 72 h the silica gel was exchanged with dry gel to ensure constant drying. To assess the gas phase composition, a particle filter (HEPA capsule, Pall Corporation, Port Washington, USA) was switched in line every 2.5 h for half an hour to remove the particle phase signal. A large orifice magnetic valve (VX3244-02F-5DZ1-B, SMC Corporation, Tokyo, Japan) was chosen to reduce particle losses inside the valve.

Data were recorded between mass to charge ratios (*m/z*) 50 to *m/z* 500. Each recorded spectrum is an average of 200 microscans, resulting in a measurement frequency of one spectrum per minute. At the beginning of the field measurements the instrument was automatically tuned on *m/z* 215 resulting in the settings listed in Table 2.1. The mass calibration of the instrument was carried out by using the recommended mass calibration solution of the manufacturer. The background of the instrument was measured at the beginning, during and at the end of the campaign by connecting zero air (Synthetic air, hydrocarbon free, Westfalen, Germany) to the inlet of the saturator. Data were recorded using XCalibur® 1.2 software, the data files were converted to plain text files and then transferred into a matrix with five minute time resolution using Matlab®, Mathworks Inc. software. Each recorded *m/z* ratio was rounded to the nominal mass. Gas phase measurements, which were recorded in 3 h time intervals, were interpolated linearly and subtracted from the total signal resulting in the particle phase signal.

Table 2.1 Instrument settings of Atmospheric Pressure Chemical Ionization Mass Spectrometer (APCI-IT-MS)

Vaporizer temperature	350 °C
Sheath gas flow	0 a.u.
Discharge current	3 µA
Discharge voltage	3 kV (±0.3 kV)
Capillary temperature	200 °C
Capillary voltage	−14 V
Tube lens offset	20 V
Multipole 1 offset	2.5 V
Lens voltage	16 V
Multipole 2 offset	5.5 V
Electron multiplier voltage	−1030 V

2.2.2 C-ToF-AMS setup during the HUMPPA-COPEC 2010 field campaign

During the measurement campaign the C-ToF AMS was operating alongside the APCI-IT-MS, and was sampling from the same main inlet. The AMS inlet port was situated approximately 2 meters downstream of the APCI-IT-MS inlet and the AMS was connected to the port using 6 mm copper tubing of 1 m length (Figure 2.1). For the purpose of intercomparison between the AMS and the APCI-IT-MS, the instruments can be considered co-located and having equivalent inlet losses.

The specifics of the C-ToF AMS have been described in detail by Drewnick et al. (2005), but in short the AMS measures aerosol particle mass and chemical composition. The AMS used in this study features an aerodynamic lens for concentrating the sampled aerosol particles in the size range of roughly 50 to 600 nm, into a narrow beam, a particle time-of-flight chamber for particle size distribution measurement, thermal vaporization of the sample at 600 °C using a porous tungsten vaporizer, 70 eV electron impact (EI) ionization of the produced vapor, and a compact time-of-flight mass spectrometer (C-ToF-MS). This particular instrument also features a shorter-than-usual particle time-of-flight chamber, which results in increased transmission of both particles and gas, and therefore also a larger air signal than in most AMS designs. The high air signal was reduced by adding 3.5 ml min^{-1} of He (AGA, 6.0 grade) to the time of flight chamber. The resulting high He signal at mass 4 Th was removed by a small RF-only quadrupole before the ion lenses and the extraction region of the ToF.

The AMS data was preprocessed using Squirrel (SeQUential Igor data RetRiEvaL) data analysis tool v.1.5. The mass concentration of aerosol particles was quantified and the measured mass was assigned into subgroups of different chemical composition; sulfates, organics, nitrates, ammonia and chlorides. For a thorough description of AMS data analysis see e.g. Allan et al. (2003) (2004). The measured data was corrected for collection efficiency (CE). A base CE value of 0.43 was selected based on a comparison with the sub-micron mass concentrations derived from the number size distribution measurements with the Differential Mobility Particle Sizer (DMPS) in the size range of 3 to 600 nm. The base CE was estimated for time periods when the aerosol acidity was neutral. For periods with non-neutralized sulfate, implicating elevated aerosol acidity, a higher value was used, based on a linear correction function similar to that of Quinn et al. (2006) and Middlebrook et al. (2012). CE anomalies caused by high mass fraction of nitrates were not observed, and the amount of nitrates remained consistently below 10 %.

The quantitativeness of the AMS results gives a good starting point for more detailed analysis. During the HUMPPA campaign, the ambient aerosol was dominated by organic chemical species with minimum concentrations near zero on a clean day and maximum of

23.1 µg/m^3 observed during a long-range transported forest fire smoke episode. On average organic species explained 69% of the submicron non-refractory mass, sulfates accounted for 20% of mass and ammonium compounds and nitrates for 7% and 4% respectively. The amount of chlorides was negligible. The dataset therefore provides a good basis especially for studying the composition of organic species using mVACES/APCI-IT-MS.

2.2.3 Laboratory setup

To test the coupling of the aerosol concentrator mVACES with APCI-IT-MS in the laboratory, secondary organic aerosol from α-pinene ozonolysis was generated in a 100 l continuous-flow reaction chamber. For this purpose gaseous (+)-α-pinene (Sigma-Aldrich, ≥99%), generated in a thermally controlled diffusion source (Thorenz et al., 2012) was mixed with ozone (1 ppm) in the reaction chamber to produce organic aerosol particles. Ozone was generated with an ozone generator (1008-RS, Dasibi Environmental Corp., Glendale, CA, USA) and directly introduced into the reaction chamber. The formed aerosol was measured online using APCI-IT-MS without mVACES. Gas phase species were removed using an activated charcoal denuder. When the reactant and aerosol concentration in the continuous-flow chamber were in steady-state, the online measurement without mVACES was started. After a few minutes the mVACES was switched in between the reaction chamber and the APCI-IT-MS, to measure the concentration enrichment factor and to investigate whether the mVACES leads to an alteration of the chemical composition of the particle phase.

For MS² experiments the same experimental setup was used to record online-MS² spectra from ozonolysis products from (+)-α-pinene (Sigma-Aldrich, ≥99%), (R)-(+)-limonene (Sigma-Aldrich, 97%) and (+)-Δ^3-carene (Fluka analytical, ≥98.5%). The collision induced dissociation (CID) of an isolated molecular ion inside the ion trap was achieved by using Helium (5.0, Westfalen AG) as collision gas. The relative collision energies were adjusted to measure a relative abundance of the molecular ion after fragmentation of 5-20%. This was achieved by setting CID energy to 26% for laboratory studies and to 30% in the field studies. Typically 30-70 of the recorded MS² spectra were averaged since the intensities during MS² measurements varied significantly.

2.2.4 Calibration of APCI-IT-MS

The APCI-IT-MS was calibrated for two different biogenic organic acids (pinic acid and pinonic acid) in the laboratory. Both acids are regarded as representative compounds formed from monoterpene oxidation in the boreal forest atmosphere. *Cis*-Pinonic acid (Sigma-Aldrich, 98% purity) was purchased as a commercially available standard, *cis*-Pinic acid is a self-synthesized standard (Moglioni et al., 2000). Zero air (hydrocarbon free) was purchased from Westfalen AG.

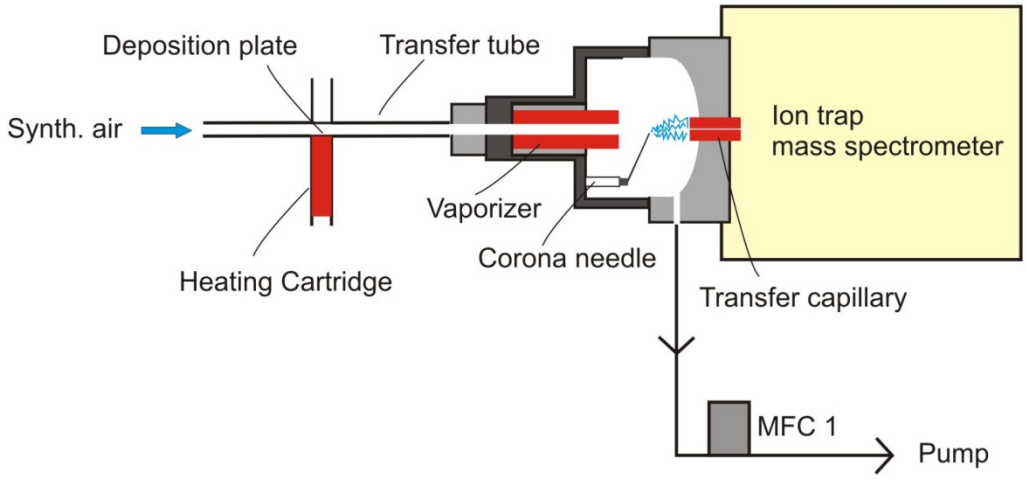

Figure 2.2 Setup for the calibration of the APCI-IT-MS.

For the calibration of the instrument, the acids were dissolved in methanol (Sigma-Aldrich, HPLC grade) and adjusted to concentrations ranging from 0.25 to 2.5 ng/µl. 10 µl of the individual solutions were deposited on a stainless steel surface. This deposition surface was installed directly in front of the ion source, a setup similar to the MOVI-CIMS setup described by Yatavelli and Thornton (2010). Figure 2.2 shows the experimental setup. The deposited compounds were evaporated by heating the deposition surface within 3 min. to approx. 120 °C. The zero air flow prior to the ion source was set to 1.0 SLPM using a mass flow controller. The transfer tube to the ion source was heated to 150 °C to avoid condensation of the evaporated acids. The resulting peak height was averaged for 5 and 10 min and related to the sampled volume within these intervals to determine the instruments response of online measurements to a certain concentration of the investigated acids (Figure 2.3). It has to be noted that the heated deposition plate was not operative during the field campaign and consequently the calibration

procedure was done after the field campaign in the laboratory. As a consequence the calibration procedure is based on the following assumptions:

(1) the vaporization of the analytes from the surface takes place in a quantitative manner without decomposition

(2) during online measurements vaporization of the analytes from particles is quantitative

(3) the instrumental performance during field measurements and laboratory calibration did not change significantly.

The recorded mass spectra during the calibration did not actually show any evidence of decomposition of the tested acids. Furthermore, the investigated *m/z* ratios did not show any significant blank signal such as the observed blank signal of palmitic acid described by Yatavelli and Thornton (2010).

2.3 Results and discussion

2.3.1 Calibration and detection limit for biogenic organic acids

Figure 2.3 (a) shows the results of 12 calibration runs at 4 different concentrations in a laboratory experiment. During heating cycles of the deposition plate, the analytes evaporate into a controlled flow of 1.0 SLPM carrier gas and produce a characteristic signal peak. The shape of the peak essentially depends on the heating rate and the volatility of the analyte. In order to use this transient signal for calibration of the online APCI-IT-MS measurements, the signals from the calibration experiments were averaged over two intervals: five and ten minutes. Equation (2.1) is used to determine the instruments response towards the absolute mass concentration. During the calibration procedure (Figure 2.2), the mass of the deposited organic acid on the deposition plate is m (µg), and the denominator expresses the volume (m^3) in which the analyte is evaporated into: the product of flow rate f (SLPM) and average time interval t (min) (red boxes: 5 min; black boxes: 10 min), resulting in the concentration c ($\mu g\, m^{-3}$). Based on the assumption that the average intensity I (counts) during the calibration procedure equals the same mass concentration during the online measurement, the linear interpolation (slope s and y-intercept b) was applied on the ambient online intensities to determine the ambient mass concentration.

$$c = \frac{m}{1 * 10^{-3} * f * t} = \left(\frac{I - b}{s}\right) \tag{2.1}$$

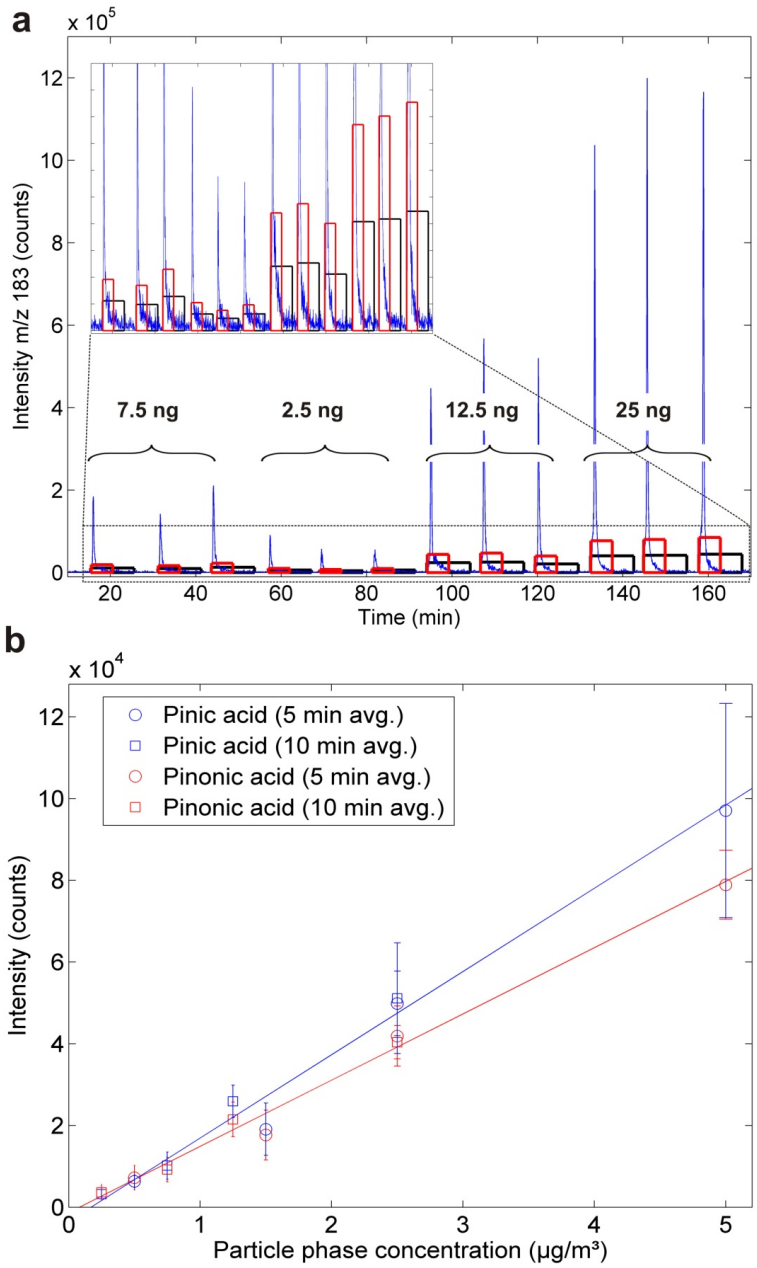

Figure 2.3 (a) Mass trace of pinonic acid (m/z 183) during calibration (blue), mean intensity for 5 minute (red) and 10 minute intervals (black). (b) Linear fit of calibration for pinonic acid (*m/z* 183, red) and pinic acid (*m/z* 185, blue).

The calibration range was adjusted to match the measured intensity range of gas and particle phase measurements of *m/z* 183 and *m/z* 185 during the HUMPPA-COPEC2010 field campaign, and showed a linear response between deposited organic acid mass and resulting average signal height. Based on the assumptions described above the detection limit (LOD) for pinonic acid in

the particle phase was determined to be about 300 ng m^{-3}, and for pinic acid about 410 ng m^{-3}. This LOD calculation was based on the blank signal intensity assuming three times standard deviation of the noise signal. The detection limit of pinonic acid and pinic acid in the gas phase at 25 °C would be 41 pptV and 54 pptV, respectively. These detection limits are in the same order of magnitude as the reported sensitivities for oleic acid in the particle phase (LOD: 200 ng m^{-3}) by Aerosol CIMS (Hearn and Smith, 2006). However, ambient concentrations of these compounds are expected to be lower than the calculated detection limits. Maximum reported particle phase concentration of pinonic acid and the isobaric overlapping caronic acid in Hyytiälä, Finland are 74 ng m^{-3} and 23 ng m^{-3}, respectively (Warnke et al., 2006). Therefore, the application of the aerosol concentrator mVACES is necessary to detect these species in the ambient air.

2.3.2 mVACES concentration efficiency

To test the concentration enrichment factor of the mVACES in the laboratory, the setup as described in chapter 2.2.3 was used. The measured total ion current (TIC) of the products formed from α-pinene ozonolysis was used to calculate the enrichment factor. Figure 2.4 shows the online mass traces of the TIC (*m/z* 50-500), a lower molecular weight range (monomeric ozonolysis products, *m/z* 160-240, hereafter monomers) and a higher molecular weight range (dimeric ozonolysis products, *m/z* 320-400, hereafter dimers). The green bars in Figure 2.4 mark the time interval in which the TIC signal was averaged to determine the enrichment factor in the laboratory. The overall calculated concentration enrichment factor determined in the laboratory as described above was 11.0 ± 2.4 (2* rel. SD).

It should be noted in Figure 2.4 that the signal intensities of the three depicted mass ranges were not constant during the individual measurement periods (i.e. with and without mVACES). This is due to the fact that the product concentration in the continuous-flow chamber changed due to differing flow rates / reaction times when working with or without mVACES. The resulting change of particle concentration (total organic aerosol mass) can affect the gas-to-particle partitioning, especially for the semi- or intermediately volatile compounds (i.e. monomers - resulting in an increased fraction of the monomers in the particle phase with increasing organic particle mass concentration). To avoid potential influences of such concentration changes on the determination of the enrichment factor, the time intervals chosen for the estimation are ‘end of the mVACES on’ vs. ‘beginning of the mVACES off’ (Figure 2.4).

Another aspect that should be considered when a VACES system is used are the losses of semi-volatile and at least partly water soluble compounds during the mVACES preconcentration by absorption within the saturator. An estimation of this amount based on the Gormley-Kennedy

equation (diffusion coefficient D=0.058 cm² s^{-1} at a flow rate of 11.0 SLPM) results in a notable loss of 30% of the gas phase fraction, assuming that the wet sponge acts as a perfect sink for gaseous organic acids. Subsequent re-equilibration between gas- and particle-phase (evaporation of SVOC from the particle phase) might result in negative artefacts. An indication for negative artefacts of semi-volatile organics can be seen in Figure 2.4 at minute 10: before switching the concentrator on, the signal of the monomers is higher than that of the dimers, and vice versa after switching on. Further concerns about possible changes in gas/aerosol partitioning might be raised by multiple temperature changes during the passage through the concentrator. Contrary to negative artefacts, Khlystov et al. (2005) showed that the concentration of water soluble semi-volatile material can be increased at small sizes after passage through the concentrator. Their maximum observed amount of positive nitrate artefacts (relative to sulphate) on a polluted day reached a factor of 2.6; organic material showed significantly less positive artefacts (factor 1.2). These positive artefacts are most probably attenuated due to losses of gas-phase organics in the saturator. Further investigation on artefact formation of the semi-volatile aerosol fraction in a water based concentrator is needed for a more precise determination of the concentration factor of semi-volatile organic compounds.

During the HUMPPA-COPEC 2010 field campaign, the concentration enrichment factor was determined by measuring the sulphate signal at *m/z* 97 with and without mVACES since (1) sulphate has a lower vapour pressure than most organic compounds and thus the influence of changes in gas/aerosol partitioning due to the mVACES is low, and (2) sulphate was sufficiently high to be measured well above background without mVACES. The concentration enrichment factor during the field measurement was 7.5 ± 2.5 (2*RSD). Sulphate concentration measured by AMS during this time was around 2 µg m^{-3}. Furthermore, the total concentration of organic acids in the particle phase during the HUMPPA-COPEC field campaign was approximated by using the average response of pinic acid and applying this response onto the sum of the signals between *m/z* 150 – *m/z* 500. By doing so, pinic acid is used as a surrogate for the quantification of organic acids based on the total signal intensities in the negative ion mode.

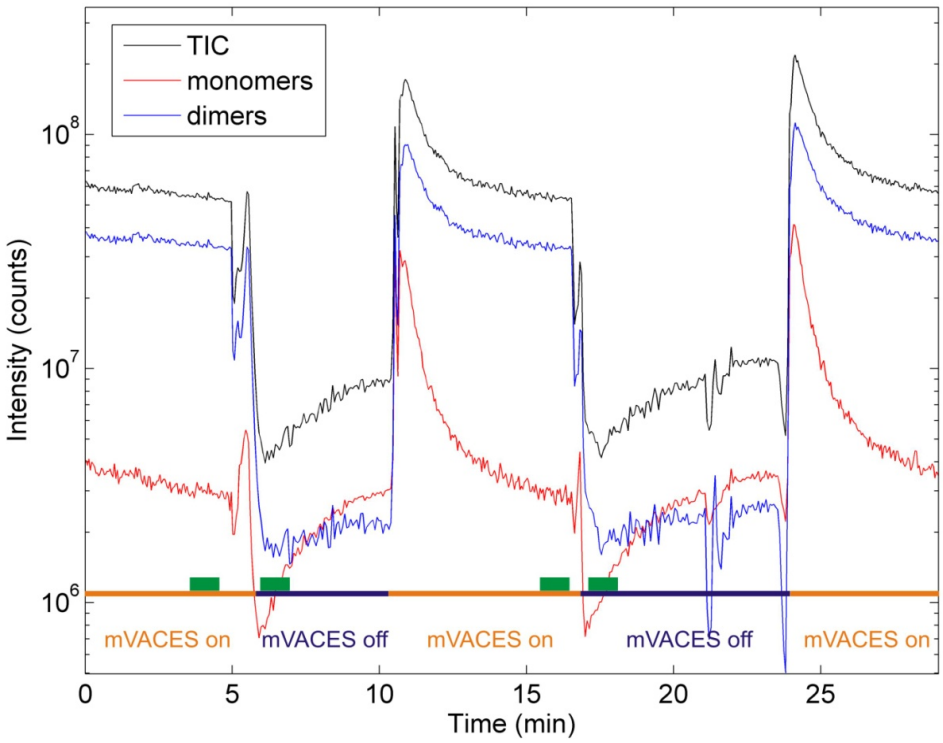

Figure 2.4 Performance of mVACES aerosol enrichment during laboratory testing. TIC: total ion current, monomers: sum of signals *m/z* 160- 240, dimers: sum of signals *m/z* 320- 400.

2.3.3 Instrument comparison

Figure 2.5 correlates the two online mass spectrometric techniques mVACES/APCI-IT-MS and AMS during the HUMPPA-COPEC 2010 field campaign. Data points are five minute averages between 16 July 2010 and 12 August 2010. Data points for time intervals in which the AMS and/or the APCI-IT-MS did not run due to power cuts or instrumental maintenance were taken out. However, 49% of the total campaign duration is still covered with simultaneous data from both instruments. The AMS data are corrected using a collection efficiency factor of 0.43. As mentioned above, the APCI-IT-MS data are the sum of the particle phase signal of *m/z* 150 to *m/z* 500, quantified by using the average response of pinic acid, regarding this acid as representative for all compounds ionized in the APCI-IT-MS negative mode. With certainty this is an assumption which does not take into account that higher weight molecular compounds might have a different response factor compared to pinic acid. Unfortunately, to our knowledge there are no literature data available yet on quantitative determination of e.g. sesquiterpene derived acids.

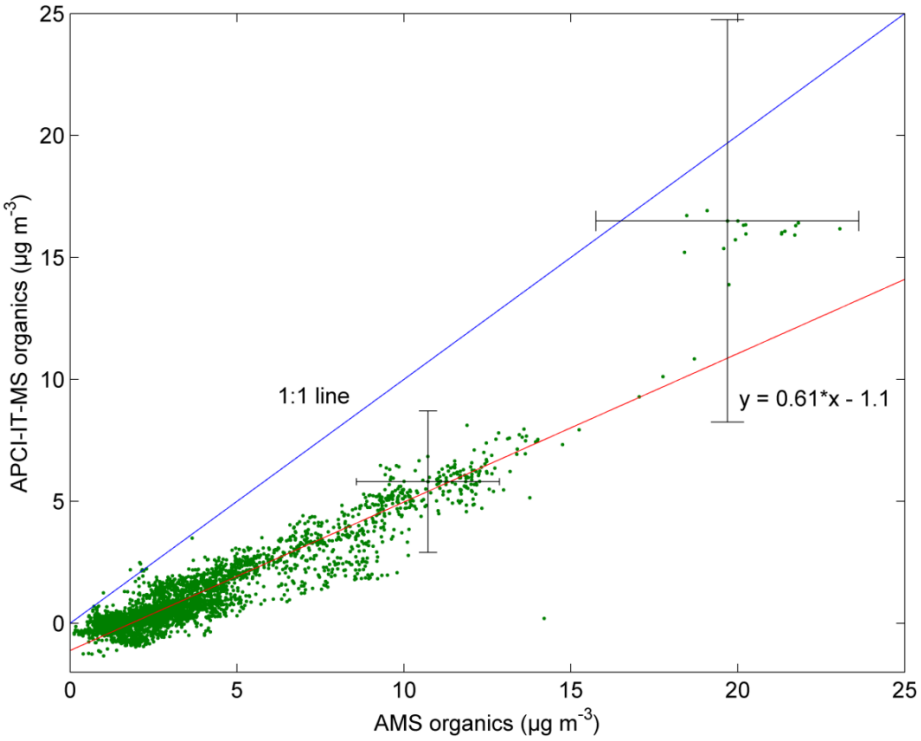

Figure 2.5 Correlation plot of organic signals from mVACES/APCI-IT-MS and C-ToF-AMS during the HUMPPA-COPEC 2010 field campaign (APCI-IT-MS signal (sum *m/z* 150-500) based on instruments response to pinic acid). Estimated errorbars for AMS uncertainty are +/- 20 % and for APCI-IT-MS uncertainty are ±50 %.

As can be seen in Figure 2.5, all data points are well below the 1:1 line. This is expected since APCI-IT-MS probably exclusively measures organic acids (or multifunctional organic molecules including carboxylic acid functional groups) and therefore does not include other organics, e.g. alkanes, alcohols, aldehydes or ketones. The campaign bulk average contribution of organic acids measured by APCI-IT-MS to total organic aerosol measured by AMS during HUMPPA-COPEC 2010 was about 60% (possibly induced by the extreme heat and biomass burning events during summer 2010 (Williams et al., 2011)). Since the sensitivity of the instrument for heat-sensitive acids (e.g. oxalic acid or malonic acid) is almost one order of magnitude lower than for the calibrated acids, the contribution of organic acids might be even higher. However, for the available data the comparison between APCI-IT-MS and AMS shows a very good correlation with a Pearson's R of 0.94 for organics.

On 29 July, at 10:00 -14:00 (local time, UTC +2), a plume from strong biomass burning events in central Russia arrived at the station. During this period the AMS measured the campaign maximum of 23.1 µg m^{-3} organic aerosol concentration. Also, the concentration of organic acids measured by the APCI-IT-MS was the highest during the whole campaign as well

as the relative contribution of acids to the total organic aerosol (see Figure 2.5). These observations suggest that the biomass burning aerosol during this event was extremely oxidized and photochemically aged– a suggestion also supported by the observed ratio of AMS organic signals on *m/z* 43 and *m/z* 44, which are commonly used as a qualitative indicator of the degree of aerosol oxidation. Unfortunately, the C-ToF-AMS was not capable to determine a reliable O:C ratio to further corroborate these findings.

2.3.4 Online MS² experiments from field and laboratory experiments

On 22 July 2010, at 13:20-15:20h (UTC +2), during the HUMPPA-COPEC 2010 campaign MS² spectra of the total organic signal (gas and particle phase) were recorded. Several individual *m/z* ratios between *m/z* 150 to *m/z* 250 were isolated (isolation width ± 0.5 amu) in the ion trap, and by subsequent addition of RF energy, collision induced dissociation caused specific fragmentation of the isolated ions. Figure 2.6 shows the resulting MS² spectrum of *m/z* 185, measured at the boreal field site together with the online MS² spectrum on *m/z* 185 of α-pinene, limonene and Δ^3-carene ozonolysis products in the laboratory. The main compound at this *m/z* ratio is supposed to be pinic acid and isobaric acids originating from other monoterpenes, e.g. 3-caric acid. Although the field MS² mass spectrum is similar to the spectra from the reaction chamber experiments, some fragments actually appear only in the field MS² spectrum, indicating that several other compounds might contribute to the signal on the same *m/z* ratio.

All of these spectra show that *m/z* 167 and *m/z* 141 are the most prominent ion signals. These fragments are the result of waterloss (18 Da) and of CO_2 (44 Da) – characteristic loss and evidence for carboxylic acid functional groups. Furthermore, the limonene spectrum shows a loss of 70 Da (potentially C_4H_6O), resulting in the fragment *m/z* 115, which is not present in the spectrum of α-pinene and Δ^3-carene ozonolysis but clearly detectable in the Hyytiälä spectrum. The *m/z* 115 signal was also described as a fragment of ketolimononic acid measured by offline ambient filter measurements from K-puszta and analysis by HPLC/ESI-MS^n (Yasmeen et al., 2011). The abundance of the MS² fragment *m/z* 115 at Hyytiälä seems surprising since the main monoterpene emissions at Hyytiälä measured by GC-MS are α-pinene and Δ^3-carene (Yassaa et al., 2012). An explanation might be that limonene is emitted in larger amounts than derived from ambient measurements or cuvette studies– possibly induced by the very high reactivity of the double unsaturated monoterpene. Due to the diversity of biogenic emissions at the Hyytiälä station, oxidation products from other volatile organic precursor molecules might also contribute to the *m/z* 115 fragment, e.g. myrcene-, camphene-, sabinene- or sesquiterpene derived acids. The loss of CO or C_2H_4 (28 Da), resulting in *m/z* 157 cannot be found in chamber experiments with the tested monoterpenes (ß-pinene also tested but not shown). The fragment *m/z* 97 can

originate from the dissociation of the sulphate group from organosulfates (detachment of HSO_4^-) or, more likely, from the dissociation of two CO_2 molecules from the molecular ion at *m/z* 185. Since pinic acid and 3-caric acid are both dicarboxylic acids, the dissociation of two CO_2 is very likely. In conclusion, we would like to speculate that the oxidation of fast reacting (e.g. myrcene) or unknown VOCs (Di Carlo et al., 2004) can form products which might explain the not-assignable fragments measured during the MS^2 experiments.

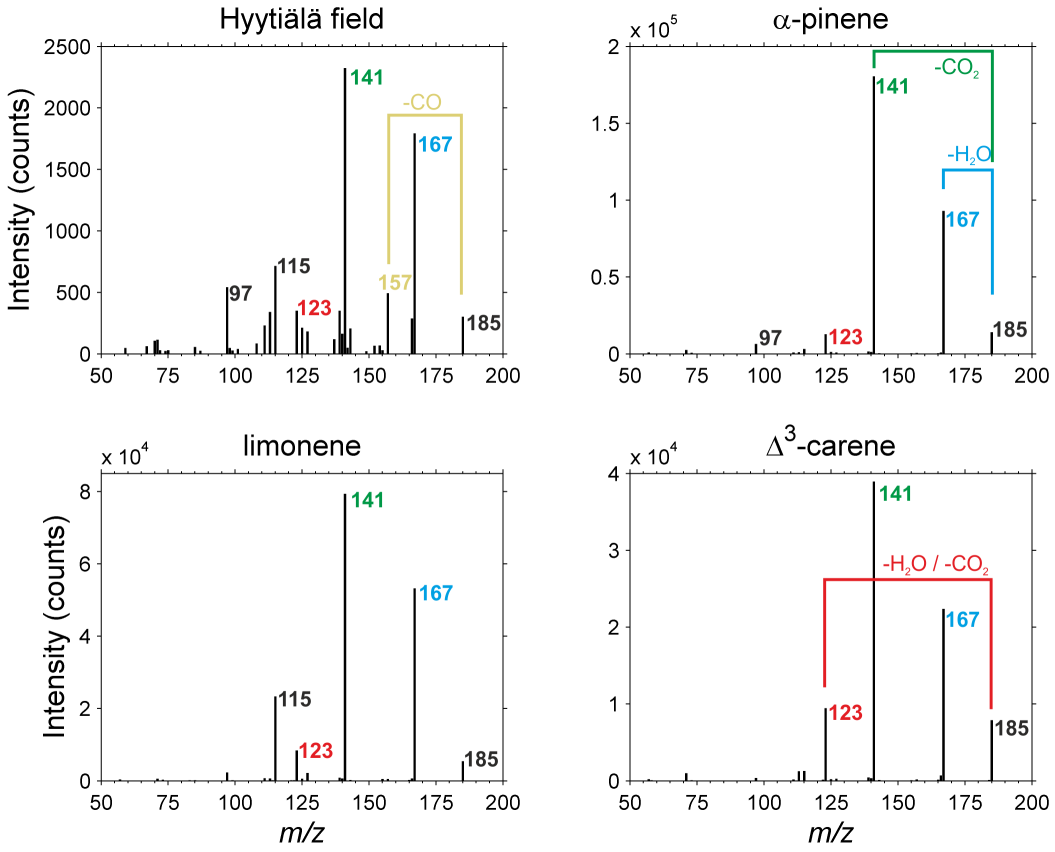

Figure 2.6 Online MS^2 experiments at Hyytiälä (CID energy 30%) and from laboratory ozonolysis using α pinene, limonene and Δ3 carene (CID energy 26%).

2.4 Conclusions

We have demonstrated for the first time the application of an online mass spectrometric technique with the ability to perform MS^2 experiments from biogenic organic acids in the field. To record the MS^2 spectra, it is essential to use soft ionization to preserve the structural information of the molecular ion before entering the detector- in our case a quadrupole ion trap. The soft ionization technique adopted here was chemical ionization at atmospheric pressure using O_2^- ions as primary ions reacting with molecules that have higher gas phase acidity. To improve the detection limit in the field, an mVACES was operated in front of the MS system. The APCI-IT-MS data were compared to C-ToF-AMS data, revealing that the two techniques are complementary mass spectrometric techniques which can lead to an improved understanding of organic aerosol formation and composition. MS^2 studies did indicate the abundance of several compounds on one nominal mass in the boreal forest environment. The overall AMS/APCI-IT-MS comparison suggests that organic acids formed a major part of organic aerosol mass during the HUMPPA-COPEC2010 campaign. Furthermore, the APCI-IT-MS technique is in principle suited to measure quantitatively rarely measured species (i.e. the suite of organic acids) in the gas phase, which can be of great help in assessing the significant missing reactivity observed in the boreal forest (Nölscher et al., 2012). For upcoming ecosystem or megacity studies, the capability to perform online high resolution mass spectrometry for more detailed observation of molecular tracer compounds would be a very valuable asset.

Acknowledgements. A. L. V. acknowledges the Max Planck Institute for Chemistry in Mainz and the Max Planck Graduate Center for financial support and the possibility to participate in the HUMPPA-COPEC 2010 field campaign. Furthermore he acknowledges the support by the SMEAR II team during the campaign and Caroline Oehm and Ottmar Moehler of the Karlsruhe Institute of Technology for the loan of the PCVI.

The entire HUMPPA-COPEC team is grateful for the support of the Hyytiälä site engineers and staff. Support of the European Community – Research Infrastructure Action under the FP6 “Structuring the European Research Area” Programme, EUSAAR Contract N° RII3-CT-2006-026140 is gratefully acknowledged.

The campaign measurements and analyses were supported by the ERC Grant ATMNUCLE (project No 227463), Academy of Finland Center of Excellence program (project No 1118615), The European Integrated project on Aerosol Cloud Climate and Air Quality Interactions EUCAARI (project No 036833-2), the EUSAAR TNA (project No 400586), and the IMECC TA (project No 4006261).

3 Organic aerosol characterization in the boreal forest environment

This chapter is a reprint of the article:

A. L. Vogel, M. Äijälä, A. L. Corrigan, H. Junninen, M. Ehn, T. Petäjä,
D. R. Worsnop, M. Kulmala, L. M. Russell, J. Williams, and T. Hoffmann

In-situ submicron organic aerosol characterization at a boreal forest research station during HUMPPA-COPEC 2010 using soft and hard ionization mass spectrometry

Atmospheric Chemistry and Physics, *13*, 10933-10950, doi:10.5194/acp-13-10933-2013, **2013**.

Abstract. The chemical composition of submicron aerosol during the comprehensive field campaign HUMPPA-COPEC 2010 at Hyytiälä, Finland is presented. The focus lies on online measurements of organic acids, which was achieved by using atmospheric pressure chemical ionization (APCI) ion trap mass spectrometry (IT-MS). These measurements were accompanied by aerosol mass spectrometry (AMS) measurements and Fourier-Transform Infrared Spectroscopy (FTIR) of filter samples, all showing a high degree of correlation. The soft ionization mass spectrometer alternated between gas phase measurements solely and measuring the sum of gas- and particle-phase.

The AMS measurements of C, H and O elemental composition show that the aerosol during the campaign was highly oxidized, which appears reasonable due to high and prolonged radiation during the boreal summer measurement period as well as the long transport times of some of the aerosol. In order to contrast ambient and laboratory aerosol, an average organic acid pattern, measured by APCI-IT-MS during the campaign, was compared to terpene ozonolysis products in a laboratory reaction chamber. Identification of single organic acid species remains a major challenge due to the complexity of the boreal forest aerosol. Unambiguous online species identification was attempted by the combinatorial approach of identifying unique fragments in the MS^2-mode of standards, and then comparing these results with MS^2 field spectra. During the campaign, unique fragments of limonene derived organic acids (limonic acid and ketolimononic acid) and of the biomass burning tracer vanillic acid were detected. Other specific fragments (neutral loss of 28 Da) in the MS^2 suggest the occurrence of semialdehydes.

Furthermore, an approach to determine the average molecular weight of the aerosol is presented. The campaign average organic molecular weight was determined to be 300 g mol^{-1}. However, a plume of aged biomass burning aerosol, arriving at Hyytiälä from Russia, contained organic compounds up to 800 Da ($\overline{MW}_{om} \approx 450$ g mol^{-1}), showing that the average molecular weight can vary significantly. The high measurement frequency of both, AMS and APCI-IT-MS, enabled the partitioning of selected organic acids between gas- and particle-phase as a function of the total particulate mass to be quantified. Surprisingly high fractions of the higher molecular weight organic acids were observed to reside in the gas phase. These observations might be a consequence of large equilibration timescales for semi-solid boreal forest aerosol, as it has been recently hypothesised by Shiraiwa and Seinfeld (2012).

3.1 Introduction

The boreal forest biome is one of the major ecosystems on earth, accounting for one third of the world´s forested area (Sabine et al., 2004). Due to biogenic volatile organic compound (BVOC) emissions from the vegetation, the boreal forest significantly affects the chemistry and physics of the atmosphere. Subsequent to the emission of the VOCs, their atmospheric oxidation results in low volatility organic compounds that contribute to the condensational growth of particles to sizes which allow them to act as cloud condensation nuclei (CCN) (Riipinen et al., 2012). By including the effects of those CCN on the radiative balance of the boreal forest in climate models, it has been shown that the previously assumed net positive radiative forcing, due to the low surface albedo (e.g. Bonan, 2008), is counteracted by a more negative cloud albedo radiative forcing, resulting in an overall cooling effect of the boreal forest on the global climate (Spracklen et al., 2008).

Many fundamental aspects of this climate feedback process, like the detailed speciation of emissions, OH-radical budgets, particle formation and aging processes, needed to be investigated in-situ to obtain a more detailed and holistic picture of the ongoing atmospheric processes. In order to clarify these issues, a large comprehensive field campaign (HUMPPA-COPEC 2010) was carried out at the Hyytiälä forest station in southern Finland from 12 July 2010 to 12 August 2010, to investigate summertime conditions in the boreal forest (Williams et al., 2011). Especially the atmospheric oxidation of volatile organic compounds (VOCs) and the subsequent secondary organic aerosol (SOA) formation is relevant for improving global climate models, since the major uncertainties are due to the particle derived direct radiative effect and to the cloud albedo effect (IPCC, 2007). The secondary fraction of organic aerosol (OA) usually makes up the largest proportion of the total aerosol mass (Zhang et al., 2007; Docherty et al., 2008; Jimenez et al., 2009). However, the huge number of different species in the organic fraction, which originates from a variety of different reactive precursors, makes it a considerable analytical challenge to resolve this complexity (Goldstein and Galbally, 2007; Hallquist et al., 2009).

The volatility of an organic compound determines whether the atmospheric processing occurs in the gas- or in the particle-phase. This is an important factor for global climate models. Since the gas-to-particle partitioning is mass dependent (Pankow, 1994a), low volatility compounds make up a larger fraction of the OA at low mass loadings. In a simplified perspective, the volatility of an organic compound can be regarded as a function of carbon and oxygen atoms (Donahue et al., 2011). Thus, it can be assumed that carboxylic acids make up a significant, if not the most significant, fraction of the particle phase, due to their reduced volatility. Furthermore, quantum mechanical calculations have shown that organic acids in the

gas phase can help to surmount the nucleation barrier by forming clusters with sulfuric acid, and thus can play an important role in new particle formation (Zhang, 2010). On the other hand, a large number of organic acids are still volatile enough to partition predominately to the gas phase, where they can be involved in oxidation processes and contribute to the overall gas phase OH reactivity. Donahue et al. (2006) argued that the large amount of these intermediate volatile organic compounds (IVOCs), which are present almost entirely in the gas phase (even can contain more mass than the condensed phase), are completely ignored by local and global models.

Recent work illustrated that the OH-initiated aging of semi-volatile organic compounds (SVOCs) and IVOCs in the gas phase is an important part in the formation of SOA (Donahue et al., 2012a) and that the first oxidation step of VOCs is only barely sufficient to form SOA at atmospheric relevant mass concentration levels (Donahue et al., 2012b).

Instruments that provide reliable measurement of single organic species, among the thousands of different compounds in the organic aerosol, are needed in order to investigate those atmospheric processes in detail. In parallel to further improvements of the aerosol mass spectrometer (AMS, Aerodyne, USA) (Jayne et al., 2000; Jimenez et al., 2003; Canagaratna et al., 2007), which operates with hard ionization, recently chemical ionization (CI) has received increasing attention. The advantage of this soft ionization technique is that it preserves the structural information of the molecule (Zahardis et al., 2011; Laskin et al., 2012; Pratt and Prather, 2012). The mass spectrometric separation after ionization can be achieved by various techniques. The most common technique measures the time of flight (ToF) of the ions formed in order to determine their mass-to-charge (*m/z*) ratio. Yatavelli et al. (2012) described this technique as highly sensitive (detection limits of organic acids in the particle phase less than 1 ng m^{-3}), providing high mass resolution (R=5000 above *m/z* 250) and high mass accuracy (±20 ppm). A different mass spectrometric technique is the ion trap mass spectrometry (IT-MS), which typically has less mass resolution and accuracy but offers the unique possibility to distinguish between isobaric species through collision induced fragmentation. Isobaric species are ubiquitous in atmospheric aerosols, since the constituents of the main precursor classes of mono- and sesquiterpenes are often isomeric (examples are given in chapter 3.3.2).

In this paper the results of the online particle measurements during HUMPPA-COPEC 2010 are presented with special emphasis on biogenic organic acids. Biogenic acids were measured online in the gas and particle phase, with high temporal resolution, by using an atmospheric pressure chemical ionization (APCI) ion trap mass spectrometer (IT-MS) in combination with a mVACES online particle concentrator (Geller et al., 2005; Vogel et al., 2013a). These measurements include, to our knowledge, the first in-situ MS^2 experiments of biogenic acids in the boreal forest. Since the Aerodyne´s C-ToF-AMS was operating simultaneously, we have

explored the potential of combining soft and hard ionization techniques to gain new insights into aerosol composition and partitioning.

3.2 Experimental

3.2.1 Field site description

From 12 July to 12 August 2010, the large field intensive HUMPPA-COPEC 2010 was carried out at the Station for Measuring Forest Ecosystem – Atmosphere Relations (SMEAR II) at Hyytiälä in Finland. During this period, the continuous long term on-site measurements were extended by a large suite of instruments for measuring gas- and particle-phase chemistry (Williams et al., 2011). The station is located in southern Finland (61°51’ N, 24°17’ E, 181 m a.s.l.) in the middle of a ~50 year old Scots pine (*Pinus sylvestris* L.) stand, with homogenous Scots pine forest forming also the main larger-scale surroundings, thus representing well the boreal coniferous forest environment (Hari and Kulmala, 2005; Kulmala et al., 2001). The town nearest to SMEAR II, Orivesi (10.000 inhabitants), is situated 15 km south of the station and the city of Tampere (215.000 inhabitants) is located approximately 50 km SW from the station. The city of Helsinki lies 200 km to the south of the station and St. Petersburg approximately 350 km south-east.

3.2.2 Field campaign instrumentation

3.2.2.1 On-line aerosol mass spectrometry

Two online and collocated (same inlet) aerosol mass spectrometers were measuring simultaneously in the main SMEAR II cottage for detailed online chemical analysis of non-refractory sub-micron particles: (1) an Atmospheric Pressure Chemical Ionization Ion Trap Mass Spectrometer (APCI-IT-MS, Finnigan LCQ; Hoffmann et al. 2002, Kückelmann et al. 2000) in conjunction with a miniature Versatile Aerosol Concentration Enrichment System (mVACES, Geller et al. 2005) as described by Vogel et al. (2013) and (2) the Aerodyne’s Compact Time of Flight Aerosol Mass Spectrometer (C-ToF-AMS, Drewnick et al. 2005). Filter samples for FTIR-analysis were taken at a distance of approximately 200 m from the main cottage.

Briefly, the APCI-IT-MS produces primary ions by corona discharge at atmospheric pressure. In the negative ion mode, gaseous compounds having a higher gas-phase acidity become ionized by proton transfer reaction with O_2^- radicals, and are then mass analyzed by the quadrupole ion trap. Prior to the discharge region source, particulate compounds become

vaporized by a heating unit. The measurable compound classes are mainly restricted to organic molecules including a carboxylic functional group (organic acids), sulphate and organic molecules with a sulphate group (e.g. organosulfates). The class of nitrophenols can be detected in the negative mode as well. Organic compounds, which show fast thermal decomposition, were measured with a much lower sensitivity than other biogenic acids. The spectrum was recorded between *m/z* 50 to 500 and one recorded spectrum per minute was averaged from 200 microscans.

The Aerosol Mass Spectrometer (Aerodyne Research Inc., Billerca, MA, U.S.A) is an instrument capable of directly measuring the chemical composition of aerosols using time-of-flight mass spectrometry. The AMS is widely used and its operation principle and data analysis methods have been described in detail elsewhere (Canagaratna et al. (2007), general information on AMS; Drewnick et al. (2005), a description of the C-ToF-AMS variant used in this study). Analysis of the AMS data has been described by e.g. Allan et al. (2003, 2004), and the analysis procedure during HUMPPA-COPEC 2010 and the general AMS data outlook during the campaign by Vogel et al. (2013).

In short, the AMS uses an aerodynamic lens to form the sample aerosol into a particle beam. This beam is then modulated by a beam chopper and directed to a particle time-of-flight (PToF) chamber for size distribution measurement. After the PToF chamber, the sample aerosol is thermally vaporized, resulting in the non-refractory aerosol particle components (i.e. those vaporizing in 600 degrees Celsius or less) transforming to gas-phase in the ionization region. The gaseous molecules are subsequently ionized via 70 eV electron ionization, forming both positive and negative ions. The positive polarity ions are selected and led to the time-of-flight mass analyzer. The analysis happens in real time, and sample is continuously collected via the inlet, while the inside of the instrument is kept in high vacuum by a differential pumping system consisting of five turbomolecular pumps.

The time of flight data from the mass analyzer is inverted to yield *m/z* mass spectra, based on which the observed signal amounts are assigned to various chemical species. Using calibration data, the amount of signal is then quantified to give out particle mass concentrations in micrograms per cubic meters for organic compounds, sulfates, nitrates, ammonia compounds and chlorides.

3.2.2.2 Off-line FTIR filter measurements

Submicron particles were collected 4 m above ground level on 37 mm Teflon filters (Pall Inc., 37 mm diameter, 1.0 μm pore size Teflon membrane), downstream of a 1 μm sharp-cut cyclone (SCC 2.229 PM1, BGI, Inc.) (Corrigan et al., 2013). The aerosol was dried to less than approximately 75% RH prior to reaching the cyclone. Filter collection times varied from 6, 9,

and 12 hours, including duplicate 24-hour filters, and were based on real-time OM values measured by the C-ToF-AMS in order to maximize resolution time while staying above the detection limit. After collection, the filters were stored at 0°C before they were analyzed in San Diego, California by a Tensor 27 spectrometer with a DTGS detector (Bruker, Billerica, MA). A peak-fitting algorithm described in Russell et al. (2009) and Takahama et al. (2013) was used to quantify organic functional groups from the FTIR spectra. Quantified organic functional groups included: alcohol, alkane, carboxcylic acid, primary amine and non-acid carbonyl. Alkene and aromatic functional groups were below the limit of quantification during the sampling period.

3.2.2.3 Black carbon aethalometer

Black carbon is not detected by the AMS, as it is not vaporized at 600°C. Therefore, a separate instrument was needed to obtain black carbon (BC) mass during the campaign. For this purpose the SMEAR II site aethalometer (Magee Scientific Corporation, Berkeley, CA 94704, USA) data was used. The instrument measures light absorption of an aerosol collector tape, at several wavelengths, to determine the mass concentration of black carbon particles. Together the AMS data on non-refractory particles and the BC data from the aethalometer form a comprehensive picture of the Hyytiälä submicron aerosol basic chemical composition.

3.2.3 Other

3.2.3.1 Laboratory experiments

In a 100 L dark continous-flow reaction chamber (glass and Teflon), (+)-α-pinene (Sigma-Aldrich, ≥99%) and (+)-3-carene (Fluka analytical, ≥98.5%), vaporized in an external thermal diffusion source, were mixed with app. 1 ppm of ozone (1008-RS, Dasibi Environmental Corp., Glendale, CA, USA) to produce secondary organic aerosol. The aerosol from this chamber was sampled directly through an activated charcoal denuder (length ~0.5 m, ID ~0.5cm) into the ion source of the APCI-IT-MS in order to record the online mass spectra.

To record the MS^2 spectra of selected authentic standards, vanillic acid (Sigma-Aldrich, ≥97%), *cis*-pinonic acid (Sigma-Aldrich, 98%) and self-synthesized pinic acid were dissolved as 0.1 mM aqueous solutions. Out of these solutions a polydisperse aerosol was generated using a TSI 3076 atomizer. Before entering the APCI ion source, the aerosol was dried using a silica diffusion dryer. Due to the lack of a standard of 3-methyl-1,2,3-butanetricarboxylic acid, the MS^2 spectrum of this compound was recorded using (–)ESI-UHR-MS after LC separation of an ambient filter sample extract, collected at the Taunus Observatory, Germany.

3.2.3.2 Trajectory analysis

Backward trajectories were obtained from the web based HYSPLIT model (HYbrid Single-Particle Lagrangian Integrated Trajectory, Draxler and Rolph G. D., 2013) which can be accessed on the NOAA Air Resources Laboratory website (http://ready.arl.noaa.gov) (Rolph, 2013). The length of the backward calculation was set to 96 hours and the arrival height at 25 m above ground level.

3.3 Results and Discussion

3.3.1 Aerosol chemical variation and source apportionment during HUMPPA-COPEC 2010

Figure 3.1 displays the temporal pattern of three different particle phase measuring techniques during the HUMPPA-COPEC 2010 campaign. The blue time series in the top panel represents the total counts of organic acids (and possibly other compound classes such as organosulfates or nitro-phenols and catechols) in the particle phase, which is the sum of the signal intensities between *m/z* 150 and *m/z* 500, measured by APCI-IT-MS. The green time series shows OA measured by the AMS, which ranged from below detection limit (day 204) to 23 µg/m³ (day 210). As can be seen, AMS organics and APCI-IT-MS show a similar pattern throughout the campaign, both capturing days 207-209 with the highest aerosol concentrations.

In the middle panel of Figure 3.1, a PMF (positive matrix factorization, see. e.g. Paatero and Tapper, 1994) solution for the AMS measurements is shown, using the solutions from Corrigan et al. (2013). The PMF analysis is one way to deconvolve the complex AMS mass spectra to yield source-specific time series and mass spectra for the different organic aerosol types. From the PMF solution space, a solution of three factors (FPEAK = −0.4) was selected, as in this solution a very clear high f43 factor (OOA-2) emerges. The FPEAK selection was based on obtaining the clearest difference in correlation profiles for the factors and auxiliary measurements (i.e. trace gases, BC, and AMS inorganics). However, the two other obtained high f44 factors had similar temporal behaviour, mass spectra and correlation profiles with auxiliary measurements, and they were thus combined to form the OOA-1 factor in this analysis. A probable interpretation for the 3 factor solution would be that the organic aerosol is divided into (1) long-range transported anthropogenic pollution (OOA-2) and (2) highly oxidized BBOA generated from Russian wildfires, and highly oxidized biogenic-related OA (OOA-1). In order to avoid possible over-interpretation of the highly aged aerosol, only the OOA-2 factor and the

(combined) OOA-1 factor are presented (The mass spectra can be found in the supplemental material).

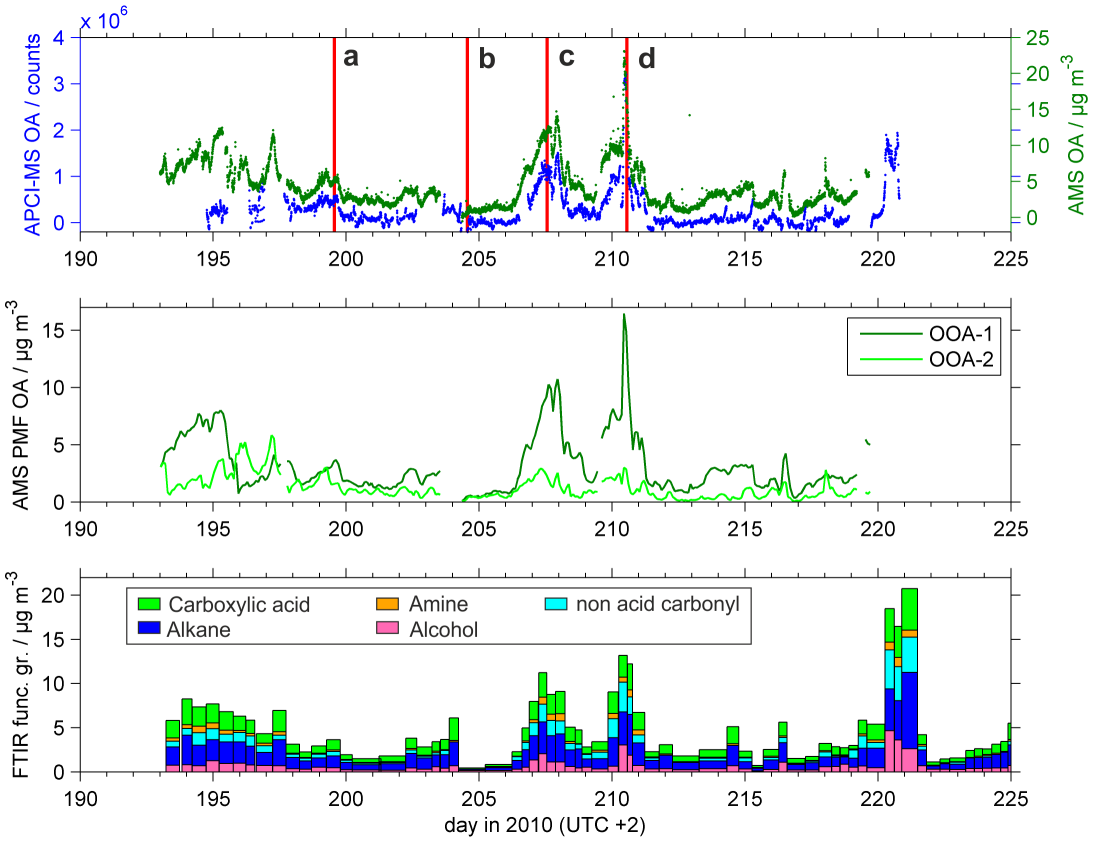

Figure 3.1 Temporal variation of organic aerosol during HUMPPA-COPEC 2010. Top panel: Summation of particle phase signals between *m/z* 150 and 500 measured by APCI-IT-MS (blue) vs. the total submicron organic mass concentration measured by AMS (green). Middle panel: Two factor PMF analysis of AMS data (OOA: Oxygenated Organic Aerosol, factor -1 and OOA-2, see text). Lower panel: Mass concentration of functional groups measured by filter-FTIR.

The lowermost time series represents the different organic functional groups (alcohol, alkane, non-acid carbonyl, amine and carboxylic acid), which were determined by filter based measurements using FTIR.

Total submicron OM measured by FTIR (lower panel) varied substantially throughout the campaign, with an average of 4.3 ± 3.9 µg m^{-3}. The highest OM concentrations, 23 µg m^{-3}, were observed with the arrival of aged biomass burning emissions from central Russia on day 222. The lowest OM concentrations, roughly 0.4 µg m^{-3}, were measured on day 204 and 205, when air masses arrived from northern Scandinavia and the Arctic Ocean. The organic functional group composition was dominated by oxygenated groups, carboxylic acid (28%), non-acid carbonyl (15%), and alcohol (15%) groups, consistent with the high O/C measured by the AMS. Despite

the fluctuation in total OM, the fraction of oxygenated organic functional groups remained frequently constant throughout the campaign.

The temporal resolution of the online measurements of the APCI-IT-MS and the AMS are 5 minute averages, AMS-PMF data are based on 30 min average intervals, and the average filter sampling time for FTIR analysis is approximately 9 hours.

The red marked periods (a-d) in the top panel are 3-hour intervals – the respective average APCI-IT-MS gas- and particle-phase mass spectra and the average chemical composition measured by AMS are shown in Figure 3.2. These intervals were chosen to illustrate how mass spectra of the gas- and particle-phase vary with different airmass histories. All four spectra are averaged between 12:00 and 15:00h (UTC +2) of the respective day.

During (a) (day 199, 18.7.2010 12:00 – 15:00h, UTC+2), the back trajectory analysis (Figure 3.3) indicates that the air masses arriving at the site were coming from the SW, descending from higher altitudes over Sweden and the Baltic sea. Average submicron particulate mass (PM) during this period was 7.2 µg/m³. The organic acid distribution in the particle phase shows a bimodal distribution with maxima around *m/z* 200 and *m/z* 300, respectively. The maximum at lower *m/z* ratios can be explained by the contribution of monoterpene derived organic acids, which are mainly measured in the range below *m/z* 230. We assume that the higher molecular weight compounds can be attributed to sesquiterpene oxidation products, aged oligomers of low molecular compounds (isoprene, glyoxal), dimers of monoterpene oxidation products or, most probably, a combination of these precursors. The *m/z* distribution in the gas phase has its maximum on *m/z* 183. Generally, the gas phase spectrum during a, c and d are very equally distributed. The small signals in the *m/z* 370-390 area are most probably cluster artefacts of smaller organic acids (e.g. 2-hydroxyterpenylic acid), as it was described by Claeys et al. (2009). Although, the air masses during (a) were coming from SW and might be influenced by Helsinki and Tampere pollution, the CO mixing ratio during this period was 103.8 ppbV, distinctly below the mean campaign CO mixing ratio of 208.5 ppbV. This suggests that the air masses are only marginally influenced by anthropogenic activities or biomass burning.

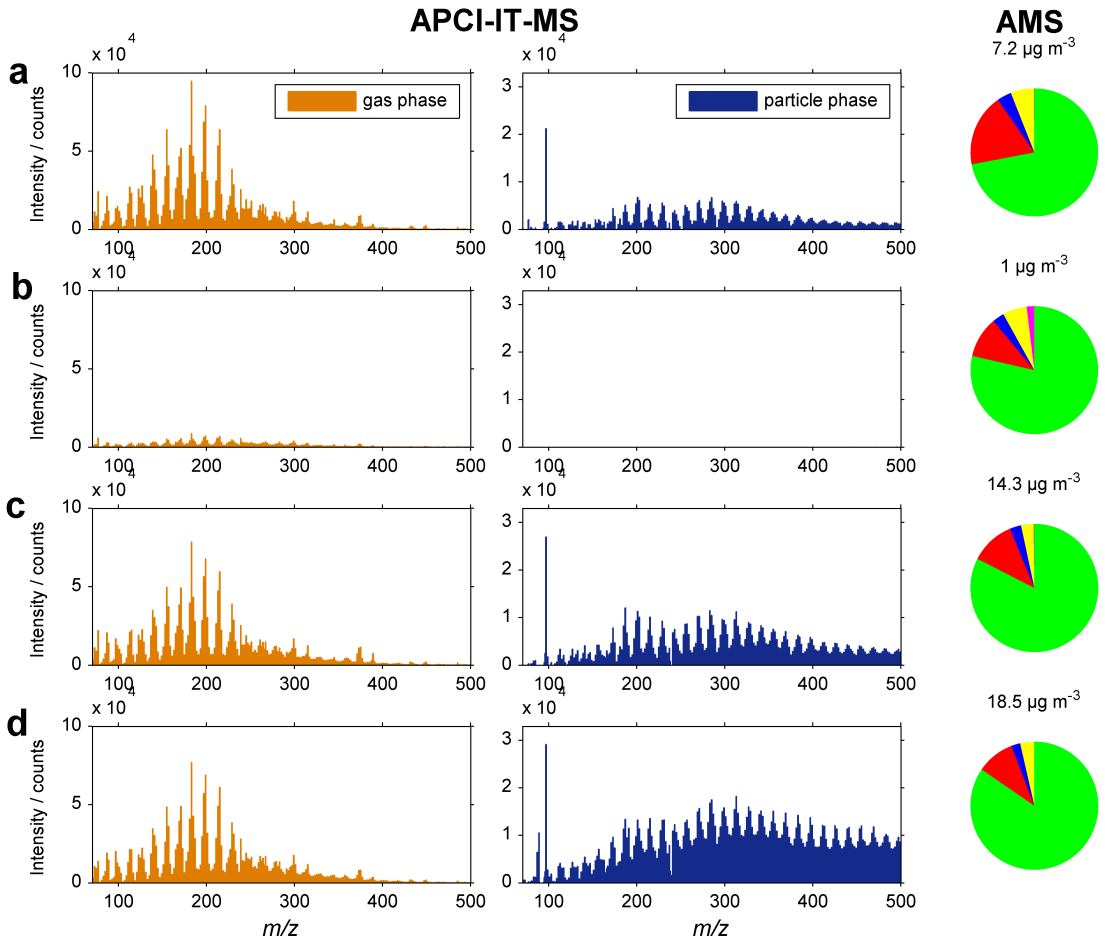

Figure 3.2 Average composition of the gas- and particle- phase on four different days during HUMPPA-COPEC 2010 (a-d, Figure 3.1) measured by APCI-IT-MS and AMS. Black carbon is not included in the AMS pie charts but in the numbered submicron mass concentration.

On day 204 (b) (23 July 2010 08:00 – 13:00h, UTC+2), the sole new particle formation (NPF) event during the campaign occurred. In general, during summertime, NPF occurs quite rarely- annual variation of NPF peaks in spring and autumn (Dal Maso et al., 2007). Back trajectory analysis of this day shows that air masses were coming from the Arctic region at high altitudes, descending over the Gulf of Bothnia and then residing approximately 12 hours over the Finnish boreal forest before arriving at the Hyytiälä station. Hence, clean air masses coming from the arctic region are favourable for NPF events during summertime, since the low number of pre-existing aerosol particles does not provide sufficient surface for condensation of low volatile species. This agrees with the observation made by Nilsson et al. (2001) who described a prevalence for NPF occurring in clean arctic air masses. Such cold air outbreaks from the arctic region form rarely during summer time. The average submicron particle phase concentration on 23 July 2010 12:00-15:00h was 0.97 µg/m³, and the nucleation event started in the morning hours. The average CO mixing ratio was 78.2 ppbV – close to the minimum CO mixing ratio

(77.5 ppbV) of the campaign, which was measured in the morning hours of the same day. The average APCI-IT-MS gas phase spectrum shows a very weak signal of organic acids, e.g. on *m/z* 183 8700 counts – the campaign average on *m/z* 183 was 72000 counts. Thus, the signal measured during (b) is only slightly above the instrumental background (~6700 counts, 3 x standard deviation (SD) of the noise signal). The particle phase signals during the NPF event are below detection limit, indicating the analytical limitations of the utilized setup.

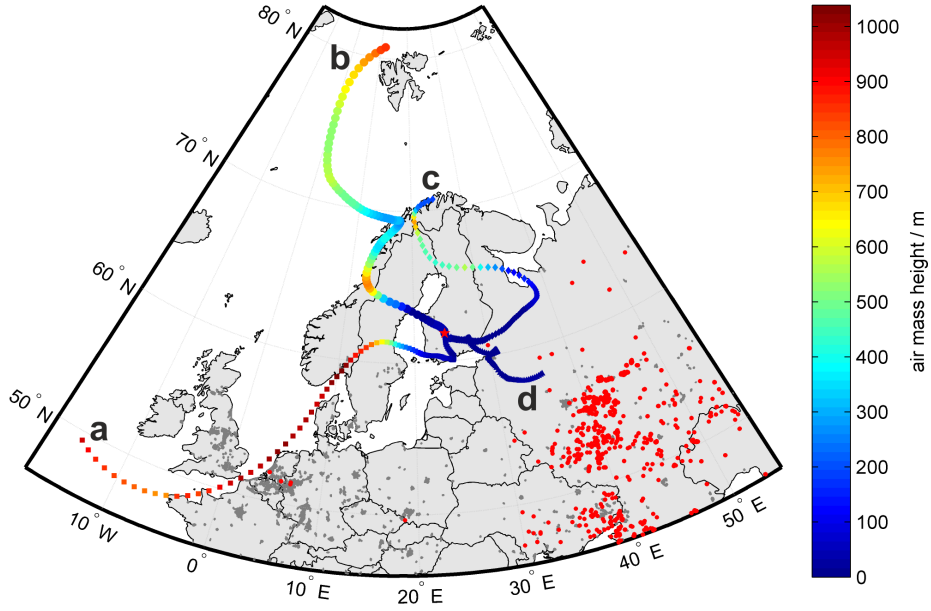

Figure 3.3 96 hours backward trajectory analysis of four different days (a-d) using the NOAA HYSPLIT model. (a) to (d) refer to the average intervals in Figure 3.1 (arrival time 14:00 h (UTC+2) of the respective day). The red star marks the SMEAR station at Hyytiälä. MODIS fire data are 100% CI fire spots between 18.07.10 and 29.07.10. Land, borders and populated areas are based on Natural Earth shapefiles (http://www.naturalearthdata.com).

Backtrajectory analysis of day 207 (c) (26 July 2010), indicates that air masses were coming from NE situated at low altitudes for approximately 72 h before arriving at the Hyytiälä station. Elevated CO levels (188.7 ppbV) are a hint for biomass burning influence and/or anthropogenic pollution from the St. Petersburg region. Average PM1 was 14.3 µg/m³ and the average mass loading of sulphates 1.6 µg/m³, both unusually high for the SMEAR II station. A bimodal distribution with two maxima at ~*m/z* 180-190 and *m/z* 280-290 appears in spectrum (c), slightly shifted towards lower *m/z* ratios compared to spectrum (a).

Comparing the particle phase spectra (c) and (d) reveals that higher molecular compounds account for a higher proportion of the total aerosol mass in (d) than in (c). The average spectrum in (d) was measured during day 210- a period of strong influence from the central Russia biomass burning events in the Nidzni-Novgorod region (Konovalov et al., 2011; Portin et al., 2012). During this time (day 210, 29 July 2010) the highest aerosol mass was measured (27.1 µg/m³ (non-refractory aerosol, AMS), 1.9 µg/m³ black carbon (aethalometer)), accompanied by the highest temperature (32.6 °C), lowest visibility and highest CO mixing ratio (437.7 ppbV). PMF analysis shows the highest fraction of f44 (OOA-1). As has been shown by Vogel et al. (2013), during this time the estimated sum of organic acids contribute more than the campaign average to the total OA mass. The O/C ratio measured by FTIR, which can be regarded as a proxy for the aerosol oxidation state, was 0.70 on this day, and thus above the average O/C ratio of the campaign (O/C = 0.56). A similar aerosol oxidation proxy for the AMS data, the ratio of signals in *m/z* 44 to *m/z* 43, also averages relatively high at 3.10 for the day in question, compared to a campaign average of 2.34. Due to the strong influence of the biomass burning, it is highly probable that the aerosol contains significant amounts of compounds which are, under normal conditions, not present in boreal forest aerosol. However, the high contribution of organic acids can be explained by the prolonged period of photochemical aging experienced by the plume before arriving at the station. The back trajectories suggest that the emitted aerosol from central Russia spent more than three days at low altitudes before arriving at Hyytiälä without encountering wet deposition. During this time, biomass burning markers, like levoglucosan and other lignin derived organic compounds, can undergo strong heterogeneous oxidation and either become volatilized, oligomerized or functionalized (Kroll et al., 2011). Functionalized (e.g. carboxylic acid functionalities) compounds can then be detected in the negative ionization mode of the APCI-IT-MS. Gas phase oxidation of additionally released VOCs through biomass burning (Andreae & Merlet, 2001) and subsequent gas-to-particle conversion increases the aerosol mass as the plume is transported to the SMEAR station. Kessler et al. (2010) illustrated the significant volatilization during the oxidation of levoglucosan. In contrast to levoglucosan, organic acids show little mass volatilization during heterogeneous OH oxidation, since the loss of carbon is roughly equivalent to the increase of oxygen (Kessler et al., 2012). Therefore it can be concluded, that the proportion of organic acids in biomass burning aerosol increases during aging not only due to heterogeneous oxidation of the aerosol constituents but also due to the oxidative volatilization of other non-acidic compounds. Lastly, it should be noted that the high temperature and the biomass burning events during the summer 2010 can be regarded as an extreme anomaly, compared to average boreal forest summer conditions (see Williams et al., 2011).

3.3.2 Ambient monoterpene oxidation products compared to simulation chamber ozonolysis of α-pinene and Δ^3-carene

A detailed knowledge of the specific VOC emission pattern of the boreal forest helps to understand the chemistry and the composition of the boreal forest aerosol. Therefore measurements of ambient VOC mixing ratios, using Adsorptive Preconcentration followed by Thermal Desorption-Gas Chromatography-Mass Spectrometry (TD-GC-MS), were carried out during the HUMPPA-COPEC 2010 campaign. Those measurements showed that the mixing ratios of the most abundant biogenic compounds (α-pinene, Δ^3-carene, ß-pinene) in ambient air ranged between a few pptV and 1.5 ppbV (Yassaa et al., 2012).

Additionally, laboratory α-pinene and Δ^3-carene dark ozonolysis experiments were conducted in the laboratory for comparison with the ambient APCI-IT-MS data. The ambient spectrum and the laboratory spectrum shown in Figure 3.4, focus on the range between *m/z* 160 and *m/z* 240, which includes the most important terpenoid acids. Although there is a certain amount of OH radicals which are formed during the terpene ozonolysis, a recent study by Hall et al. (2013) shows that the additional oxidation of α-pinene ozonolysis products by OH radicals leads to the fragmentation of the dimeric products and an overall increase of the oxidation state. Therefore we like to mention that the different oxidative environment between laboratory and ambient air might result in different products which cannot be distinguished by the used method.

The ambient data are a three hour average of 26 July 2010 12:00 – 15:00 (UTC+2). The partitioning of specific compounds between gas- and particle-phase during the campaign will be discussed in chapter 3.3.5 – this chapter focuses on the discussion of the chemical composition.

Three main conclusions can be drawn from the pattern of the ambient mass spectra (Figure 3.4, middle panel):

(1) The regular pattern of Δ *m/z* 14 between the major signals in the particle phase can be attributed to an increasing number of CH_2 groups in the carbon backbone. The gas phase does not show this Δ *m/z* 14 pattern as clearly as the particle phase.

(2) The low signals on even *m/z* ratios can be attributed to ^{13}C-containing molecules since the pattern follows the odd *m/z* pattern and ratios to the monoisotopic ion are within the expected intensity distribution. However, the presence of nitrogen containing organic acids cannot be ruled out since the instrumental ionization method might suppress compounds with a higher gas-phase basicity.

(3) By comparing the gas- and particle-phase signal distribution in one peak cluster (e.g. from *m/z* 176 to *m/z* 192), it becomes obvious that the maximum particle phase signals are shifted towards higher masses.

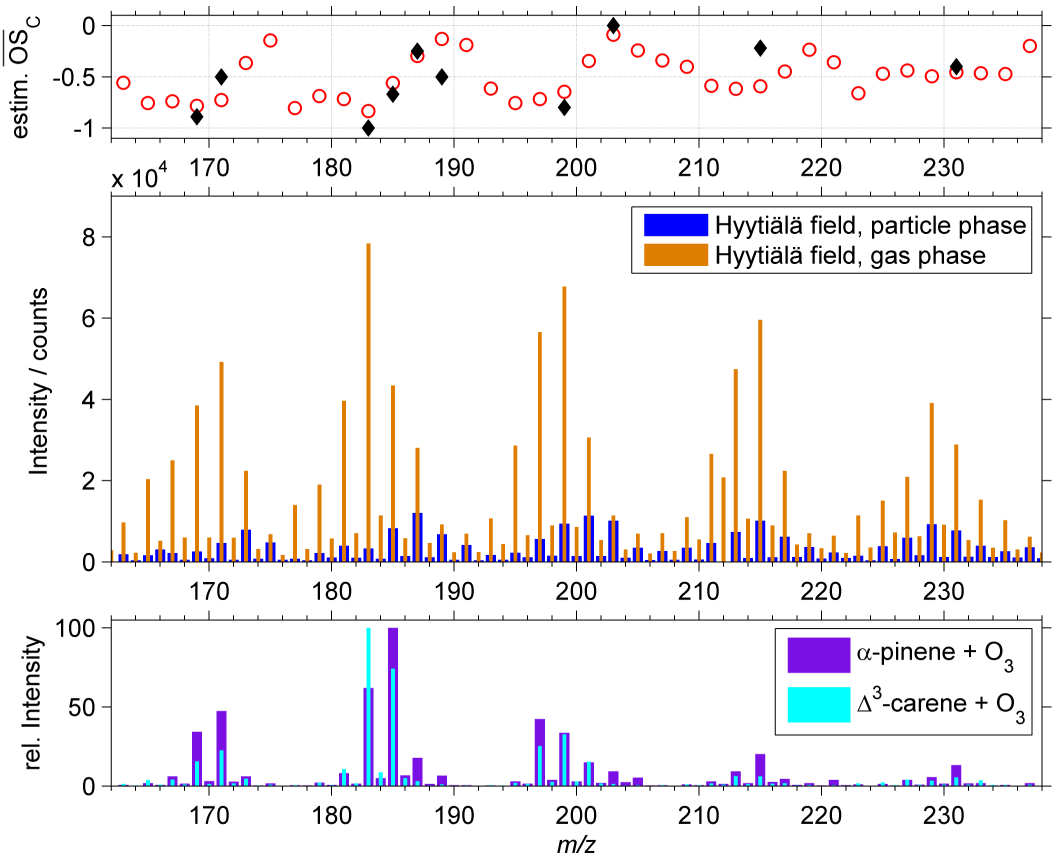

Figure 3.4 Top panel: Estimated average oxidation states (red circles) derived from oxidation states of literature terpenoid organic acids (black diamonds, see Table 3.1). Middle panel: Average spectrum of organic acids in the ambient air measured with APCI-IT-MS in the negative mode on day 207 (26 July 2010 12:00 – 15:00h (UTC+2)). Bottom panel: Average spectrum of laboratory dark ozonolysis experiments with α-pinene and Δ^3-carene.

The last observation can be explained by a different average carbon oxidation ($\overline{OS}_C$) state of the respective compounds in one peak cluster, meaning that the maximum gas phase compounds (e.g. all compounds on *m/z* 183) are on average less oxidized than the maximum particle phase compounds (e.g. all compounds on *m/z* 187). Since $\overline{OS}_C$ is strongly related to volatility, an approach to determine $\overline{OS}_C$ from the measured ratio between the particle- and the gas-phase signal (supplementary material) resulted in values between -1 and 0 (Figure 3.4, top panel). A clear repetitive character of an increasing oxidation state in the three peak clusters < *m/z* 206 can be seen. As it has recently been shown by ESI-UHRMS of filter samples from Hyytiälä, $\overline{OS}_C$ values of single compounds in ambient aerosol from Hyytiälä fall in the range between -1 and 1 (Kourtchev et al., 2013). To which extent highly oxidized compounds ($\overline{OS}_C$>0) contribute to the total aerosol mass and how those compounds are formed, needs to be investigated in future measurements.

Table 3.1 Considered literature organic acids for the estimation of $\overline{OS_C}$

compound	elem. comp.	*m/z* ([M-H]$^-$)	$\overline{OS_C}$ [a]	PP/GP [b]	Reference
Norpinonic acid	$C_9H_{14}O_3$	169	-0.89	6.6e-2	Yu et al., 1998
Norpinic acid	$C_8H_{12}O_4$	171	-0.50	9.4e-2	Hoffmann et al., 1998
Pinonic acid	$C_{10}H_{16}O_3$	183	-1.00	4.2e-2	Yu et al., 1998
Pinic acid	$C_9H_{14}O_4$	185	-0.67	1.9e-1	Yu et al., 1998
2-hydroxyterpenylic acid	$C_8H_{12}O_5$	187	-0.25	4.3e-1	Claeys et al., 2009
Diaterpenylic acid	$C_8H_{14}O_5$	189	-0.50	7.4e-1	Claeys et al., 2009
10-hydroxypinonic acid	$C_{10}H_{16}O_4$	199	-0.80	1.4e-1	Glasius et al., 1999
MBTCA	$C_8H_{12}O_6$	203	0.00	8.8e-1	Szmigielski et al., 2007
Diaterebic acid acetate	$C_9H_{14}O_6$	217	-0.22	1.7e-1	Iinuma et al., 2009
Diaterpenylic acid acetate	$C_{10}H_{16}O_6$	231	-0.40	2.7e-1	Claeys et al., 2009

[a] after $\overline{OS_C} \approx 2O/C - H/C$ (Kroll et al., 2011)
[b] PP: particle phase, GP:gas phase, average signal measured during day 207 (26 July 2010 12:00 – 15:00h (UTC+2)) (see supp. mat. for estimation of avg. oxidation state of unattributed *m/z* ratios)

Comparison between the ambient gas phase spectrum (middle panel, Figure 3.4) and the Δ^3-carene- and α-pinene-ozonolysis spectrum (bottom panel, Figure 3.4), shows the same number of peak clusters and that the peak cluster in the *m/z* 180 to 190 region is the most dominant one. The spectral pattern of both monoterpene precursors in the laboratory (Δ^3-carene- and α-pinene) are similarly distributed, which can be explained by the fact that ozonolysis of different monoterpenes results in a highly similar product distribution (Glasius et al., 2000). Furthermore, it can be seen that the ambient gas-phase spectrum is more similar to the chamber spectrum than the ambient particle-phase spectrum. This is most probably because the aerosol in the chamber does not undergo the same degree of heterogeneous aging as the ambient aerosol.

Although the spectra comparison might suggests that single species cause one *m/z* signal, the main signals in the spectra cannot be attributed unambiguously to one certain compound. This is due to the possible presence of isobaric compounds, and thus we cannot state with certainty how much one compound contributes to one *m/z* signal. To give a concrete example: regarding only α-pinene oxidation, several different compounds are formed, which have the same molecular weight. E.g. the signal on *m/z* 185 can be assigned to *cis*-pinic acid ($C_9H_{14}O_4$). *Cis*-pinic acid is a main oxidation product of α-pinene and ß-pinene (Hoffmann et al., 1998; Yu et al., 1999; Glasius et al., 1999). In addition, other isobaric organic acids like 10-hydroxynorpinonic acid and 4-hydroxypinalic-3-acid, formed in the α-pinene/ozone reaction, can contribute to the signal *m/z* 185 as well (Yu et al., 1999; Jaoui and Kamens, 2003).

Other mono- and sesquiterpene precursors form isobaric products, all consisting of $C_9H_{14}O_4$ as well, and thus contributing to the *m/z* 185 signal:

1. Δ^3-carene forms 3-caric acid and OH-3-caralic acid (Yu et al., 1998; Ma et al., 2009),
2. limonene forms ketolimononic acid and limonic acid (Jaoui et al., 2006; Gomez-Gonzalez et al., 2012),
3. sabinene forms sabinic acid and hydroxy norsabinonic acid (Yu et al., 1999),
4. myrtenol forms 9-hydroxynorpinonic acid (Glasius et al., 1999),
5. ß-pinene forms homoterpenylic acid (Yasmeen et al., 2010),
6. ß-caryophyllene forms 2-(carboxymethyl)-3,3-dimethylcyclobutanecarboxylic acid (Alfarra et al., 2012).

In total this results in twelve possible isobaric species in SOA with the elemental composition of $C_9H_{14}O_4$, an indication of the complexity of the organic fraction of atmospheric aerosols even under relatively well defined boreal conditions with minor anthropogenic influences.

Furthermore, due to the unit mass resolution of the instrument used, it cannot be ruled out that other non-isomeric compounds contribute to the *m/z* 185 signal as well, e.g. undecanoic acid ($C_{11}H_{22}O_2$), or organic acids with the elemental composition of e.g. $C_{10}H_{18}O_3$ or $C_8H_{10}O_5$. However, Warnke et al. (2006) showed by HPLC-(−)ESI-MS of filter samples from Hyytiälä, that 3-caric acid and *cis*-pinic acid are the most abundant organic acids on *m/z* 185 in the particle phase of the boreal forest aerosol, which is in agreement with the previous assumption that α-pinene and Δ^3-carene are the major monoterpenoic precursors at Hyytiälä.

Despite of the similarity between ambient and laboratory SOA, some minor signals only appear in the ambient spectrum, e.g. *m/z* 177, *m/z* 191, *m/z* 193, *m/z* 207. To our knowledge organic acids of these molecular masses have neither been found in ambient filter samples nor have been predicted by chemical mechanism models. Either these signals are real, emerging from unstable compounds, which cannot be captured by filter measurements, or these signals are fragmentation or cluster artefacts generated during the online ionization process.

The ambient particle phase spectrum in Figure 3.4 (middle panel, blue bars) shows the strongest signals on *m/z* 173, *m/z* 187, *m/z* 201, *m/z* 215 and *m/z* 229 - a the regular pattern of Δ *m/z* 14 occurs. In the following discussion we want to focus on *m/z* 187, *m/z* 203 and *m/z* 231, since compounds with a molecular weight related to these *m/z* ratios have been described in the literature. As mentioned above, the higher partitioning of *m/z* 187 and *m/z* 203 to the particle phase when compared to *m/z* 183 and *m/z* 199 can be explained by a higher oxidation state. Compared to the rapid formation of first generation acids (*m/z* 183, e.g. *cis*-pinonic acid) in chamber experiments, further atmospheric oxidation towards higher oxidized compounds takes

minutes to hours. This is the reason why higher oxidized compounds are not observed in the SOA chamber spectrum as strong as in the ambient spectrum.

Claeys et al. (2009) reported the measurement of 2-hydroxyterpenylic acid (MW 188, $C_8H_{12}O_5$) which was present in ambient PM 2.5 filter samples from a mixed coniferous/ deciduous forest 12 km NE of Antwerp, Belgium. Since this compound is not very abundant in chamber generated α-pinene SOA, Claeys et al. suggested that it is formed via oxidation of the first generation terpenylic acid. The high signal in the particle phase at *m/z* 187 might suggest that the compounds contributing to this signal are less volatile than e.g. the dicarboxylic acid *cis*-pinic acid (*m/z* 185). However, 2-hydroxyterpenylic acid is most probably more volatile than *cis*-pinic acid as it possesses one carbon atom and one carboxylic acid group less. Another identified carboxylic acid that would appear at *m/z* 187 is ketolimonic acid ($C_8H_{12}O_5$), which consists also of one carbon atom less than *cis*-pinic acid, but which contains two carboxylic acid functional groups and one keto-function (Jaoui et al., 2006; Rossignol et al., 2012). Thus, ketolimonic acid is approximately one order of magnitude less volatile than *cis*-pinic acid and therefore might reasonably explain the high signal of *m/z* 187 in the particle phase. Furthermore, Yasmeen et al. (2011) suggested hydroxylated norpinic acid as a possible compound at *m/z* 187, however, unambiguous identification has not been made so far.

The signal *m/z* 203 can tentatively be assigned to the compound 3-methyl-1,2,3-butanetricarboxylic acid ($C_8H_{12}O_6$, MBTCA), which forms during aerosol aging by gas phase OH-radical induced oxidation of *cis*-pinonic acid (Szmigielski et al., 2007; Mueller et al., 2012). Kourtchev et al. (2008) measured MBTCA concentrations based on filter sampling/LC-MS measurements in the range from 1.6 to 99.3 ng/m³. The maximum value of *m/z* 203 during the HUMPPA-COPEC campaign was measured on day 210. This confirms that MBTCA can be regarded as an aerosol aging marker for biogenic SOA, since the backtrajectory on day 210 indicates several days of intensive photochemical aging over the boreal forest. MBTCA has a high O/C ratio (0.75) and is expected to partition almost completely to the particle phase. Nevertheless, a significant amount of *m/z* 203 was measured in the gas phase. Possible explanations for this observation are isobaric interference of other more volatile organic compounds (see chapter 3.3.3) and a biased partitioning due to an amorphous aerosol phase state (see chapter 3.3.5).

In chamber studies of α-pinene and limonene ozonolysis, the signal *m/z* 231 has been described by Warscheid and Hoffmann (2002), who suggest several highly oxidized products with the composition of $C_{10}H_{16}O_6$. Claeys et al., (2009) propose diaterpenylic acid acetate as a SOA tracer for α-pinene photooxidation, which has been measured in daytime PM 2.5 ambient aerosol. Diaterpenylic acid acetate has also been identified as an oxidation product of 1,8-cineol (Iinuma et al., 2009b).

To conclude this section, it is worth mentioning that the structural identification becomes more complex with increasing molecular mass and therefore it cannot be concluded with certainty which exact compound contributes to which extent to the total signal at a specific *m/z* ratio. However, having the possibility to perform in-situ MS^2 experiments of one selected *m/z* ratio, which can comprise several different compounds, enables identification of the fragmentation markers, and helps to elucidate the chemical structure of unknown compounds.

3.3.3 In-situ MS^2 measurements

Figure 3.5 shows the major neutral losses from four different *m/z* ratios measured in the gas and particle phase during the HUMPPA-COPEC 2010 campaign compared to the neutral losses of standard compounds of the same masses (*m/z* 167: vanillic acid, *m/z* 183: pinonic acid, *m/z* 185: pinic acid and *m/z* 203: MBTCA). The fragmentation was achieved by using the CID (*collision induced dissociation*) mode, which briefly means that the target molecules of one *m/z* ratio were isolated and subsequently fragmented by collisions with helium atoms inside the ion trap. The measurements were carried out on 22 July 2010 13:20-15:20h (UTC +2) - air masses during this period came from the south-west. The experimental setup did not allow for measuring the fragmentation pattern of particle phase compounds exclusively. MS^2-fragments with a relative intensity less than 10% (of the base peak) are attributed to the "other" bin. Specific fragments which can be attributed to structural elements were included despite low intensities (e.g. 15 Da loss due to a CH_3 radical cleavage). In the supplementary material all measured MS^2 raw spectra are depicted.

The difference between online MS^2 described here and offline MS^2 spectra after chromatographic separation is that the online technique generates fragments of all isobaric compounds present, whereas the offline technique generates fragments which can unambiguously be assigned to one compound (assuming a complete chromatographic separation). Yasmeen et al. (2011) recently published an overview of MS^n spectra of several terpenoic acids using HPLC-(−)ESI-MS^n measurements of filter extracts (selected isobaric compounds at *m/z* 183, *m/z* 185, *m/z* 187 and *m/z* 203). These spectra allow for unambiguous differentiation between different biogenic organic acids. Typically, organic acids show the neutral loss of water (18 Da) and CO_2 (44 Da) - which can be observed during both: online- and offline MS^2. However, other neutral losses which are more characteristic can help to confirm the identity of known compounds or support the structural elucidation of unknown compounds. In general, the MS^2-field spectra show many more fragments than during online MS^2-studies of terpene ozonolysis chamber experiments (Vogel et al., 2013) or after chromatographic separation (Yasmeen et al., 2011).

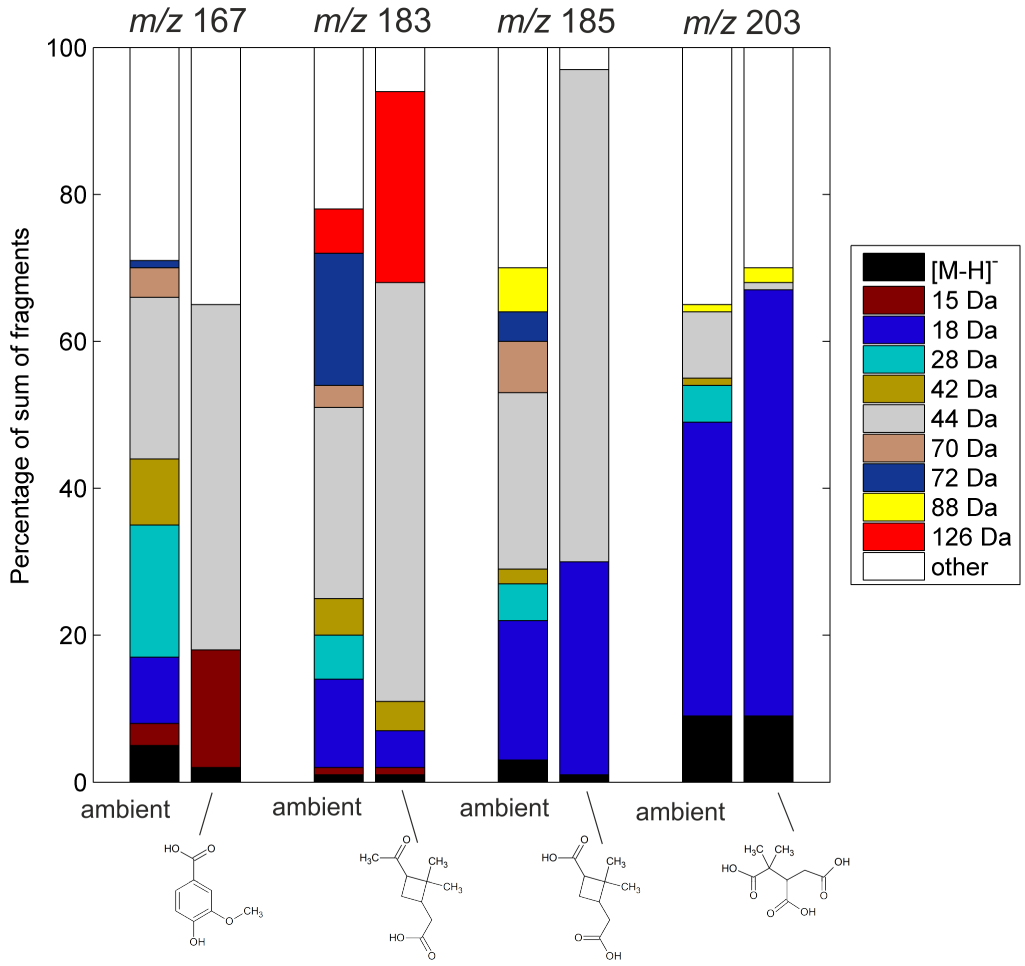

Figure 3.5 Neutral losses of four distinct *m/z* ratios during online MS^2 on 22 July 2010 13:20-15:20h (UTC +2) compared with MS^2-spectra of authentic standards of vanillic acid (*m/z* 167), *cis*-pinonic acid (*m/z* 183) and *cis*-pinic acid (*m/z* 185). The MS^2-spectrum of MBTCA (*m/z* 203) is taken from an ambient filter sample measured with ESI-MS^2 after chromatographic separation.

Among others, one organic acid which contributes to the signal at *m/z* 167 is vanillic acid ($C_8H_8O_4$). Vanillic acid has been described, among many other methoxyphenols, as a biomass burning tracer (Simoneit et al., 1993), which can be directly emitted during burning processes or formed through heterogeneous reaction of coniferyl alcohol and ozone (Net et al., 2011). Justesen (2001) reported that the loss of 15 Da during MS^2 is a common neutral loss from methoxy-phenolic structures and can be attributed to the cleavage of a CH_3-radical from the methoxy group. The standard MS^2-spectrum of vanillic acid shows a stronger loss of the 15 Da fragment, suggesting that other organic acids than vanillic acid contribute to the signal measured on *m/z* 167.

Offline MS^2 spectra of the compounds on *m/z* 183, *cis*-pinonic acid and *cis*-caronic acid, show that the strongest neutral loss is 44 Da and 72 Da, respectively (Yasmeen et al., 2011).

Both neutral losses are observed in the online-MS^2 spectrum, especially the loss of 72 Da contributes substantially, compared to the fragmentation pattern of other *m/z* ratios. However, the 72 Da fragment does not occur in the standard MS^2 spectrum of *cis*-pinonic acid, supporting the fact that the 72 Da fragment originates from *cis*-caronic acid. This indicates a high abundance of *cis*-caronic acid in the ambient aerosol. Furthermore, Yasmeen et al. did show by MS^3 analysis of the fragment ions *m/z* 139 and *m/z* 111 that the strongest ion formed from both acids was measured on *m/z* 57. This signal appears in the online measurements already during MS^2 (loss of 126 Da). This particular fragment was not measured at other *m/z* ratios and therefore can be regarded as an unambiguous marker fragment for the identification of *cis*-pinonic and *cis*-caronic acid. The neutral loss of 28 Da in the field experiment has not been described in the literature-possible fragments are CO or C_2H_4. The authentic standard *cis*-pinonic acid shows a small signal of the neutral loss of 15 Da, however, a reasonable fragmentation scheme explaining this fragment would be speculative.

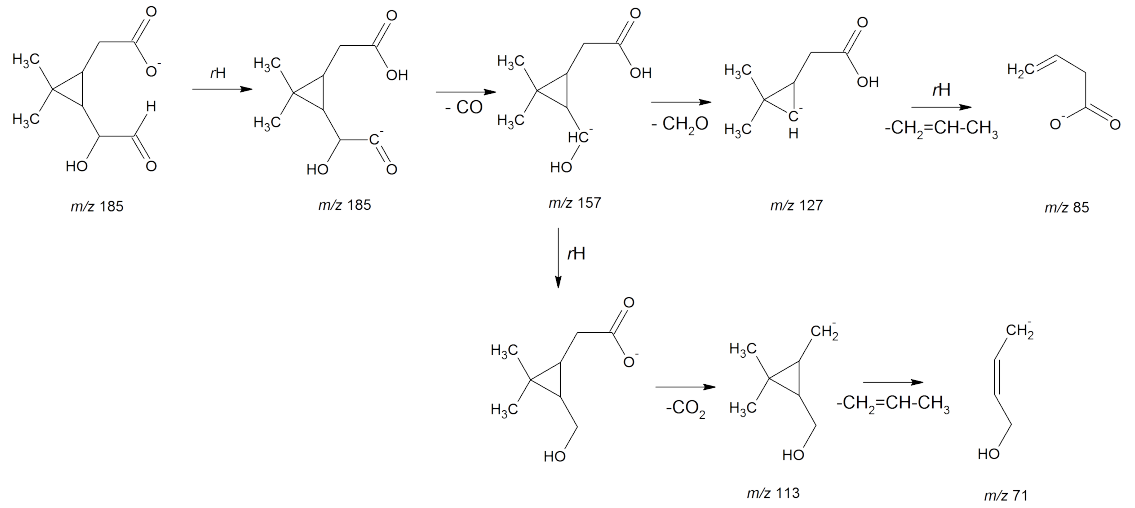

Figure 3.6 Proposed MS^2 fragmentation mechanism of OH-3-caralic acid.

The most pronounced neutral losses of *m/z* 185 are 18 Da and 44 Da. Furthermore, the MS^2 pattern shows a strong ion signal at *m/z* 97 (loss of 88 Da) which can be regarded as an evidence for a dicarboxylic acid (cleavage of 2 CO_2). This seems reasonable since *cis*-pinic acid, *cis*-caric acid and limonic acid are dicarboxylic acids. Surprisingly, only limonic acid shows the signal *m/z* 97 in offline MS^2 (Yasmeen et al., 2011). As can be seen in Figure 3.5, the neutral losses of *cis*-pinic acid are mainly water and CO_2. However, another unique fragment in the ambient MS^2 appears on *m/z* 115 (neutral loss of 70 Da) – it can be observed online and offline. Yasmeen et al. suggested a McLafferty type rearrangement of ketolimononic acid resulting in the ion at *m/z* 115. This indicates that limonic acid and ketolimononic acid are significantly abundant in the ambient aerosol at Hyytiälä. The loss of a neutral 28 Da fragment from the molecular ion *m/z* 185 might

be attributed to CO, and therefore a possible indication for semialdehydes, e.g. 4-hydroxypinalic-3-acid (Jaoui and Kamens, 2003) or the Δ^3-carene derivative OH-3-caralic acid (Ma et al., 2009). Unfortunately, these compounds are not available commercially. One possible fragmentation mechanism of OH-3-caralic acid is proposed in Figure 3.6, giving an explanation for the neutral loss of 28 Da. All of the proposed fragments in Figure 3.6 can be found in the online MS^2 spectrum of *m/z* 185, some of them only at low intensities (see supplemental material for the MS^2 spectrum of *m/z* 185). If the semialdehydes partition to a high degree to the gas phase or if oxidation during filter sampling occurs, it can be explained why the neutral loss of 28 Da has up to now not been observed in MS^2 studies of ambient filter measurements.

The MS^2 fragmentation pattern of *m/z* 203 shows the strongest loss of water compared to the pattern of the other *m/z* ratios. Due to the lack of a MBTCA standard, the shown reference MS^2 spectrum refers to the measurement of an ambient filter after chromatographic separation. However, the spectra shown are consistent with the observations made by Yasmeen et al., where two different MW 204 compounds in ambient nighttime aerosol show the ion *m/z* 185 during MS^2. Offline MS^3 from MBTCA shows a weak signal on *m/z* 115 which corresponds to the loss of two carboxylic acid groups, which was also observed during the ambient online MS^2 measurement of *m/z* 203 (neutral loss of 88 Da). The loss of 28 Da indicates that further unidentified organic acids might contribute to the signal on *m/z* 203.

3.3.4 Average OA molecular weight

Since a soft ionization process is used, which in general generates molecular ions, it is obvious to use this information to determine the average molecular weight of the organic fraction $\overline{MW}_{om}$ in the particle phase. The average molecular weight is of particular importance for the calculation of gas-to-particle partitioning coefficients, as it was recently stressed by Pankow (2011).

The average molecular weight in the particulate phase can be described by the number average molecular weight $\overline{MW}_n$ (Eq. (3.1)), or the weight average molecular weight $\overline{MW}_w$ (Eq. (3.2)), where N_i is the number of molecules i (represented by the *m/z*-intensity) and M_i is the molecular mass of i (Kalberer et al., 2006).

$$\overline{MW}_n = \frac{\sum N_i M_i}{\sum N_i} \tag{3.1}$$

$$\overline{MW}_w = \frac{\sum N_i M_i^2}{\sum N_i M_i} \tag{3.2}$$

Figure 3.7 shows a negative ion mode spectrum of the particle phase signal (90 min average) during 29 July 2010 13:00-14:30 (UTC+2). In this particular spectrum the calculation of $\overline{MW}_n$ and $\overline{MW}_w$ results in 454 g mol^{-1} and 518 g mol^{-1}, respectively. It should be stressed that the figure is not representative for the campaign average, but it indicates that OA components can exceed 500 Da significantly in transported plumes from biomass burning events.

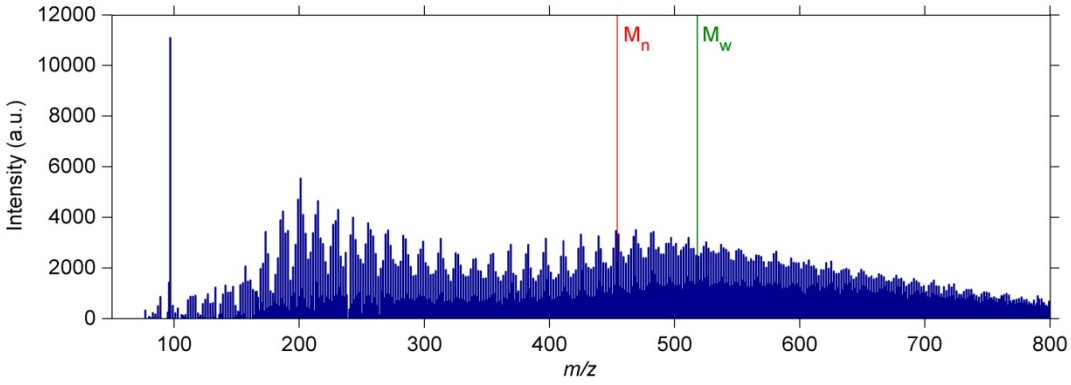

Figure 3.7 Average spectrum of compounds measured in the negative APCI mode on 29 July 2010 13:00-14:30 (UTC+2) during a period influenced by the severe biomass burning in central Russia. M_n is the number average molecular weight and M_w the weight average molecular weight.

Using Eq. (3.1) to calculate $\overline{MW}_{om}$ of each scan and averaging the values over the duration of the campaign results in $\overline{MW}_{om} \approx 300$ g mol^{-1}, which is on the upper end of the range described by Kiss et al. (2003). For simplicity, in the calculation of the campaign average $\overline{MW}_{om}$, the ideal case that all ions are singly charged, do not fragment and have similar ionization efficiencies was assumed. Furthermore, the calculation includes the assumption that the molar mass distribution of the ions, which are formed in the negative mode, is equal to the molar mass distribution of all compounds in the particle phase. The determination of $\overline{MW}_{om}$ using mass spectrometry can be seriously biased as is extensively discussed in the supplemental material. Nevertheless, Kiss et al. (2003) demonstrated by using two different techniques for the determination of $\overline{MW}_{om}$, namely electrospray ionization mass spectrometry and vapor pressure osmometry, that both techniques agree quite well with a slight shift towards lower values obtained with the MS method.

In previous field work by Williams et al. (2010) a $\overline{MW}_{om}$ of 220 g mol^{-1} was observed by using TAG (Thermal Desorption Aerosol Gas Chromatograph). Kalberer et al. (2006) observed $\overline{MW}_{om}$-values between 300 and 400 g mol^{-1} in a smog chamber experiment with isoprene and α-pinene by the use of MALDI-MS (Matrix Assisted Laser Desorption Ionization-MS). This shows that $\overline{MW}_{om}$ is on average variable in the range between 200 and 400 g mol^{-1}. Under exceptional circumstances (e.g. aged biomass burning aerosol) the average molecular weight can exceed this range.

3.3.5 Gas-to-particle partitioning of organic acids

The modelled gas-to-particle partitioning of three distinct biogenic organic acids, which are substantially different in their volatility, is represented by the solid lines in Figure 3.8. The organic acids in question are *cis*-pinonic acid, *cis*-pinic acid and MBTCA, which are first and second generation oxidation products from specific monoterpenes. Equation (3.3), based on the partitioning model of Liang and Pankow (1996), was used to calculate the fraction in particle phase $f_{p,i}$ of the compound i as a function of the mass concentration of absorptive particulate matter PM (µg m^{-3}) and the partitioning coefficient $K_{p,i}$ (m^3 µg^{-1}) of the compound i. To determine $f_{p,i}$ from the measurements, the signal of species i in the particle-phase F_i was divided by the sum of the gas-phase signal A_i and the particle-phase signal F_i:

$$f_{p,i} = \frac{K_{p,i}PM}{1 + K_{p,i}PM} = \frac{F_i}{F_i + A_i}. \tag{3.3}$$

The equilibrium partitioning coefficient $K_{p,i}$ (m^3 µg^{-1}) (Eq. (3.4); Pankow, 1994) depends on the fraction of PM that is organic matter f_{om}, on the temperature T (K), on the average molecular weight of the particulate organic matter $\overline{MW}_{om}$ (g mol^{-1}), on the activity coefficient γ_i (which describes the non-ideal particle-molecule interactions) and on the pure liquid vapour pressure $p^o_{L,i}$ (Torr) of the respective compound i. R is the gas constant, 760 a pressure conversion factor and 10^6 a mass conversion factor:

$$K_{p,i} = \frac{f_{om}760RT}{\overline{MW}_{om}\gamma_i p^o_{L,i}10^6}. \tag{3.4}$$

To model the gas-to-particle partitioning of the compounds *cis*-pinonic acid, *cis*-pinic acid and MBTCA, the partitioning coefficient of each compound($K_{p,PNOA}$, $K_{p,PNA}$, $K_{p,MBTCA}$) was calculated using Eq. (3.4) with the following parameters: the campaign average value f_{om}=0.64, T=294 K, $\overline{MW}_{om}$=300 g mol^{-1}, γ_i=1, and the predicted vapor pressure at 294 K (see Tab. 1) using the SIMPOL.1 group contribution method (Pankow and Asher, 2008). The organic matter factor f_{om} was determined by dividing the campaign average of OA (AMS-data) by the total aerosol mass incl. black carbon (AMS and Aethalometer). The resulting $K_{p,i}$ for the three acids are shown in Table 3.2 and represented by the solid lines in Figure 3.8. The C_i^*-value (µg m^{-3}) in Table 3.2 is the saturation concentration, which is the inverse of the partitioning coefficient $K_{p,i}$, both describing the volatility of the compound *i* in a mixture (Donahue et al., 2006).

Table 3.2 Modelled and measured partitioning coefficients of three distinct organic acids.

	***Cis*-Pinonic acid**	***Cis*-Pinic Acid**	**MBTCA**
$p_{L,i}^o$ (Torr)[a]	2.55 x 10^{-5}	4.28 x 10^{-7}	3.16 x 10^{-10}
$K_{p,i}$(m^3 µg^{-1})[b]	1.5 x 10^{-3}	9.1 x 10^{-2}	124
C^* (µg m^{-3})[b]	667	11	8.1 x 10^{-3}
	***m/z* 183 Hyytiälä**	***m/z* 185 Hyytiälä**	***m/z* 203 Hyytiälä**
$K_{p,i}$(m^3 µg^{-1})[c]	3.6 x 10^{-3}	1.1 x 10^{-2}	4.9 x 10^{-2}
C^* (µg m^{-3})[c]	278	91	20

[a] predicted by the SIMPOL.1 model at 294 K (Pankow and Asher, 2008).
[b] based on a, campaign average values of f_{om}=0.64 and $\overline{MW}_{om}$=300 g mol^{-1}, *T*=294 K and γ_i=1.
[c] campaign average fit using Eq. (3).

The online partitioning measurements of the related *m/z* ratios of the three acids are represented by one hour average points during the time when APCI-IT-MS and AMS were running simultaneously. The corresponding *PM* values are averaged in the same time intervals from AMS and Aethalometer data. All values below 0.7 µg m^{-3} were taken out due to uncertainty in the measurements. The resulting data points of each *m/z* ratio are fitted using Eq. (3.3). The resulting $K_{p,i}$ values are stated in Table 3.2 and the fit of the partitioning data is represented by the dotted lines in Figure 3.8.

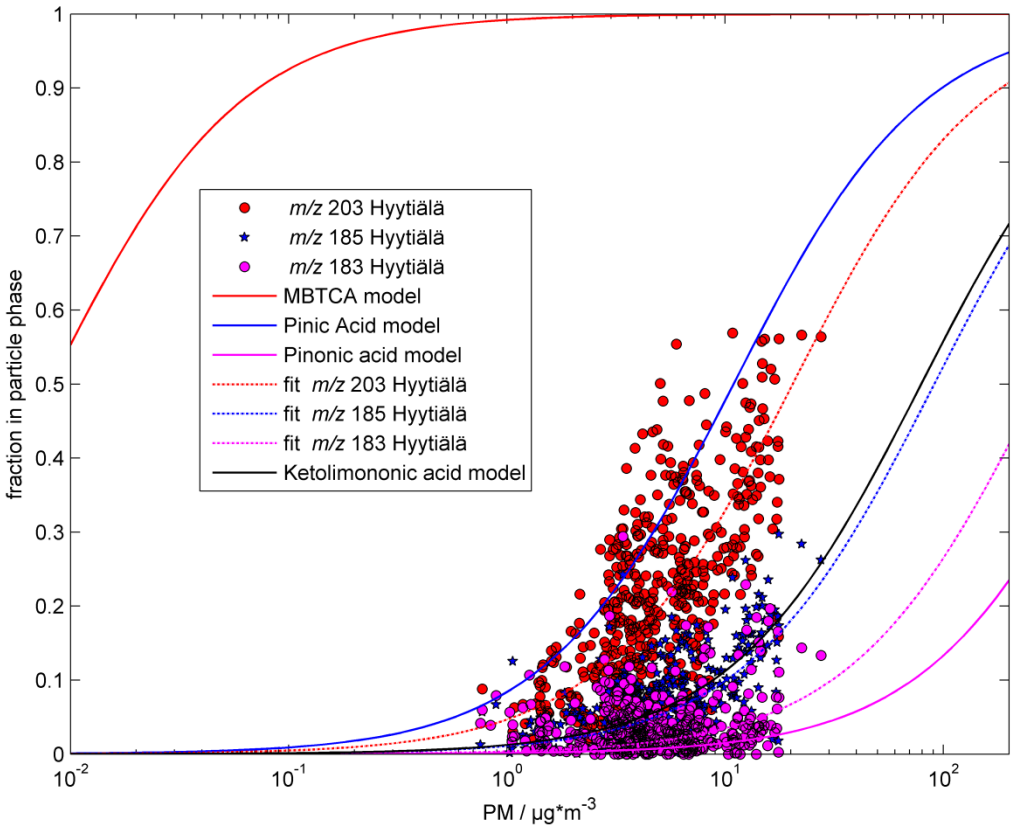

Figure 3.8 Modelled (solid lines) gas-to-particle partitioning of three distinct organic acids versus the measured (dashed lines) gas-to-particle partitioning of the respective *m/z* ratios. The model assumes instantaneous partitioning (liquid particle phase). The measured data points are averaged on an hourly basis. For clarity, separated *m/z* data points are shown in the supplementary material.

By comparing the model predictions with the measured *m/z* partitioning values, it can be seen that model and observation do show the same trend in volatility from the highest volatile *cis*-pinonic acid to the lowest volatile MBTCA. However, the huge offset between the partitioning model and the measurements (especially for *m/z* 203) does not necessarily mean that either the model or the measurement is wrong, because isobaric interference of more volatile compounds on the same *m/z* ratio can shift the measured partitioning significantly. For example, as it has been shown in chapter 3.3.3, the signal at *m/z* 185 does not only emerge from one acid. Predicting the vapor pressure for the *m/z* 185 ketolimononic acid at T=294 K results in $p^{o}_{L,KETOLMNOA}$ = 3.1 x 10^{-6} Torr, suggesting that ketolimononic acid is almost one order of magnitude more volatile than *cis*-pinic acid. The predicted partitioning of ketolimononic acid fits well to the observations at *m/z* 185 as it is shown by the black solid line in Figure 3.8. Thus,

isobaric interferences of organic species having different vapor pressures might be one explanation for the observed differences between model and measurements.

Furthermore, the model assumes that the particles are in a liquid state and that all of the particulate matter is involved in the partitioning and that equilibrium is reached very fast (instantaneous equilibrium). However, recent studies indicate that ambient particles can occur in a glassy or semi-solid state which implicates much slower diffusion exchange between the surface and the inner core of a particle (Virtanen et al., 2010; Shiraiwa et al., 2011). Therefore, the equilibration timescale of the partitioning of organic compounds between gas- and particle-phase has to be taken into account, since the assumption of instantaneous equilibration can lead to discrepancies in the mass distribution between gas- and particle-phase. Recently, Shiraiwa and Seinfeld (2012) demonstrated that the gas-to-particle partitioning of semi- and low-volatile compounds is far from equilibrium if the particle phase is in a semi-solid state. As a consequence, the instantaneous partitioning model underestimates the concentration of low-volatile compounds in the gas-phase by several orders of magnitude. In fact, our findings of unexpected high gas-phase concentrations can also be interpreted as experimental evidence that the aerosol during HUMPPA-COPEC was highly viscous and therefore the partitioning not nearly in equilibrium. We are aware of the fact that the application of a water based concentrator changes the gas-to-particle partitioning, however, the gas phase concentration was calculated as a lower limit estimate (see supplementary material) and thus the partitioning might be shifted even more towards the gas phase.

The observed scattering of the compounds around the fitted function in Figure 3.8 can be explained by a varying f_{om}-value. To illustrate the influence of f_{om} on the partitioning, Figure 3.9 shows the signals of *m/z* 203 (30 min average) including the respective color coded f_{om} value, which was measured by AMS (and Aethalometer for BC) simultaneously. Using Eq. (3.4) with f_{om} =0.3 to 1.0 based on the basis of the fit of all measured data points with $p^{o}_{L,m/z\,203}$=8.2 x 10^{-7} and f_{om}=0.64 (campaign average), shows that the broad distribution of the partitioning of one *m/z* ratio substantially depends on the f_{om} value, as it is predicted by the model.

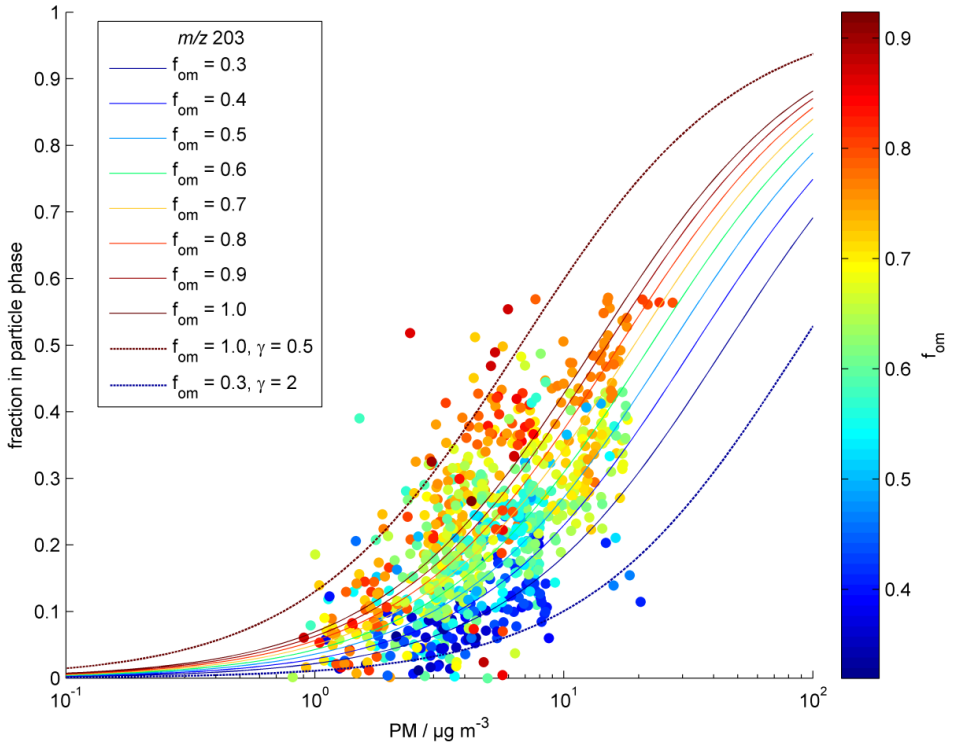

Figure 3.9 Measured gas-to-particle partitioning of *m/z* 203 with colour coded organic matter fraction. All modelled functions are based on the average fit of all data points with the average campaign of f_{om}=0.64 and γ=1. The measured data points are averaged on a basis of 30 minutes.

The remaining bias between model and observation can most probably be explained by non-unity γ_i-values. If the activity coefficients is larger than 1, the particle phase is forced to separate, due to e.g. non-solubility between polar and non-polar molecules. In turn, an activity coefficient < 1 tends to stabilize the particle phase due to intermolecular binding forces. As it can be seen in Figure 3.9, both phenomena can be observed. To explain the offset above f_{om}=1, it is assumed that the organic molecules are highly oxidized, so that they can build up strong intermolecular binding forces (hydrogen bonding). Thus, the activity coefficient becomes < 1 and the fraction in the particle phase increases. This is illustrated by the dashed red line which is based on f_{om}=1 and γ_i=0.5. The other case is that the activity coefficient > 1 describes destabilizing forces such as “salting out” effects, which results in a higher fraction in the gas-phase. The dashed blue line (f_{om}=0.3 and γ_i=2) shows this tendency pushing semi-volatile compounds into the gas phase.

3.4 Conclusions

The organic aerosol composition during the HUMPPA-COPEC 2010 boreal forest field study was presented with special attention towards the organic acid fraction. Good agreement between online APCI-IT-MS and AMS and offline FTIR measurements was achieved. AMS-PMF analysis indicated that the aerosol was highly oxidized, especially during the arrival of an aged biomass burning plume from the Russian wildfires. During this biomass burning plume, the soft ionization APCI-IT-MS measured high MW organic acids compounds up to 800 Da in the particle phase.

Comparison between laboratory experiments and ambient measurements showed that the chamber generated α-pinene and Δ^3-carene SOA is in terms of the mass spectral pattern more similar to the ambient gas-phase than to the ambient particle-phase, most probably due to aging processes of the particle phase in ambient air. Concerning the online identification of single organic acid species, it has been shown that a first step to overcome the problem of isobaric interference is utilizing the MS^2 technique, which can generate distinctive structural fragments. Unattributed MS^2 fragments indicate the existence of unidentified compounds in the ambient gas- and particle-phase at Hyytiälä. Applying this technique in future field studies for measuring MS^n of either gas- or particle-phase solely, can resolve how far isobaric compounds partition to a different extent between gas- and particle-phase due to different functionality / volatility. Further improvement of this technique can open up the possibility of unambiguous online identification and quantification of isobaric species in ambient organic aerosol.

It has been shown that the utilization of complementary online mass spectrometric techniques, such as the combination of APCI-IT-MS and AMS, enables to determine the gas- to particle-partitioning of specific *m/z* ratios at a high temporal resolution. It has been considered that, despite the abundance of unidentified compounds, the phase state (and thus the equilibration timescale) of aerosol particles might account for the high observed gas-phase concentrations of low volatile organic compounds. Therefore, in future campaigns it might be essential to measure the phase state of particles in order to study its effect on the partitioning of low volatile organic compounds.

Acknowledgements. ALV and TH gratefully acknowledge the Max Planck Institute for Chemistry in Mainz and the Max Planck Graduate Center for financial support and the possibility to participate in the HUMPPA-COPEC 2010 field campaign. Furthermore they acknowledge the support by the SMEAR II team during the campaign, Caroline Oehm and Ottmar Moehler of the Karlsruhe Institute of Technology for the loan of the PCVI and Horst Fischer and Rainer

Königstedt for the distribution of the CO data. ALC gratefully acknowledges support by the Department of Energy Office of Science Graduate Fellowship Program (DOE SCGF).

The entire HUMPPA-COPEC team is grateful for the support of the Hyytiälä site engineers and staff. Support of the European Community – Research Infrastructure Action under the FP6 "Structuring the European Research Area" Programme, EUSAAR Contract N° RII3-CT-2006-026140 is gratefully acknowledged.

The campaign measurements and analyses were supported by the ERC Grant ATMNUCLE (project No 227463), Academy of Finland Center of Excellence program (project No 1118615), The European Integrated project on Aerosol Cloud Climate and Air Quality Interactions EUCAARI (project No 036833-2), the EUSAAR TNA (project No 400586), and the IMECC TA (project No 4006261).

The authors gratefully acknowledge the NOAA Air Resources Laboratory (ARL) for the provision of the HYSPLIT transport and dispersion model and READY website (http://ready.arl.noaa.gov) used in this publication.

4 Resolving aerosol chemistry by complementary mass spectrometric techniques

This chapter is a reprint of the manuscript:

A. L. Vogel, J. Schneider, C. Müller-Tautges, G. J. Phillips, M. Krüger, D. Rose, U. Makkonen, H. Hakola, J. Crowley, U. Pöschl, and T. Hoffmann

Aerosol chemistry resolved by mass spectrometry-insights into ambient new particle formation and CCN activity of organic aerosols

in preparation (**2014**).

Abstract. The prediction of the number concentration and physico-chemical properties of atmospheric aerosol particles is a current scientific challenge in atmospheric science that requires knowledge of the underlying physical processes and the involved chemical compounds. In this work, we used different complementary online mass spectrometric techniques, such as atmospheric pressure chemical ionization (APCI) mass spectrometry (MS) and electron impact ionization (EI) aerosol mass spectrometry (AMS) to precisely measure submicron aerosol composition at a rural mountaintop research station in central Germany. During a new particle formation (NPF) event, the online APCI-MS detected signals of compounds with molecular masses >250 Da. The analysis of co-located filter samples by liquid chromatography (LC) coupled to ultrahigh resolution mass spectrometry (UHRMS) revealed that several signals can be attributed to sesquiterpene oxidation products (e.g. $C_{15}H_{24}O_5$). Those compounds might be important players in the initial particle growth and thus in the competition between growth and loss due to coagulation of particles. Furthermore, the comparison between total submicron sulfate and purely inorganic sulfate measured by AMS and ion chromatography, respectively, indicated that occasionally inorganic sulfate accounts only for ~70% of the total sulfate. This led us to the conclusion that ~30% of the sulfate is bonded to organic molecules. Simultaneous online APCI-MS and filter LC-UHRMS measurements confirmed the significant presence of several organosulfates (OS) and nitrooxy organosulfates (NOS). The MS based analysis together with co-located CCN (cloud condensation nuclei) counter measurements allowed us to observe that freshly formed aerosol particles and the bonding of sulfate to organic molecules leads to significantly reduced hygroscopicity (κ), compared to κ-values that would be expected from the organic fraction determined by AMS, solely.

4.1 Introduction

One of the major uncertainties in global climate models is the role of aerosol particles, caused by their high spatial and temporal variation throughout the atmosphere (IPCC, 2013). The ability of aerosol particles to indirectly influence the radiative budget of the planet by acting as cloud condensation nuclei (CCN) requires insight into their sources, properties and transformation processes (Andreae and Rosenfeld, 2008; Hallquist et al., 2009). It has been shown that throughout the northern hemisphere, the organic fraction of submicron particles accounts for 20-90% (Zhang et al., 2007) and that most of the particulate organic compounds are secondary in nature (Jimenez et al., 2009). The highly diverse composition of the aerosols organic fraction (Goldstein and Galbally, 2007) might conceal important interactions between the chemistry and physico-chemical properties of submicron particles. It has been demonstrated that the size of aerosol particles greatly affects their CCN ability (Dusek et al., 2006). However, there

is strong evidence that the growth of particles to atmospherically relevant sizes is dominated by organic compounds (Riipinen et al., 2012), but the underlying chemistry responsible for the growth remains poorly elucidated.

Thanks to emerging analytical techniques, such as chemical ionization mass spectrometry (CI-MS), that face the challenge of resolving the chemical complexity of the organic aerosol (OA) fraction at low concentrations and high temporal resolution (Aljawhary et al., 2013; Lopez-Hilfiker et al., 2013; Vogel et al., 2013a; Yatavelli et al., 2012; Holzinger et al., 2010), a more detailed analysis of aerosol particles becomes feasible. Such elaborate analysis is necessary since submicron OA cannot be regarded as one chemical class with uniform properties. Chemical transformation of the organic fraction, also known as aging, can significantly alter the aerosols physical and physico-chemical properties on short timescales. Oxidative aging processes can occur in form of fragmentation, functionalization or oligomerization processes, of which the two latter ones result in increasing aerosol mass (Kroll et al., 2011).

Aging processes appear to be highly diverse with regard to the phase where they take place: Aging can occur due to reactive uptake of gaseous oxidants (heterogeneous aging) (Shilling et al., 2007; George et al., 2007; Kessler et al., 2012; Zeng et al., 2013), due to repartitioning following gas phase oxidation of semi-volatiles (condensational aging) (Robinson et al., 2007; Donahue et al., 2012a; Tkacik et al., 2012; Iinuma et al., 2013) or due to condensed phase chemistry such as oligomerization or organosulfate formation (homogeneous aging) ((Kalberer et al., 2004; Offenberg et al., 2006; Mueller et al., 2008; Surratt et al., 2008; Ma et al., 2012). However, the atmospheric implication such as the ultimate impact of different aging processes on the CCN ability of submicron particles remains highly uncertain.

What has been demonstrated is that the organic mass fraction measured by Aerodyne´s aerosol mass spectrometer (AMS) can be used to approximate the effective aerosol particle hygroscopicity (e.g., Gunthe et al., 2011; Rose et al., 2011). Field measurement also have demonstrated that particles show a reduced hygroscopicity and thus CCN efficiency during new particle formation (Wiedensohler et al., 2009; Dusek et al., 2010) or during summer time along with higher amounts of fresh organic emissions (Asmi et al., 2012), both indicating that oxidative aging of organic precursors has an important effect on the particle hygroscopicity. Unfortunately, AMS measurements barely account for the chemical complexity of the organic fraction, such as the differentiation between inorganic sulfate and sulfate emerging from organosulfates (OS) (Liggio and Li, 2006; Farmer et al., 2010). Thus, due to the occurrence of organosulfates, measurements are not only biased regarding the ratio between the inorganic and organic fraction. Also the O/C ratio, which is often used to parameterize the hygroscopicity of the organic fraction (e.g. Chang et al., 2010; Lambe et al., 2011), would be systematically underestimated. Evidence for the ubiquitous abundance of OS and nitrooxy organosulfates (NOS) has been provided in a

variety of studies using different measurement techniques (Romero and Oehme, 2005; Reemtsma et al., 2006; Surratt et al., 2007; Surratt et al., 2008; Iinuma et al., 2007; Kristensen and Glasius, 2011; Gomez-Gonzalez et al., 2012). Quantification of the contribution of organosulfates to the total organic matter (OM) is a current challenge- average contributions vary between 5 to 10% (Tolocka and Turpin, 2012), and upper-bound estimations amount up to 30% or 50% (Surratt et al., 2008; Lukacs et al., 2009). Isoprene derived OS were detected also by online-MS techniques in the free troposphere (Froyd et al., 2010) and in the south-eastern US (Hatch et al., 2011a). Hatch and co-workers also have shown a strong diurnal cycle of the OS concentrations (Hatch et al., 2011b), suggesting that different chemical pathways might be involved in the formation (e.g. Lin et al., 2012 and references therein) and that meteorological conditions show a strong influence on the concentration levels.

The objective of this work was to characterize the ambient organic aerosol fraction at a rural mountaintop station using state-of-the-art analytical techniques. We used two complementary online aerosol mass spectrometers, the AMS measuring the aerosol inorganic and organic fraction and a chemical ionization mass spectrometer operating at atmospheric pressure (APCI-MS) for measuring organic species which are ionized in the negative mode- both providing a high measurement frequency. The APCI-MS technique allowed for measuring the extent of aging by the ratio of two secondary biogenic organic acids. Semi-online ion chromatography was applied for measuring the total inorganic sulfate to identify periods with organosulfates present and to quantify the fraction of sulfate originating from organosulfates. Unambiguous determination of the elemental composition of organic species (organic acids, organosulfates and nitrooxy organosulfates) was achieved by the analysis of co-located filter samples using ultrahigh performance liquid chromatography coupled to electrospray ionization ultrahigh resolution mass spectrometry (UHPLC-ESI-UHRMS). Simultaneously, the effective particle hygroscopicity was measured using a CCN counter in order to assess the relevance of particle age and chemical composition on the cloud formation ability of submicron aerosol particles.

4.2 Experimental

4.2.1 Field site description

Measurements were conducted during the INUIT-TO campaign at the rural mountaintop research station at Mt. Kleiner Feldberg, located in central Germany (Taunus Observatorium, 826 m a.s.l., operated by the Goethe-University/Frankfurt) in August 2012. The surrounding area is dominated by Norway spruce, the large scale area to the north-west dominated by mixed

forests and agricultural lands. To the north-west, the area is sparsely populated, whereas in the south to south-east the heavily populated Rhine-Main area with the cities Frankfurt, Wiesbaden and Mainz lies in a distance of approximately 30 km.

All measurements were arranged closely with the inlets at the same altitude and at a distance of <10 m (Fig. S4.1) Exhausts of pumps were, after filtering and leading through activated charcoal, released together in a ~20 m long and flexible tube towards the downwind side.

4.2.2 Online (−)APCI-MS

The setup of the online APCI-MS in conjunction with an aerosol concentrator (Geller 2005) is described in detail by Vogel et al. (2013). Briefly the APCI-MS vaporizes an aerosol particle stream in a heated ceramic tube (350 °C) and subsequent capillary discharge produces O_2^--ions which act as the chemical ionization reagent for the vaporized compounds. Molecules which have a higher gas phase acidity than O_2^- (e.g. organic acids, organosulfates) become ionized by proton transfer. The ionization is carried out at atmospheric pressure, thus the preservation of the chemical structure of the analytes is achieved by the chemical ionization process and by collisional stabilization.

Different to the described setup by Vogel et al. (2013), in this work the HEPA-filter/valve setup between the concentrator and the APCI-MS was replaced by a charcoal denuder in order to remove gaseous species (see Fig. S4.2). This procedure enables to measure more precisely during low particle concentrations. Furthermore, 1 LPM of sheath air (Synthetic air, Westfalen) was added to the ion source and the capillary temperature was set to 100 °C. Blank values were measured daily by manually plugging a HEPA filter in front of the concentrator. The mean signal height on each mass-to-charge ratio (*m/z*) during the blank filter intervals were linearly interpolated and subtracted from the measured signal. Mass spectra were aquired between *m/z* 80 and *m/z* 500 and 200 micro scans were averaged into one recorded spectrum resulting in a measurement frequency of approximately one mass spectrum per minute.

4.2.3 Offline UHPLC/(−)ESI-UHRMS/ data analysis

PTFE-coated quartz fibre filters (Pallflex T60A20, Pall Life Science, USA) were used for sampling the excess PM 2.5 inlet air flow (~27.5 LPM) between 6 and 30 hours throughout the campaign (Fig. S4.2). The filters were stored in glass vials at -18 °C until analysis. A field blank sample was collected by placing a filter in the filter holder at the field site for approximately half an hour without sample flow and applying the same extraction and analysis procedure in the

laboratory. Depending on the sampled volume, one quarter or a half of the filter was cut into small pieces and extracted with 1.5 mL methanol (HPLC grade) using a vortex shaker for 30 min. The extraction step was repeated twice with 1 mL of methanol and the combined extracts were evaporated to dryness under a gentle stream of nitrogen at 30°C. The residue was dissolved in 10% methanol solution and directly measured by LC-MS in order to avoid esterification reactions.

The measurements were carried out using an UHPLC system (Dionex UltiMate 3000, Thermo Scientific, Germany) with a Hypersil Gold column (C18, 50 x 2.0 mm, 1.9 µm particle size, Thermo Scientific). During the measurements the auto sampler temperature was set to 20 °C, the column compartment temperature was 25 °C. Eluent A (ultrapure water with 2% acetonitrile and 0.04% formic acid) and B (acetonitrile with 2% ultrapure water) were used in gradient mode with a flow rate of 500 µL/min. The optimized gradient was 1% B at 0 min, 1 % B at 1 min, 20 % B at 2 min, 20 % B at 5 min, 30 % B at 6 min, 50 % B at 7 min, 99 % B at 7.5 min and 99% B at 8 min. The injection volume was 10 µL per run and each filter extract was measured in triplicate.

High resolution mass spectra were obtained using a Q-Exactive mass spectrometer (Thermo Scientific, Germany) equipped with a HESI (heated electrospray ionization) ion source at 120 °C. The HESI source was operated in negative ion mode with 60 psi sheath gas, 20 psi aux gas (both nitrogen), 320 °C capillary temperature and -3.3 kV spray voltage. The full-MS mode was used with a scan range of *m/z* 80 – 500 and a resolution setting of R=70000 at *m/z* 200. Mass calibration was carried out using the Pierce ESI Negative Calibration Solution with additional 4-hydroxybutanoic-acid to calibrate for masses smaller than 250 Da.

The resulting data were analysed by the non-target screening approach using a commercially available software (SIEVE®, Thermo Scientific). A threshold value of 1e5 counts in the two dimensional space of retention time 0.7 – 7 min vs. *m/z* 80 to 500 of the LC-MS analysis of all filter samples was applied. The software automatically searches for peaks above the threshold value which are significantly different from the blank chromatogram. Furthermore, it assigns signals emerging from isotopes and ion-clusters by the same retention time and exact mass difference to the molecular ion compound. To the resulting list of the exact masses at a certain retention time, the elemental composition was assigned by XCalibur 2.2 (Thermo Scientific) using the following constraints: #^{12}C: 1 to 45, #^{1}H: 1 to 60, #^{14}N: 0 to 10, #^{16}O: 2 to 45, #^{31}P: 0 to 2, #^{32}S: 0 to 4 and #^{35}Cl: 0 to 2 and a mass tolerance of ±2 ppm. Resulting neutral formulas with a non-integer or negative double bond equivalent (DBE) were removed. Chemically unreasonable molecules involving several heteroatoms in one molecular formula or chemically impossible O/C and H/C-ratios were sorted out as well. Additionally, the abundance and intensity height of the ^{13}C isotopic peak was checked to finally verify the elemental composition

attribution. Due to low intensities on filter #5, which was sampled during a nucleation event, particular *m/z* ratios of the LC-MS data were analysed manually.

4.2.4 Aerosol Mass Spectrometer (AMS)

The submicron mass concentrations and size distributions of nonrefractory particulate organic matter ('organics'), sulphate ('SO_4'), nitrate ('NO_3'), ammonium ('NH_4'), and chloride ('Chl') were measured with a C-ToF-AMS (compact time-of-flight aerosol mass spectrometer; Drewnick et al., 2005). The C-ToF-AMS was connected to a PM1 inlet sampling approximately 2 m above the roof of the upper container (10 m above ground level). The particle size measurement was calibrated using PSL particles at the beginning of the campaign, the ionization efficiency (IE) was calibrated twice during the campaign with 400 and 450 nm NH_4NO_3 particles, the relative ionization efficiency for sulfate was additionally calibrated with $(NH_4)_2SO_4$ particles (RIE_NH_4 = 4.14, RIE_SO_4 = 0.47). Comparison of the total mass concentration measured by the AMS added to the black carbon concentration measured by a MAAP to a PM1 measurement (Grimm EDM) yielded a collection efficiency (CE) of unity.

4.2.5 Monitor for Aerosols and Gases in Ambient Air (MARGA)

The MARGA system (Rumsey et al., 2013) is a commercialized version of the GRAEGOR analyser developed by ECN, Netherlands (Brink et al., 2009; Thomas et al., 2009), and produced by Metrohm Applikon BV, Netherlands. The instrument was deployed inside a ventilated metal cabinet on the roof of the observatory. The methodology and instrument description is contained in references above and so a brief description of the method follows. The air sample was drawn, at 1 m^3 h^{-1}, through a short, <25 cm length of high density polyethylene (HDPE) tube, through Teflon coated PM10 cutoff cyclone into a wet rotating denuder (WRD). The WRD consists of two concentric glass tubes wetted with IC grade water. The gases are efficiently denuded in the WRD, but the low mobility of particles prevents them from diffusing to the walls of the WRD (Wyers et al., 1993). The air sample then enters the steam-jet aerosol collector (SJAC) (Khlystov et al., 1995) where the water soluble particle fraction is condensed using steam and collected. The samples from both the WRD and SJAC are analyzed online every hour using both cation and anion chromatography ion chromatography. The MARGA system commonly reports gas-phase and particle-phase ammonium, calcium, sodium, magnesium, nitrate, nitrite, chloride and sulfate. From concentrations of the ions, concentrations of ambient components may be inferred, e.g. HCl from the gas-phase chloride signal. In some cases the analytical ion may result from more

than one ambient species and care must be taken when interpreting MARGA signals (Phillips et al., 2013), e.g. N_2O_5 and HNO_3 can give rise to NO_3^- in the gas-phase as measured during INUIT-TO. The detection system is continuously calibrated by the use of an internal standard of LiBr. In addition, before starting the ambient measurements standard solutions were injected to check the retention times and the analytical system. The MARGA system measures very reactive analytes and therefore care must be taken with the inlet systems as significant losses of gases such as HNO_3 can occur. Our inlet system including cyclone were cleaned after approximately 2 weeks of operation.

4.2.6 CCN counter

The number concentration of CCN was measured using a continuous-flow streamwise thermal gradient CCN counter (CCNC), commercially available from Droplet Measurement Technologies, Inc. (DMT, CCN-100, Roberts and Nenes, 2005). The instrument was coupled to a Differential Mobility Analyzer (DMA, TSI 3071, selecting quasi-monodisperse aerosol) and to a condensation particle counter (CPC, TSI 3762, detecting the number concentration of aerosol particles (CN)) to measure size-resolved CCN efficiency spectra, i.e., the size-resolved fraction of activated particles at a certain water vapor supersaturation (Frank et al., 2006; Rose et al., 2008). The effective water vapor supersaturation (S) in the CCNC was alternately set to 0.1, 0.2, 0.3, 0.5 and 0.7%. It was calibrated regularly during the campaign with ammonium sulfate aerosol particles applying the method described in Rose et al. (2008) (using Köhler model AP3). The recorded CCN efficiency spectra (CCN/CN) were corrected for multiple charges, the DMA transfer function, and different counting efficiencies of the CCNC and the CPC (Frank et al., 2006; Rose et al., 2010). From the diameter at which the CCN efficiency spectrum at a certain S reaches half its maximum value (activation diameter D_a) the hygroscopicity parameter κ was calculated using Eq. 6 of Petters and Kreidenweis (2007). The κ parameter can be used to describe the influence of chemical composition on the CCN activity of aerosol particles. Its values reach from zero for completely insoluble materials like pure soot or mineral dust to 1.28 for sodium chloride aerosol. Typical values for organic aerosol and ammonium sulfate are κ ~ 0.1 and ~ 0.6, respectively (Petters and Kreidenweis, 2007; and references therein). On average, mixed aerosol of continental background tend to cluster around κ ~ 0.3 (e.g., Pöschl et al., 2009).

4.2.7 Mobile Laboratory (MoLa)

Additional particle, gas phase and meteorological measurements were performed by the mobile laboratory (MoLa) which is described in detail by Drewnick et al. (2012). Briefly, the particle size distribution between 6 and 560 nm (electrical mobility) was determined by a Fast Mobility Particle Sizer (FMPS, Model 3091, TSI Inc., USA). For the mass closure of the submicron particle population (see 4.2.4), the black carbon concentration was determined by a multi angle absorption photometer (MAAP, Thermo Electron Corp., USA) and the total PM 1 mass by an environmental dust monitor (EDM, Model EDM180, Grimm Aerosoltechnik, Germany). O_3, SO_2, CO and NO_x mixing ratios were recorded by the AirPointer (Recordum Messtechnik GmbH, Austria), meteorological parameters by a WXT520 (Vaisala, Finland) met station and the solar radiation by a CMP3 pyranometer (Campbell Scientific, Inc., UK).

4.3 Results and Discussion

4.3.1 Observation of ambient organic aerosol nucleating and aging

Simultaneously to the C-ToF-AMS measurements, the highly time resolved measurements of the APCI-MS are depicted in the upper panel of Figure 4.1. The particle concentration during the INUIT-TO 2012 campaign mass was strongly affected by the air mass history and meteorological conditions (e.g. strong decrease in number and mass after the passage of a cold front on 16 August 2012). From 22 August 2012 on, particle number and mass as well as ozone and temperature ranged at very low values, since the air masses were transported rapidly from the Atlantic.

4.3.1.1 Nucleation

It can very clearly be seen that several new particle formation (NPF) events occurred during the campaign. The most prominent NPF event on 16 August was triggered by a cold front (accompanied by precipitation) passing the station during the night. During the early stage of this particular NPF event, the organic aerosol concentration ranged around 300 ng m^{-3} (Figure 4.2). Meanwhile, the APCI-MS measured signals above background levels despite the low mass concentration. The mean intensity of the APCI-MS signal at mass/charge (*m/z*) 203 during the particle formation event is one order of magnitude higher than the background signal (the time when the aerosol was removed by a HEPA filter in front of the aerosol concentrator). The occurrence (although we cannot quantify the concentration) of *m/z* 203 during the nucleation is

surprising, since the most abundant compound at *m/z* 203 is the tricarboxylic acid MBTCA (Szmiegielski et al., 2007) which is an established aerosol aging marker. With an approximated vapor pressure of 2.7e-10 Torr (at 293.15 K) by the SIMPOL.1 model (Pankow and Asher, 2008) and the occurrence during NPF, this compound might substantially enhance the growth of freshly nucleated particles, especially because of its formation via gas phase oxidation of pinonic acid (Pierce et al., 2011; Donahue et al., 2012a).

The high signals, which were measured by the APCI-MS but not by the AMS around 11:00 h, are caused by super micron particles, corroborated by aerodynamic particle sizer (APS) measurements. In contrast to the AMS, the APCI-MS is not size selective, and thus measures the bulk composition of particles that pass the PM 2.5 pre-separator.

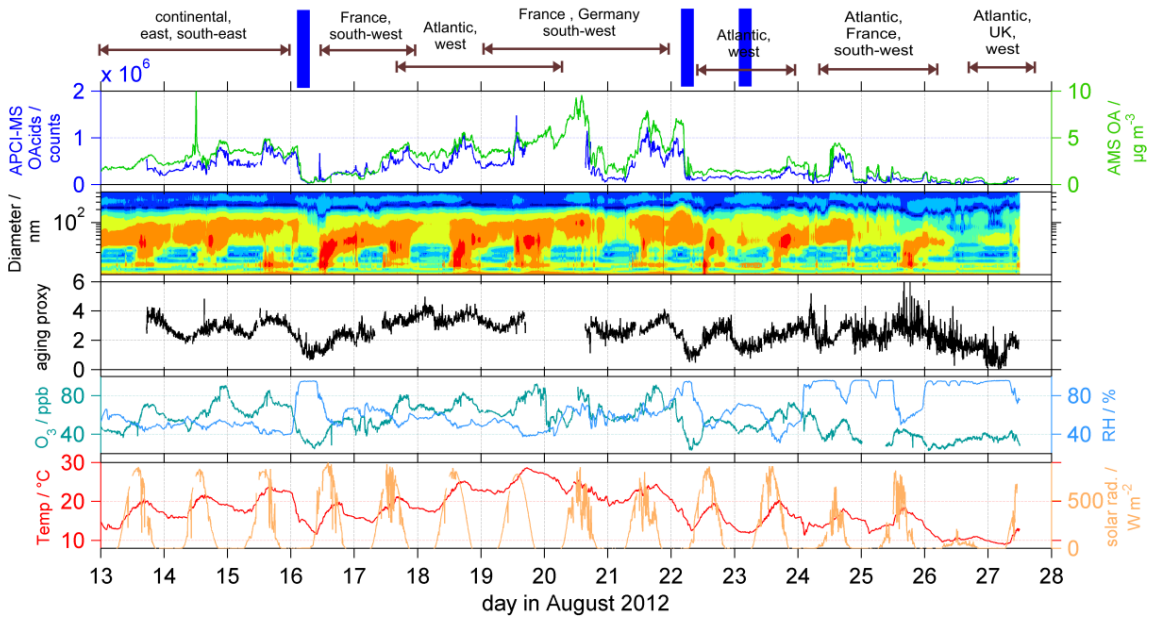

Figure 4.1 Temporal variation during the INUIT-TO 2012 campaign. The airmass histories were determined by the 96h backtrajectory analysis using the Hysplit model (Draxler and Rolph, 2013). Blue bars represent the passages of cold fronts. APCI-MS OAcids represents the PM 2.5 APCI-MS signals in the negative ionization mode (which is dominated by organic acids) between *m/z* 150 and *m/z* 500. AMS OA refers to the organic aerosol determined by C-ToF-AMS. The submicron aerosol size distribution was measured by a fast scanning mobility particle sizer (FMPS). The aging proxy is derived from the APCI-MS signal ratio *m/z* 203 / *m/z* 185 – a proxy for aging extent of secondary biogenic aerosol. Low values indicate fresh biogenic aerosol, whereas high values indicate high oxidative aging of biogenic aerosol.

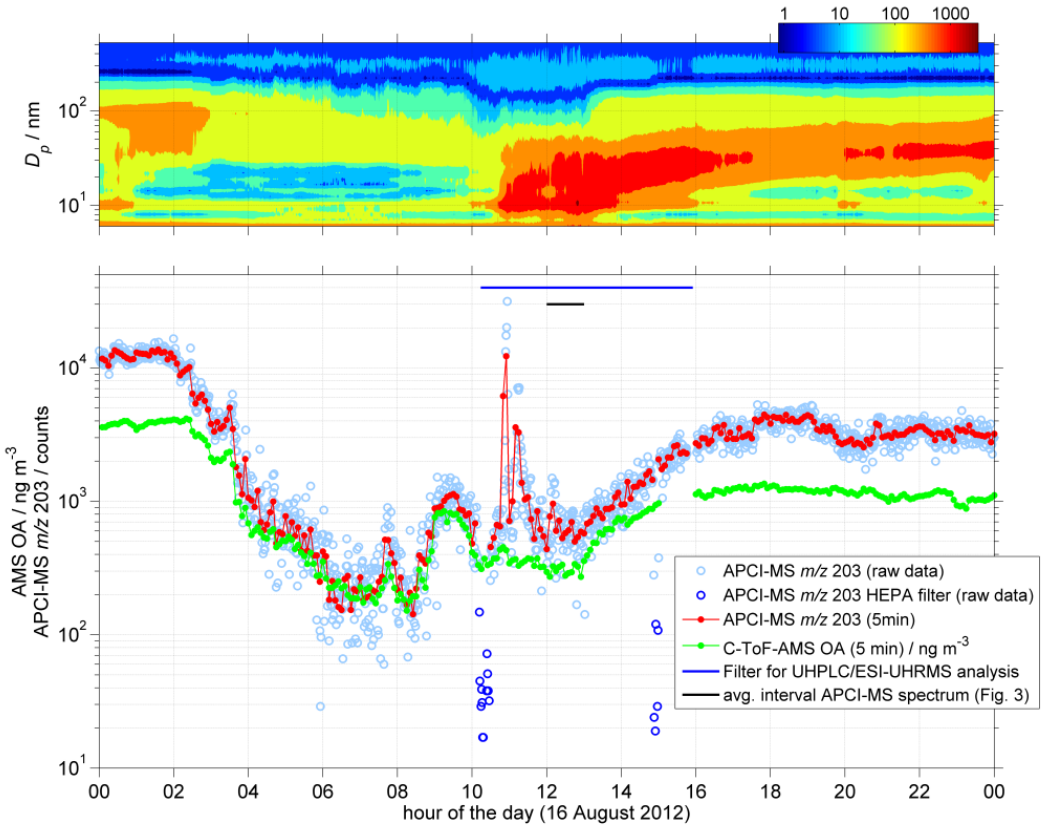

Figure 4.2 FMPS number size distribution, APCI-MS (*m/z* 203) and AMS signal variation during the new particle formation event on 16 August 2012. The raw data of the APCI-MS signal at *m/z* 203 are depicted as light blue circles. The dark blue circles represent the blank signals at *m/z* 203, when a HEPA filter was used to remove particles in front of the aerosol concentrator.

The average APCI-MS mass spectrum during the new particle formation event (average time 12:00 – 13:00 h, represented by the black bar in Figure 4.2) is compared to the average APCI-MS mass spectrum of the entire campaign (Figure 4.3 A). The signal intensitiy distribution of the campaign average spectrum shows a bimodal character. The base peak occurs at *m/z* 203 and the highest peak of the larger mode at *m/z* 299. During the new particle formation event, this bimodality cannot be observed- the base peak of the spectrum occurs at *m/z* 299. The disappearance of the mode at smaller *m/z* ratios between the two mass spectra can be explained by the partitioning theory (Pankow, 1994b), which implies that a species of a certain volatility partitions with increasing particle mass to a greater extent into the particle phase.

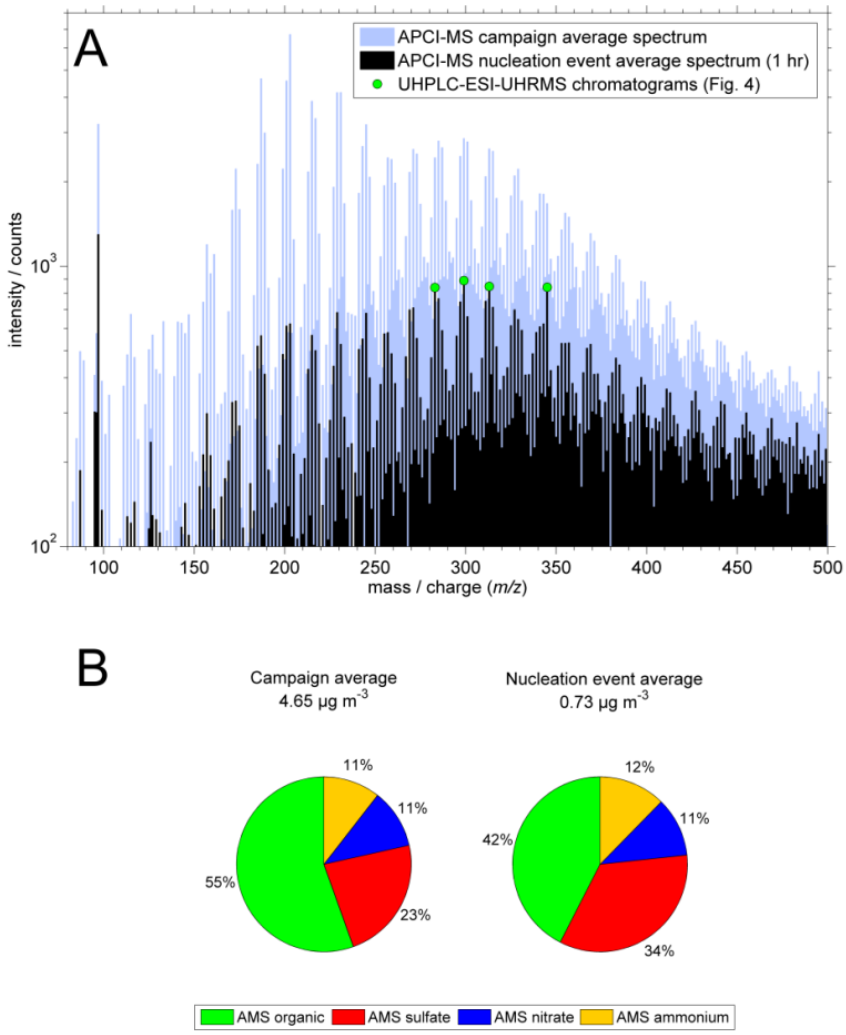

Figure 4.3 (A) The campaign average APCI-MS spectrum and a one hour average spectrum of the organic aerosol during the nucleation event on 16 August 2012. The green marked signals refer to the LC-UHRMS analysis (see Fig. 4.4) of the nucleation event filter (see Fig. 4.2). (B) Submicron aerosol composition during the campaign and the nucleation event measured by the C-ToF-AMS.

Volatility of organic molecules is, beside their functionalities, also affected by their molecular weight. Thus, it explains that the compounds of the smaller *m/z* mode are less present in the particle phase during nucleation due to their semi-volatile character. However, those compounds appear to be important for the growth of particles to larger sizes. AMS measurements also show that the organic fraction (Figure 4.3 B) during the nucleation event is lower compared to the campaign average- indicating that the growth of the particles is substantially driven by the condensation of organic compounds.

When using online CIMS techniques, one always has to keep in mind that signals can be caused by molecular ion clusters. To address this issue, a filter which was sampled for 6 hours solely during the nucleation event (Figure 4.2, blue bar) was analysed by LC-UHRMS in order to confirm the existence of the compounds. According to the four highest APCI-MS signals during the nucleation event (*m/z* 283, 299, 313 and 345), these nominal masses were checked for signals in the LC-MS analysis. The chromatogram of the accurate mass at *m/z* 283.1555 can be attributed to the elemental composition of $C_{15}H_{24}O_5$ (Figure 4.4 A). It shows the abundance of five isomers which seem to be partly hydrophobic due to the relatively long retention time on the reversed phase column. An oxidation compound of the sesquiterpene ß-caryophyllene on this accurate mass has been described by Chan et al. (2011), namely hydrated ß-oxocaryophyllonic acid. The abundance of five isomers suggests that different sesquiterpene precursors form similar oxidation products. The estimation of the vapor pressure of the hydrated ß-oxocaryophyllonic acid by the SIMPOL.1 model results in 3.9e-12 Torr (at 293.15 K), thus two orders of magnitude less volatile than the tricarboxylic acid MBTCA. This extremely low vapor pressure, combined with the high abundance in the mass spectrum during new particle formation, makes this compound an ideal candidate for the initial growth of sub-10-nm particles, possibly playing a crucial role (due to the different functional groups) in the stabilisation of nano-clusters.

The extracted ion chromatogram (EIC) of *m/z* 299.1502 is shown in Figure 4.4 B. Three distinct and chromatographically well resolved isomers can be observed. Although the intensities are very low, the peaks show a very low standard deviation and are significantly different from the field blank sample. According to the accurate mass, the elemental composition of the compounds at *m/z* 299.1502 can be determined with high certainty to $C_{15}H_{24}O_6$. As it was mentioned in the discussion of the *m/z* 283 compounds, an elemental composition with 15 carbon atoms suggests that the observed compounds are oxidation products of sesquiterpenes ($C_{15}H_{24}$). To our knowledge, a molecule consisting of the elemental composition $C_{15}H_{24}O_6$ has not been observed in ambient nor in laboratory generated secondary organic aerosol so far. Since the LC-MS analysis was conducted in the negative ESI-mode, this compound should contain at least one carboxylic acid functional group. If we assume that the remaining oxygen atoms are due to two hydroxyl- and two keto-functional groups (similar to the hydrated ß-oxocaryophyllonic acid), the SIMPOL.1 model predicts an equilibrium vapor pressure of 1.7e-13 Torr (at 293.15 K).

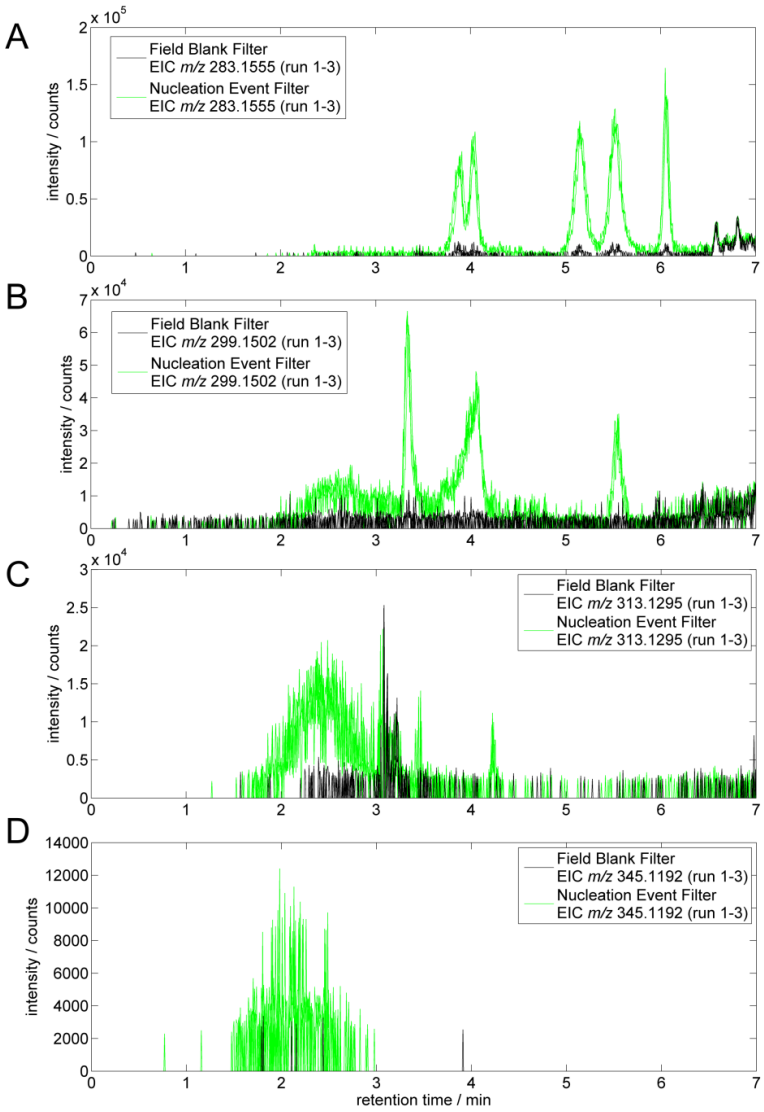

Figure 4.4 Extracted Ion Chromatogramss (EIC / ± 5 ppm) of the most significant abundant exact masses on the depicted nominal masses in Figure 4.3 (*m/z* 283, 299, 313 and 345). The exact mass of 283.1555 refers to the molecular formula $C_{15}H_{24}O_5$ (1.4 ppm), 299.1502 to $C_{15}H_{24}O_6$ (0.6 ppm), 313.1295 to $C_{15}H_{22}O_7$ (0.7 ppm) and 345.1192 to $C_{15}H_{22}O_9$ (0.3 ppm).

The two other marked high signals in the APCI-MS nucleation spectrum at *m/z* 313 and 345 do not reveal proper signals in the LC-MS analysis, although there is a broad enhancement in the exact mass traces of *m/z* 313.1295 and *m/z* 345.1192 compared to the field blank samples. These exact masses would refer to the elemental composition of $C_{15}H_{22}O_7$ and $C_{15}H_{22}O_9$, respectively. One can imagine that the further incorporated oxygen is associated with a further reduction of the vapor pressure and the presence of additional functional groups. Together with the high abundance during the nucleation event measured by online APCI-MS, it can be concluded that these observations are a strong evidence for the participation of sesquiterpene oxidation products

in the initial growth of newly formed particles in a rural forested site in central Germany during summertime.

4.3.1.2 Aging

Considering once again the achievement by the APCI-MS to measure signals on individual *m/z* ratios throughout the campaign well above background levels, it opens up the possibility to measure a new proxy of the aging state of biogenic organic aerosol (middle panel Figure 4.1). This proxy is the ratio of two organic acids: the aging marker MBTCA (*m/z* 203) divided by the first generation pinic acid (PA, *m/z* 185). It was first described by Müller and Hoffmann (unpublished results) along with APCI-MS aging studies of α-pinene SOA at the large ambient photo-oxidation chamber SAPHIR at Jülich, Germany. This proxy is especially suited for measuring the extent of biogenic aerosol oxidation as these two acids emerge from monoterpene oxidation. During the chamber experiment at Jülich, it was observed that the ratio steadily increased during photochemical oxidation of α-pinene SOA, however, even after the two days of aging in the chamber, the ratio was below unity. Such low values were not observed during the entire field campaign, which indicates that chamber oxidation barely accounts for the oxidative potential in ambient air. In principal, the ratio of those two acids can be determined by filter-LC-MS as well, but as it is shown in Figure S4.3, the offline method shows by nature less temporal variability and a systematic underestimation during periods with an increased aging ratio. In Figure 4.1, the time series of this aging proxy clearly depicts that the aerosol during the nucleation event is freshly formed- shown by a ratio of the two acids close to unity. From this event on, the ratio *m/z* 203 / *m/z* 185 increases for almost 36 hours until it reaches the level from the day before the passage of the cold front. On several days, the slope of the aging proxy shows a diurnal pattern- increasing during daytime and decreasing during night time. In order to link organic aerosol age to the aerosol hygroscopicity, we will address this parameterization and the temporal fluctuation throughout the campaign in chapter 4.3.4 once again.

4.3.2 Online mass spectrometry measuring organosulfates and nitrooxy organosulfates

The time series shown in Figure 4.5A,C,E focusses on the second week of the campaign, during which transient periods showed a strong bias between sulfate measuring instruments. As it can be seen in Figure 4.5 A, the comparison of the AMS with the MARGA data indicate that the AMS measures increased values of sulfate especially during the night of 21 to 22 August 2012. This observation is a strong indication for the presence of organic bonded sulfate (obSO4) in the ambient aerosol. The mass fraction of obSO4 of the total sulfate, which is determined by the deviation from the 1:1 line in Figure 4.5 B, amounts up to 38% during the 22 August 2012. The average of the mass fraction of obSO4 during the whole depicted period (20 – 27 August) is 10%.

The signal on *m/z* 97 of the APCI-MS measurements (Figure 4.5 C) can be assigned to inorganic sulfate (HSO_4^-), and thus resolving the temporal variation of sulfate based on a higher measurement frequency compared to the MARGA. Due to the preservation of the molecular structure of OS in the chemical ionization process, the signal on *m/z* 97 is less affected by sulfate originating from the fragmentation of OS as it is observed in the AMS measurements. Therefore the APCI-MS *m/z* 97 time series represents more accurately the pure inorganic sulfate. Although, the APCI-MS was not calibrated for sulfate during the campaign, the APCI-MS sulfate concentration was calculated based on APCI-MS *m/z* 97 counts correlated to the MARGA measurements of sulfate (R^2=0.86, Fig. S4.4). On the basis of the higher measurement frequency of the APCI-MS compared to the MARGA, the maximum fraction of sulfate bonded to organics amounts up to approximately 50% during the event in the night of 22 August 2012. However, due to the possibility of isobaric interference of other compounds than sulfate on APCI-MS *m/z* 97, in the following analysis, the quantitative amount of obSO4 was determined by the deviation between AMS and MARGA sulfate measurements.

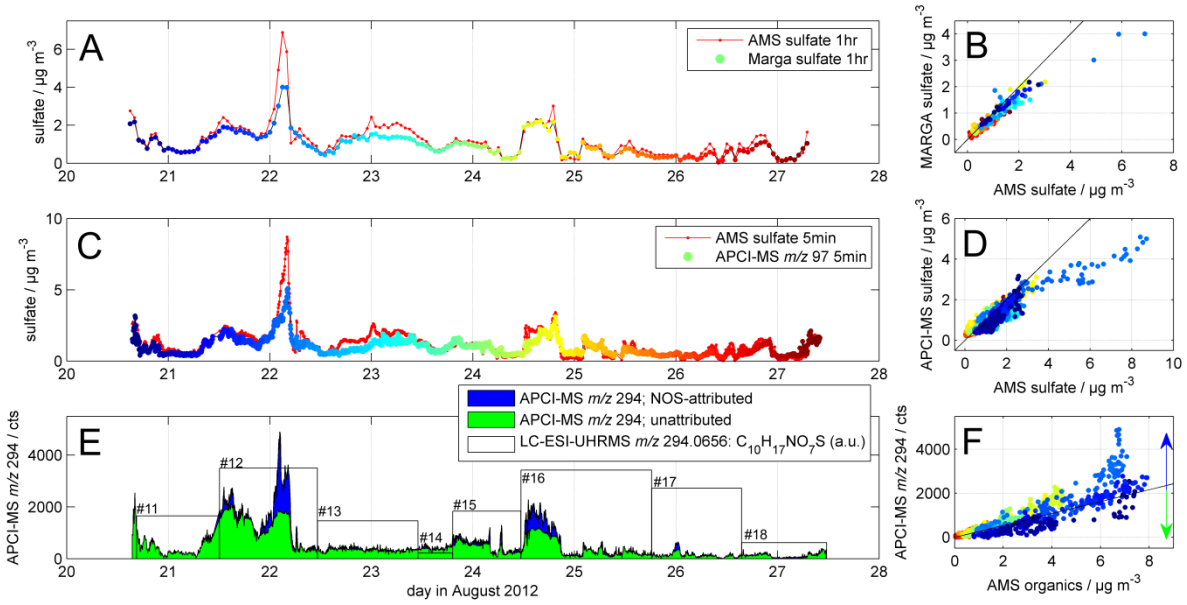

Figure 4.5 (A+B) Comparison of MARGA and AMS sulfate at one hour time resolution. (C+D) Comparison of AMS sulfate and APCI-MS *m/z* 97, which is converted to sulfate concentration based on the MARGA data (Fig. S4.4). The black lines in B and D represent the 1:1 line and the color codes time. (E) APCI-MS *m/z* 294 was divided into the blue signal which is attributed to $C_{10}H_{17}NO_7S$ and the green signal which is attributed to other isobaric interference. This attribution is derived from the black line in F, which is the linear fit of APCI-MS *m/z* 294 vs. AMS organics when nitrate & sulfate were below 2 µg/m3. The white bars in E represent the filter LC-UHRMS analysis, showing the integral of all five $C_{10}H_{17}NO_7S$ isomers (see Figure 4.6).

The assumption of high concentrations of (nitrooxy) organosulfates ((N)OS), which is concluded from the bias between AMS and MARGA sulfate measurements, is furthermore supported by the time series of particular APCI-MS *m/z* ratios. Coinciding with the measured divergence of sulfate during 22 August 2012, the signal of *m/z* 294 was strongly enhanced (Figure 4.5 E). In previous studies, the nitrooxy organosulfate $C_{10}H_{17}NO_7S$ (295 Da) was identified from filter measurements of ambient aerosols in a variety of studies (Surratt et al., 2007; Surratt et al., 2008; Iinuma et al., 2007; Kristensen and Glasius, 2011; Yttri et al., 2011; Lin et al., 2012; Lin et al., 2013). The molecular ion of this compound appears on *m/z* 294. The filter/LC-UHRMS measurements indicate that other isobaric interferences can be observed as well (Figure 4.6), which cumulate in the online APCI-MS signal at *m/z* 294. In order to estimate the contribution of $C_{10}H_{17}NO_7S$ to the total signal of *m/z* 294, the signal of this particular mass-to-charge ratio was correlated to the AMS OA signal when AMS sulfate and nitrate both were below 2 µg/m^3 (since the occurrence of OS coincides with high nitrate and sulfate). The linear fit of this correlation is represented by the black line in Figure 4.5 F. The assumption that all data points above this line can be attributed to the NOS-compound $C_{10}H_{17}NO_7S$, and all below to

compounds other than the nitrooxy organosulfate, results in the NOS-attributed and non-NOS-attributed (unattributed) time series in Figure 4.5 E. This time series clearly shows when the transient periods with enhanced concentrations of the nitrooxy organosulfate $C_{10}H_{17}NO_7S$ occurred.

The unambiguous identification and proof for the presence of the nitrooxy organosulfate at *m/z* 294 was achieved by analysing filter samples using LC-UHRMS. As it can be seen in the lower panel of Figure 4.6, which is the average signal over the entire chromatogram of filter #12, four major signals of a different elemental composition emerge at *m/z* 294. The peak of the nitrooxy organosulfate $C_{10}H_{17}NO_7S$ is the most intense, and the chromatogram resolves the presence of five different isomers of this elemental composition.

The relative variation of the integrated intensity of all five $C_{10}H_{17}NO_7S$ isomers between the different filter samples is shown in Figure 4.5 E, represented by the white bars. Filter #12 and filter #16 are showing the highest intensity, which is in agreement with the largest areas of the NOS-attributed APCI-MS *m/z* 294 signal. A comparison of filter #13 and #14 reveals that filter #13, which was sampled overnight, shows an increased signal of the NOS 294, whereas filter #14, which was sampled only during daytime, does not. During this period, the online APCI-MS depicts that there is almost no variation between night and day. A possible reason for this observation might be that reactions on the filter proceed during the night-time sampling. Therefore we avoid to draw conclusions in terms of quantitative interpretation of night- and daytime filter samples, since the filter sampling can seriously be affected by (in this case night-time-positive-) sampling artefacts.

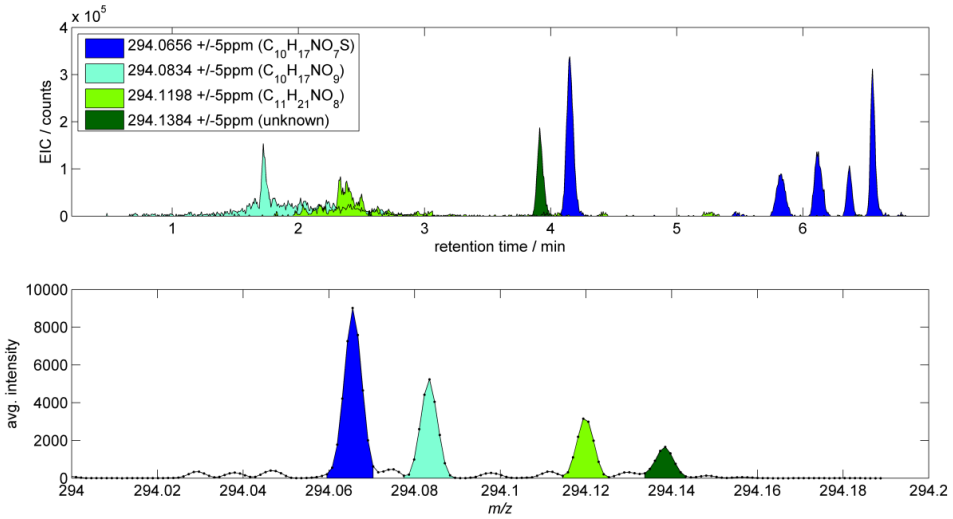

Figure 4.6 The chromatogram of the accurate mass at *m/z* 294.0656 resolves that five different isomers occur on this exact mass. The UHPLC-ESI-UHRMS analysis separates four compounds on the nominal mass at *m/z* 294 which cannot be resolved by the online APCI-MS.

4.3.3 Composition group classification of organics by offline LC/ESI-UHRMS and online APCI-MS analysis

The presence of five nitrooxy organosulfates of the elemental composition $C_{10}H_{17}NO_7S$ has been demonstrated- now we provide evidence for a large number of other OS and NOS. The non-target-analysis of the negative ion mode measurements resulted in 407 components occurring above the signal threshold value of 1e5 counts. To 261 out of these 407 components, a molecular formula with a mass deviation of less than 2 ppm could be assigned. The comprehensive list of the 261 different compounds (156 different molecular formulas) is given in the supplementary material (Table S4.1 a-d). All signals could be classified into CHO, CHNO, CHOS or CHNOS subgroups. Some chlorine containing compounds were observed, but it turned out that those signals emerged from chlorine adducts of other compounds. The functionalities of the four subgroups cannot be retrieved from the elemental composition, but since it was measured in the negative ionization mode, the CHO and CHNO compounds should contain at least one carboxylic acid function, whereas the compounds from the CHOS and CHNOS group can also be detected in the negative mode due to a R-OSO_3H moiety. This would involve organosulfates and nitrooxy organosulfates belonging to the CHOS and CHNOS group, respectively. The numerically largest group is the CHO-subgroup accounting for 35 % of all molecular formulas, followed by the CHNOS subgroup with 26 %, followed by the CHOS-subgroup with 21 %. The CHNO subgroup is the numerically smallest group accounting for only 18 % of all molecular formulas.

The obtained information on the elemental composition by the LC-UHRMS analysis, together with the temporal variation (between 20 August and 27 August) measured by APCI-MS, was used to investigate the temporal correlation of CHO, CHOS and CHNOS subgroups (Figure 4.7). Representative for the CHO group we chose *m/z* 187 and *m/z* 203, for the CHOS group *m/z* 209 and *m/z* 279 and for the CHNOS group *m/z* 294 and *m/z* 296. A high temporal correlation between different compounds suggests same sources or similar atmospheric formation pathways. By comparing different *m/z* signals of the same group (e.g. *m/z* 209 vs. *m/z* 279), a high degree of correlation can be observed ($R^2 \geq 0.92$). From previous studies, it is known that the organic acid $C_8H_{12}O_6$ (*m/z* 203) and $C_8H_{12}O_5$ (*m/z* 187) are of both biogenic origin (Szmigielski et al., 2007; Yasmeen et al., 2012), which results in a high degree of correlation (R^2=0.99). In contrast, the correlation between the two CHO compounds $C_8H_{12}O_6$ (*m/z* 203) and $C_9H_6O_5$ (*m/z* 193) is much lower (R^2=0.78) (not shown). The high DBE of the compound $C_9H_6O_5$ suggests that this compound is aromatic in character. The aromatic character does not necessarily imply that this compound is of anthropogenic origin. However, due to the lower coefficient of correlation

compared to the correlation between other biogenic compounds, it can be stated that the compound $C_9H_6O_5$ is most probably of anthropogenic origin.

During the transient periods with increased concentrations of sulfate, organosulfates (CHOS group) show an increased signal compared to organic acids (CHO group) (Figure 4.7). Even more pronounced is the signal of nitrooxy organosulfates (CHNOS group) versus the signal of organic acids during the periods of elevated sulfate concentrations.

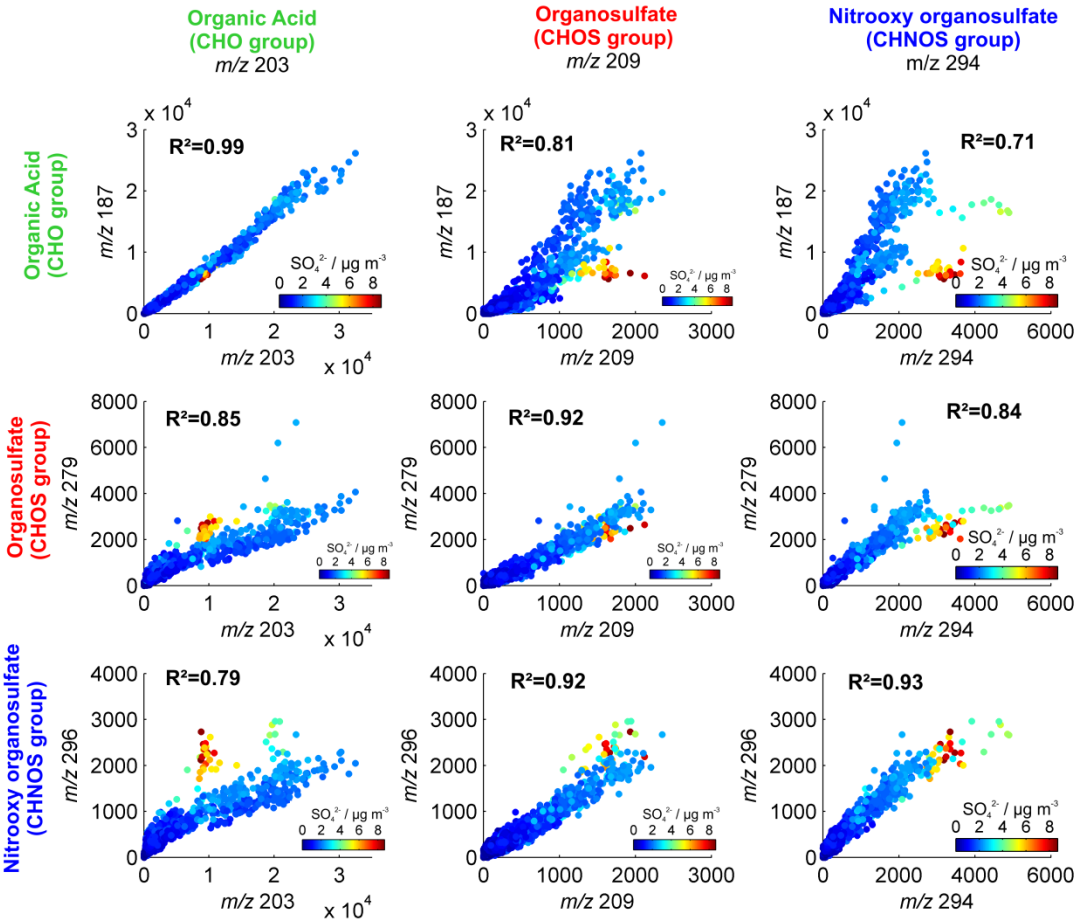

Figure 4.7 Temporal correlation analysis of particular *m/z* signals measured by the online APCI-MS in the time period between 20 August 2012 and 28 August 2012. The signals at *m/z* 187 and *m/z* 203 represent the CHO group, *m/z* 209 and *m/z* 279 the CHOS subgroup and *m/z* 294 and *m/z* 296 the CHNOS subgroup. It is referred to Table S4.1, showing that isobaric interference of compounds from different subgroups were not detected above the threshold value of 1e5 counts by the LC-UHRMS analysis.

The observation that particular *m/z* ratios, which are classified to the same composition group, show a high degree of correlation, whereas the correlation between different groups is less pronounced, suggests the implementation of this analysis upon the whole measured mass range by the APCI-MS in order to classify *m/z* signals into composition groups. Therefore, the squared

correlation coefficient matrix for all *m/z* ratios (between *m/z* 80 and *m/z* 500) was calculated (Fig. S4.5) (negative R-values were set to zero). In Figure 4.8 each R^2 of the nominal masses in the range between *m/z* 150 to *m/z* 400 is plotted against *m/z* 203 (upper panel) and *m/z* 294 (lower panel). In this figure it can be seen to what extent a signal of one particular *m/z* ratio is resembling the temporal variation of *m/z* 203 (representing the CHO group) and *m/z* 294 (representing the CHNOS group), respectively. In order to draw firm conclusions, the temporal correlation analysis was combined with the molecular composition information by the LC-UHRMS analysis. Each signal in Figure 4.8 which is labelled by a color-coded circle, represents one or more compounds which show a distinctive peak in LC-MS analysis. The color code classifies the signals by their elemental composition group. Since the online APCI-MS is not a high resolution mass spectrometer, compounds of a different molecular composition can coincide at one *m/z* ratio (e.g. *m/z* 227, 266, 308).

What can be learned from this kind of analysis is that the majority of the measured signals by the online APCI-MS can be attributed to compounds which were also detected by the LC-MS analysis. As it can be seen in the upper panel of Figure 4.8, the majority of compounds belonging to the CHO group are highly correlated to *m/z* 203 ($R^2 \geq 0.95$). In contrast, all CHO compounds show a lower temporal correlation to the CHNOS-containing compound at *m/z* 294 ($R^2 \leq 0.85$). Furthermore, it can be seen that the greater the mass difference between a CHO compound and *m/z* 203, the degree of correlation decreases. However, it cannot be stated that this is an effect which displays the real atmospheric variability between different molecules, because at higher *m/z* ratios the probability of isobaric interference increases, and thus minor contribution of other isobar molecules might also be a reason for the decreasing correlation trend.

Regarding the correlation to *m/z* 294, it turns out that several different compounds of the CHNOS group are enhanced during the period with high sulfate and nitrate concentrations, and therefore show a high degree of correlation to the *m/z* 294 signal. Furthermore, it can be seen that some CHNO-compounds show a higher degree of correlation than organosulfates from the CHOS group (e.g. *m/z* 264, 278, 336, 348). This observation suggests that under the prevailing conditions the CHOS compounds probably further react to from CHNOS-compounds.

Furthermore, this kind of analysis may shed light on the formation routes of terpene derived OS, which are not completely elucidated. The study by Minerath et al. (2008) revealed that the rate of OS formation by alcohol-sulfuric acid esterification is kinetically insignificant under atmospherically relevant timescales. Instead it was found that the reactive uptake of epoxides can explain the formation of organosulfates (Iinuma et al., 2009a; Minerath et al., 2009). Despite this finding, the formation of the most abundant nitrooxy organosulfate $C_{10}H_{17}NO_7S$ still cannot be explained by the epoxide pathway, as it is discussed by Lin et al. (2012), and it stands to reason that NO_3 night time chemistry might be involved. A consequence of the high correlation of other

NOS to *m/z* 294 might be that the NO_3 night time chemistry is also an important formation pathway for those compounds which in principal incorporate sufficient oxygen atoms necessary to explain formation via the the epoxide pathway, but in fact are formed by via the NO_3 radical chemistry.

Another interesting aspect is that the IEPOX-derived organosulfate $C_5H_{12}SO_7$ (Surratt et al., 2010; Hatch et al., 2011a) does not considerably contribute to the signal at *m/z* 215, but so do the isobar organic acids $C_9H_{12}O_6$ and $C_{10}H_{16}O_5$ resulting in a high correlation to *m/z* 203. The LC-MS analysis indicates that the highly polar IEPOX derived OS $C_5H_{12}SO_7$ elutes from the column within the solvent peak, thus we do not rule out that this compound is an important compound in the ambient aerosol at the Kleiner Feldberg field station.

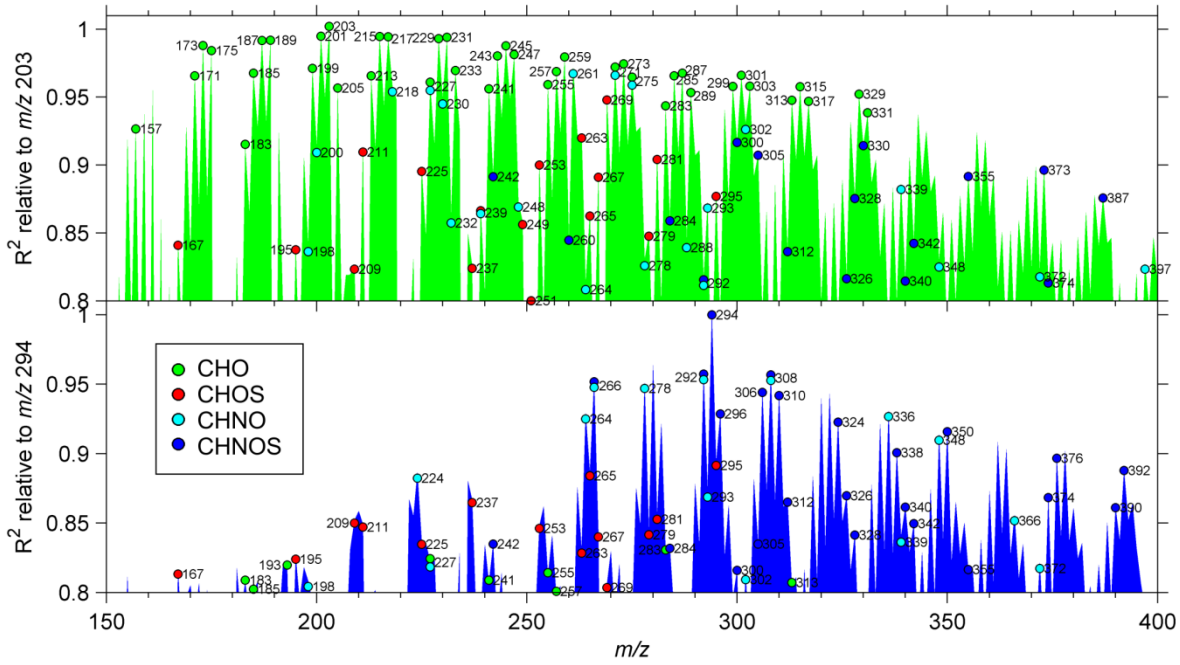

Figure 4.8 Temporal correlation analysis (20 to 28 August 2012) between the APCI-MS signals *m/z* 150 to *m/z* 400 and APCI-MS *m/z* 203 (primarily $C_8H_{12}O_6$, upper panel) and APCI-MS *m/z* 294 (primarily $C_{10}H_{17}NO_7S$, lower panel). The identified molecular formulas by the LC-UHRMS analysis (Table S4.1) are depicted as color coded circles according to the elemental composition group (CHO, CHOS, CHNO or CHNOS).

What cannot be concluded from Figure 4.8 is a quantitative estimation of the OS and NOS concentration, since it shows only the degree of the temporal correlation. However, elucidating which OS (and NOS) compounds are the most abundant molecules and estimating the total fraction of OS would be very valuable for assessing their atmospheric implications. Therefore, a

period with low concentrations of (nitrooxy) organosulfates (low OS) was compared to the period with enhanced concentrations of (nitrooxy) organosulfates (high OS) (Figure 4.9). The average spectra of both periods were normalized on their base peak (*m/z* 203) and depicted on top of each other (middle panel). It can be seen that *m/z* 97, 123 and 125 are strongly enhanced during the high OS periods. The higher signal of *m/z* 97 and *m/z* 125 can be attributed to the enhanced concentration of inorganic sulfate and nitrate (HSO_4^- and HNO_3*NO_3^-), respectively. The enhanced contribution of *m/z* 123 cannot be attributed with certainty (possible explanations are the cluster ions CH_3NO_2*NO_3^- or C_2H_7NO*NO_3^-). Furthermore, above *m/z* 200, many signals emerge that are enhanced during the high OS period. In the lower panel of Figure 4.9, the difference between the two normalized spectra is depicted. Again the LC-UHRMS results (Table S4.1) appear in the spectrum as color-coded circles. Almost all *m/z* ratios related to CHOS, CHNO and CHNOS compounds are increased during the high OS period. A two sample t-test proves that the signals assigned to CHOS-, CHNO- and CHNOS-compounds are significantly enhanced, compared to the CHO-attributed signals which scatter around zero.

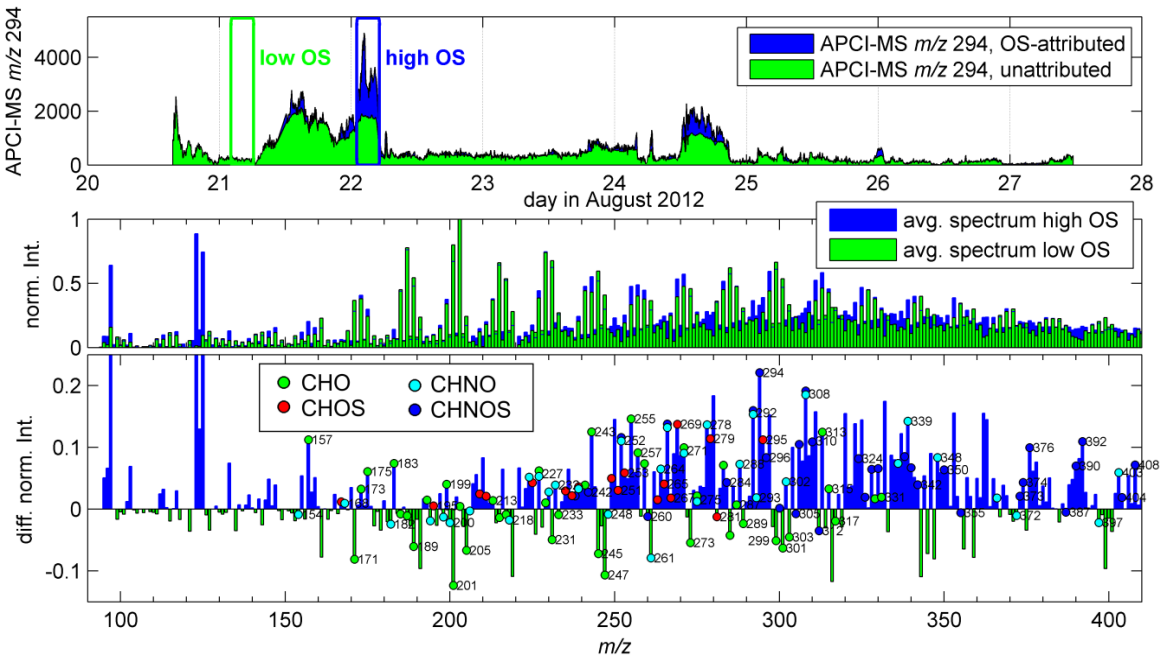

Figure 4.9 APCI-MS mass spectra comparison of periods showing low and high organosulfate concentrations. The mass spectra in the middle panel are normalized on the base peak (in both spectra *m/z* 203). The undermost panel shows the difference between the two normalized spectra. The identified molecular formulas by the LC-UHRMS analysis are depicted as color coded circles according to the elemental composition group (CHO, CHOS, CHNO or CHNOS).

The most pronounced difference between those two periods arises at *m/z* 294 and amounts up to 20% increase during the high OS period. A variety of other (nitrooxy) organosulfates can be observed in the spectrum, in total substantially contributing to the bias between AMS and MARGA sulfate concentrations. Further strongly enhanced CHNOS compounds appear on *m/z* 292 and 308 which could be identified as $C_{11}H_{19}NO_6S$ and $C_{13}H_{27}NO_5S$ by the LC-MS analysis. This probably implies that not only monoterpenes (C_{10}-compounds) are involved in the formation of organosulfates.

In order to estimate the average molecular weight of the organosulfates (OS and NOS), all signals which are confirmed by LC-UHRMS as CHOS- or CHNOS-compounds are used for the calculation of the number weighted average molecular weight ($\overline{MW_n}$). Of course, using MS techniques for measuring $\overline{MW_n}$ can only provide a rough estimation, since the different molecules can be substantially different in their ionization efficiency (Vogel et al., 2013b; Kalberer et al., 2006; Kiss et al., 2003). However, $\overline{MW_n}$ of the CHOS-assigned signals solely results in 258 g/mol and $\overline{MW_n}$ of the CHNOS-assigned signals results in 320 g/mol. The vast majority of CHOS and CHNOS compounds incorporate only one sulphur atom. If we assume that this sulfur is incorporated into the molecules by a sulfate group, the average molecular weight of the organic part of the CHOS molecules would refer to 161 g/mol (258 g/mol − 97 g/mol). We obtain the same result for the CHNOS compounds: 320 g/mol – 62 g/mol – 97 g/mol = 161 g/mol. Using this average molecular weight of the OS´s organic moiety, it is possible to calculate the organosulfate fraction contributing to the total OA. The mean sulfate concentrations determined by AMS and MARGA during the high OS event are 4.9 and 3.2 µg/m^3, respectively. Thus, the amount of sulfate which is bonded to organics is 1.7 µg/m^3 translating into 17.3 mmol/m^3. Using 161 g/mol as an average molecular weight of the organic moiety of organosulfates, results in 2.8 µg/m^3 OA due to organosulfates. The average OA during the high OS event is 6.1 µg/m^3, thus 46% of the OA signal would be caused by organosulfates. However, it has to be emphasized that the APCI-MS obviously does not to measure all organosulfate species, since a strong deviation between MARGA and AMS sulfate was observed also during the night of 23 August, which cannot be explained by enhanced APCI-MS mass traces. We assume that small organosulfates decompose during the APCI ionization (e.g. isoprene or glyoxal derived organosulfates (Surratt et al., 2010; Galloway et al., 2009). This fact would shift the average molecular weight towards lower values, resulting in a lower contribution of OS to total OA. Thus, the contribution of 46% organosulfates to the total OA mass has to be regarded as an upper-limit estimation.

To conclude this section, the extremely high OS-fraction in OA is a current best estimation of a transient event and further studies are needed in order to investigate the fraction and frequency of the occurrence of organosulfates. The application of online high resolution mass

spectrometric techniques, which are able to resolve e.g. the isobar compounds $C_{10}H_{17}NO_7S$ and $C_{10}H_{17}NO_9$ at *m/z* 294, will contribute to a better understanding of this subject. Furthermore, authentic standards or at least adequate surrogate standards are needed in order to quantify the organosulfate fraction more reliably.

4.3.4 Impact of oxidative aging and organic bonded sulfate on particle hygroscopicity

As the submicron aerosol during the campaign has been characterized in detail, the impact of the chemical composition on the effective hygroscopicity (κ) of the CCN active particles was investigated. We hypothesize that particles, which contain high amounts of sulfate that is bonded to organic molecules, show a decreased hygroscopicity compared to particles in which sulfate appears to be purely inorganic. Decreased values of κ, caused by a high fraction of organic bonded sulfate (f_{obSO4}), can be counteracted by a highly aged organic fraction. Therefore we estimate f_{obSO4} by the difference between MARGA and AMS sulfate (Figure 4.10 D) and the particle aging state by the ratio of the APCI-MS signals *m/z* 203 / *m/z* 185 (Figure 4.10 C).

In contrast to the work by Gunthe et al. (2011) and Dusek et al. (2010), the following analysis focusses only on the κ parameter derived from CCN measurements performed at the lowest supersaturation (S=0.11%), which is most closely representing the aerosol bulk composition. The composition of smaller diameters (κ derived from higher supersaturations) was not considered because the utilized instruments, which provide a more detailed picture of the organic fraction (APCI-MS and MARGA), are not capable to measure size resolved chemical composition. At the supersaturation of S=0.11%, the critical particle diameter for CCN activation, which is used to derive κ, was observed to be in the size range of 120 to 220 nm (predominantly in the range 130 to 180 nm), whereas for larger supersaturations the activation diameters were much smaller. Depending on D_a (at S=0.11%), the size resolved chemical composition by the C-ToF-AMS was hourly averaged and calculated for the size bins between 120-150 nm (for D_a<150 nm) and between 150-180 nm (for D_a>150nm). An average density of 1.5 g/cm^3 was assumed in order to calculate the electrical mobility into the vacuum aerodynamic mobility. The size resolved NH_4 concentrations were calculated from the SO_4 and NO_3 concentrations under the assumption that the aerosol was fully neutralized.

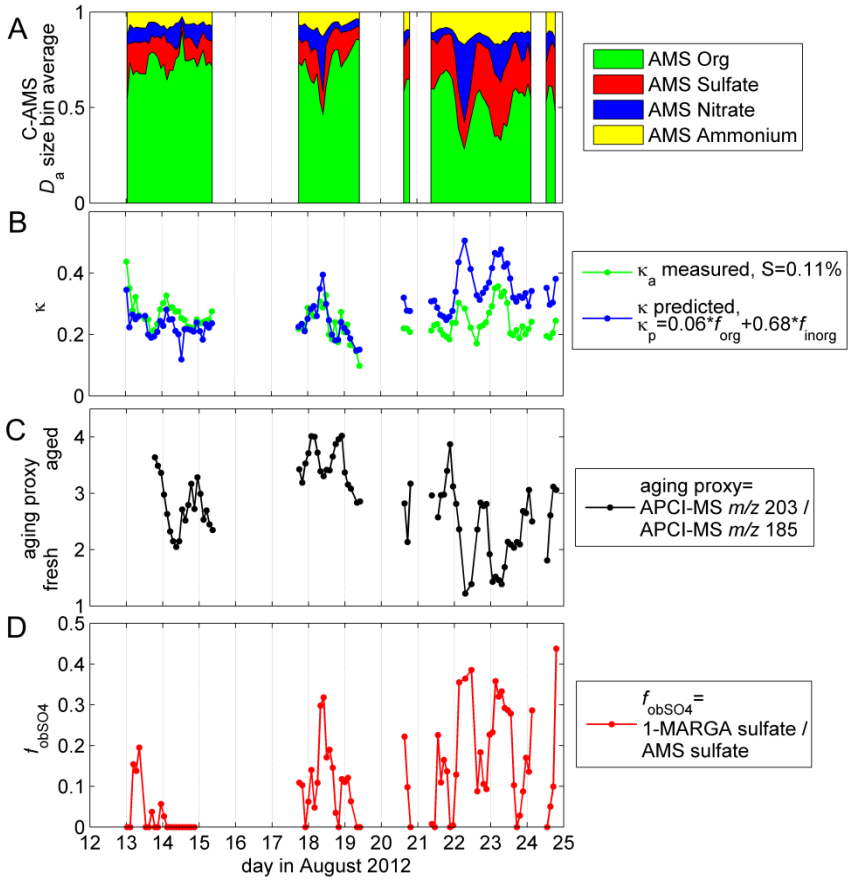

Figure 4.10 (A) Size resolved aerosol chemical fractions determined by C-ToF-AMS. (B) κ_a values which are determined from the CCNc measurements at the lowest supersaturation of S=0.11%. κ_p, was calculated from the Gunthe et al. (2011) parameterisation. (C) Biogenic aerosol aging proxy *m/z* 203 / *m/z* 185 at the temporal resolution of the CCNc measurements. (D) Fraction of organic bonded sulfate determined by the difference between MARGA and AMS sulfate measurements.

Figure 4.10 B clearly depicts that the predicted κ-value (calculated from the AMS fractions by the Gunthe et al. (2011) parameterisation) fits very well to the observed κ_a between the 13 August and 19 August, despite a short period on 14 August where the predicted κ-value (κ_p) underestimates the actually measured value of κ_a. During 18 August f_{obSO4} is increased to 30%, and coincidently κ_p is slightly larger than k_a. The largest offset between measured and predicted κ can be observed from 22 August on, when the f_{obSO4} was continuously high and the organic aerosol sparsely aged. To recall the observations from previous chapters, the highest fraction of organosulfates was measured by the APCI-MS during the night of 22 August. Thus it emerges that if the highly hygroscopic sulfate and nitrate is bonded to monoterpenes, that are sparsely hygroscopic, the resulting total hygroscopicity appears to be lower from what would be expected

by the AMS measurements. This implies that chemical reactions between anthropogenic inorganic emissions and biogenic organic emissions results in less hygroscopic particles, compared to the oxidation pathways leading towards pure sulfuric acid particles and organic oxidation products. To which extent these inorganic/organic interactions influence the indirect cooling effect of anthropogenic SO_2 emissions has to be evaluated in future studies.

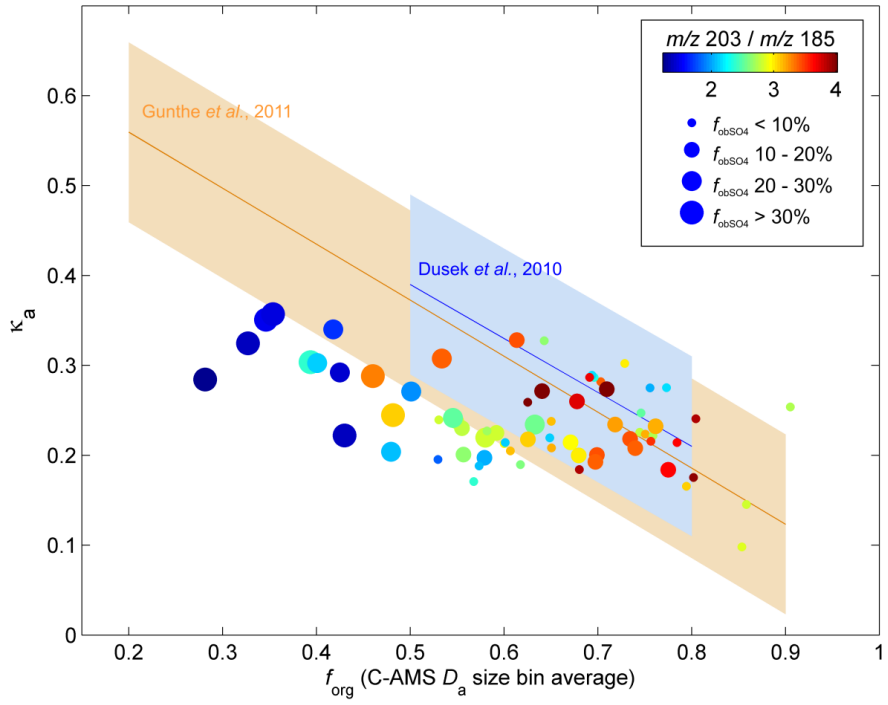

Figure 4.11 The size resolved AMS organic fraction vs. the effective hygroscopicity parameter κ_a of CCN active particles at S=0.11%. The size of the data points represents the fraction of organic bonded sulfate and the color the extent of the aerosol age (blue: fresh aerosol, red: aged aerosol). The orange and blue line represent the parameterisation of κ derived from f_{org}. The shaded area represents the uncertainty of the f_{org}-derived parameterisation.

In Figure 4.11, the size resolved organic fraction is plotted against the measured κ_a at S=0.11% as in the previous work by Gunthe et al. (2011) and Dusek et al. (2010). The APCI-MS aging proxy (Figure 4.10) and the fraction of sulfate that is bonded to organics is depicted by colour and size coded data points, respectively. It can clearly be seen that the measured κ agrees with the AMS dependent parameterisation when the fraction of organic bonded sulfate is low and the aerosol moderately to highly aged (represented by small reddish points). However, the parameterisation is not applicable with decreasing aerosol age (blue to green points) and/or an increasing fraction of organic bonded sulfate (large points). The observed overestimation of κ by

the AMS-parameterisation can, under certain conditions, be larger than 0.2 and thus significantly different from the uncertainty of the measurements. Most of the data points that show a reduced κ are affected by both chemical effects: sparsely aged and a high f_{obSO4}. However, a few data points suggest that aging effects alone can explain a reduction of κ of more than 0.1. Vice versa, two data points show high f_{obSO4} and are highly aged, but appear below the expected κ-values. To conclude, one can estimate that both effects have significant influence on the hygroscopicity, but for a more thoroughly analysis of the chemical effects, future studies which are based on larger data sets are required.

4.4 Conclusions and outlook

We have demonstrated that the utilization of comprehensive analytical techniques contributes valuable insights in the chemistry of organic aerosols during new particle formation and helps to understand the hygroscopicity behaviour of CCN-active particles. It is incontestable that the size of aerosol particles is the most important variable in determining the CCN activity of aerosol particles. However, the size distribution is affected by (1) the number of pre-existing particles on which low volatile compounds can condense on and (2) chemical reactions of the aerosol constituents such as aging or oligomerization processes. Therefore, it is crucial to understand the formation and particle growth processes which seem to be governed by the condensation of highly oxidized organic acids, whose formation pathways remain largely unidentified. The determination of the molecular formula by ultrahigh resolution mass spectrometry of a nucleation event filter, suggests that the oxidation products of sesquiterpenes (e.g. $C_{15}H_{24}O_5$) are due to their low vapour pressure key players in the growth of newly formed clusters, and possibly important for the stabilization of sub-3-nm clusters due to several different functional groups.

Secondly, it has been shown that high amounts of a variety of organosulfates and nitrooxy organosulfates were observed by online APCI-MS and co-located filter sampling for UHPLC-ESI-UHRMS analysis. During a particular night time event, the fraction of organic bonded sulfate (f_{obSO4}) was determined to be larger than 30%. Periods of a large f_{obSO4} also occurred when APCI-MS measurements did not indicate high amounts of (nitrooxy) organosulfates, suggesting that certain organosulfates cannot be measured by the APCI-MS method. Thus, further development of ambient ionization techniques is needed in order to make labile organic compounds accessible by mass spectrometry. Since the chemical composition of large particles is not seriously affecting the CCN-destiny of a particle (because larger particles are already activated at lower supersaturations) it should be an analytical aim to achieve size resolved

chemical analysis of particle sizes where chemical composition can become the crucial factor whether a particle grows to a cloud droplet or not.

Acknowledgements: This work was supported by the Max Planck Graduate Center with the Johannes Gutenberg-Universität Mainz (MPGC).

ALV gratefully acknowledges the support of Heinz Bingemer and the Uni Frankfurt mechanics staff for technical assistance, Ottmar Möhler for the loan of the PCVI and Thomas Klimach for the FMPS data analysis.

The authors gratefully acknowledge the NOAA Air Resources Laboratory (ARL) for the provision of the HYSPLIT transport and dispersion model and READY website (http://ready.arl.noaa.gov) used in this publication.

5 Conclusions and Outlook

The field application of a soft ionization mass spectrometric technique for the analysis of organic compounds that form stable negative ions has been demonstrated within this thesis. Due to low particle phase concentrations of organic compounds in the ambient environment, the aerosol was enriched prior to the MS by using a miniature versatile aerosol concentration enrichment system (mVACES). It has been demonstrated, that the application of the concentrator enriches the aerosol mass by approximately one order of magnitude which allows for the operation of an APCI-IT-MS at ambient concentration levels.

The application of the system in a field study at the boreal forest research station in Hyytiälä, Finland, facilitated the quantitative measurements of the gas-to-particle partitioning of organic acids. *In-situ* MS/MS studies revealed the occurrence of isobaric compounds which can show a significantly different partitioning behaviour. For example, evidence for two isobar compounds, pinic acid and ketolimononic acid, was provided by MS/MS experiments of *m/z* 185. These compounds have the same elemental composition, but contain different functional groups, hence affecting the vapour pressure which results in a different partitioning behaviour of up to one order of magnitude. This observation demonstrates that solely the information on the elemental composition is not sufficient to reliably predict gas-to-particle partitioning. Moreover, it was found that the partitioning of low volatile organic compounds (LVOCs), such as a tricarboxylic acid, which are expected to partition completely into the particle phase, occurred to a large extent in the gas phase. MS/MS spectra of this compound showed the minor abundance of other isobaric compounds. Hence, it was concluded that this partitioning behaviour results from the large aerosol equilibration timescales that can be caused by (1) continuous production of the LVOCs in the gas phase or (2) a semi-solid phase state of the particles that reduces bulk diffusion, resulting in a decreased uptake of low volatile compounds into the particle phase.

As the partitioning of oxidation products between the gas and particle phase can significantly affect the particulate mass and thus the size of atmospheric particles, it is important to clarify those micro-scale processes through observations. The approach of measuring the partitioning of single molecular compounds presented within this work is promising. Associated uncertainties through the application of the aerosol concentrator can easily be reduced by the application of state-of-the-art mass spectrometers that are more sensitive and therefore making the concentration step obsolete. Modern MS techniques can provide information of the molecular composition through high mass resolution and precision as well as provide insights into the molecular structure of the analytes through the *in-situ* MS/MS capability.

Within the field study at the Mt. Kleiner Feldberg, Germany, high molecular weight compounds were observed by the online APCI-MS during a new particle formation event. Co-located filter sampling allowed for the determination of the elemental composition of single organic compounds that occurred during nucleation. The observation that organic compounds which appear during nucleation incorporate 15 carbon atoms, suggests that oxidation products of sesquiterpenes are involved in the growth of newly formed particles. The high average oxidation state of the observed compounds indicates that their vapor pressure is low enough to participate in nucleation processes.

Furthermore, evidence for the abundance of organosulfates during particular periods could also be demonstrated by the applied complementary MS techniques. The effect of oxidative aging and of the occurrence of organosulfates on the particle hygroscopicity has been investigated. Further field and laboratory measurements are necessary in order to examine to which extent the occurrence of organosulfates can alter the hygroscopicity of particles. Estimations from the field observations show that the hygroscopicity parameter kappa can be decreased by ~0.2 when a large fraction of sulfate is chemically bonded to organic molecules. The formation mechanisms of organosulfates also need to be investigated in future laboratory studies, since their formation can largely increase the particle mass of organic aerosols.

This thesis has shown that the application of complementary mass spectrometric techniques within field studies enables to gain detailed insight into the chemical composition and transformation processes of atmospheric aerosols. The application at different environments, such as in the tropics, in the marine boundary layer or at semi-arid regions might shed light into the variety of unknown but atmospherically relevant chemical species in organic aerosols. Further long-term field deployment of online soft ionization techniques is important to study seasonal cycles of ambient aerosol composition. The application in urban areas for the investigation of the atmospheric degradation of pollutants can reveal new findings that are closely related to human health issues. Further improvement of soft-ionization methods is also needed in order to investigate those compounds by online mass spectrometry that usually undergo fragmentation upon heating.

6 References

Albrecht, B. A.: Aerosols, Cloud Microphysics, and Fractional Cloudiness, Science, 245, 1227–1230, doi:10.1126/science.245.4923.1227, 1989.

Alfarra, M. R., Hamilton, J. F., Wyche, K. P., Good, N., Ward, M. W., Carr, T., Barley, M. H., Monks, P. S., Jenkin, M. E., Lewis, A. C., and McFiggans, G. B.: The effect of photochemical ageing and initial precursor concentration on the composition and hygroscopic properties of beta-caryophyllene secondary organic aerosol, Atmospheric Chemistry and Physics, 12, 6417–6436, doi:10.5194/acp-12-6417-2012, 2012.

Aljawhary, D., Lee, A. K. Y., and Abbatt, J. P. D.: High-resolution chemical ionization mass spectrometry (ToF-CIMS): application to study SOA composition and processing, Atmospheric Measurement Techniques, 6, 3211–3224, doi:10.5194/amt-6-3211-2013, 2013.

Allan, J. D., Delia, A. E., Coe, H., Bower, K. N., Alfarra, Jimenez, J. L., Middlebrook, A. M., Drewnick, F., Onasch, T. B., Canagaratna, Jayne, J. T., and Worsnop: A generalised method for the extraction of chemically resolved mass spectra from aerodyne aerosol mass spectrometer data, Journal of Aerosol Science, 35, 909–922, doi:10.1016/j.jaerosci.2004.02.007, 2004.

Allan, J. D., Jimenez, J. L., Williams, P. I., Alfarra, Bower, K. N., Jayne, J. T., Coe, H., and Worsnop: Quantitative sampling using an Aerodyne aerosol mass spectrometer - 1. Techniques of data interpretation and error analysis, Journal of Geophysical Research-Atmospheres, 108, doi:10.1029/2002JD002358, 2003.

Altieri, K. E., Turpin, B. J., and Seitzinger, S. P.: Oligomers, organosulfates, and nitrooxy organosulfates in rainwater identified by ultra-high resolution electrospray ionization FT-ICR mass spectrometry, Atmospheric Chemistry and Physics, 9, 2533–2542, 2009.

Andreae, M. O., Jones, C. D., and Cox, P. M.: Strong present-day aerosol cooling implies a hot future, Nature, 435, 1187–1190, doi:10.1038/nature03671, 2005.

Andreae, M. O. and Merlet, P.: Emission of trace gases and aerosols from biomass burning, Global Biochemical Cycles, 15, 955-966, doi:10.1029/2000GB001382, 2001.

Andreae, M. O. and Rosenfeld, D.: Aerosol-cloud-precipitation interactions. Part 1. The nature and sources of cloud-active aerosols, Earth Science Reviews, 89, 13–41, doi:10.1016/j.earscirev.2008.03.001, 2008.

Asmi, E., Freney, E., Hervo, M., Picard, D., Rose, C., Colomb, A., and Sellegri, K.: Aerosol cloud activation in summer and winter at puy-de-Dome high altitude site in France, Atmospheric Chemistry and Physics, 12, 11589–11607, doi:10.5194/acp-12-11589-2012, 2012.

Bartmess, J. E., NIST Chemistry WebBook: Negative Ion Energetics Data: http://webbook.nist.gov, 2013.

Bateman, A. P., Laskin, J., Laskin, A., and Nizkorodov, S. A.: Applications of High-Resolution Electrospray Ionization Mass Spectrometry to Measurements of Average Oxygen to Carbon Ratios in Secondary Organic Aerosols, Environmental Science & Technology, 46, 8315–8324, doi:10.1021/es3017254, 2012.

Bonan, G. B.: Forests and climate change: Forcings, feedbacks, and the climate benefits of forests, Science, 320, 1444–1449, doi:10.1126/science.1155121, 2008.

Boucher, O. and Lohmann, U.: The Sulfate-CCN-Cloud Albedo Effect - A Sensitivity Study with 2 General-Circulation Models, Tellus Series B-Chemical and Physical Meteorology, 47, 281–300, doi:10.1034/j.1600-0889.47.issue3.1.x, 1995.

Boulter, J. E., Cziczo, D. J., Middlebrook, A. M., Thomson, D. S., and Murphy, D. M.: Design and performance of a pumped counterflow virtual impactor, Aerosol Science and Technology, 40, 969–976, doi:10.1080/02786820600840984, 2006.

Brink, H. ten, Otjes, R., Jongejan, P., and Kos, G.: Monitoring of the ratio of nitrate to sulphate in size-segregated submicron aerosol in the Netherlands, Atmospheric Research, 92, 270–276, doi:10.1016/j.atmosres.2008.12.003, 2009.

Brüggemann, M., Vogel, A. L., and Hoffmann, T.: Analysis of organic aerosols using a micro-orifice volatilization impactor (MOVI) coupled to an atmospheric-pressure chemical ionization mass spectrometer (APCI-MS), European Journal of Mass Spectrometry, accepted, 2014.

Canagaratna, M. R., Jayne, J. T., Jimenez, J. L., Allan, J. D., Alfarra, M. R., Zhang, Q., Onasch, T. B., Drewnick, F., Coe, H., Middlebrook, A. M., Delia, A., Williams, L. R., Trimborn, A. M., Northway, M. J., DeCarlo, P. F., Kolb, C. E., Davidovits, P., and Worsnop, D. R.: Chemical and microphysical characterization of ambient aerosols with the aerodyne aerosol mass spectrometer, Mass Spectrometry Reviews, 26, 185–222, doi:10.1002/mas.20115, 2007.

Cantrell, W. and Heymsfield, A.: Production of ice in tropospheric clouds - A review, Bulletin of the American Meteorological Society, 86, 795–807, doi:10.1175/BAMS-86-6-795, 2005.

Carlton, A. G., Wiedinmyer, C., and Kroll, J. H.: A review of Secondary Organic Aerosol (SOA) formation from isoprene, Atmospheric Chemistry and Physics, 9, 4987–5005, 2009.

Carroll, D. I., Dzidic, I., Stillwell, R. N., Haegele, K. D., and Horning, E. C.: Atmospheric pressure ionization mass spectrometry. Corona discharge ion source for use in a liquid chromatograph-mass spectrometer-computer analytical system, Analytical Chemistry, 47, 2369–2373, doi:10.1021/ac60364a031, 1975.

Chang, R. Y.-W., Slowik, J. G., Shantz, N. C., Vlasenko, A., Liggio, J., Sjostedt, S. J., Leaitch, W. R., and Abbatt, J. P. D.: The hygroscopicity parameter (kappa) of ambient organic aerosol at a field site subject to biogenic and anthropogenic influences: relationship to degree of aerosol oxidation, Atmospheric Chemistry and Physics, 10, 5047–5064, doi:10.5194/acp-10-5047-2010, 2010.

Chan, M. N., Surratt, J. D., Chan, A. W. H., Schilling, K., Offenberg, J. H., Lewandowski, M., Edney, E. O., Kleindienst, T. E., Jaoui, M., Edgerton, E. S., Tanner, R. L., Shaw, S. L., Zheng, M., Knipping, E. M., and Seinfeld, J. H.: Influence of aerosol acidity on the chemical composition of secondary organic aerosol from beta-caryophyllene, Atmospheric Chemistry and Physics, 11, 1735–1751, doi:10.5194/acp-11-1735-2011, 2011.

Charlson, R. J., Schwartz, S. E., Hales, J. M., Cess, R. D., Coakley, J. A., Hansen, J. E., and Hofmann, D. J.: Climate Forcing by Anthropogenic Aerosols, Science, 255, 423–430, doi:10.1126/science.255.5043.423, 1992.

Claeys, M., Iinuma, Y., Szmigielski, R., Surratt, J. D., Blockhuys, F., van Alsenoy, C., Boege, O., Sierau, B., Gomez-Gonzalez, Y., Vermeylen, R., van der Veken, P., Shahgholi, M., Chan, A. W. H., Herrmann, H., Seinfeld, J. H., and Maenhaut, W.: Terpenylic Acid and Related Compounds from the Oxidation of alpha-Pinene: Implications for New Particle Formation and Growth above Forests, Environmental Science & Technology, 43, 6976–6982, doi:10.1021/es9007596, 2009.

Claeys, M., Wang, W., Ion, A. C., Kourtchev, I., Gelencser, A., and Maenhaut, W.: Formation of secondary organic aerosols from isoprene and its gas-phase oxidation products through reaction with hydrogen peroxide, Atmospheric Environment, 38, 4093–4098, doi:10.1016/j.atmosenv.2004.06.001, 2004.

Clegg, S. L., Brimblecombe, P., and Wexler, A. S.: Thermodynamic model of the system H+-NH4+-Na+-SO42--NB3--Cl--H2O at 298.15 K, Journal of Physical Chemistry A, 102, 2155–2171, doi:10.1021/jp973043j, 1998.

Cooks, R. G., Glish, G. L., McLuckey, S. A., and Kaiser, R. E.: Ion Trap Mass Spectrometry, Chemical & Engineering News, 69, doi:10.1021/cen-v069n012.p026, 1991.

Corrigan, A. L., Russell, L. M., Takahama, S., Äijälä, M., Ehn, M., Junninen, H., Rinne, J., Petäjä, T., Kulmala, M., Vogel, A. L., Hoffmann, T., Ebben, C. J., Geiger, F. M., Chhabra, P., Seinfeld, J. H., Worsnop, D. R., Song, W., Auld, J., and Williams, J.: Biogenic and biomass burning organic aerosol in a boreal forest at Hyytiälä, Finland, during HUMPPA-COPEC 2010, Atmospheric Chemistry and Physics, 13, 12233–12256, doi:10.5194/acp-13-12233-2013, 2013.

Dal Maso, M., Sogacheva, L., Aalto, P. P., Riipinen, I., Komppula, M., Tunved, P., Korhonen, L., Suur-Uski, V., Hirsikko, A., Kurten, T., Kerminen, V.-M., Lihavainen, H., Viisanen, Y., Hansson, H.-C., and Kulmala, M.: Aerosol size distribution measurements at four Nordic field stations: identification, analysis and trajectory analysis of new particle formation bursts, Tellus Series B-Chemical and Physical Meteorology, 59, 350–361, doi:10.1111/j.1600-0889.2007.00267.x, 2007.

Di Carlo, P., Brune, W. H., Martinez, M., Harder, H., Lesher, R., Ren, X. R., Thornberry, T., Carroll, M. A., Young, V., Shepson, P. B., Riemer, D., Apel, E., and Campbell, C.: Missing OH reactivity in a forest: Evidence for unknown reactive biogenic VOCs, Science, 304, 722–725, doi:10.1126/science.1094392, 2004.

Docherty, K. S., Stone, E. A., Ulbrich, I. M., DeCarlo, P. F., Snyder, D. C., Schauer, J. J., Peltier, R. E., Weber, R. J., Murphy, S. M., Seinfeld, J. H., Grover, B. D., Eatough, D. J., and Jimenez, J. L.: Apportionment of Primary and Secondary Organic Aerosols in Southern California during the 2005 Study of Organic Aerosols in Riverside (SOAR-1), Environmental Science & Technology, 42, 7655–7662, doi:10.1021/es8008166, 2008.

Donahue, N. M., Epstein, S. A., Pandis, S. N., and Robinson, A. L.: A two-dimensional volatility basis set: 1. organic-aerosol mixing thermodynamics, Atmospheric Chemistry and Physics, 11, 3303–3318, doi:10.5194/acp-11-3303-2011, 2011.

Donahue, N. M., Henry, K. M., Mentel, T. F., Kiendler-Scharr, A., Spindler, C., Bohn, B., Brauers, T., Dorn, H. P., Fuchs, H., Tillmann, R., Wahner, A., Saathoff, H., Naumann, K.-H., Moehler, O., Leisner, T., Mueller, L., Reinnig, M.-C., Hoffmann, T., Salo, K., Hallquist, M., Frosch, M., Bilde, M., Tritscher, T., Barmet, P., Praplan, A. P., DeCarlo, P. F., Dommen, J., Prevot, A. S. H., and Baltensperger, U.: Aging of biogenic secondary organic aerosol via gas-phase OH radical reactions, Proceedings of the National Academy of Sciences of the United States of America, 109, 13503–13508, doi:10.1073/pnas.1115186109, 2012a.

Donahue, N. M., Kroll, J. H., Pandis, S. N., and Robinson, A. L.: A two-dimensional volatility basis set - Part 2: Diagnostics of organic-aerosol evolution, Atmospheric Chemistry and Physics, 12, 615–634, doi:10.5194/acp-12-615-2012, 2012b.

Donahue, N. M., Robinson, A. L., Stanier, C. O., and Pandis, S. N.: Coupled partitioning, dilution, and chemical aging of semivolatile organics, Environmental Science & Technology, 40, 2635–2643, doi:10.1021/es052297c, 2006.

Draxler, R.R. and Rolph, G.D.: HYSPLIT (HYbrid Single-Particle Lagrangian Integrated Trajectory) Model access via NOAA ARL READY Website (http://ready.arl.noaa.gov/HYSPLIT.php). NOAA Air Resources Laboratory, Silver Spring, MD, 2013.

Drewnick, F., Boettger, T., Weiden-Reinmueller, S.-L. von der, Zorn, S. R., Klimach, T., Schneider, J., and Borrmann, S.: Design of a mobile aerosol research laboratory and data

processing tools for effective stationary and mobile field measurements, Atmospheric Measurement Techniques, 5, 1443–1457, doi:10.5194/amt-5-1443-2012, 2012.

Drewnick, F., Hings, S. S., Alfarra, M. R., Prevot, A. S. H., and Borrmann, S.: Aerosol quantification with the Aerodyne Aerosol Mass Spectrometer: detection limits and ionizer background effects, Atmospheric Measurement Techniques, 2, 33–46, 2009.

Drewnick, F., Hings, S. S., DeCarlo, P., Jayne, J. T., Gonin, M., Fuhrer, K., Weimer, S., Jimenez, J. L., Demerjian, K. L., Borrmann, S., and Worsnop: A new time-of-flight aerosol mass spectrometer (TOF-AMS) - Instrument description and first field deployment, Aerosol Science and Technology, 39, 637–658, doi:10.1080/02786820500182040, 2005.

Dreyfus, M. A., Adou, K., Zucker, S. M., and Johnston, M. V.: Organic aerosol source apportionment from highly time-resolved molecular composition measurements, Atmospheric Environment, 43, 2901–2910, doi:10.1016/j.atmosenv.2009.03.008, 2009.

Dreyfus, M. A. and Johnston, M. V.: Rapid sampling of individual organic aerosol species in ambient air with the photoionization aerosol mass spectrometer, Aerosol Science and Technology, 42, 18–27, doi:10.1080/02786820701785112, 2008.

Dusek, U., Frank, G. P., Curtius, J., Drewnick, F., Schneider, J., Kuerten, A., Rose, D., Andreae, M. O., Borrmann, S., and Poeschl, U.: Enhanced organic mass fraction and decreased hygroscopicity of cloud condensation nuclei (CCN) during new particle formation events, Geophysical Research Letters, 37, doi:10.1029/2009GL040930, 2010.

Dusek, U., Frank, G. P., Hildebrandt, L., Curtius, J., Schneider, J., Walter, S., Chand, D., Drewnick, F., Hings, S., Jung, D., Borrmann, S., and Andreae, M. O.: Size matters more than chemistry for cloud-nucleating ability of aerosol particles, Science, 312, 1375–1378, doi:10.1126/science.1125261, 2006.

Farmer, D. K. and Jimenez, J. L.: Real-time Atmospheric Chemistry Field Instrumentation, Analytical Chemistry, 82, 7879–7884, doi:10.1021/ac1010603, 2010.

Farmer, D. K., Matsunaga, A., Docherty, K. S., Surratt, J. D., Seinfeld, J. H., Ziemann, P. J., and Jimenez, J. L.: Response of an aerosol mass spectrometer to organonitrates and organosulfates and implications for atmospheric chemistry, Proceedings of the National Academy of Sciences of the United States of America, 107, 6670–6675, doi:10.1073/pnas.0912340107, 2010.

Frank, G. P., Dusek, U., and Andreae, M. O.: Technical note: A method for measuring size-resolved CCN in the atmosphere, Atmospheric Chemistry and Physics Discussions, 6, 4879–4895, doi:10.5194/acpd-6-4879-2006, 2006.

Froyd, K. D., Murphy, S. M., Murphy, D. M., Gouw, J. A. de, Eddingsaas, N. C., and Wennberg, P. O.: Contribution of isoprene-derived organosulfates to free tropospheric aerosol mass, Proceedings of the National Academy of Sciences of the United States of America, 107, 21360–21365, doi:10.1073/pnas.1012561107, 2010.

Galloway, M. M., Chhabra, P. S., Chan, A. W. H., Surratt, J. D., Flagan, R. C., Seinfeld, J. H., and Keutsch, F. N.: Glyoxal uptake on ammonium sulphate seed aerosol: reaction products and reversibility of uptake under dark and irradiated conditions, Atmospheric Chemistry and Physics, 9, 3331–3345, 2009.

Geddes, S., Nichols, B., Todd, K., Zahardis, J., and Petrucci, G. A.: Near-infrared laser desorption/ionization aerosol mass spectrometry for measuring organic aerosol at atmospherically relevant aerosol mass loadings, Atmospheric Measurement Techniques, 3, 1175–1183, doi:10.5194/amt-3-1175-2010, 2010.

Geller, M. D., Biswas, S., Fine, P. A., and Sioutas, C.: A new compact aerosol concentrator for use in conjunction with low flow-rate continuous aerosol instrumentation, Journal of Aerosol Science, 36, 1006–1022, doi:10.1016/j.jaerosci.2004.11.015, 2005.

George, I. J., Vlasenko, A., Slowik, J. G., Broekhuizen, K., and Abbatt, J. P. D.: Heterogeneous oxidation of saturated organic aerosols by hydroxyl radicals: uptake kinetics, condensed-phase products, and particle size change, Atmospheric Chemistry and Physics, 7, 4187–4201, 2007.

Glasius, M., Duane, M., and Larsen, B. R.: Determination of polar terpene oxidation products in aerosols by liquid chromatography-ion trap mass spectrometry, Journal of Chromatography A, 833, 121–135, doi:10.1016/S0021-9673(98)01042-5, 1999.

Glasius, M., Lahaniati, M., Calogirou, A., Di Bella, D., Jensen, N. R., Hjorth, J., Kotzias, D., and Larsen, B. R.: Carboxylic acids in secondary aerosols from oxidation of cyclic monoterpenes by ozone, Environmental Science & Technology, 34, 1001–1010, doi:10.1021/es990445r, 2000.

Goldstein, A. H. and Galbally, I. E.: Known and unexplored organic constituents in the earth's atmosphere, Environmental Science & Technology, 41, 1514–1521, doi:10.1021/es072476p, 2007.

Gomez-Gonzalez, Y., Wang, W., Vermeylen, R., Chi, X., Neirynck, J., Janssens, I. A., Maenhaut, W., and Claeys, M.: Chemical characterisation of atmospheric aerosols during a 2007 summer field campaign at Brasschaat, Belgium: sources and source processes of biogenic secondary organic aerosol, Atmospheric Chemistry and Physics, 12, 125–138, doi:10.5194/acp-12-125-2012, 2012.

Guenther, A., Hewitt, C. N., Erickson, D., Fall, R., Geron, C., Graedel, T., Harley, P., Klinger, L., Lerdau, M., McKay, W. A., Pierce, T., Scholes, B., Steinbrecher, R., Tallamraju, R., Taylor, J., and Zimmerman, P.: A global model of natural volatile organic compound emissions, Journal of Geophysical Research-Atmospheres, 100, 8873–8892, doi:10.1029/94JD02950, 1995.

Gunthe, S. S., Rose, D., Su, H., Garland, R. M., Achtert, P., Nowak, A., Wiedensohler, A., Kuwata, M., Takegawa, N., Kondo, Y., Hu, M., Shao, M., Zhu, T., Andreae, M. O., and Poeschl, U.: Cloud condensation nuclei (CCN) from fresh and aged air pollution in the megacity region of Beijing, Atmospheric Chemistry and Physics, 11, 11023–11039, doi:10.5194/acp-11-11023-2011, 2011.

Hall, W. A., Pennington, M. R., and Johnston, M. V.: Molecular Transformations Accompanying the Aging of Laboratory Secondary Organic Aerosol, Environmental Science and Technology, 47, 2230–2237, doi:10.1021/es303891q, 2013.

Hallquist, M., Wenger, J. C., Baltensperger, U., Rudich, Y., Simpson, D., Claeys, M., Dommen, J., Donahue, N. M., George, C., Goldstein, A. H., Hamilton, J. F., Herrmann, H., Hoffmann, T., Iinuma, Y., Jang, M., Jenkin, M. E., Jimenez, J. L., Kiendler-Scharr, A., Maenhaut, W., McFiggans, G., Mentel, T. F., Monod, A., Prevot, A. S. H., Seinfeld, J. H., Surratt, J. D., Szmigielski, R., and Wildt, J.: The formation, properties and impact of secondary organic aerosol: current and emerging issues, Atmospheric Chemistry and Physics, 9, 5155–5236, 2009.

Hamilton, J. F., Alfarra, Wyche, K. P., Ward, M. W., Lewis, A. C., McFiggans, G. B., Good, N., Monks, P. S., Carr, T., White, I. R., and Purvis, R. M.: Investigating the use of secondary organic aerosol as seed particles in simulation chamber experiments, Atmospheric Chemistry and Physics, 11, 5917–5929, doi:10.5194/acp-11-5917-2011, 2011.

Hari, P. and Kulmala, M.: Station for measuring ecosystem-atmosphere relations (SMEAR II), Boreal Environment Research, 10, 315–322, 2005.

Hatch, L. E., Creamean, J. M., Ault, A. P., Surratt, J. D., Chan, M. N., Seinfeld, J. H., Edgerton, E. S., Su, Y., and Prather, K. A.: Measurements of Isoprene-Derived Organosulfates in Ambient Aerosols by Aerosol Time-of-Flight Mass Spectrometry - Part 1: Single Particle

Atmospheric Observations in Atlanta, Environmental Science & Technology, 45, 5105–5111, doi:10.1021/es103944a, 2011a.

Hatch, L. E., Creamean, J. M., Ault, A. P., Surratt, J. D., Chan, M. N., Seinfeld, J. H., Edgerton, E. S., Su, Y., and Prather, K. A.: Measurements of Isoprene-Derived Organosulfates in Ambient Aerosols by Aerosol Time-of-Flight Mass Spectrometry-Part 2: Temporal Variability and Formation Mechanisms, Environmental Science & Technology, 45, 8648–8655, doi:10.1021/es2011836, 2011b.

Heald, C. L., Jacob, D. J., Park, R. J., Russell, L. M., Huebert, B. J., Seinfeld, J. H., Liao, H., and Weber, R. J.: A large organic aerosol source in the free troposphere missing from current models, Geophysical Research Letters, 32, doi:10.1029/2005GL023831, 2005.

Hearn, J. D. and Smith, G. D.: Reactions and mass spectra of complex particles using Aerosol CIMS, International Journal of Mass Spectrometry, 258, 95–103, doi:10.1016/j.ijms.2006.05.017, 2006.

Hoffmann, T., Bandur, R., Hoffmann, S., and Warscheid, B.: On-line characterization of gaseous and particulate organic analytes using atmospheric pressure chemical ionization mass spectrometry, Spectrochimica Acta Part B-Atomic Spectroscopy, 57, 1635–1647, doi:10.1016/S0584-8547(02)00111-8, 2002.

Hoffmann, T., Bandur, R., Marggraf, U., and Linscheid, M.: Molecular composition of organic aerosols formed in the alpha-pinene/O-3 reaction: Implications for new particle formation processes, Journal of Geophysical Research-Atmospheres, 103, 25569–25578, doi:10.1029/98JD01816, 1998.

Hoffmann, T., Huang, R.-J., and Kalberer, M.: Atmospheric Analytical Chemistry, Analytical Chemistry, 83, 4649–4664, doi:10.1021/ac2010718, 2011.

Hohaus, T., Trimborn, D., Kiendler-Scharr, A., Gensch, I., Laumer, W., Kammer, B., Andres, S., Boudries, H., Smith, K. A., Worsnop, D. R., and Jayne, J. T.: A new aerosol collector for quasi on-line analysis of particulate organic matter: the Aerosol Collection Module (ACM) and first applications with a GC/MS-FID, Atmospheric Measurement Techniques, 3, 1423–1436, doi:10.5194/amt-3-1423-2010, 2010.

Holzinger, R., Williams, J., Herrmann, F., Lelieveld, J., Donahue, N. M., and Rockmann, T.: Aerosol analysis using a Thermal-Desorption Proton-Transfer-Reaction Mass Spectrometer (TD-PTR-MS): a new approach to study processing of organic aerosols, Atmospheric Chemistry and Physics, 10, 2257–2267, 2010.

Hu, Q. Z., Noll, R. J., Li, H. Y., Makarov, A., Hardman, M., and Cooks, R. G.: The Orbitrap: a new mass spectrometer, Journal of Mass Spectrometry, 40, 430–443, doi:10.1002/jms.856, 2005.

Iinuma, Y., Boege, O., Graefe, R., and Herrmann, H.: Methyl-Nitrocatechols: Atmospheric Tracer Compounds for Biomass Burning Secondary Organic Aerosols, Environmental Science & Technology, 44, 8453–8459, doi:10.1021/es102938a, 2010.

Iinuma, Y., Boege, O., Kahnt, A., and Herrmann, H.: Laboratory chamber studies on the formation of organosulfates from reactive uptake of monoterpene oxides, Physical Chemistry Chemical Physics, 11, 7985–7997, doi:10.1039/b904025k, 2009a.

Iinuma, Y., Boege, O., Keywood, M., Gnauk, T., and Herrmann, H.: Diaterebic Acid Acetate and Diaterpenylic Acid Acetate: Atmospheric Tracers for Secondary Organic Aerosol Formation from 1,8-Cineole Oxidation, Environmental Science & Technology, 43, 280–285, doi:10.1021/es802141v, 2009b.

Iinuma, Y., Kahnt, A., Mutzel, A., Boege, O., and Herrmann, H.: Ozone-Driven Secondary Organic Aerosol Production Chain, Environmental Science & Technology, 47, 3639–3647, doi:10.1021/es305156z, 2013.

Iinuma, Y., Muller, C., Berndt, T., Boge, O., Claeys, M., and Herrmann, H.: Evidence for the existence of organosulfates from beta-pinene ozonolysis in ambient secondary organic aerosol, Environmental Science & Technology, 41, 6678–6683, doi:10.1021/es070938t, 2007.

IPCC: Climate Change 2007: The Physical Science Basis. Contribution of Working Group I to the Fourth Assessment Report of the Intergovernmental Panel on Climate Change: Summary for Policymakers., Cambridge University Press, Cambridge, United Kingdom and New York, NY, USA., Cambridge, United Kingdom and New York, NY, USA, viii, 996, 2007.

IPCC: Climate Change 2013: The Physical Science Basis. Contribution of Working Group I to the Fifth Assessment Report of the Intergovernmental Panel on Climate Change: Summary for Policymakers., Cambridge University Press, Cambridge, United Kingdom and New York, NY, USA, 2013.

Jang, M. S., Czoschke, N. M., Lee, S., and Kamens, R. M.: Heterogeneous atmospheric aerosol production by acid-catalyzed particle-phase reactions, Science, 298, 814–817, doi:10.1126/science.1075798, 2002.

Jaoui, M., Corse, E., Kleindienst, T. E., Offenberg, J. H., Lewandowski, M., and Edney, E. O.: Analysis of secondary organic aerosol compounds from the photooxidation of d-limonene in the presence of NOX and their detection in ambient PM2.5, Environmental Science & Technology, 40, 3819–3828, doi:10.1021/es052566z, 2006.

Jaoui, M. and Kamens, R. M.: Gaseous and particulate oxidation products analysis of a mixture of alpha-pinene plus beta-pinene/O-3/air in the absence of light and alpha-pinene plus beta-pinene/NOx/air in the presence of natural sunlight, Journal of Atmospheric Chemistry, 44, 259–297, doi:10.1023/A:1022977427523, 2003.

Jayne, J. T., Leard, D. C., Zhang, X. F., Davidovits, P., Smith, K. A., Kolb, C. E., and Worsnop: Development of an aerosol mass spectrometer for size and composition analysis of submicron particles, Aerosol Science and Technology, 33, 49–70, doi:10.1080/027868200410840, 2000.

Jimenez, J. L., Canagaratna, M. R., Donahue, N. M., Prevot, A. S. H., Zhang, Q., Kroll, J. H., DeCarlo, P. F., Allan, J. D., Coe, H., Ng, N. L., Aiken, A. C., Docherty, K. S., Ulbrich, I. M., Grieshop, A. P., Robinson, A. L., Duplissy, J., Smith, J. D., Wilson, K. R., Lanz, V. A., Hueglin, C., Sun, Y. L., Tian, J., Laaksonen, A., Raatikainen, T., Rautiainen, J., Vaattovaara, P., Ehn, M., Kulmala, M., Tomlinson, J. M., Collins, D. R., Cubison, M. J., Dunlea, E. J., Huffman, J. A., Onasch, T. B., Alfarra, M. R., Williams, P. I., Bower, K., Kondo, Y., Schneider, J., Drewnick, F., Borrmann, S., Weimer, S., Demerjian, K., Salcedo, D., Cottrell, L., Griffin, R., Takami, A., Miyoshi, T., Hatakeyama, S., Shimono, A., Sun, J. Y., Zhang, Y. M., Dzepina, K., Kimmel, J. R., Sueper, D., Jayne, J. T., Herndon, S. C., Trimborn, A. M., Williams, L. R., Wood, E. C., Middlebrook, A. M., Kolb, C. E., Baltensperger, U., and Worsnop, D. R.: Evolution of Organic Aerosols in the Atmosphere, Science, 326, 1525–1529, doi:10.1126/science.1180353, 2009.

Jimenez, J. L., Jayne, J. T., Shi, Q., Kolb, C. E., Worsnop, Yourshaw, I., Seinfeld, J. H., Flagan, R. C., Zhang, X. F., Smith, K. A., Morris, J. W., and Davidovits, P.: Ambient aerosol sampling using the Aerodyne Aerosol Mass Spectrometer, Journal of Geophysical Research-Atmospheres, 108, doi:10.1029/2001JD001213, 2003.

Justesen, U.: Collision-induced fragmentation of deprotonated methoxylated flavonoids, obtained by electrospray ionization mass spectrometry, Journal of Mass Spectrometry, 36, 169–178, doi:10.1002/jms.118, 2001.

Kahnt, A., Iinuma, Y., Mutzel, A., Böge, O., Claeys, M., and Herrmann, H.: Campholenic aldehyde ozonolysis: a possible mechanism for the formation of specific biogenic secondary

organic aerosol constituents, Atmospheric Chemistry and Physics Discussions, 13, 22487–22534, doi:10.5194/acpd-13-22487-2013, 2013.

Kalberer, M., Paulsen, D., Sax, M., Steinbacher, M., Dommen, J., Prevot, A. S., Fisseha, R., Weingartner, E., Frankevich, V., Zenobi, R., and Baltensperger, U.: Identification of polymers as major components of atmospheric organic aerosols, Science, 303, 1659–1662, doi:10.1126/science.1092185, 2004.

Kalberer, M., Sax, M., and Samburova, V.: Molecular size evolution of oligomers in organic aerosols collected in urban atmospheres and generated in a smog chamber, Environmental Science & Technology, 40, 5917–5922, doi:10.1021/es0525760, 2006.

Kampf, C. J., Jakob, R., and Hoffmann, T.: Identification and characterization of aging products in the glyoxal/ammonium sulfate system - implications for light-absorbing material in atmospheric aerosols, Atmospheric Chemistry and Physics, 12, 6323–6333, doi:10.5194/acp-12-6323-2012, 2012.

Kanakidou, M., Seinfeld, J. H., Pandis, S. N., Barnes, I., Dentener, F. J., Facchini, M. C., van Dingenen, R., Ervens, B., Nenes, A., Nielsen, C. J., Swietlicki, E., Putaud, J. P., Balkanski, Y., Fuzzi, S., Horth, J., Moortgat, G. K., Winterhalter, R., Myhre, C. E., Tsigaridis, K., Vignati, E., Stephanou, E. G., and Wilson, J.: Organic aerosol and global climate modelling: a review, Atmospheric Chemistry and Physics, 5, 1053–1123, 2005.

Kesselmeier, J. and Staudt, M.: Biogenic volatile organic compounds (VOC): An overview on emission, physiology and ecology, Journal of Atmospheric Chemistry, 33, 23–88, doi:10.1023/A:1006127516791, 1999.

Kessler, S. H., Nah, T., Daumit, K. E., Smith, J. D., Leone, S. R., Kolb, C. E., Worsnop, D. R., Wilson, K. R., and Kroll, J. H.: OH-Initiated Heterogeneous Aging of Highly Oxidized Organic Aerosol, Journal of Physical Chemistry A, 116, 6358–6365, doi:10.1021/jp212131m, 2012.

Kessler, S. H., Smith, J. D., Che, D. L., Worsnop, D. R., Wilson, K. R., and Kroll, J. H.: Chemical Sinks of Organic Aerosol: Kinetics and Products of the Heterogeneous Oxidation of Erythritol and Levoglucosan, Environmental Science & Technology, 44, 7005–7010, doi:10.1021/es101465m, 2010.

Khlystov, A., Wyers, G. P., and Slanina, J.: The Steam-Jet Aerosol Collector, Atmospheric Environment, 29, 2229–2234, doi:10.1016/1352-2310(95)00180-7, 1995.

Khlystov, A., Zhang, Q., Jimenez, J. L., Stanier, C., Pandis, S. N., Canagaratna, Fine, P., Misra, C., and Sioutas, C.: In situ concentration of semi-volatile aerosol using water-condensation technology, Journal of Aerosol Science, 36, 866–880, doi:10.1016/j.jaerosci.2004.11.005, 2005.

Kiss, G., Tombacz, E., Varga, B., Alsberg, T., and Persson, L.: Estimation of the average molecular weight of humic-like substances isolated from fine atmospheric aerosol, Atmospheric Environment, 37, 3783–3794, doi:10.1016/S1352-2310(03)00468-0, 2003.

Konovalov, I. B., Beekmann, M., Kuznetsova, I. N., Yurova, A., and Zvyagintsev, A. M.: Atmospheric impacts of the 2010 Russian wildfires: integrating modelling and measurements of an extreme air pollution episode in the Moscow region, Atmospheric Chemistry and Physics, 11, 10031–10056, doi:10.5194/acp-11-10031-2011, 2011.

Kourtchev, I., Fuller, S., Aalto, J., Ruuskanen, T. M., McLeod, M. W., Maenhaut, W., Jones, R., Kulmala, M., and Kalberer, M.: Molecular Composition of Boreal Forest Aerosol from Hyytiala, Finland, Using Ultrahigh Resolution Mass Spectrometry, Environmental Science & Technology, 47, 4069–4079, doi:10.1021/es3051636, 2013.

Kourtchev, I., Ruuskanen, T. M., Keronen, P., Sogacheva, L., Dal Maso, M., Reissell, A., Chi, X., Vermeylen, R., Kulmala, M., Maenhaut, W., and Claeys, M.: Determination of isoprene

and alpha-/beta-pinene oxidation products in boreal forest aerosols from Hyytiala, Finland: diel variations and possible link with particle formation events, Plant Biology, 10, 138–149, doi:10.1055/s-2007-964945, 2008.

Kreidenweis, S. M., Petters, M. D., and DeMott, P. J.: Deliquescence-controlled activation of organic aerosols, Geophysical Research Letters, 33, doi:10.1029/2005GL024863, 2006.

Kristensen, K. and Glasius, M.: Organosulfates and oxidation products from biogenic hydrocarbons in fine aerosols from a forest in North West Europe during spring, Atmospheric Environment, 45, 4546–4556, doi:10.1016/j.atmosenv.2011.05.063, 2011.

Kroll, J. H., Donahue, N. M., Jimenez, J. L., Kessler, S. H., Canagaratna, M. R., Wilson, K. R., Altieri, K. E., Mazzoleni, L. R., Wozniak, A. S., Bluhm, H., Mysak, E. R., Smith, J. D., Kolb, C. E., and Worsnop, D. R.: Carbon oxidation state as a metric for describing the chemistry of atmospheric organic aerosol, Nature Chemistry, 3, 133–139, doi:10.1038/NCHEM.948, 2011.

Kroll, J. H. and Seinfeld, J. H.: Chemistry of secondary organic aerosol: Formation and evolution of low-volatility organics in the atmosphere, Atmospheric Environment, 42, 3593–3624, doi:10.1016/j.atmosenv.2008.01.003, 2008.

Kuckelmann, U., Warscheid, S., and Hoffmann, T.: On-line characterization of organic aerosols formed from biogenic precursors using atmospheric pressure chemical ionization mass spectrometry, Analytical Chemistry, 72, 1905–1912, doi:10.1021/ac991178a, 2000.

Kulmala, M., Asmi, A., Lappalainen, H. K., Baltensperger, U., Brenguier, J.-L., Facchini, M. C., Hansson, H.-C., Hov, O., O'Dowd, C. D., Pöschl, U., Wiedensohler, A., Boers, R., Boucher, O., Leeuw, G. de, van der Gon, H. A. C. D., Feichter, J., Krejci, R., Laj, P., Lihavainen, H., Lohmann, U., McFiggans, G., Mentel, T., Pilinis, C., Riipinen, I., Schulz, M., Stohl, A., Swietlicki, E., Vignati, E., Alves, C., Amann, M., Ammann, M., Arabas, S., Artaxo, P., Baars, H., Beddows, D. C. S., Bergstrom, R., Beukes, J. P., Bilde, M., Burkhart, J. F., Canonaco, F., Clegg, S. L., Coe, H., Crumeyrolle, S., D'Anna, B., Decesari, S., Gilardoni, S., Fischer, M., Fjaeraa, A. M., Fountoukis, C., George, C., Gomes, L., Halloran, P., Hamburger, T., Harrison, R. M., Herrmann, H., Hoffmann, T., Hoose, C., Hu, M., Hyvarinen, A., Horrak, U., Iinuma, Y., Iversen, T., Josipovic, M., Kanakidou, M., Kiendler-Scharr, A., Kirkevag, A., Kiss, G., Klimont, Z., Kolmonen, P., Komppula, M., Kristjansson, J.-E., Laakso, L., Laaksonen, A., Labonnote, L., Lanz, V. A., Lehtinen, K. E. J., Rizzo, L. V., Makkonen, R., Manninen, H. E., McMeeking, G., Merikanto, J., Minikin, A., Mirme, S., Morgan, W. T., Nemitz, E., O'Donnell, D., Panwar, T. S., Pawlowska, H., Petzold, A., Pienaar, J. J., Pio, C., Plass-Duelmer, C., Prevot, A. S. H., Pryor, S., Reddington, C. L., Roberts, G., Rosenfeld, D., Schwarz, J., Seland, O., Sellegri, K., Shen, X. J., Shiraiwa, M., Siebert, H., Sierau, B., Simpson, D., Sun, J. Y., Topping, D., Tunved, P., Vaattovaara, P., Vakkari, V., Veefkind, J. P., Visschedijk, A., Vuollekoski, H., Vuolo, R., Wehner, B., Wildt, J., Woodward, S., Worsnop, D. R., van Zadelhoff, G.-J., Zardini, A. A., Zhang, K., van Zyl, P. G., Kerminen, V.-M., Carslaw, K. S., and Pandis, S. N.: General overview: European Integrated project on Aerosol Cloud Climate and Air Quality interactions (EUCAARI) - integrating aerosol research from nano to global scales, Atmospheric Chemistry and Physics, 11, 13061–13143, doi:10.5194/acp-11-13061-2011, 2011.

Kulmala, M., Hameri, K., Aalto, P. P., Makela, J. M., Pirjola, L., Nilsson, E. D., Buzorius, G., Rannik, U., Dal Maso, M., Seidl, W., Hoffman, T., Janson, R., Hansson, H. C., Viisanen, Y., Laaksonen, A., and O'Dowd, C. D.: Overview of the international project on biogenic aerosol formation in the boreal forest (BIOFOR), Tellus Series B-Chemical and Physical Meteorology, 53, 324–343, doi:10.1034/j.1600-0889.2001.530402.x, 2001.

Kulmala, M., Kontkanen, J., Junninen, H., Lehtipalo, K., Manninen, H. E., Nieminen, T., Petaja, T., Sipila, M., Schobesberger, S., Rantala, P., Franchin, A., Jokinen, T., Jarvinen, E., Aijala, M., Kangasluoma, J., Hakala, J., Aalto, P. P., Paasonen, P., Mikkila, J., Vanhanen, J., Aalto,

J., Hakola, H., Makkonen, U., Ruuskanen, T., Mauldin, R. L., III, Duplissy, J., Vehkamaki, H., Back, J., Kortelainen, A., Riipinen, I., Kurten, T., Johnston, M. V., Smith, J. N., Ehn, M., Mentel, T. F., Lehtinen, K. E. J., Laaksonen, A., Kerminen, V.-M., and Worsnop, D. R.: Direct Observations of Atmospheric Aerosol Nucleation, Science, 339, 943–946, doi:10.1126/science.1227385, 2013.

Laaksonen, A., Korhonen, P., Kulmala, M., and Charlson, R. J.: Modification of the Kuhler equation to include soluble trace gases and slightly soluble substances, Journal of the Atmospheric Sciences, 55, 853–862, doi:10.1175/1520-0469(1998)055<0853:MOTKHE>2.0.CO;2, 1998.

Lambe, A. T., Onasch, T. B., Massoli, P., Croasdale, D. R., Wright, J. P., Ahern, A. T., Williams, L. R., Worsnop, D. R., Brune, W. H., and Davidovits, P.: Laboratory studies of the chemical composition and cloud condensation nuclei (CCN) activity of secondary organic aerosol (SOA) and oxidized primary organic aerosol (OPOA), Atmospheric Chemistry and Physics, 11, 8913–8928, doi:10.5194/acp-11-8913-2011, 2011.

Laskin, A., Laskin, J., and Nizkorodov, S. A.: Mass spectrometric approaches for chemical characterisation of atmospheric aerosols: critical review of the most recent advances, Environmental Chemistry, 9, 163–189, doi:10.1071/EN12052, 2012.

LeClair, J. P., Collett, J. L., and Mazzoleni, L. R.: Fragmentation Analysis of Water-Soluble Atmospheric Organic Matter Using Ultrahigh-Resolution FT-ICR Mass Spectrometry, Environmental Science & Technology, 46, 4312–4322, doi:10.1021/es203509b, 2012.

Liang, C. K. and Pankow, J. F.: Gas/particle partitioning of organic compounds to environmental tobacco smoke: Partition coefficient measurements by desorption and comparison to urban particulate material, Environmental Science & Technology, 30, 2800–2805, doi:10.1021/es960050x, 1996.

Liggio, J. and Li, S.-M.: Organosulfate formation during the uptake of pinonaldehyde on acidic sulfate aerosols, Geophysical Research Letters, 33, doi:10.1029/2006GL026079, 2006.

Lim, H. J. and Turpin, B. J.: Origins of primary and secondary organic aerosol in Atlanta: Results' of time-resolved measurements during the Atlanta supersite experiment, Environmental Science & Technology, 36, 4489–4496, doi:10.1021/es0206487, 2002.

Lim, Y. B., Tan, Y., Perri, M. J., Seitzinger, S. P., and Turpin, B. J.: Aqueous chemistry and its role in secondary organic aerosol (SOA) formation, Atmospheric Chemistry and Physics, 10, 10521–10539, doi:10.5194/acp-10-10521-2010, 2010.

Lin, P., Yu, J. Z., Engling, G., and Kalberer, M.: Organosulfates in Humic-like Substance Fraction Isolated from Aerosols at Seven Locations in East Asia: A Study by Ultra-High-Resolution Mass Spectrometry, Environmental Science & Technology, 46, 13118–13127, doi:10.1021/es303570v, 2012.

Lin, Y.-H., Knipping, E. M., Edgerton, E. S., Shaw, S. L., and Surratt, J. D.: Investigating the influences of SO2 and NH3 levels on isoprene-derived secondary organic aerosol formation using conditional sampling approaches, Atmospheric Chemistry and Physics, 13, 8457–8470, doi:10.5194/acp-13-8457-2013, 2013.

Lohmann, U. and Feichter, J.: Global indirect aerosol effects: a review, Atmospheric Chemistry and Physics, 5, 715–737, 2005.

Lopez-Hilfiker, F. D., Mohr, C., Ehn, M., Rubach, F., Kleist, E., Wildt, J., Mentel, T. F., Lutz, A., Hallquist, M., Worsnop, D., and Thornton, J. A.: A novel method for on-line analysis of gas and particle composition: description and evaluation of a Filter Inlet for Gases and AEROsols (FIGAERO), Atmospheric Measurement Techniques Discussions, 6, 9347–9395, doi:10.5194/amtd-6-9347-2013, 2013.

Lukacs, H., Gelencser, A., Hoffer, A., Kiss, G., Horvath, K., and Hartyani, Z.: Quantitative assessment of organosulfates in size-segregated rural fine aerosol, Atmospheric Chemistry and Physics, 9, 231–238, 2009.

Makarov, A.: Electrostatic axially harmonic orbital trapping: A high-performance technique of mass analysis, Analytical Chemistry, 72, 1156–1162, doi:10.1021/ac991131p, 2000.

Mauderly, J. L. and Chow, J. C.: Health effects of organic aerosols, Inhalation Toxicology, 20, 257–288, doi:10.1080/08958370701866008, 2008.

Ma, Y., Chen, J., and Wang, L.: Characteristics and Formation Mechanisms of Atmospheric Organosulfates, Progress in Chemistry, 24, 2277–2286, 2012.

Ma, Y., Porter, R. A., Chappell, D., Russell, A. T., and Marston, G.: Mechanisms for the formation of organic acids in the gas-phase ozonolysis of 3-carene, Physical Chemistry Chemical Physics, 11, 4184–4197, doi:10.1039/b818750a, 2009.

McFiggans, G., Artaxo, P., Baltensperger, U., Coe, H., Facchini, M. C., Feingold, G., Fuzzi, S., Gysel, M., Laaksonen, A., Lohmann, U., Mentel, T. F., Murphy, D. M., O'Dowd, C. D., Snider, J. R., and Weingartner, E.: The effect of physical and chemical aerosol properties on warm cloud droplet activation, Atmospheric Chemistry and Physics, 6, 2593–2649, 2006.

Middlebrook, A. M., Bahreini, R., Jimenez, J. L., and Canagaratna, M. R.: Evaluation of Composition-Dependent Collection Efficiencies for the Aerodyne Aerosol Mass Spectrometer using Field Data, Aerosol Science and Technology, 46, 258–271, doi:10.1080/02786826.2011.620041, 2012.

Minerath, E. C., Casale, M. T., and Elrod, M. J.: Kinetics feasibility study of alcohol sulfate esterification reactions in tropospheric aerosols, Environmental Science & Technology, 42, 4410–4415, doi:10.1021/es8004333, 2008.

Minerath, E. C., Schultz, M. P., and Elrod, M. J.: Kinetics of the Reactions of Isoprene-Derived Epoxides in Model Tropospheric Aerosol Solutions, Environmental Science & Technology, 43, 8133–8139, doi:10.1021/es902304p, 2009.

Mitchum, R. K. and Korfmacher, W. A.: Atmospheric Pressure Ionization Mass Spectrometry, Analytical Chemistry, 55, 1485–&, 1983.

Moglioni, A. G., Garcia-Exposito, E., Aguado, G. P., Parella, T., Branchadell, V., Moltrasio, G. Y., and Ortuno, R. M.: Divergent routes to chiral cyclobutane synthons from (-)-alpha-pinene and their use in the stereoselective synthesis of dehydro amino acids, Journal of Organic Chemistry, 65, 3934–3940, doi:10.1021/jo991773c, 2000.

Mohr, C., Lopez-Hilfiker, F. D., Zotter, P., Prevot, A. S. H., Xu, L., Ng, N. L., Herndon, S. C., Williams, L. R., Franklin, J. P., Zahniser, M. S., Worsnop, D. R., Knighton, W. B., Aiken, A. C., Gorkowski, K. J., Dubey, M. K., Allan, J. D., and Thornton, J. A.: Contribution of Nitrated Phenols to Wood Burning Brown Carbon Light Absorption in Detling, United Kingdom during Winter Time, Environmental Science & Technology, 47, 6316–6324, doi:10.1021/es400683v, 2013.

Mueller, L., Reinnig, M.-C., Naumann, K. H., Saathoff, H., Mentel, T. F., Donahue, N. M., and Hoffmann, T.: Formation of 3-methyl-1,2,3-butanetricarboxylic acid via gas phase oxidation of pinonic acid - a mass spectrometric study of SOA aging, Atmospheric Chemistry and Physics, 12, 1483–1496, doi:10.5194/acp-12-1483-2012, 2012.

Mueller, L., Reinnig, M.-C., Warnke, J., and Hoffmann, T.: Unambiguous identification of esters as oligomers in secondary organic aerosol formed from cyclohexene and cyclohexene/alpha-pinene ozonolysis, Atmospheric Chemistry and Physics, 8, 1423–1433, 2008.

Murphy, D. M., Cziczo, D. J., Froyd, K. D., Hudson, P. K., Matthew, B. M., Middlebrook, A. M., Peltier, R. E., Sullivan, A., Thomson, D. S., and Weber, R. J.: Single-particle mass

spectrometry of tropospheric aerosol particles, Journal of Geophysical Research-Atmospheres, 111, doi:10.1029/2006JD007340, 2006.

Nenes, A., Charlson, R. J., Facchini, M. C., Kulmala, M., Laaksonen, A., and Seinfeld, J. H.: Can chemical effects on cloud droplet number rival the first indirect effect?, Geophysical Research Letters, 29, doi:10.1029/2002GL015295, 2002.

Net, S., Alvarez, E. G., Gligorovski, S., and Wortham, H.: Heterogeneous reactions of ozone with methoxyphenols, in presence and absence of light, Atmospheric Environment, 45, 3007–3014, doi:10.1016/j.atmosenv.2011.03.026, 2011.

Ng, N. L., Canagaratna, M. R., Jimenez, J. L., Chhabra, P. S., Seinfeld, J. H., and Worsnop, D. R.: Changes in organic aerosol composition with aging inferred from aerosol mass spectra, Atmospheric Chemistry and Physics, 11, 6465–6474, doi:10.5194/acp-11-6465-2011, 2011.

Ng, N. L., Canagaratna, M. R., Zhang, Q., Jimenez, J. L., Tian, J., Ulbrich, I. M., Kroll, J. H., Docherty, K. S., Chhabra, P. S., Bahreini, R., Murphy, S. M., Seinfeld, J. H., Hildebrandt, L., Donahue, N. M., DeCarlo, P. F., Lanz, V. A., Prevot, A. S. H., Dinar, E., Rudich, Y., and Worsnop, D. R.: Organic aerosol components observed in Northern Hemispheric datasets from Aerosol Mass Spectrometry, Atmospheric Chemistry and Physics, 10, 4625–4641, doi:10.5194/acp-10-4625-2010, 2010.

Ng, N. L., Kwan, A. J., Surratt, J. D., Chan, A. W. H., Chhabra, P. S., Sorooshian, A., Pye, H. O. T., Crounse, J. D., Wennberg, P. O., Flagan, R. C., and Seinfeld, J. H.: Secondary organic aerosol (SOA) formation from reaction of isoprene with nitrate radicals (NO3), Atmospheric Chemistry and Physics, 8, 4117–4140, 2008.

Nguyen, T. B., Lee, P. B., Updyke, K. M., Bones, D. L., Laskin, J., Laskin, A., and Nizkorodov, S. A.: Formation of nitrogen- and sulfur-containing light-absorbing compounds accelerated by evaporation of water from secondary organic aerosols, Journal of Geophysical Research-Atmospheres, 117, doi:10.1029/2011JD016944, 2012.

Nilsson, E. D., Paatero, J., and Boy, M.: Effects of air masses and synoptic weather on aerosol formation in the continental boundary layer, Tellus Series B-Chemical and Physical Meteorology, 53, 462–478, doi:10.1034/j.1600-0889.2001.530410.x, 2001.

Ning, Z., Moore, K. F., Polidori, A., and Sioutas, C.: Field validation of the new miniature Versatile Aerosol Concentration Enrichment System (mVACES), Aerosol Science and Technology, 40, 1098–1110, doi:10.1080/02786820600996422, 2006.

Nizkorodov, S. A., Laskin, J., and Laskin, A.: Molecular chemistry of organic aerosols through the application of high resolution mass spectrometry, Physical Chemistry Chemical Physics, 13, 3612–3629, doi:10.1039/c0cp02032j, 2011.

Nölscher, A. C., Williams, J., Sinha, V., Custer, T., Song, W., Johnson, A. M., Axinte, R., Bozem, H., Fischer, H., Pouvesle, N., Phillips, G., Crowley, J. N., Rantala, P., Rinne, J., Kulmala, M., Gonzales, D., Valverde-Canossa, J., Vogel, A. L., Hoffmann, T., Ouwersloot, H. G., Arellano, J. V.-G. de, and Lelieveld, J.: Summertime total OH reactivity measurements from boreal forest during HUMPPA-COPEC 2010, Atmospheric Chemistry and Physics, 12, 8257–8270, doi:10.5194/acp-12-8257-2012, 2012.

Offenberg, J. H., Kleindienst, T. E., Jaoui, M., Lewandowski, M., and Edney, E. O.: Thermal properties of secondary organic aerosols, Geophysical Research Letters, 33, doi:10.1029/2005GL024623, 2006.

Paatero, P. and Tapper, U.: Positive matrix factorization: A non-negative factor model with optimal utilization of error estimates of data values, Environmetrics, 5, 111–126, doi:10.1002/env.3170050203, 1994.

Pankow, J. F.: An absorption model of gas/particle partitioning of organic compounds in the atmosphere, Atmospheric Environment, 28, 185–188, doi:10.1016/1352-2310(94)90093-0, 1994a.

Pankow, J. F.: An absorption model of the gas/aerosol partitioning involved in the formation of secondary organic aerosol, Atmospheric Environment, 28, 189–193, doi:10.1016/1352-2310(94)90094-9, 1994b.

Pankow, J. F.: On the ability of the gas/particle partitioning constant K-p to consider the effects of mean MW and the presence of high MW compounds, Atmospheric Environment, 45, 1213–1216, doi:10.1016/j.atmosenv.2010.11.041, 2011.

Pankow, J. F. and Asher, W. E.: SIMPOL.1: a simple group contribution method for predicting vapor pressures and enthalpies of vaporization of multifunctional organic compounds, Atmospheric Chemistry and Physics, 8, 2773–2796, 2008.

Perry, R. H., Cooks, R. G., and Noll, R. J.: Orbitrap mass spectrometry: instrumentation, ion motion and applications, Mass Spectrometry Reviews, 27, 661–699, doi:10.1002/mas.20186, 2008.

Petters, M. D. and Kreidenweis, S. M.: A single parameter representation of hygroscopic growth and cloud condensation nucleus activity, Atmospheric Chemistry and Physics, 7, 1961–1971, 2007.

Phillips, G. J., Makkonen, U., Schuster, G., Sobanski, N., Hakola, H., and Crowley, J. N.: The detection of nocturnal N2O5 as HNOr3 by alkali- and aqueous-denuder techniques, Atmospheric Measurement Techniques, 6, 231–237, doi:10.5194/amt-6-231-2013, 2013.

Pierce, J. R., Riipinen, I., Kulmala, M., Ehn, M., Petaja, T., Junninen, H., Worsnop, D. R., and Donahue, N. M.: Quantification of the volatility of secondary organic compounds in ultrafine particles during nucleation events, Atmospheric Chemistry and Physics, 11, 9019–9036, doi:10.5194/acp-11-9019-2011, 2011.

Pope, C. A. and Dockery, D. W.: Health effects of fine particulate air pollution: Lines that connect, Journal of the Air & Waste Management Association, 56, 709–742, 2006.

Pope, C. A., III, Ezzati, M., and Dockery, D. W.: Fine-Particulate Air Pollution and Life Expectancy in the United States, New England Journal of Medicine, 360, 376–386, doi:10.1056/NEJMsa0805646, 2009.

Portin, H., Mielonen, T., Leskinen, A., Arola, A., Parjala, E., Romakkaniemi, S., Laaksonen, A., Lehtinen, K. E. J., and Komppula, M.: Biomass burning aerosols observed in Eastern Finland during the Russian wildfires in summer 2010-Part 1: In-situ aerosol characterization, Atmospheric Environment, 47, 269–278, doi:10.1016/j.atmosenv.2011.10.067, 2012.

Pöschl, U.: Atmospheric aerosols: Composition, transformation, climate and health effects, Angewandte Chemie-International Edition, 44, 7520–7540, doi:10.1002/anie.200501122, 2005.

Pöschl, U., Rose, D., and Andreae, M. O.: Climatologies of cloud-related aerosols: Part 2: particle hygroscopicity and cloud condensation nucleus activity, in: Clouds in the perturbed climate system: Their relationship to energy balance, atmospheric dynamics, and precipitation, Heintzenberg, J., Charlson, R. J. (Eds.), MIT Press, Cambridge, Mass, 57–72, 2009.

Prather, K. A., Hatch, C. D., and Grassian, V. H.: Analysis of Atmospheric Aerosols, Annual Review of Analytical Chemistry, 1, 485–514, doi:10.1146/annurev.anchem.1.031207.113030, 2008.

Pratt, K. A. and Prather, K. A.: Mass spectrometry of atmospheric aerosolsuRecent developments and applications. Part II: On-line mass spectrometry techniques, Mass Spectrometry Reviews, 31, 17–48, doi:10.1002/mas.20330, 2012.

Prenni, A. J., Petters, M. D., Kreidenweis, S. M., DeMott, P. J., and Ziemann, P. J.: Cloud droplet activation of secondary organic aerosol, Journal of Geophysical Research-Atmospheres, 112, doi:10.1029/2006JD007963, 2007.

Quinn, P. K., Bates, T. S., Coffman, D., Onasch, T. B., Worsnop, D., Baynard, T., Gouw, J. A. de, Goldan, P. D., Kuster, W. C., Williams, E., Roberts, J. M., Lerner, B., Stohl, A., Pettersson, A., and Lovejoy, E. R.: Impacts of sources and aging on submicrometer aerosol properties in the marine boundary layer across the Gulf of Maine, Journal of Geophysical Research-Atmospheres, 111, doi:10.1029/2006JD007582, 2006.

Ramanathan, V. and Carmichael, G.: Global and regional climate changes due to black carbon, Nature Geoscience, 1, 221–227, doi:10.1038/ngeo156, 2008.

Ramanathan, V., Crutzen, P. J., Kiehl, J. T., and Rosenfeld, D.: Atmosphere - Aerosols, climate, and the hydrological cycle, Science, 294, 2119–2124, doi:10.1126/science.1064034, 2001.

Ravishankara, A. R.: Heterogeneous and multiphase chemistry in the troposphere, Science, 276, 1058–1065, doi:10.1126/science.276.5315.1058, 1997.

Raymond, T. M. and Pandis, S. N.: Formation of cloud droplets by multicomponent organic particles, Journal of Geophysical Research-Atmospheres, 108, doi:10.1029/2003JD003503, 2003.

Reemtsma, T., These, A., Venkatachari, P., Xia, X., Hopke, P. K., Springer, A., and Linscheid, M.: Identification of fulvic acids and sulfated and nitrated analogues in atmospheric aerosol by electrospray ionization Fourier transform ion cyclotron resonance mass spectrometry, Analytical Chemistry, 78, 8299–8304, doi:10.1021/ac061320p, 2006.

Reinnig, M.-C., Warnke, J., and Hoffmann, T.: Identification of organic hydroperoxides and hydroperoxy acids in secondary organic aerosol formed during the ozonolysis of different monoterpenes and sesquiterpenes by on-line analysis using atmospheric pressure chemical ionization ion trap mass spectrometry, Rapid Communications in Mass Spectrometry, 23, 1735–1741, doi:10.1002/rcm.4065, 2009.

Riipinen, I., Yli-Juuti, T., Pierce, J. R., Petaja, T., Worsnop, D. R., Kulmala, M., and Donahue, N. M.: The contribution of organics to atmospheric nanoparticle growth, Nature Geoscience, 5, 453–458, doi:10.1038/ngeo1499, 2012.

Roberts, G. C. and Nenes, A.: A continuous-flow streamwise thermal-gradient CCN chamber for atmospheric measurements, Aerosol Science and Technology, 39, 206–221, doi:10.1080/027868290913988, 2005.

Robinson, A. L., Donahue, N. M., Shrivastava, M. K., Weitkamp, E. A., Sage, A. M., Grieshop, A. P., Lane, T. E., Pierce, J. R., and Pandis, S. N.: Rethinking organic aerosols: Semivolatile emissions and photochemical aging, Science, 315, 1259–1262, doi:10.1126/science.1133061, 2007.

Rolph, G.D., Real-time Environmental Applications and Display sYstem (READY) Website (http://ready.arl.noaa.gov). NOAA Air Resources Laboratory, Silver Spring, MD, 2013.

Romero, F. and Oehme, M.: Organosulfates - A new component of humic-like substances in atmospheric aerosols?, Journal of Atmospheric Chemistry, 52, 283–294, doi:10.1007/s10874-005-0594-y, 2005.

Rose, D., Gunthe, S. S., Mikhailov, E., Frank, G. P., Dusek, U., Andreae, M. O., and Pöschl, U.: Calibration and measurement uncertainties of a continuous-flow cloud condensation nuclei

counter (DMT-CCNC): CCN activation of ammonium sulfate and sodium chloride aerosol particles in theory and experiment, Atmospheric Chemistry and Physics, 8, 1153–1179, 2008.

Rose, D., Gunthe, S. S., Su, H., Garland, R. M., Yang, H., Berghof, M., Cheng, Y. F., Wehner, B., Achtert, P., Nowak, A., Wiedensohler, A., Takegawa, N., Kondo, Y., Hu, M., Zhang, Y., Andreae, M. O., and Poeschl, U.: Cloud condensation nuclei in polluted air and biomass burning smoke near the mega-city Guangzhou, China -Part 2: Size-resolved aerosol chemical composition, diurnal cycles, and externally mixed weakly CCN-active soot particles, Atmospheric Chemistry and Physics, 11, 2817–2836, doi:10.5194/acp-11-2817-2011, 2011.

Rose, D., Nowak, A., Achtert, P., Wiedensohler, A., Hu, M., Shao, M., Zhang, Y., Andreae, M. O., and Poeschl, U.: Cloud condensation nuclei in polluted air and biomass burning smoke near the mega-city Guangzhou, China - Part 1: Size-resolved measurements and implications for the modeling of aerosol particle hygroscopicity and CCN activity, Atmospheric Chemistry and Physics, 10, 3365–3383, 2010.

Rosenfeld, D., Lohmann, U., Raga, G. B., O'Dowd, C. D., Kulmala, M., Fuzzi, S., Reissell, A., and Andreae, M. O.: Flood or drought: How do aerosols affect precipitation?, Science, 321, 1309–1313, doi:10.1126/science.1160606, 2008.

Rossignol, S., Chiappini, L., Perraudin, E., Rio, C., Fable, S., Valorso, R., and Doussin, J. F.: Development of a parallel sampling and analysis method for the elucidation of gas/particle partitioning of oxygenated semi-volatile organics: a limonene ozonolysis study, Atmospheric Measurement Techniques, 5, 1459–1489, doi:10.5194/amt-5-1459-2012, 2012.

Rumsey, I. C., Cowen, K. A., Walker, J. T., Kelly, T. J., Hanft, E. A., Mishoe, K., Rogers, C., Proost, R., Beachley, G. M., Lear, G., Frelink, T., and Otjes, R. P.: An assessment of the performance of the Monitor for AeRosols and GAses in ambient air (MARGA): a semi-continuous method for soluble compounds, Atmospheric Chemistry and Physics Discussions, 13, 25067–25124, doi:10.5194/acpd-13-25067-2013, 2013.

Russell, L. M., Takahama, S., Liu, S., Hawkins, L. N., Covert, D. S., Quinn, P. K., and Bates, T. S.: Oxygenated fraction and mass of organic aerosol from direct emission and atmospheric processing measured on the R/V Ronald Brown during TEXAQS/GoMACCS 2006, Journal of Geophysical Research-Atmospheres, 114, doi:10.1029/2008JD011275, 2009.

Sabine, C. L., Heimann, M., Artaxo, P., Bakker, D. C. E., Chen, C. A., Field, C. B., Gruber, N., Quéré, C., Prinn, R., Richey, J. E., Romero Lankao, P., Satahaye, J. A., and Valentin, R. (Eds.): Current Status and Past Trends of the Global Carbon Cycle: The global carbon cycle: Integrating humans, climate, and the natural world, SCOPE, 62, Island Press, Washington, 1 online resource (xxiv, 526, 2004.

Satheesh, S. K. and Moorthy, K. K.: Radiative effects of natural aerosols: A review, Atmospheric Environment, 39, 2089–2110, doi:10.1016/j.atmosenv.2004.12.029, 2005.

Saukko, E., Kuuluvainen, H., and Virtanen, A.: A method to resolve the phase state of aerosol particles, Atmospheric Measurement Techniques, 5, 259–265, doi:10.5194/amt-5-259-2012, 2012.

Schwartz, J., Dockery, D. W., and Neas, L. M.: Is daily mortality associated specifically with fine particles?, Journal of the Air & Waste Management Association, 46, 927–939, 1996.

Seinfeld, J. H. and Pandis, S. N.: Atmospheric chemistry and physics: From air pollution to climate change, 2nd ed., J. Wiley, Hoboken, N.J, xxviii, 1203, 2006.

Shapiro, E. L., Szprengiel, J., Sareen, N., Jen, C. N., Giordano, M. R., and McNeill, V. F.: Light-absorbing secondary organic material formed by glyoxal in aqueous aerosol mimics, Atmospheric Chemistry and Physics, 9, 2289–2300, 2009.

Shilling, J. E., Chen, Q., King, S. M., Rosenoern, T., Kroll, J. H., Worsnop, D. R., DeCarlo, P. F., Aiken, A. C., Sueper, D., Jimenez, J. L., and Martin, S. T.: Loading-dependent elemental

composition of alpha-pinene SOA particles, Atmospheric Chemistry and Physics, 9, 771–782, 2009.

Shilling, J. E., King, S. M., Mochida, M., and Martin, S. T.: Mass spectral evidence that small changes in composition caused by oxidative aging processes alter aerosol CCN properties, Journal of Physical Chemistry A, 111, 3358–3368, doi:10.1021/jp068822r, 2007.

Shiraiwa, M., Ammann, M., Koop, T., and Poeschl, U.: Gas uptake and chemical aging of semisolid organic aerosol particles, Proceedings of the National Academy of Sciences of the United States of America, 108, 11003–11008, doi:10.1073/pnas.1103045108, 2011.

Shiraiwa, M. and Seinfeld, J. H.: Equilibration timescale of atmospheric secondary organic aerosol partitioning, Geophysical Research Letters, 39, doi:10.1029/2012GL054008, 2012.

Simoneit, B. R. T., Rogge, W. F., Mazurek, M. A., Standley, L. J., Hildemann, L. M., and Cass, G. R.: Lignin pyrolysis products, lignans, and resin acids as specific tracers of plant classes in emissions from biomass combustion, Environmental Science & Technology, 27, 2533–2541, doi:10.1021/es00048a034, 1993.

Smith, J. N. and Rathbone, G. J.: Carboxylic acid characterization in nanoparticles by thermal desorption chemical ionization mass spectrometry, International Journal of Mass Spectrometry, 274, 8–13, doi:10.1016/j.ijms.2008.04.008, 2008.

Spracklen, D. V., Bonn, B., and Carslaw, K. S.: Boreal forests, aerosols and the impacts on clouds and climate, Philosophical Transactions of the Royal Society a-Mathematical Physical and Engineering Sciences, 366, 4613–4626, doi:10.1098/rsta.2008.0201, 2008.

Sun, Y., Zhang, Q., Macdonald, A. M., Hayden, K., Li, S. M., Liggio, J., Liu, P. S. K., Anlauf, K. G., Leaitch, W. R., Steffen, A., Cubison, M., Worsnop, D. R., van Donkelaar, A., and Martin, R. V.: Size-resolved aerosol chemistry on Whistler Mountain, Canada with a high-resolution aerosol mass spectrometer during INTEX-B, Atmospheric Chemistry and Physics, 9, 3095–3111, 2009.

Surratt, J. D., Chan, A. W. H., Eddingsaas, N. C., Chan, M., Loza, C. L., Kwan, A. J., Hersey, S. P., Flagan, R. C., Wennberg, P. O., and Seinfeld, J. H.: Reactive intermediates revealed in secondary organic aerosol formation from isoprene, Proceedings of the National Academy of Sciences of the United States of America, 107, 6640–6645, doi:10.1073/pnas.0911114107, 2010.

Surratt, J. D., Gomez-Gonzalez, Y., Chan, A. W. H., Vermeylen, R., Shahgholi, M., Kleindienst, T. E., Edney, E. O., Offenberg, J. H., Lewandowski, M., Jaoui, M., Maenhaut, W., Claeys, M., Flagan, R. C., and Seinfeld, J. H.: Organosulfate formation in biogenic secondary organic aerosol, Journal of Physical Chemistry A, 112, 8345–8378, doi:10.1021/jp802310p, 2008.

Surratt, J. D., Kroll, J. H., Kleindienst, T. E., Edney, E. O., Claeys, M., Sorooshian, A., Ng, N. L., Offenberg, J. H., Lewandowski, M., Jaoui, M., Flagan, R. C., and Seinfeld, J. H.: Evidence for organosulfates in secondary organic aerosol, Environmental Science & Technology, 41, 517–527, doi:10.1021/es062081q, 2007.

Surratt, J. D., Murphy, S. M., Kroll, J. H., Ng, a. L. N., Hildebrandt, L., Sorooshian, A., Szmigielski, R., Vermeylen, R., Maenhaut, W., Claeys, M., Flagan, R. C., and Seinfeld, J. H.: Chemical composition of secondary organic aerosol formed from the photooxidation of isoprene, Journal of Physical Chemistry A, 110, 9665–9690, doi:10.1021/jp061734m, 2006.

Svenningsson, B., Rissler, J., Swietlicki, E., Mircea, M., Bilde, M., Facchini, M. C., Decesari, S., Fuzzi, S., Zhou, J., Monster, J., and Rosenorn, T.: Hygroscopic growth and critical supersaturations for mixed aerosol particles of inorganic and organic compounds of atmospheric relevance, Atmospheric Chemistry and Physics, 6, 1937–1952, 2006.

Szmigielski, R., Surratt, J. D., Gomez-Gonzalez, Y., van der Veken, P., Kourtchev, I., Vermeylen, R., Blockhuys, F., Jaoui, M., Kleindienst, T. E., Lewandowski, M., Offenberg, J.

H., Edney, E. O., Seinfeld, J. H., Maenhaut, W., and Claeys, M.: 3-methyl-1,2,3-butanetricarboxylic acid: An atmospheric tracer for terpene secondary organic aerosol, Geophysical Research Letters, 34, doi:10.1029/2007GL031338, 2007.

Takahama, S., Johnson, A., and Russell, L. M.: Quantification of Carboxylic and Carbonyl Functional Groups in Organic Aerosol Infrared Absorbance Spectra, Aerosol Science and Technology, 47, 310–325, doi:10.1080/02786826.2012.752065, 2013.

ThermoFisher Scientific Inc., Schematic of the Q Exactive: http://planetorbitrap.com/q-exactive#tab:schematic.

Thomas, R. M., Trebs, I., Otjes, R., Jongejan, P. A. C., Brink, H. ten, Phillips, G., Kortner, M., Meixner, F. X., and Nemitz, E.: An Automated Analyzer to Measure Surf ace-Atmosphere Exchange Fluxes of Water Soluble Inorganic Aerosol Compounds and Reactive Trace Gases, Environmental Science & Technology, 43, 1412–1418, doi:10.1021/es8019403, 2009.

Thorenz, U. R., Kundel, M., Mueller, L., and Hoffmann, T.: Generation of standard gas mixtures of halogenated, aliphatic, and aromatic compounds and prediction of the individual output rates based on molecular formula and boiling point, Analytical and Bioanalytical Chemistry, 404, 2177–2183, doi:10.1007/s00216-012-6202-5, 2012.

Thornberry, T., Murphy, D. M., Thomson, D. S., Gouw, J. de, Warneke, C., Bates, T. S., Quinn, P. K., and Coffman, D.: Measurement of Aerosol Organic Compounds Using a Novel Collection/Thermal-Desorption PTR-ITMS Instrument, Aerosol Science and Technology, 43, 486–501, doi:10.1080/02786820902763132, 2009.

Tkacik, D. S., Presto, A. A., Donahue, N. M., and Robinson, A. L.: Secondary Organic Aerosol Formation from Intermediate-Volatility Organic Compounds: Cyclic, Linear, and Branched Alkanes, Environmental Science & Technology, 46, 8773–8781, doi:10.1021/es301112c, 2012.

Tobias, H. J. and Ziemann, P. J.: Compound identification in organic aerosols using temperature-programmed thermal desorption particle beam mass spectrometry, Analytical Chemistry, 71, 3428–3435, doi:10.1021/ac990056f, 1999.

Tolocka, M. P. and Turpin, B.: Contribution of Organosulfur Compounds to Organic Aerosol Mass, Environmental Science & Technology, 46, 7978–7983, doi:10.1021/es300651v, 2012.

Topping, D., Connolly, P., and McFiggans, G.: Cloud droplet number enhanced by co-condensation of organic vapours, Nature Geoscience, 6, 443–446, doi:10.1038/NGEO1809, 2013.

Turpin, B. J., Huntzicker, J. J., and Hering, S. V.: Investigation of organic aerosol sampling artefacts in the Los Angeles basin, Atmospheric Environment, 28, 3061–3071, doi:10.1016/1352-2310(94)00133-6, 1994.

Twomey, S.: The Influence of Pollution on the Shortwave Albedo of Clouds, Journal of the Atmospheric Sciences, 34, 1149–1152, doi:10.1175/1520-0469(1977)034<1149:TIOPOT>2.0.CO;2, 1977.

Veres, P., Roberts, J. M., Warneke, C., Welsh-Bon, D., Zahniser, M., Herndon, S., Fall, R., and Gouw, J. de: Development of negative-ion proton-transfer chemical-ionization mass spectrometry (NI-PT-CIMS) for the measurement of gas-phase organic acids in the atmosphere, International Journal of Mass Spectrometry, 274, 48–55, doi:10.1016/j.ijms.2008.04.032, 2008.

Virtanen, A., Joutsensaari, J., Koop, T., Kannosto, J., Yli-Pirila, P., Leskinen, J., Makela, J. M., Holopainen, J. K., Poeschl, U., Kulmala, M., Worsnop, D. R., and Laaksonen, A.: An amorphous solid state of biogenic secondary organic aerosol particles, Nature, 467, 824–827, doi:10.1038/nature09455, 2010.

Vogel, A. L., Aijala, M., Brueggemann, M., Ehn, M., Junninen, H., Petaja, T., Worsnop, D. R., Kulmala, M., Williams, J., and Hoffmann, T.: Online atmospheric pressure chemical ionization ion trap mass spectrometry (APCI-IT-MSn) for measuring organic acids concentrated bulk aerosol - a laboratory and field study, Atmospheric Measurement Techniques, 6, 431–443, doi:10.5194/amt-6-431-2013, 2013a.

Vogel, A. L., Aijala, M., Corrigan, A. L., Junninen, H., Ehn, M., Petaja, T., Worsnop, D. R., Kulmala, M., Russell, L. M., Williams, J., and Hoffmann, T.: In situ submicron organic aerosol characterization at a boreal forest research station during HUMPPA-COPEC 2010 using soft and hard ionization mass spectrometry, Atmospheric Chemistry and Physics, 13, 10933–10950, 2013b.

Volkamer, R., Jimenez, J. L., San Martini, F., Dzepina, K., Zhang, Q., Salcedo, D., Molina, L. T., Worsnop, D. R., and Molina, M. J.: Secondary organic aerosol formation from anthropogenic air pollution: Rapid and higher than expected, Geophysical Research Letters, 33, doi:10.1029/2006GL026899, 2006.

Warnke, J., Bandur, R., and Hoffmann, T.: Capillary-HPLC-ESI-MS/MS method for the determination of acidic products from the oxidation of monoterpenes in atmospheric aerosol samples, Analytical and Bioanalytical Chemistry, 385, 34–45, doi:10.1007/s00216-006-0340-6, 2006.

Warscheid, B. and Hoffmann, T.: On-line measurements of a-pinene ozonolysis products using an atmospheric pressure chemical ionisation ion-trap mass spectrometer, Atmospheric Environment, 35, 2927–2940, doi:10.1016/S1352-2310(00)00513-6, 2001.

Warscheid, B. and Hoffmann, T.: Direct analysis of highly oxidised organic aerosol constituents by on-line ion trap mass spectrometry in the negative-ion mode, Rapid Communications in Mass Spectrometry, 16, 496–504, doi:10.1002/rcm.602, 2002.

Went, F. W.: Blue Hazes in the Atmosphere, Nature, 187, 641–643, doi:10.1038/187641a0, 1960.

Wiedensohler, A., Cheng, Y. F., Nowak, A., Wehner, B., Achtert, P., Berghof, M., Birmili, W., Wu, Z. J., Hu, M., Zhu, T., Takegawa, N., Kita, K., Kondo, Y., Lou, S. R., Hofzumahaus, A., Holland, F., Wahner, A., Gunthe, S. S., Rose, D., Su, H., and Poeschl, U.: Rapid aerosol particle growth and increase of cloud condensation nucleus activity by secondary aerosol formation and condensation: A case study for regional air pollution in northeastern China, Journal of Geophysical Research-Atmospheres, 114, doi:10.1029/2008JD010884, 2009.

Williams, B. J., Goldstein, A. H., Kreisberg, N. M., and Hering, S. V.: In situ measurements of gas/particle-phase transitions for atmospheric semivolatile organic compounds, Proceedings of the National Academy of Sciences of the United States of America, 107, 6676–6681, doi:10.1073/pnas.0911858107, 2010.

Williams, J., Crowley, J., Fischer, H., Harder, H., Martinez, M., Petaja, T., Rinne, J., Back, J., Boy, M., Dal Maso, M., Hakala, J., Kajos, M., Keronen, P., Rantala, P., Aalto, J., Aaltonen, H., Paatero, J., Vesala, T., Hakola, H., Levula, J., Pohja, T., Herrmann, F., Auld, J., Mesarchaki, E., Song, W., Yassaa, N., Nölscher, A. C., Johnson, A. M., Custer, T., Sinha, V., Thieser, J., Pouvesle, N., Taraborrelli, D., Tang, M. J., Bozem, H., Hosaynali-Beygi, Z., Axinte, R., Oswald, R., Novelli, A., Kubistin, D., Hens, K., Javed, U., Trawny, K., Breitenberger, C., Hidalgo, P. J., Ebben, C. J., Geiger, F. M., Corrigan, A. L., Russell, L. M., Ouwersloot, H. G., Arellano, J. V.-G. de, Ganzeveld, L., Vogel, A. L., Beck, M., Bayerle, A., Kampf, C. J., Bertelmann, M., Koellner, F., Hoffmann, T., Valverde, J., Gonzalez, D., Riekkola, M.-L., Kulmala, M., and Lelieveld, J.: The summertime Boreal forest field measurement intensive (HUMPPA-COPEC-2010): an overview of meteorological and chemical influences, Atmospheric Chemistry and Physics, 11, 10599–10618, doi:10.5194/acp-11-10599-2011, 2011.

Wong, P. S. H., Cooks, R. G.: Ion Trap Mass Spectrometry: http://www.currentseparations.com/issues/16-3/cs16-3c.pdf.

Wyers, G. P., Oties, R. P., and Slanina, J.: A continuous-flow denuder for the measurement of ambient concentrations and surface-exchange fluxes of ammonia, Atmospheric Environment. Part A. General Topics, 27, 2085–2090, doi:10.1016/0960-1686(93)90280-C, 1993.

Yasmeen, F., Szmigielski, R., Vermeylen, R., Gomez-Gonzalez, Y., Surratt, J. D., Chan, A. W. H., Seinfeld, J. H., Maenhaut, W., and Claeys, M.: Mass spectrometric characterization of isomeric terpenoic acids from the oxidation of alpha-pinene, beta-pinene, d-limonene, and Delta(3)-carene in fine forest aerosol, Journal of Mass Spectrometry, 46, 425–442, doi:10.1002/jms.1911, 2011.

Yasmeen, F., Vermeylen, R., Maurin, N., Perraudin, E., Doussin, J.-F., and Claeys, M.: Characterisation of tracers for aging of alpha-pinene secondary organic aerosol using liquid chromatography/negative ion electrospray ionisation mass spectrometry, Environmental Chemistry, 9, 236–246, doi:10.1071/EN11148, 2012.

Yasmeen, F., Vermeylen, R., Szmigielski, R., Iinuma, Y., Boege, O., Herrmann, H., Maenhaut, W., and Claeys, M.: Terpenylic acid and related compounds: precursors for dimers in secondary organic aerosol from the ozonolysis of alpha- and beta-pinene, Atmospheric Chemistry and Physics, 10, 9383–9392, doi:10.5194/acp-10-9383-2010, 2010.

Yassaa, N., Song, W., Lelieveld, J., Vanhatalo, A., Baeck, J., and Williams, J.: Diel cycles of isoprenoids in the emissions of Norway spruce, four Scots pine chemotypes, and in Boreal forest ambient air during HUMPPA-COPEC-2010, Atmospheric Chemistry and Physics, 12, 7215–7229, doi:10.5194/acp-12-7215-2012, 2012.

Yatavelli, R. L. N., Lopez-Hilfiker, F., Wargo, J. D., Kimmel, J. R., Cubison, M. J., Bertram, T. H., Jimenez, J. L., Gonin, M., Worsnop, D. R., and Thornton, J. A.: A Chemical Ionization High-Resolution Time-of-Flight Mass Spectrometer Coupled to a Micro Orifice Volatilization Impactor (MOVI-HRToF-CIMS) for Analysis of Gas and Particle-Phase Organic Species, Aerosol Science and Technology, 46, 1313–1327, doi:10.1080/02786826.2012.712236, 2012.

Yatavelli, R. L. N. and Thornton, J. A.: Particulate Organic Matter Detection Using a Micro-Orifice Volatilization Impactor Coupled to a Chemical Ionization Mass Spectrometer (MOVI-CIMS), Aerosol Science and Technology, 44, 61–74, doi:10.1080/02786820903380233, 2010.

Yoshinari, K.: Theoretical and numerical analysis of the behavior of ions injected into a quadrupole ion trap mass spectrometer, Rapid Communications in Mass Spectrometry, 14, 215–223, doi:10.1002/(SICI)1097-0231(20000229)14:4<215:AID-RCM867>3.0.CO;2-T, 2000.

Yttri, K. E., Simpson, D., Nojgaard, J. K., Kristensen, K., Genberg, J., Stenstrom, K., Swietlicki, E., Hillamo, R., Aurela, M., Bauer, H., Offenberg, J. H., Jaoui, M., Dye, C., Eckhardt, S., Burkhart, J. F., Stohl, A., and Glasius, M.: Source apportionment of the summer time carbonaceous aerosol at Nordic rural background sites, Atmospheric Chemistry and Physics, 11, 13339–13357, doi:10.5194/acp-11-13339-2011, 2011.

Yu, J. Z., Cocker, Griffin, R. J., Flagan, R. C., and Seinfeld, J. H.: Gas-phase ozone oxidation of monoterpenes: Gaseous and particulate products, Journal of Atmospheric Chemistry, 34, 207–258, doi:10.1023/A:1006254930583, 1999.

Yu, J. Z., Flagan, R. C., and Seinfeld, J. H.: Identification of products containing -COOH, -OH, and -C=O in atmospheric oxidation of hydrocarbons, Environmental Science & Technology, 32, 2357–2370, doi:10.1021/es980129x, 1998.

Zahardis, J., Geddes, S., and Petrucci, G. A.: Improved Understanding of Atmospheric Organic Aerosols via Innovations in Soft Ionization Aerosol Mass Spectrometry, Analytical Chemistry, 83, 2409–2415, doi:10.1021/ac102737k, 2011.

Zeng, G., Holladay, S., Langlois, D., Zhang, Y., and Liu, Y.: Kinetics of Heterogeneous Reaction of Ozone with Linoleic Acid and its Dependence on Temperature, Physical State, RH, and Ozone Concentration, Journal of Physical Chemistry A, 117, 1963–1974, doi:10.1021/jp308304n, 2013.

Zhang, Q., Jimenez, J. L., Canagaratna, M. R., Allan, J. D., Coe, H., Ulbrich, I., Alfarra, M. R., Takami, A., Middlebrook, A. M., Sun, Y. L., Dzepina, K., Dunlea, E., Docherty, K., DeCarlo, P. F., Salcedo, D., Onasch, T., Jayne, J. T., Miyoshi, T., Shimono, A., Hatakeyama, S., Takegawa, N., Kondo, Y., Schneider, J., Drewnick, F., Borrmann, S., Weimer, S., Demerjian, K., Williams, P., Bower, K., Bahreini, R., Cottrell, L., Griffin, R. J., Rautiainen, J., Sun, J. Y., Zhang, Y. M., and Worsnop, D. R.: Ubiquity and dominance of oxygenated species in organic aerosols in anthropogenically-influenced Northern Hemisphere midlatitudes, Geophysical Research Letters, 34, doi:10.1029/2007GL029979, 2007.

Zhang, Q., Jimenez, J. L., Canagaratna, M. R., Ulbrich, I. M., Ng, N. L., Worsnop, D. R., and Sun, Y.: Understanding atmospheric organic aerosols via factor analysis of aerosol mass spectrometry: a review, Analytical and Bioanalytical Chemistry, 401, 3045–3067, doi:10.1007/s00216-011-5355-y, 2011.

Zhang, R.: Getting to the Critical Nucleus of Aerosol Formation, Science, 328, 1366–1367, doi:10.1126/science.1189732, 2010.

7 Appendix

A. Supplementary material to chapter 3

B. Supplementary material to chapter 4

C. List of related publications and presentations

D. Acknowledgements

E. Curriculum vitae

A. Supplementary material to chapter 3

"In-situ submicron organic aerosol characterization at a boreal forest research station during HUMPPA-COPEC 2010 using soft and hard ionization mass spectrometry"

Alexander L. Vogel, Mikko Äijälä, Ashley L. Corrigan, Heikki Junninen, Mikael Ehn, Tuukka Petäjä, Douglas R. Worsnop, Markku Kulmala, Lynn M. Russell, Jonathan Williams and Thorsten Hoffmann

1. AMS Positive Matrix Factorization Spectra

As it was described in the manuscript, the AMS factor analysis (Corrigan et al., 2013) resulted in a three factor solution (FPEAK=−0.4). Factor OOA-1 comprises two merged factors having high f44, since both factors had a very similar temporal behavior, uniform mass spectra and showed similar correlation to auxiliary measurements. The factor OOA-2 shows high f43 and was higher during the beginning of the campaign (see Figure 1).

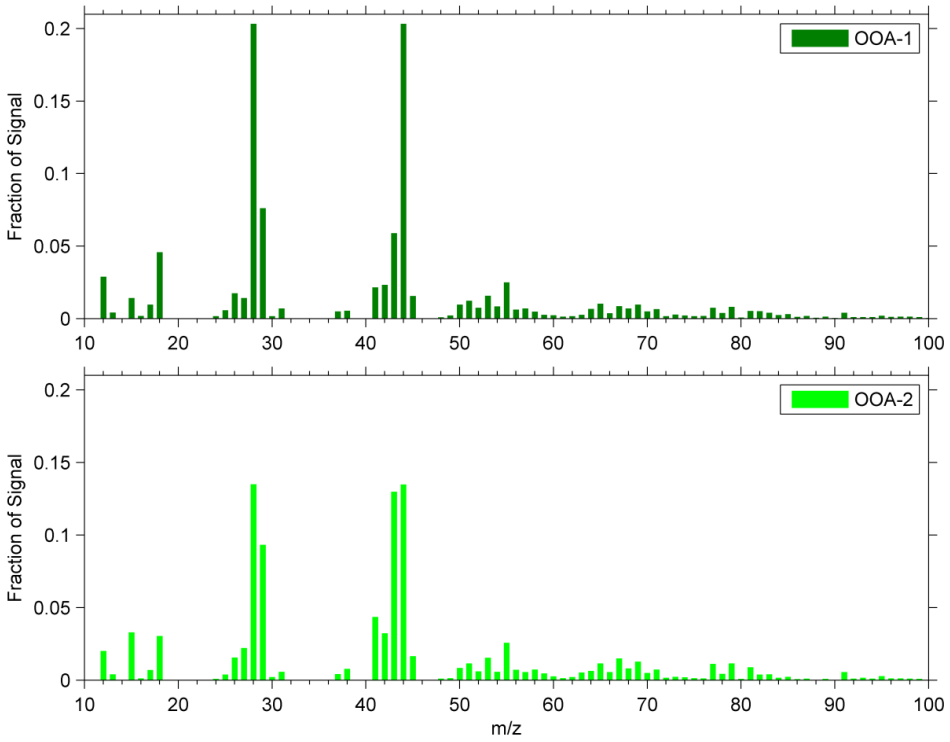

Figure S3.12 Mass spectra of AMS positive matrix factorization solution

2. Estimation of the average Oxidation States

The average molecular oxidation state $\overline{OS_C}$ (Kroll, 2011) in the top panel of Fig. 4 was estimated for all signals in the range between *m/z* 163 and *m/z* 237 in the following practice: The average oxidation states of biogenic organic acids in this mass range which are described in literature (Tab. 2) were calculated after Eq. (S1) (Kroll et al., 2011):

$$\overline{OS_C} = 2\,O/C - H/C \tag{S1}$$

For those acids, the ratio between particle phase (PP) and gas phase (GP) was calculated, based on the average of the measurements on 26 July 2010 12:00 – 15:00h (UTC+2) (the average mass spectra of this period are shown in Fig. 4, middle panel) and then plotted against $\overline{OS_C}$ (Fig. S2) with

$$Q = PP/GP. \tag{S2}$$

A single term exponential fit resulted in R^2=0.55, and was used to determine the $\overline{OS_C}$ of all unattributed *m/z* ratios resulting in the red circles in the upper panel of Fig. 4. This approach does not account for the fact that multiple organic acids appear on one *m/z* ratio, however, it nicely illustrates the repetitive character of an increasing oxidation state within the discussed mass range. This approach cannot be applied on a broader mass range, since the volatility is not only governed by the oxidation state but also by the molecular mass.

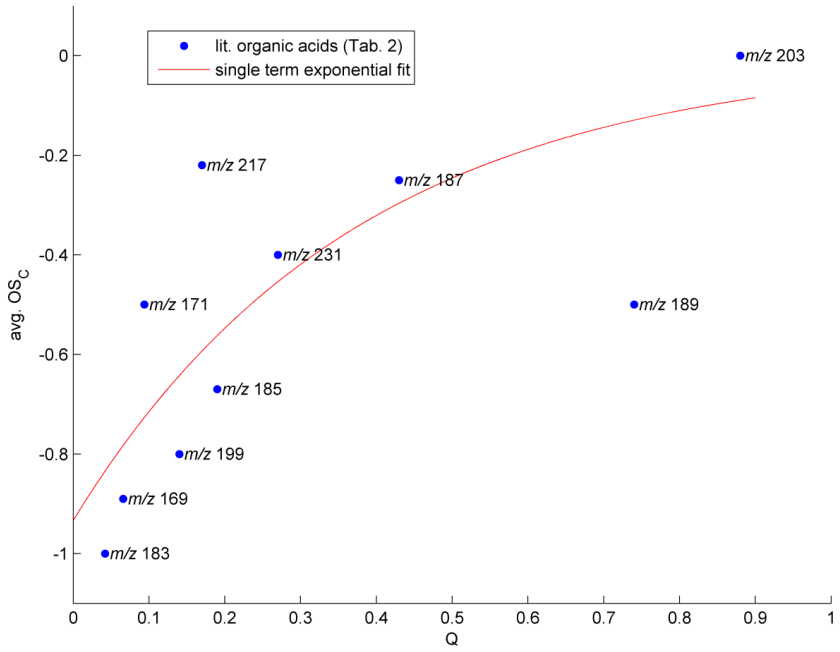

Figure S3.13 Exponential fit to determine the average oxidation state in Fig. 4

3. Online MS^2 spectra

For completeness, all online-MS^2 spectra, recorded during the HUMPPA-COPEC campaign on 22 July 2010 13:20-15:20h (UTC +2), are depicted in the following table.

m/z 115 CID energy: 30 a.u. Average scans: 47	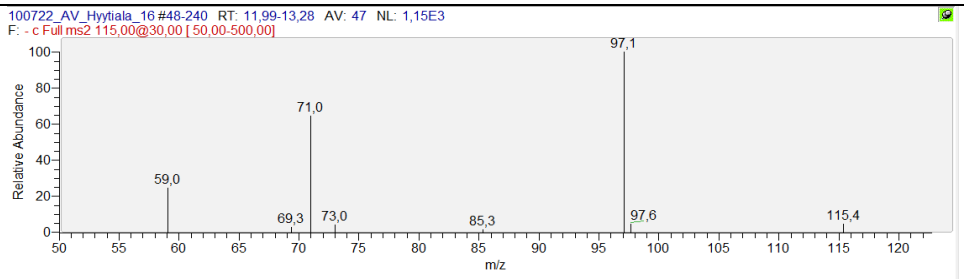
m/z 123 CID energy: 30 a.u. Average scans: 41	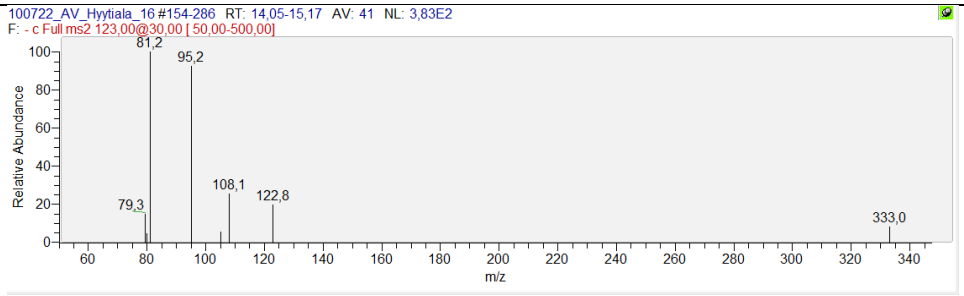
m/z 129 CID energy: 30 a.u. Average scans: 36	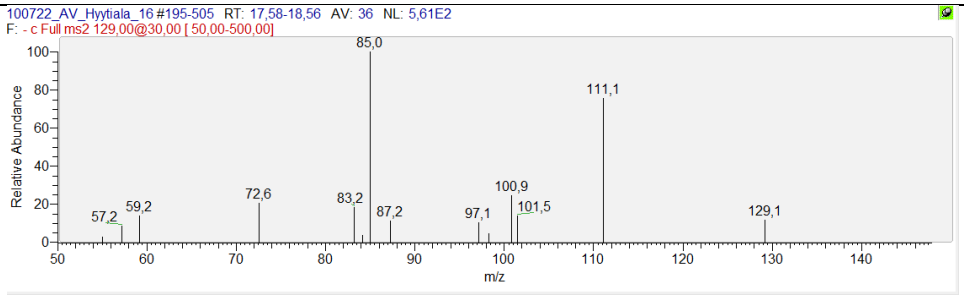
m/z 137 CID energy: 30 a.u. Average scans: 35	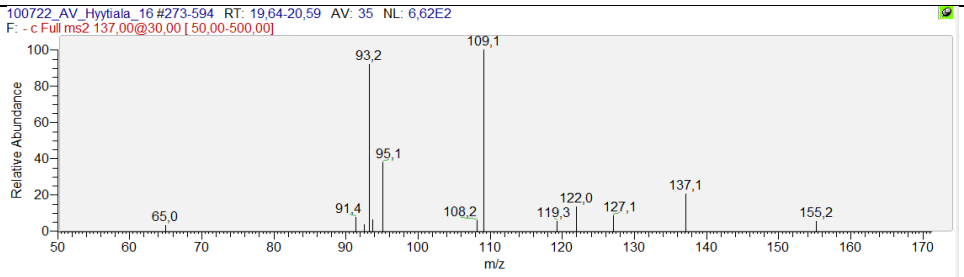
m/z 139 CID energy: 30 a.u. Average scans: 43	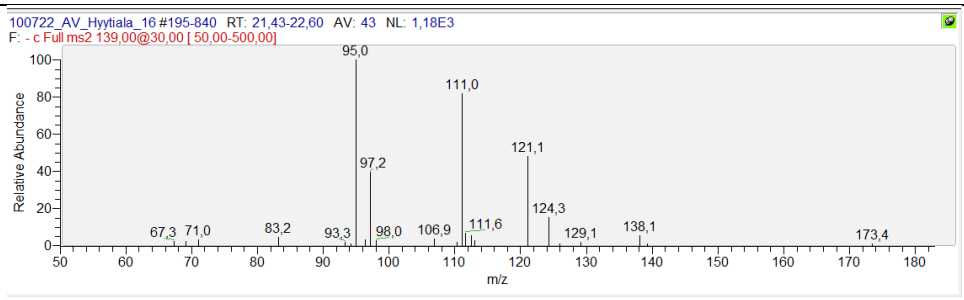

m/z 141 CID energy: 30 a.u. Average scans: 33	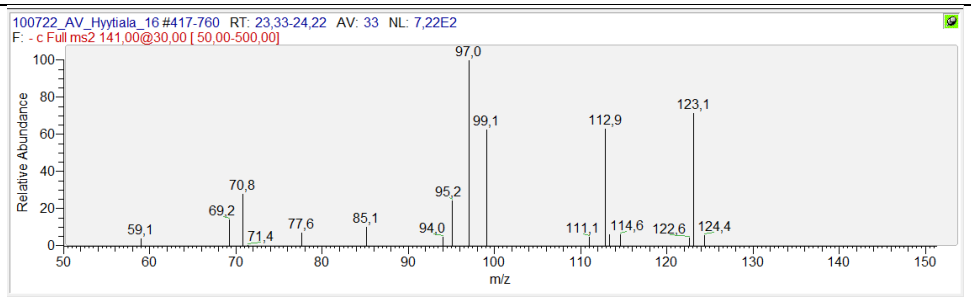
m/z 143 CID energy: 30 a.u. Average scans: 21	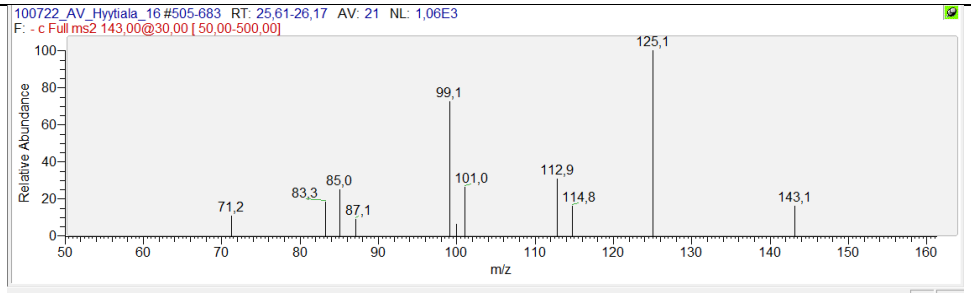
m/z 153 CID energy: 30 a.u. Average scans: 40	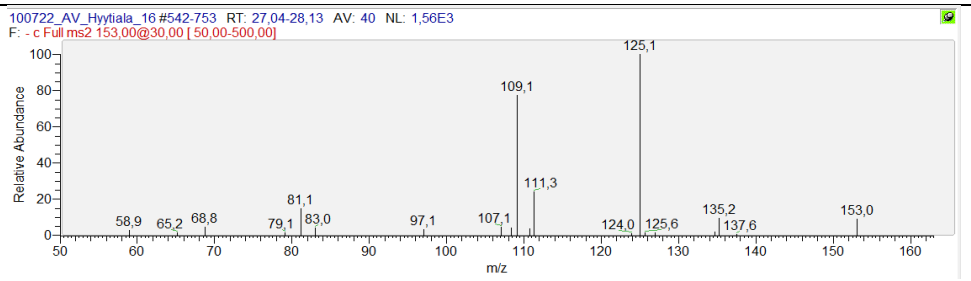
m/z 155 CID energy: 30 a.u. Average scans: 33	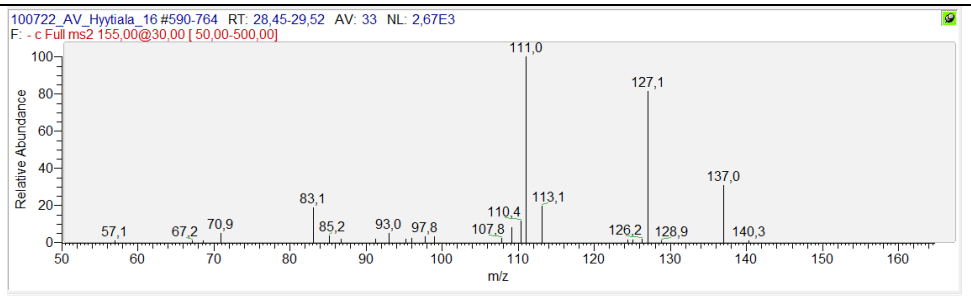
m/z 157 CID energy: 30 a.u. Average scans: 43	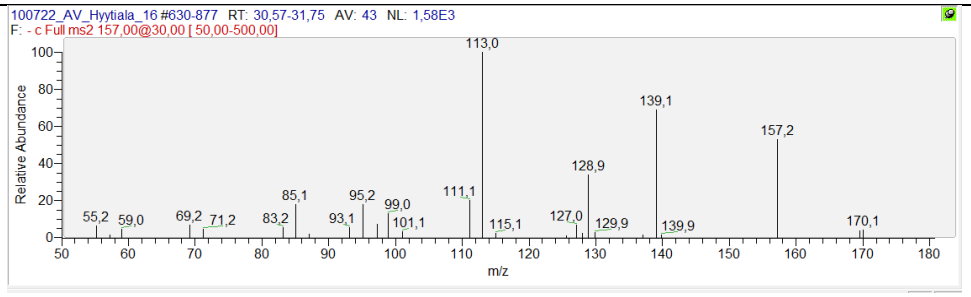
m/z 167 CID energy: 30 a.u. Average scans: 28	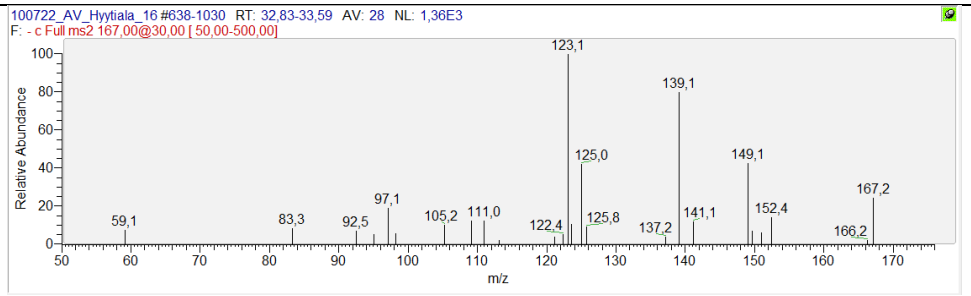

m/z 169 CID energy: 30 a.u. Average scans: 44	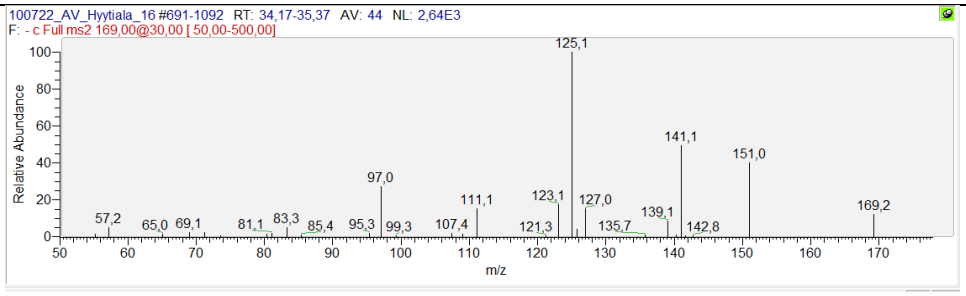
m/z 171 CID energy: 30 a.u. Average scans: 35	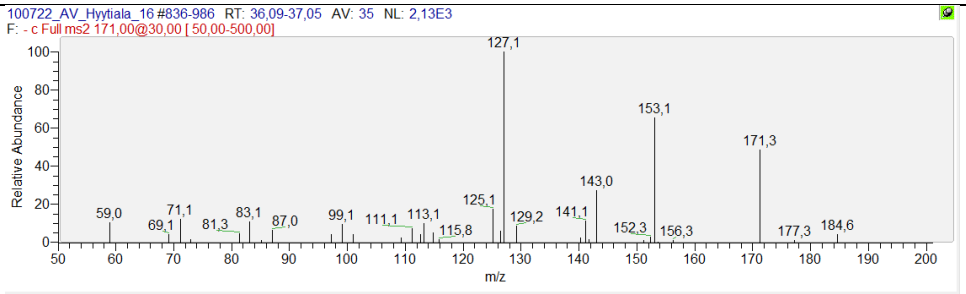
m/z 181 CID energy: 30 a.u. Average scans: 19	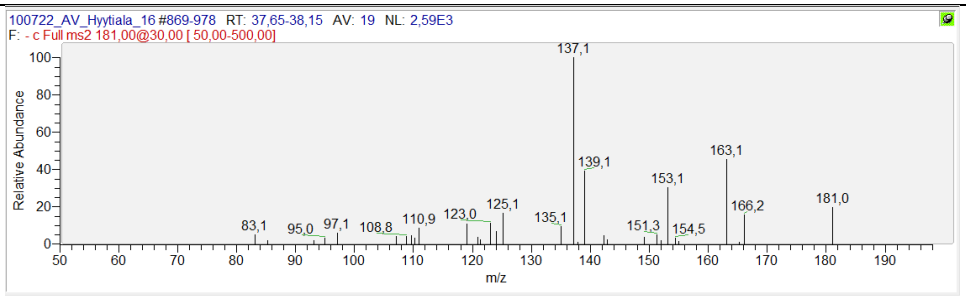
m/z 183 CID energy: 30 a.u. Average scans: 42	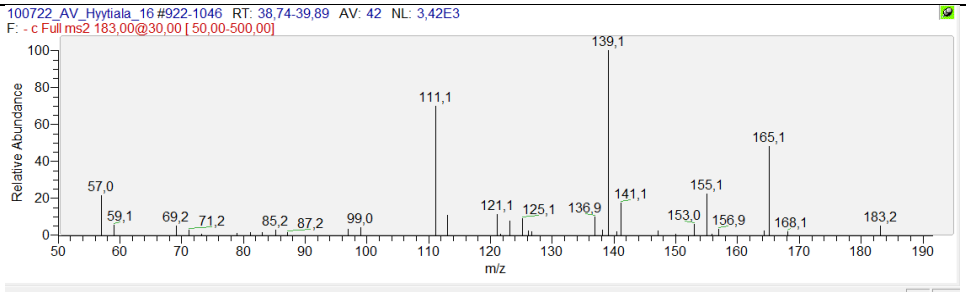
m/z 185 CID energy: 30 a.u. Average scans: 33	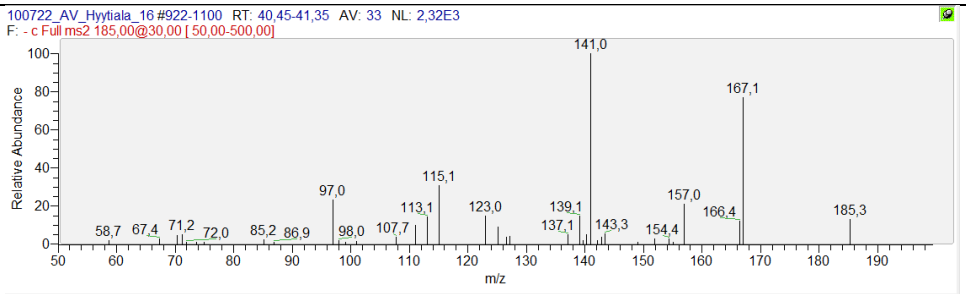

m/z 187 CID energy: 30 a.u. Average scans: 22	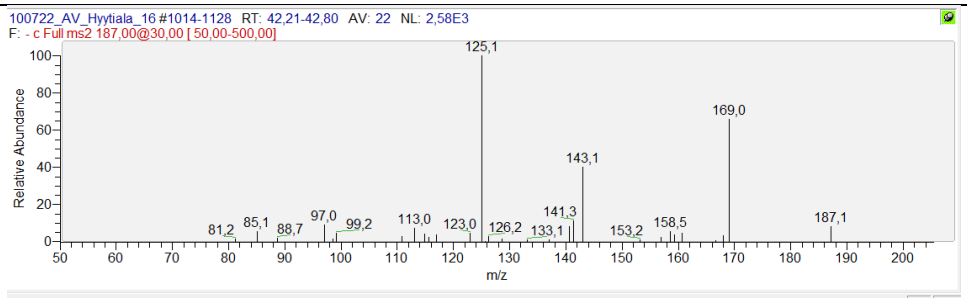
m/z 197 CID energy: 30 a.u. Average scans: 25	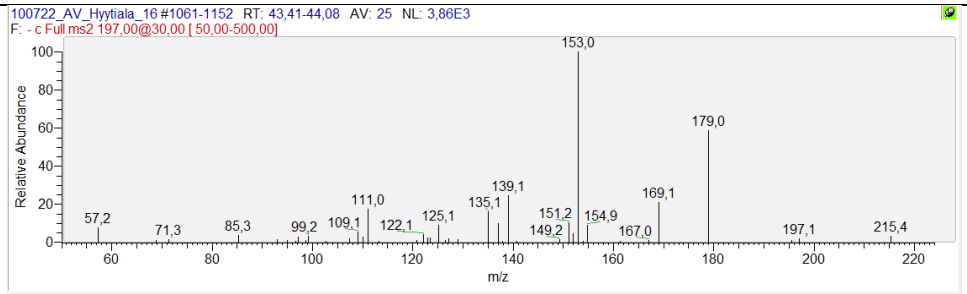
m/z 199 CID energy: 30 a.u. Average scans: 27	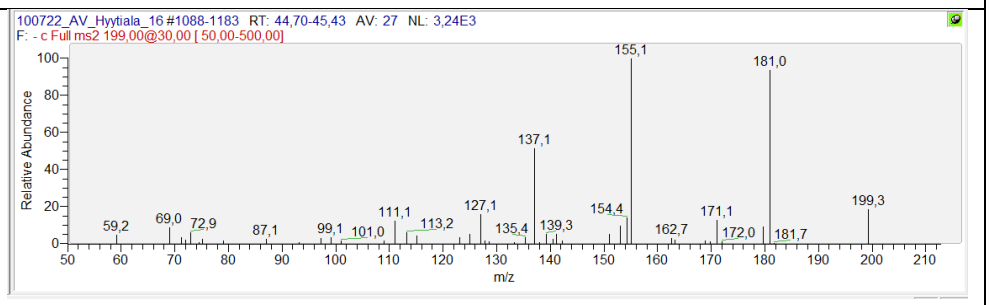
m/z 201 CID energy: 30 a.u. Average scans: 24	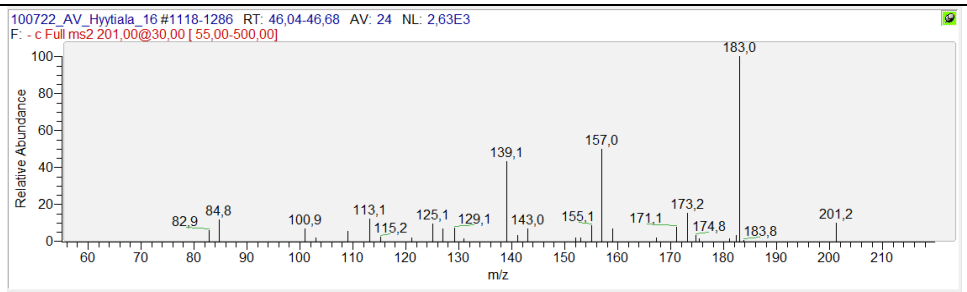
m/z 203 CID energy: 30 a.u. Average scans: 42	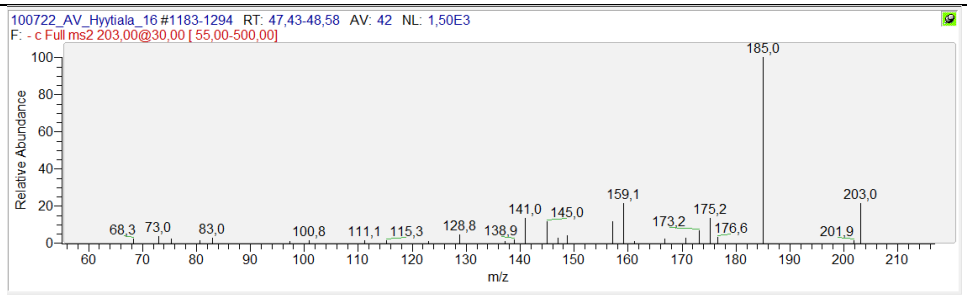

m/z 213 CID energy: 30 a.u. Average scans: 40	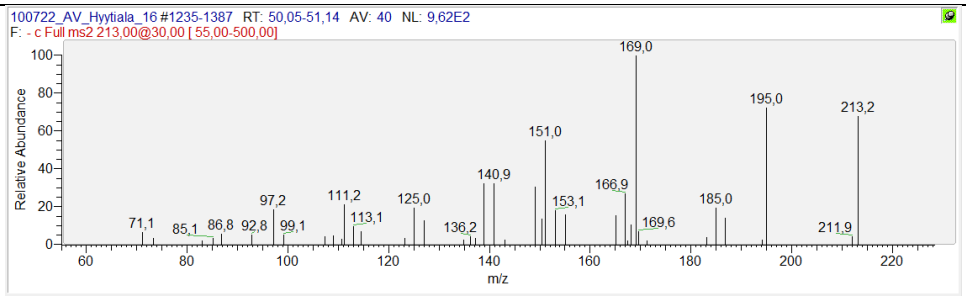
m/z 215 CID energy: 30 a.u. Average scans: 244	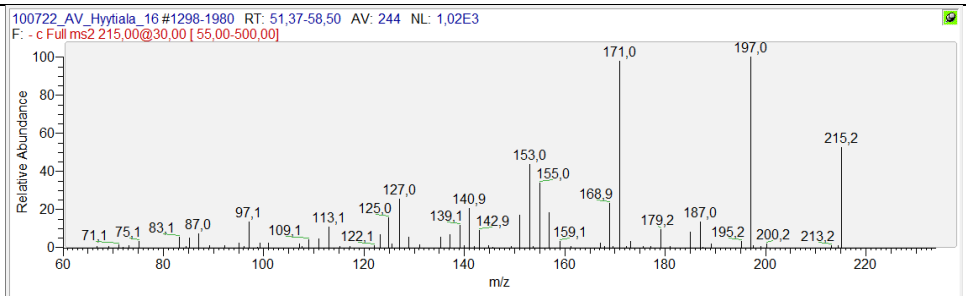
m/z 217 CID energy: 30 a.u. Average scans: 39	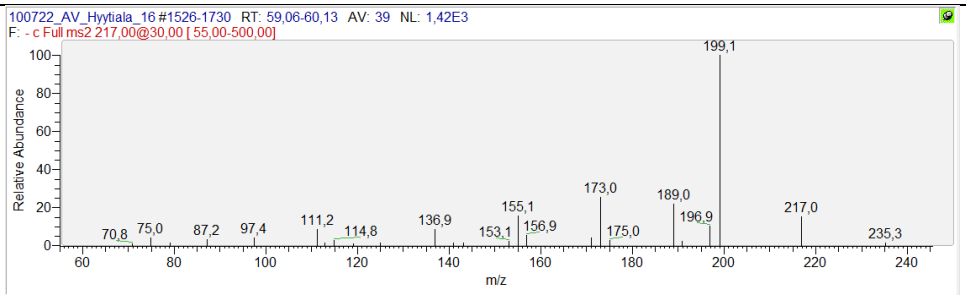
m/z 229 CID energy: 30 a.u. Average scans: 91	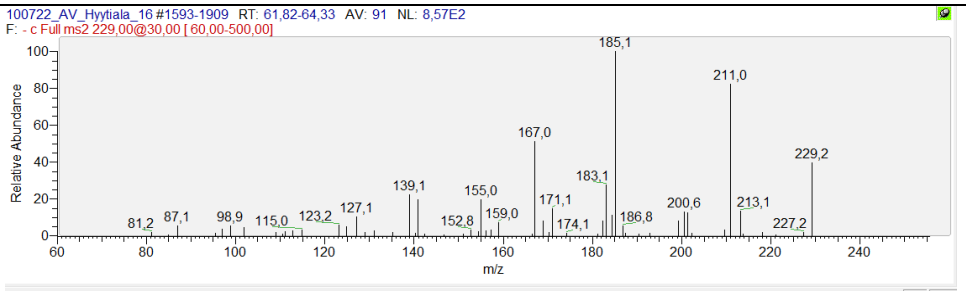
m/z 231 CID energy: 30 a.u. Average scans: 43	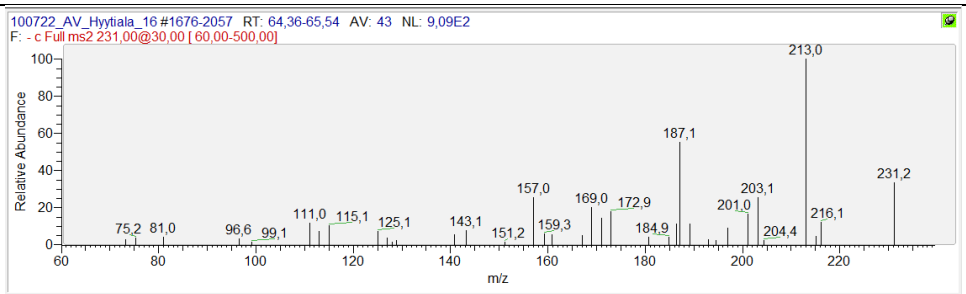

m/z 245 CID energy: 30 a.u. Average scans: 56	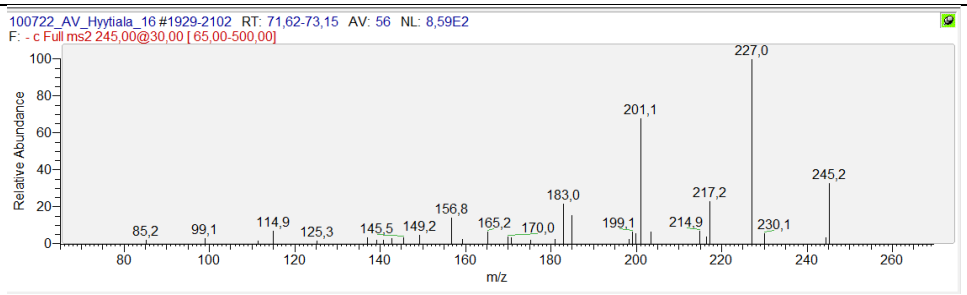
m/z 259 CID energy: 30 a.u. Average scans: 97	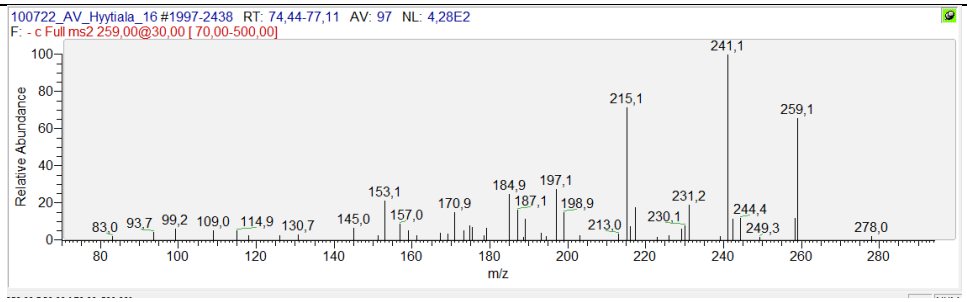

4. Average molecular weight determination

As it is mentioned in chapter 3.3.4, the determination of the average molecular weight can be seriously biased by the following phenomena: The determination can lead towards an underprediction of $\overline{MW}_{om}$ by multiply charged ions, fragmentation of the ions or by a higher ionization efficiency of low molecular weight compounds (Kiss et al., 2003; Graber and Rudich, 2006). $\overline{MW}_{om}$ can be biased towards an overprediction caused by a higher ionization efficiency of high molecular weight compounds, mass discrimination effects of small *m/z* ratios or by cluster formation.

Stenson et al. (2002) showed by the use of an ultra-high mass resolution technique (ESI-FTICR-MS) that virtually all ions formed from humic and fulvic acid standards were singly charged. Testing several organic acids in the mass range of 120-200 Da in the laboratory supported these findings.

Concerning the issue of fragmentation it has to be distinguished between heat induced fragmentation and fragmentation due to the ionization process itself. Caldwell et al. (1989) described the thermal decomposition of small dicarboxylic acids (malonic acid and succinic acid) at temperatures as low as 120 °C. In this work, the signal of ions < *m/z* 150 have low intensities compared to higher masses. Besides the fact that small dicarboxylic acids decompose very fast, those small weight acids are also affected by mass discrimination effects in the ion optics. These effects depend on the RF-voltage of the ion optics and can vary with different settings (e.g. the width of the spectrum). Aufmhoff et al. (2011) stated a mass discrimination effect of ≤ 2 comparing *m/z* 125 to *m/z* 160 for an identical constructed ion trap. Since small weight dicarboxylic acids were described as the most abundant species in OA at a semiurban site (Khwaja, 1995), the thermal decomposition and mass discrimination effects of those small weight dicarboxylic acids might bias the picture of organic acids in the particulate phase substantially towards higher masses. Regarding the decomposition rate during the ionization process itself, it is commonly known that chemical ionization at atmospheric pressure is one of the techniques showing the smallest decomposition rates. Actually, the APCI technique shows less fragmentation than CI (which operates at a lower pressure regime), because the proton transfer in the ion/molecule reaction can leave an amount of internal energy in the product ion, which is sufficient for fragmentation of the product ion (Bartmess, 1989). At atmospheric pressure, the product ion can be stabilized rapidly by transferring the internal energy in a collision with a neutral molecule (Mitchum and Korfmacher, 1983).

Furthermore, the fragmentation of higher molecular weight compounds is different from small molecules. In short: Reemtsma and These (2003) showed that fragmentation of high molecular weight compounds is accompanied by hydrogen shifts, leading up to unity of the odd/even (or M/M+1) distribution. The mass spectral pattern below *m/z* 200 in Fig. 4 does show

only a slight evidence for a biased odd/even distribution. E.g. the ratio of *m/z*187 to *m/z* 188 is 0.14. The 95% confidence interval (n=16 scans) of this ratio ranges from C_8 (0.09) to C_{14} (0.18) compounds. Since a C_{14}-carboxylic acid with the mass of 189 Da is not reasonable, a possible explanation might be that hydrogen atoms shift due to fragmentation, or organic compounds including nitrogen. However, the upper limit value of 0.18 is still far away from unity, and thus fragmentation of higher molecular weight compounds, which is accompanied by hydrogen shifts, seems not to be a major issue.

Finally, the major uncertainty in predicting $\overline{MW_{om}}$ is based on different ionization efficiencies of different organic compounds. This seems reasonable since different carboxylic acids do show a strong variation in gas-phase acidity, which results in compound dependent ionization efficiency. Unfortunately, the affinity between the negative ion O_2^- and the analyte molecule cannot be assigned to certain chemical properties or to functional group contributions (Sekimoto et al., 2012) and further fundamental studies on the ionization process at atmospheric pressure are needed.

5. Gas-to-particle partitioning

As mentioned in the text, the gas-phase concentration might even be higher than observed, since the application of the water based concentrator might result in an underprediction of water soluble gas-phase species due to diffusive losses in the saturator. These losses in the gas phase (app. 30 %) were not taken into account in calculating the partitioning between gas and particle phase.

Furthermore, the behavior of semi-volatile compounds in the condenser is highly uncertain-nevertheless, for the calculation of the partitioning it was assumed that the semi-volatile acids in the gas phase condense onto the particle surface and thus get enriched as strong as the particle phase compounds while passing the virtual impactor (see Vogel et al. 2013 or Geller et al. 2005). This assumption leads to a lowermost estimate of the gas phase concentration of the semi-volatile compounds. However, future measurements of the gas-to-particle partitioning are needed in order to better understand the impact of the phase state of organic aerosols.

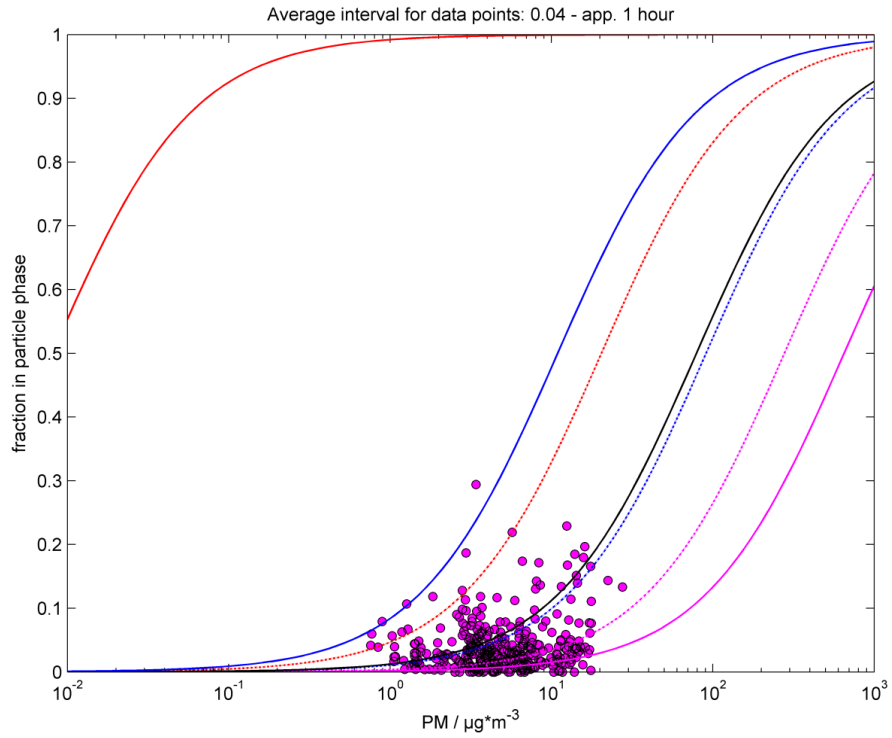

Figure S3.14a Gas-to-particle partitioning of *m/z* 183

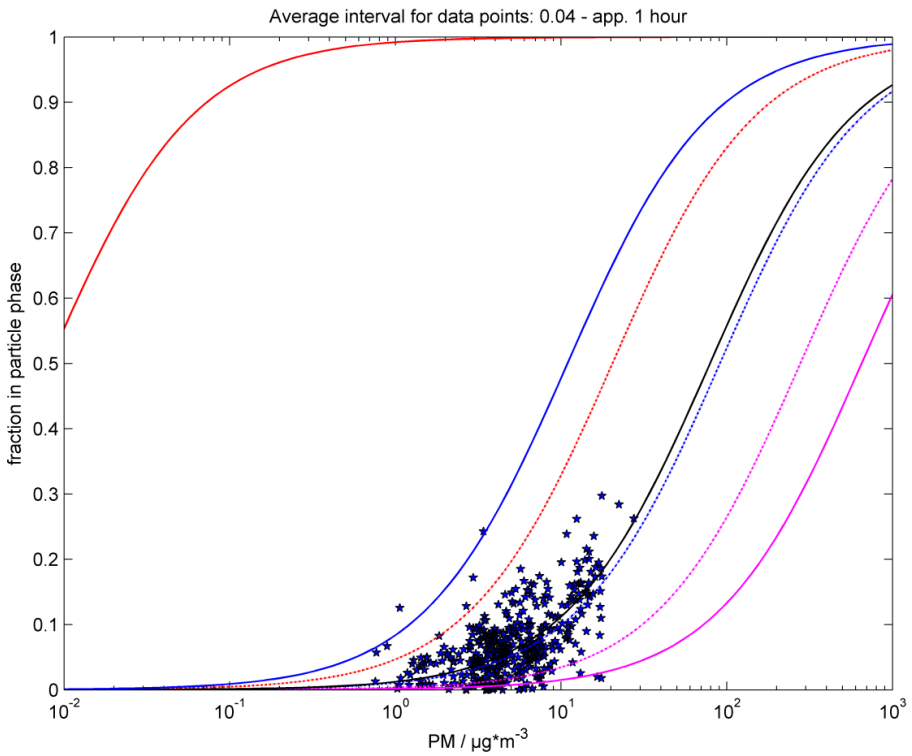

Figure S3.3b Gas-to-particle partitioning of m/z 185

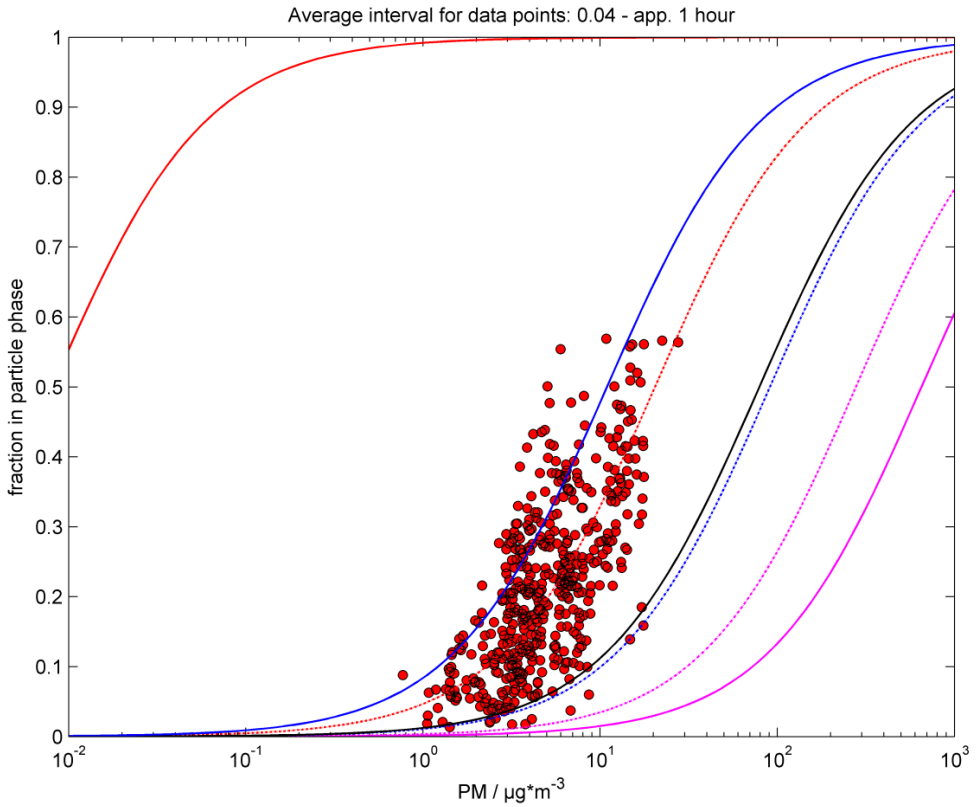

Figure S3.3c Gas-to-particle partitioning of m/z 203

References

Aufmhoff, H., Hanke, M., Uecker, J., Schlager, H., and Arnold, F.: An ion trap CIMS instrument for combined measurements of atmospheric OH and H2SO4: First test measurements above and inside the planetary boundary layer, International Journal of Mass Spectrometry, 308, doi:10.1016/j.ijms.2011.07.016, 2011.

Bartmess, J. E.: Gas-Phase Equilibrium Affinity Scales and Chemical Ionization Mass-Spectrometry, Mass Spectrometry Reviews, 8, doi:10.1002/mas.1280080502, 1989.

Caldwell, G., Renneboog, R., and Kebarle, P.: Gas phase acidities of aliphatic carboxylic acids, based on measurements of proton transfer equilibria, Canadian Journal of Chemistry-Revue Canadienne De Chimie, 67, doi:10.1139/v89-092, 1989.

Graber, E. R. and Rudich, Y.: Atmospheric HULIS: How humic-like are they? A comprehensive and critical review, Atmospheric Chemistry and Physics, 6, 729–753, 2006.

Khwaja, H. A.: Atmospheric concentrations of carboxylic acids and related compounds at a semiurban site, Atmospheric Environment, 29, doi:10.1016/1352-2310(94)00211-3, 1995.

Kroll, J. H., Donahue, N. M., Jimenez, J. L., Kessler, S. H., Canagaratna, M. R., Wilson, K. R., Altieri, K. E., Mazzoleni, L. R., Wozniak, A. S., Bluhm, H., Mysak, E. R., Smith, J. D., Kolb, C. E., and Worsnop, D. R.: Carbon oxidation state as a metric for describing the chemistry of atmospheric organic aerosol, Nature Chemistry, 3, 133–139, doi:10.1038/nchem.948, 2011.

Mitchum, R. K. and Korfmacher, W. A.: Atmospheric Pressure Ionization Mass Spectrometry, Analytical Chemistry, 55, 1983.

Reemtsma, T. and These, A.: On-line coupling of size exclusion chromatography with electrospray ionization-tandem mass spectrometry for the analysis of aquatic fulvic and humic acids, Analytical Chemistry, 75, doi:10.1021/ac0261294, 2003.

Sekimoto, K., Sakai, M., and Takayama, M.: Specific Interaction Between Negative Atmospheric Ions and Organic Compounds in Atmospheric Pressure Corona Discharge Ionization Mass Spectrometry, Journal of the American Society for Mass Spectrometry, 23, doi:10.1007/s13361-012-0363-5, 2012.

Stenson, A. C., Landing, W. M., Marshall, A. G., and Cooper, W. T.: Ionization and fragmentation of humic substances in electrospray ionization Fourier transform-ion cyclotron resonance mass spectrometry, Analytical Chemistry, 74, doi:10.1021/ac020019f, 2002.

B. Supplementary material to chapter 4

"Aerosol chemistry resolved by mass spectrometry- insights into ambient new particle formation and CCN activity of organic aerosols"

Alexander L. Vogel[a], Johannes Schneider[b], Christina Müller-Tautges[a], Gavin J. Phillips[c], Mira Krüger[d], Diana Rose[d], Ulla Makkonen[e], Hannele Hakola[e], John Crowley[c], Ulrich Pöschl[d], and Thorsten Hoffmann[a]

[a]Institute for Inorganic Chemistry and Analytical Chemistry, Johannes Gutenberg-University Mainz, Mainz, Germany

[b]Max Planck Institute for Chemistry, Particle Chemistry Department, Mainz, Germany

[c]Max Planck Institute for Chemistry, Air Chemistry Department, Mainz, Germany

[d]Max Planck Institute for Chemistry, Multiphase Chemistry Department, Mainz, Germany

[e]Finnish Meteorological Institute, Helsinki, Finland

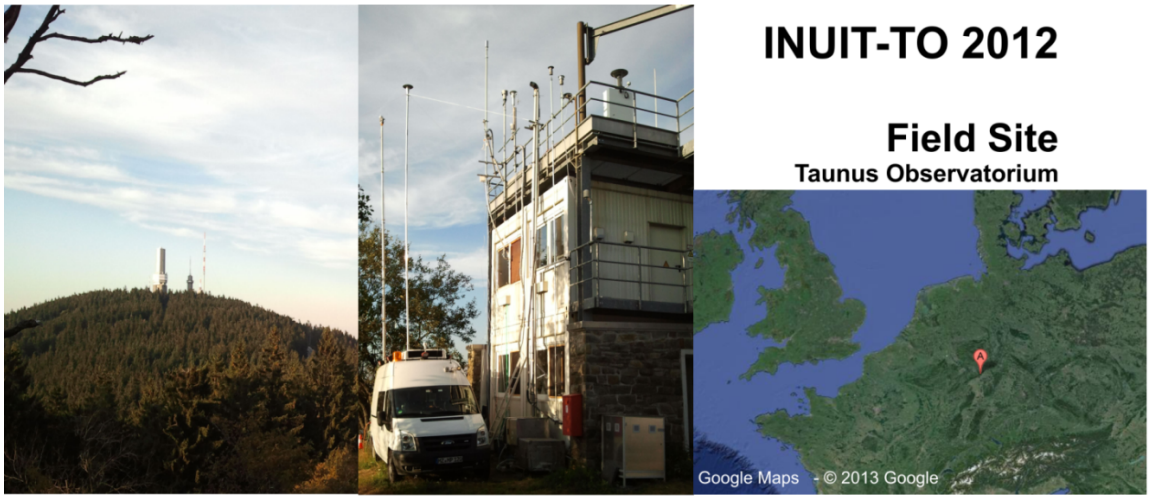

Figure S4.1. Field Site during INUIT-TO 2012 campaign at the Taunus Observatorium (826 m a.s.l.).

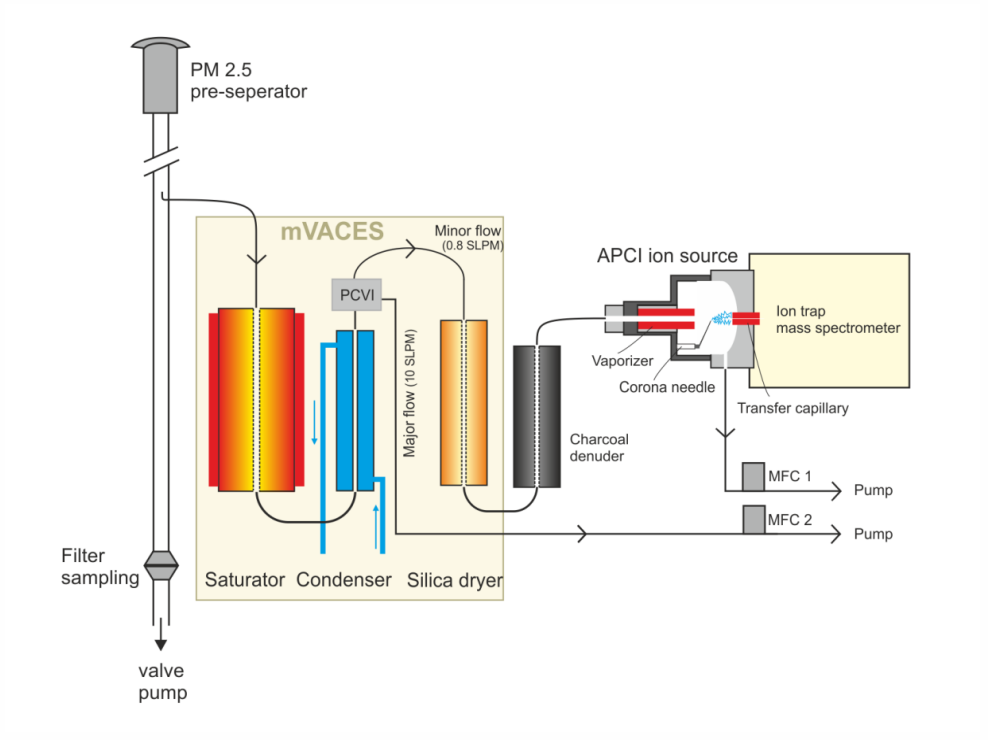

Figure S4.2. Experimental setup of the mVACES/APCI-MS and filter sampling for UHPLC-ESI-UHRMS analysis (modified from Vogel et al. 2013).

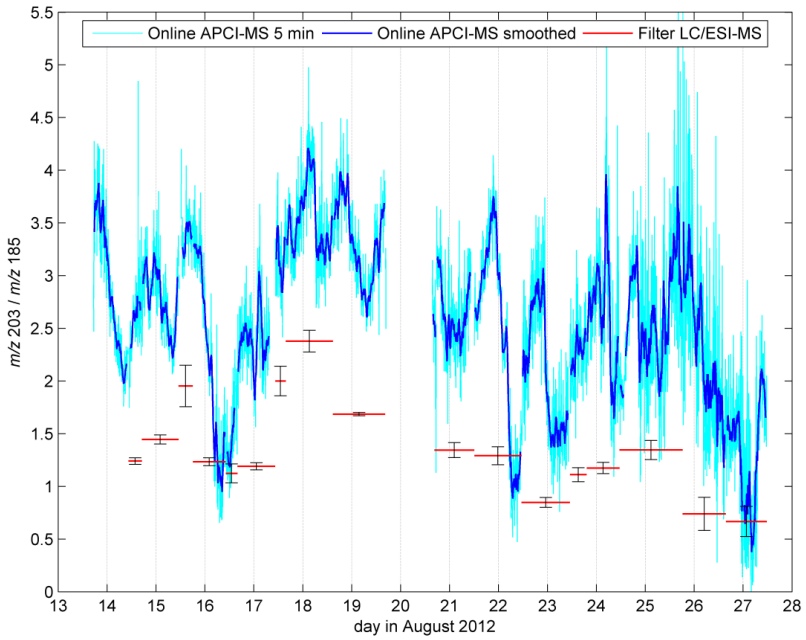

Figure S4.3. Aging proxy (m/z 203 / m/z 185) determined by online APCI-MS and by filter based LC-MS analysis.

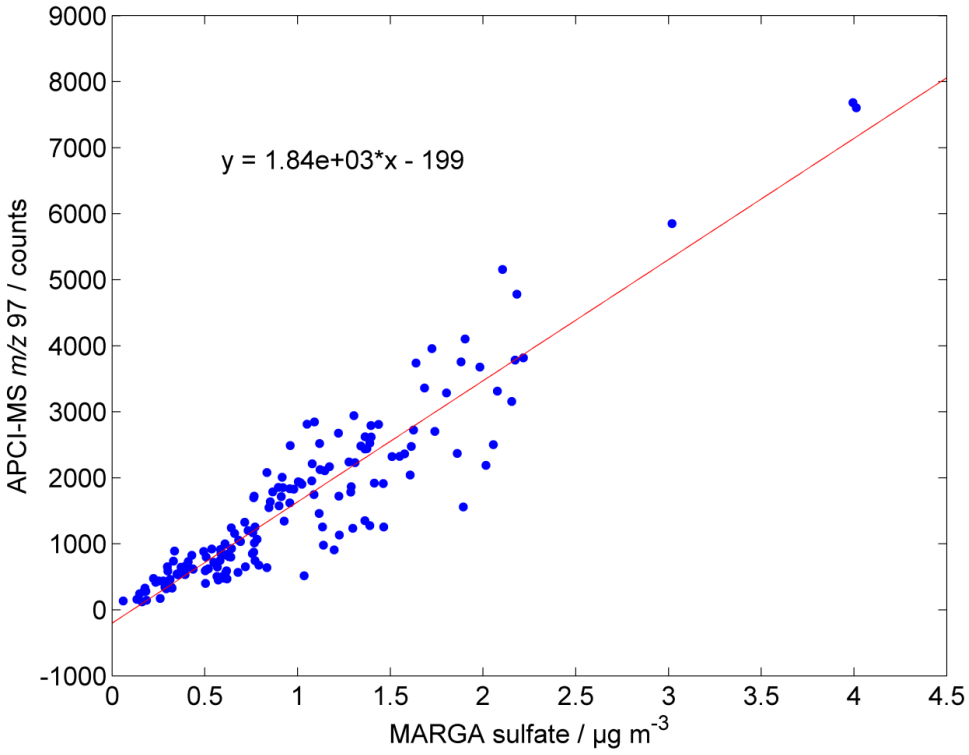

Figure S4.4. MARGA sulfate (ion chromatography) vs online APCI-MS of m/z 97 ($HSO4^-$). Linear fit used for the sulfate calibration of the APCI-MS sulfate signal.

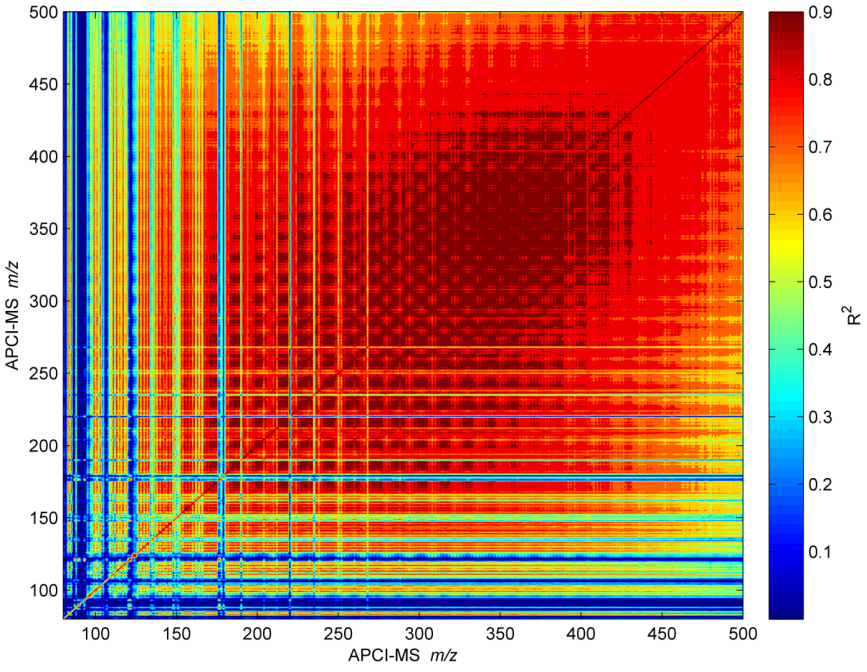

Figure S4.5. Correlation matrix of the time period 20 – 27 August of the APCI-MS spectrum.

Table S4.1a. CHO containing organic compounds on filter samples during Inuit-TO 2012 determined by UHPLC/(−)ESI-UHRMS.

measured *m/z* [M-H]⁻	elemental composition	mass deviation / ppm	DBE	$\overline{OS_C}$	retention time / min	literature
157.0507	$C_7H_{10}O_4$	0.305	3	-0.29	1.60	Gomez-Gonzales 2012
157.0871	$C_8H_{14}O_3$	0.461	2	-1.00	2.16	Kourtchev 2013
171.0664	$C_8H_{12}O_4$	0.397	3	-0.50	0.86; 1.90	Claeys 2009; Hoffmann 1998
173.0456	$C_7H_{10}O_5$	0.019	3	0.00	1.13	Bateman 2012
175.0613	$C_7H_{12}O_5$	0.133	2	-0.29	1.14	
183.0664	$C_9H_{12}O_4$	0.480	4	-0.44	2.10	
185.0457	$C_8H_{10}O_5$	0.288	4	0.00	2.46	
185.0820	$C_9H_{14}O_4$	0.420	3	-0.67	1.80; 1.92; 2.18, 2.29	e.g. Yu 1998
187.0614	$C_8H_{12}O_5$	0.231	3	-0.25	1.39; 1.64; 1.79	Claeys 2009, Gomez-Gonzalez 2012, Kourtchev 2013
189.0407	$C_7H_{10}O_6$	0.945	3	0.29	1.15, 1.53	
189.0770	$C_8H_{14}O_5$	0.599	2	-0.50	1.41	Yasmeen 2012
193.0144	$C_9H_6O_5$	0.381	7	0.44	1.95	
199.0619	$C_9H_{12}O_5$	1.021	4	-0.22	2.72	
201.0411	$C_8H_{10}O_6$	1.287	4	0.25	1.03; 1.63	
201.0771	$C_9H_{14}O_5$	0.613	3	-0.44	1.54; 1.92; 1.99	Iinuma 2013, Kahnt 2013
203.0563	$C_8H_{12}O_6$	0.437	3	0.00	1.75	Szmiegielski 2007
203.0927	$C_9H_{16}O_5$	0.754	2	-0.67	1.72; 2.06	
205.0719	$C_8H_{14}O_6$	0.335	2	-0.25	1.29; 1.59	Shilling 2009
213.0775	$C_{10}H_{14}O_5$	1.001	4	-0.40	1.96; 2.06	Kahnt 2013
215.0567	$C_9H_{12}O_6$	1.063	4	0.00	1.52; 1.78	Hamilton 2011
215.0926	$C_{10}H_{16}O_5$	0.108	3	-0.60	2.23; 2.36	Iinuma 2013, Kahnt 2013
217.0719	$C_9H_{14}O_6$	0.408	3	-0.22	1.84; 1.97; 2.07; 2.39	Iinuma 2009
227.0567	$C_{10}H_{12}O_6$	0.875	5	0.00	1.52	
227.0928	$C_{11}H_{16}O_5$	0.939	4	-0.55	1.99; 2.15; 2.22	
229.0717	$C_{10}H_{14}O_6$	-0.486	4	-0.20	1.72; 2.15	Iinuma 2013, Kahnt 2013
229.1082	$C_{11}H_{18}O_5$	0.363	3	-0.73	2.59; 2.79	
231.0875	$C_{10}H_{16}O_6$	0.340	3	-0.40	2.39	Claeys 2009
233.0670	$C_9H_{14}O_7$	0.575	3	0.00	1.44	
233.1032	$C_{10}H_{18}O_6$	0.508	2	-0.60	1.59; 1.74	
241.0510	$C_{14}H_{10}O_4$	0.821	10	-0.14	4.42	
241.1085	$C_{12}H_{18}O_5$	0.718	4	-0.67	2.34	
243.0876	$C_{11}H_{16}O_6$	0.117	4	-0.36	1.99; 2.67	
245.0667	$C_{10}H_{14}O_7$	0.098	4	0.00	1.4-1.9	
245.1031	$C_{11}H_{18}O_6$	0.320	3	-0.55	1.4-3.0	
247.0825	$C_{10}H_{16}O_7$	0.259	3	-0.20	1.62	
255.1242	$C_{13}H_{20}O_5$	0.953	4	-0.77	2.91; 4.07	Chan 2011
257.1398	$C_{13}H_{22}O_5$	1.100	3	-0.92	4.97	
259.0824	$C_{11}H_{16}O_7$	0.208	4	-0.18	1.4-2.5	
259.1188	$C_{12}H_{20}O_6$	0.167	3	-0.67	1.5-3.0	
271.1190	$C_{13}H_{20}O_6$	1.027	4	-0.62	2.48	
271.1555	$C_{14}H_{24}O_5$	0.859	3	-1.00	2.84	Chan 2011
273.0982	$C_{12}H_{18}O_7$	0.783	4	-0.33	1.2-2.8	
273.1346	$C_{13}H_{22}O_6$	0.909	3	-0.77	1.7-4.0	
275.1139	$C_{12}H_{20}O_7$	0.886	3	-0.50	1.0-3.0	
275.0775	$C_{11}H_{16}O_8$	1.052	4	0.00	0.8-2.5	
283.1555	$C_{15}H_{24}O_5$	0.611	4	-0.93	3.90; 4.05; 5.17; 5.54; 6.06	Chan 2011
285.0981	$C_{13}H_{18}O_7$	0.575	5	-0.31	1.3-3.0	
285.1346	$C_{14}H_{22}O_6$	0.731	4	-0.71	1.5-4.0	Chan 2011
287.1138	$C_{13}H_{20}O_7$	0.745	4	-0.46	1.2-3.2	
289.0931	$C_{12}H_{18}O_8$	0.862	4	-0.17	1.2-2.8	
289.1295	$C_{13}H_{22}O_7$	0.843	3	-0.62	1.5-3.0	
299.1138	$C_{14}H_{20}O_7$	0.447	5	-0.43	1.5-3.5	
299.1502	$C_{15}H_{24}O_6$	0.629	4	-0.80	2.0-4.0	
301.0930	$C_{13}H_{18}O_8$	0.529	5	-0.15	1.0-3.0	

301.1294	$C_{14}H_{22}O_7$	0.511	4	-0.57	1.5-4.0	
303.1087	$C_{13}H_{20}O_8$	0.426	4	-0.31	1.0-3.0	
313.1295	$C_{15}H_{22}O_7$	0.651	5	-0.53	1.5-4.0	Chan 2011
313.1661	$C_{16}H_{26}O_6$	0.984	4	-0.88	6.71	
315.1089	$C_{14}H_{20}O_8$	1.013	5	-0.29	1.5-3.0	
317.1243	$C_{14}H_{22}O_8$	0.250	4	-0.43	1.2-3.5	
329.1243	$C_{15}H_{22}O_8$	0.210	5	-0.40	1.5-3.5	
331.1037	$C_{14}H_{20}O_9$	0.709	5	-0.14	1.0-3.0	

* not found by SIEVE® due to bad chromatographic separation, but peak intensity was >1e5 counts (used peak threshold value)

Table S4.1b. CHNO containing organic compounds on filters samples during Inuit-TO 2012 determined by UHPLC/(−)ESI-UHRMS.

measured *m/z* [M-H]$^-$	elemental composition	mass deviation / ppm	DBE	retention time / min	literature
154.0147	$C_6H_5NO_4$	0.708	5	2.51	Mohr 2013
168.0304	$C_7H_7NO_4$	0.53	5	2.32	Iinuma 2010
182.0097	$C_7H_5NO_5$	0.794	6	2.33	
194.0097	$C_8H_5NO_5$	0.281	7	2.55	
198.1138	$C_{10}H_{17}NO_3$	0.673	3	2.02	
200.0931	$C_9H_{15}NO_4$	1.093	3	1.52	
206.1191	$C_{12}H_{17}NO_2$	0.184	5	3.08	
218.0308	$C_7H_9NO_7$	0.528	4	2.28	
224.1294	$C_{12}H_{19}NO_3$	0.728	4	3.08	
227.0312	$C_8H_8N_2O_6$	0.884	6	3.46	
230.0461	$C_{12}H_9NO_4$	0.474	9	6.91	
232.0466	$C_8H_{11}NO_7$	0.496	4	2.46	
239.0312	$C_9H_8N_2O_6$	0.505	7	2.95	
248.0414	$C_8H_{11}NO_8$	0.284	4	2.04; 2.33	
252.1091	$C_9H_{19}NO_7$	0.535	1	1.49	
261.0152	$C_{11}H_6N_2O_6$	-1.836	10	1.75	
264.0727	$C_9H_{15}NO_8$	0.267	3	2.55	
266.0522	$C_8H_{13}NO_9$	0.435	3	1.49; 2.09	Surratt 2006
271.0422	$C_6H_{12}N_2O_{10}$	0.599	2	2.20; 2.39; 2.53; 2.68;3.04	
271.1670	$C_{13}H_{24}N_2O_4$	0.773	3	1.73	
275.0307	$C_{12}H_8N_2O_6$	-0.87	10	2.06	
278.0883	$C_{10}H_{17}NO_8$	0.505	3	2.34	
288.1460	$C_{13}H_{23}NO_6$	1.108	3	2.94	
292.0680	$C_{10}H_{15}NO_9$	1.218	4	2.96	
293.0256	$C_8H_{10}N_2O_{10}$	-1.221	5	1.76	
302.1617	$C_{14}H_{25}NO_6$	0.858	3	2.23	
308.0992	$C_{11}H_{19}NO$	1.025	3	3.30; 3.46; 5.10	
336.0936	$C_{12}H_{19}NO_{10}$	1.134	4	2.47	
336.1306	$C_{13}H_{23}NO_9$	1.087	3	2.34	
339.1049	$C_{11}H_{20}N_2O_{10}$	0.153	3	4.61; 4.94; 6.22	
348.1303	$C_{14}H_{23}NO_9$	-0.128	4	2.33	Chan 2011
366.1417	$C_{14}H_{25}NO_{10}$	0.439	3	2.75	
372.2393	$C_{19}H_{35}NO_6$	0.481	3	6.68	
397.1472	$C_{14}H_{26}N_2O_{11}$	0.295	3	6.21; 6.82	
403.2458	$C_{19}H_{36}N_2O_7$	0.112	3	6.84	

Table S4.1c. CHOS containing organic compounds on filters samples during Inuit-TO 2012 determined by UHPLC/(−)ESI-UHRMS.

measured *m/z* [M-H]$^-$	elemental composition	mass deviation / ppm	DBE	retention time / min	literature
167.0385	$C_5H_{12}O_4S$	-0.017	0	1.80; 1.92; 2.22	Lin 2012
195.0700	$C_7H_{16}O_4S$	0.651	0	4.63	
209.0134	$C_6H_{10}O_6S$	0.852	2	0.88; 1.07	
209.0497	$C_7H_{14}O_5S$	0.586	1	1.65; 1.92	Lin 2012
209.0855	$C_8H_{18}O_4S$	0.751	0	6.69	
211.0284	$C_6H_{12}O_6S$	0.843	1	1.14; 1.25; 1.57	
225.0442	$C_7H_{14}O_6S$	0.835	1	1.72	Nguyen 2012, Lin 2012
235.0655	$C_9H_{16}O_5S$	1.031	2	1.63; 2.00; 2.25; 3.53	Surratt 2008, Kristensen 2011, Lin 2012
237.0442	$C_8H_{14}O_6S$	0.497	2	1.03; 1.54; 1.59	Surratt 2008, Altieri 2009, Nguyen 2012, Lin 2012
239.0233	$C_7H_{12}O_7S$	0.558	2	0.62; 0.72; 1.06	Surratt 2008, Altieri 2009, Nguyen 2012, Lin 2013
249.0811	$C_{10}H_{18}O_5S$	1.575	2	2.6	Iinuma 2007, Surratt 2007, Surratt 2008, Kristensen 2011, Yttri 2011, Lin 2012
251.0600	$C_9H_{16}O_6S$	0.589	2	1.93	Surratt 2008, Altieri 2009, Nguyen 2012, Lin 2012
253.0393	$C_8H_{14}O_7S$	1.396	2	1.30; 1.44; 1.82	Surratt 2008, Altieri 2009, Nguyen 2012
253.0762	$C_9H_{18}O_6S$	0.979	1	2.63; 2.95	Lin 2012
263.0965	$C_{11}H_{20}O_5S$	0.807	2	6.91	Yttri 2011
265.0399	$C_9H_{14}O_7S$	0.805	3	1.21; 1.44; 1.71; 2.00	Nguyen 2012
267.0186	$C_8H_{12}O_8S$	0.819	3	0.72; 1.41	Nguyen 2012
267.0548	$C_9H_{16}O_7S$	0.873	2	1.59; 1.68; 1.72; 1.97;2.41	Surratt 2008, Altieri 2009, Nguyen 2012, Lin 2012
267.0919	$C_{10}H_{20}O_6S$	1.826	1	2.48	Lin 2012
269.0344	$C_8H_{14}O_8S$	1.259	2	1.17; 1.39	
269.0714	$C_9H_{18}O_7S$	2.056	1	1.55; 1.85	
279.0549	$C_{10}H_{16}O_7S$	1.194	3	1.27; 1.87	Surratt 2007, Surratt 2008, Altieri 2009, Kristensen 2011, Yttri 2011, Nguyen 2012, LeClair 2012, Lin 2012, Lin 2013
281.0336	$C_9H_{14}O_8S$	0.814	3	1.68; 2.03; 2.17	Nguyen 2012
281.0715	$C_{10}H_{18}O_7S$	1.541	2	1.50; 1.95; 2.02	Surratt 2008, Altieri 2009, Nguyen 2012, Lin 2012, Lin 2013
295.0871	$C_{11}H_{20}O_7S$	1.807	2	2.25	Lin 2012

Table S4.1d. CHNOS containing organic compounds on filters samples during Inuit-TO 2012 determined by UHPLC/(−)ESI-UHRMS.

measured *m/z* $[M-H]^-$	elemental composition	mass deviation / ppm	DBE	retention time / min	literature
238.0758	$C_8H_{17}NO_5S$	0.644	1	1.70	
241.9983	$C_5H_9NO_8S$	0.702	2	1.30; 1.44; 1.65; 2.08	Lin 2012
252.0918	$C_9H_{19}NO_5S$	0.807	1	1.44	
260.0084	$C_5H_{11}NO_9S$	0.135	1	1.53	Surratt 2007, Surratt 2008,Altieri 2009, Lin 2013
266.1074	$C_{10}H_{21}NO_5S$	1.027	1	2.45	
284.0091	$C_7H_{11}NO_9S$	0.758	3	1.77	
292.0868	$C_{11}H_{19}NO_6S$	1.399	3	2.01	
294.0659	$C_{10}H_{17}NO_7S$	1.409	3	4.15; 5.82; 6.12; 6.37; 6.55	Surratt 2007, Iinuma 2007, Surratt 2008, Altieri 2009, Kristensen 2011, Yttri 2011, Lin 2012, Lin 2013
296.0450	$C_9H_{15}NO_8S$	0.877	3	2.29; 2.68	Surratt 2008, Yttri 2011, Kristensen 2011, Lin 2012, Lin 2013
300.0340	$C_{15}H_{11}NO_4S$	0.361	11	2.47	
304.9936	$C_5H_{10}N_2O_{11}S$	0.876	2	1.69; 1.95; 2.08; 2.17; 2.52; 2.65	Ng 2008, Surratt 2008, Altieri 2009, Lin 2012
306.1022	$C_{12}H_{21}NO_6S$	0.616	3	2.33	
308.1543	$C_{13}H_{27}NO_5S$	0.886	1	3.09	
310.0610	$C_{10}H_{17}NO_8S$	0.902	3	2.43; 2.64; 2.88; 3.21	Surratt 2007, Surratt 2008, LeClair 2012, Lin 2012
312.0404	$C_9H_{15}NO_9S$	1.426	3	2.02; 2.28	Surratt 2008
312.0768	$C_{10}H_{19}NO_8S$	0.992	2	2.81	Lin 2012
324.0399	$C_{10}H_{15}NO_9S$	0.417	4	2.37	Surratt 2008
326.0560	$C_{10}H_{17}NO_9S$	1.089	3	1.92; 2.17	Surratt 2007, Surratt 2008, Kristensen 2011, LeClair 2012, Lin 2012
328.0352	$C_9H_{15}NO_{10}S$	0.977	3	2.05; 2.23; 2.36; 2.74	
330.0146	$C_8H_{13}NO_{11}S$	0.745	3	1.24; 1.72	
338.1287	$C_{13}H_{25}NO_7S$	0.751	2	1.92	
340.0350	$C_{10}H_{15}NO_{10}S$	0.178	4	2.42	
342.0503	$C_{10}H_{17}NO_{10}S$	0.644	3	1.96; 2.03; 2.83; 2.92; 3.30; 3.40	Surratt 2008, Altieri 2009, Kristensen 2011, LeClair 2012, Lin 2012
349.9790	$C_5H_9N_3O_{13}S$	0.654	3	6.13; 6.20	Ng 2008
355.0461	$C_{10}H_{16}N_2O_{10}S$	0.99	4	6.9	Surratt 2008, Lin 2012
373.0559	$C_{10}H_{18}N_2O_{11}S$	0.554	3	2.57; 2.73; 3.1; 3.31; 3.87	Surratt 2008, Kristensen 2011, Lin 2012
374.2014	$C_{18}H_{33}NO_5S$	0.462	3	6.7	
376.2167	$C_{18}H_{35}NO_5S$	0.513	2	6.97	
387.0360	$C_{10}H_{16}N_2O_{12}S$	0.600	4	6.75	Surratt 2008
390.0180	$C_{10}H_{17}NO_{11}S_2$	0.885	3	2.5	
390.1964	$C_{18}H_{33}NO_6S$	0.765	3	6.6; 6.9	
392.2121	$C_{18}H_{35}NO_6S$	0.888	2	6.52	
404.1755	$C_{18}H_{31}NO_7S$	0.282	4	6.65; 6.85	
408.2068	$C_{18}H_{35}NO_7S$	0.229	2	6.91	

C. List of related publications and presentations

Peer-reviewed publications:

Williams, J., Crowley, J., Fischer, H., Harder, H., Martinez, M., Petaja, T., Rinne, J., Back, J., Boy, M., Dal Maso, M., Hakala, J., Kajos, M., Keronen, P., Rantala, P., Aalto, J., Aaltonen, H., Paatero, J., Vesala, T., Hakola, H., Levula, J., Pohja, T., Herrmann, F., Auld, J., Mesarchaki, E., Song, W., Yassaa, N., Nölscher, A. C., Johnson, A. M., Custer, T., Sinha, V., Thieser, J., Pouvesle, N., Taraborrelli, D., Tang, M. J., Bozem, H., Hosaynali-Beygi, Z., Axinte, R., Oswald, R., Novelli, A., Kubistin, D., Hens, K., Javed, U., Trawny, K., Breitenberger, C., Hidalgo, P. J., Ebben, C. J., Geiger, F. M., Corrigan, A. L., Russell, L. M., Ouwersloot, H. G., Arellano, J. V.-G. de, Ganzeveld, L., Vogel, A. L., Beck, M., Bayerle, A., Kampf, C. J., Bertelmann, M., Koellner, F., Hoffmann, T., Valverde, J., Gonzalez, D., Riekkola, M.-L., Kulmala, M., and Lelieveld, J.: The summertime Boreal forest field measurement intensive (HUMPPA-COPEC-2010): an overview of meteorological and chemical influences, *Atmospheric Chemistry and Physics*, 11, 10599–10618, doi:10.5194/acp-11-10599-2011, **2011**.

Nölscher, A. C., Williams, J., Sinha, V., Custer, T., Song, W., Johnson, A. M., Axinte, R., Bozem, H., Fischer, H., Pouvesle, N., Phillips, G., Crowley, J. N., Rantala, P., Rinne, J., Kulmala, M., Gonzales, D., Valverde-Canossa, J., Vogel, A. L., Hoffmann, T., Ouwersloot, H. G., Arellano, J. V.-G. de, and Lelieveld, J.: Summertime total OH reactivity measurements from boreal forest during HUMPPA-COPEC 2010, *Atmospheric Chemistry and Physics*, 12, 8257–8270, doi:10.5194/acp-12-8257-2012, **2012**.

Vogel, A. L., Äijälä, M., Brüggemann, M., Ehn, M., Junninen, H., Petäjä, T., Worsnop, D. R., Kulmala, M., Williams, J., and Hoffmann T.: Online atmospheric pressure chemical ionization ion trap mass spectrometry (APCI-IT-MS^n) for measuring organic acids in concentrated bulk aerosol – a laboratory and field study, *Atmospheric Measurement Techniques*, 6, 431–443, doi:10.5194/amt-6-431-2013, **2013**.

Huang, R.-J., Thorenz, U. R., Kundel, M., Venables, D. S., Ceburnis, D., Ho, K. F., Chen, J., Vogel, A. L., Küpper, F. C., Smyth, P. P. A., Nitschke, U., Stengel, D. B., Berresheim, H., O'Dowd, C. D., and Hoffmann, T.: The seaweeds *Fucus vesiculosus* and *Ascophyllum nodosum* are significant contributors to coastal iodine emissions, *Atmospheric Chemistry and Physics*, 13, 5255-5264, doi:10.5194/acp-13-5255-2013, **2013**.

Vogel, A. L., Aijala, M., Corrigan, A. L., Junninen, H., Ehn, M., Petaja, T., Worsnop, D. R., Kulmala, M., Russell, L. M., Williams, J., and Hoffmann, T.: In situ submicron organic aerosol characterization at a boreal forest research station during HUMPPA-COPEC 2010 using soft and hard ionization mass spectrometry, *Atmospheric Chemistry and Physics*, 13, 10933–10950, doi:10.5194/acp-13-10933-2013**, 2013**.

Corrigan, A. L., Russell, L. M., Takahama, S., Äijälä, M., Ehn, M., Junninen, H., Rinne, J., Petäjä, T., Kulmala, M., Vogel, A. L., Hoffmann, T., Ebben, C. J., Geiger, F. M., Chhabra, P., Seinfeld, J. H., Worsnop, D. R., Song, W., Auld, J., and Williams, J.: Biogenic and biomass burning organic aerosol in a boreal forest at Hyytiälä, Finland, during HUMPPA-COPEC 2010, *Atmospheric Chemistry and Physics*, 13, 12233–12256, doi:10.5194/acp-13-12233-2013, **2013**.

Brüggemann, M., Vogel, A. L., and Hoffmann, T.: Analysis of organic aerosols using a micro-orifice volatilization impactor (MOVI) coupled to an atmospheric-pressure chemical ionization mass spectrometer (APCI-MS), *European Journal of Mass Spectrometry*, accepted, **2014**.

Yatavelli, R. L. N., Stark, H., Day, D. A., Thompson, S. L., Campuzano-Jost, P., Palm, B. B., Vogel, A. L., Hoffmann, T., Äijälä, M., Kimmel, J. R., Canagaratna, M. R., Cubison, M. J., Thornton, J. A., Jayne, J. T., Worsnop, D. R., and Jimenez J. L.: Constraining the Contribution of Organic Acids to Northern Hemispheric Organic Aerosol Using Particle-Phase Acid-CIMS and AMS Datasets, *Geophysical Research Letters*, in preparation, **2014**.

Vogel, A. L., Schneider, J., Müller-Tautges, C., Phillips, G. J., Krüger, M., Rose, D., Makkonen, U., Hakola, H., Crowley, J., Pöschl, U., and Hoffmann, T.: Aerosol chemistry resolved by mass spectrometry- insights into ambient new particle formation and CCN activity of organic aerosols, in preparation, **2014**.

Oral Presentations:

Vogel, A. L., Bayerle, A., Kampf, C., Ehn, M., Junninen, H., Petäjä, T., Williams, J., and Hoffmann T.: Online analysis of aerosol over a boreal forest in Hyytiälä, Finland using mVACES/(−)APCI-IT-MS, *1st HUMPPA-COPEC2010 data meeting*, Helsiniki, Finland, December 2010.

Vogel, A. L., Bayerle, A., Kampf, C., Äijälä, M., Nölscher, A., Ehn, M., Junninen, H., Petäjä, T., Williams, J., and Hoffmann T.Organic acid measurements in gas and particle phase using APCI-MS during HUMPPA –COPEC10, *2nd HUMPPA-COPEC2010 data meeting*, Ringberg/Tegernsee, Germany, March 2011.

Vogel, A. L., Äijälä, M., Ehn, M., Junninen, H., Petäjä, T., Worsnop, D. R., Kulmala, M., Williams, J., and Hoffmann, T.: Online analysis of organic acids in gas- and particle phase during HUMPPA-COPEC-campaign, *European Aerosol Conference*, Manchester, UK, September 2011.

Vogel, A. L., Brüggemann, M., Äijälä, M., Ehn, M., Junninen, H., Corrigan, A. L., Petäjä, T., Worsnop, D. R., Russell, L. M., Kulmala, M., Williams, J., and Hoffmann, T.: Online measurement of biogenic organic acids in the boreal forest using atmospheric pressure chemical ionization mass spectrometry (APCI-MS), *European Geosciences Union General Assembly*, Vienna, Austria, April 2012.

Poster Presentations:

Vogel, A. L., Beck, M., Äijälä, M., Ehn, M., Junninen, H., Petäjä, T., Worsnop, D. R., Kulmala, M., Williams, J., and Hoffmann, T.: Field measurement of secondary organic aerosol in a boreal forest site in southern Finland using on-line soft ionization ion trap mass spectrometry, *ANAKON*, Zürich, Switzerland, March 2011.

Vogel, A. L., Äijälä, M., Ehn, M., Junninen, H., Petäjä, T., Worsnop, D. R., Kulmala, M., Williams, J., and Hoffmann, T.: Online analysis of organic acids in gas- and particle phase during HUMPPA-COPEC-campaign, *European Aerosol Conference*, Manchester, UK, September 2011.

Vogel, A. L. and Hoffmann, T.: *In-situ* MS^n von biogenen Carbonsäuren in Aerosolpartikeln, *ANAKON*, Essen, Germany, March 2013.

Vogel, A. L., Äijälä, M., Ehn, M., Junninen, H., Petäjä, T., Worsnop, D. R., Kulmala, M., Williams, J., Schneider, J, and Hoffmann, T.: Online soft ionization mass spectrometry for measuring organic acids in biogenic aerosol, *European Geosciences Union General Assembly*, Vienna, Austria, April 2013.